Stabilisation of Non-equilibrium Melt in A Linear Polyethylene in the Presence of Reduced Graphene Oxide Nanoplatelets

by

Kangsheng Liu

Doctoral Thesis

Submitted in partial fulfillment of the requirements
for the award of Doctor of Philosophy

Department of Materials

School of Aeronautical, Automotive, Chemical and Materials Engineering

Loughborough University

Loughborough LE11 3TU, Leicestershire

England, United Kingdom (U.K.)

05/2015

Contents

Acknowledgements

First and foremost I would like to thank my two supervisors, Dr Sara Ronca and Professor Sanjay Rastogi. It has been my privilege to be their PhD student. I appreciate all their contributions of time, discussions, suggestions, and funding to make my PhD life encouraged and productive.

I would like to acknowledge, Ele der Boer, with whom I developed decent friendship in the group, for the fantastic social activities he has organised and enthusiastic academic debates on the rheology and crystallisation experiments and results, though many times we did not agree with each other. I do admit, the discussions provoked some of my new ideas. I also want to thank another two honorary group members, Dr Dario Romano and Dr Efren Andablo-Reyes who worked with me over my whole PhD project. I have gained knowledge from Dario who has expertise in polymer chemistry and Efren who is an experienced rheologist. Also thank them for the great time that we spent together in my social life.

Regarding to beamtime in European Synchrotron Radiation Facilities (ESRF), I would like to thank a past member in the group who also shares decent friendship with me, Dr Nilesh Patil, for the help he has offered for my first time at ESRF. Also thank beam scientist Dr Daniel Hermida Merino for his help of setting up the equipment.

Thank my PhD friends in the department, CJ, Sian, Emma, Bailj, et al. for nice coffee time and discussions we had in the department or Holywell cafeteria.

Furthermore I would like to thank:

- Loughborough University for the financial support;
- Sponsoring company Teijin Aramid for financial support;
- The people in the department of materials who provided me training on equipments that I used during my project, for instance, Giuseppe Forte, Zhaoxia Zhou and Keith Yendall;
- Nick Tops in Teijin Aramid for the drawing of the disentangled UHMWPE composites and mechanical properties measurements;
- Professor Yefeng Yao in East Normal China University for solid-state NMR measurements and professional discussions;

- Professor Mo Song, my Masters supervisor, for his valuable suggestions on my future career
- Dr Yogesh Deshmukh in Maastricht University and Dr Xu Jianjun in DSM for some quick X-ray shots on some of my samples for my paper.

I also want to thank my friends Qi Shi, Yuchen Lu, Zuliang Hong, Tongyu Wu, Luis Drakes, Yujia Kang, for becoming a part of my life. I would like to thank Georgie Court for inviting me to visit her family during Easter and Christmas times and for having fantastic social time in the first year of my PhD. I would also like to thank all my friends in Lufbra Rag for the unforgettable experience I have ever had in my life in charity. Thank my current lovely host family who I live with, Fiona, Peter, Sophie and Helen, for their warm hospitality over the last year of my PhD.

I also would like to thank the members on my examination board, Dr Xujin Bao and Professor Jamie Hobbs, for their time and interest on my project.

Lastly but the most important part, I would like to thank my parents and my sister for their encouragement, support and understanding whenever it is needed, and I am very looking forward to seeing my lovely new-born nephew as soon as I submit my thesis.

Dedicated to my family

Abstract

In this thesis, investigation on stabilisation of non-equilibrium melt in the presence of high aspect ratio reduced graphene oxide nanosheets (rGON) was carried out. The non-equilibrium melt was prepared by melting disentangled ultrahigh molecular weight polyethylene (UHMWPE) which was synthesised using homogeneous single-site catalytic system. Rheological analyses of the disentangled UHMWPE/rGON nanocomposites prepared by physical mixing conclusively demonstrate the transformation of the melt from non-equilibrium state to equilibrium state is suppressed when the filler was added. The suppression effect on the transformation reached maximum at a certain filler content and the non-equilibrium melt state was retained within the experimental time, indicating the existence of strong filler-chain interaction that hindered the chain thermodynamics. In order to have better understanding of the suppression on the transformation, thermal analysis was performed on the non-equilibrium melts to follow the influence of non-equilibrium polymer melt on crystallisation kinetics of disentangled UHMWPE with and without rGON. The analysis was carried out by means of differential scanning calorimetry (DSC), and the changes in enthalpic relaxation process were found in good agreement with the rheological response of the melts. Thermal analysis showed the presence of two endothermic peaks in a sample of non-equilibrium melt that was left to crystallise under isothermal condition after melting. The high temperature endothermic peak (141.5 °C) was related to melting of crystals obtained on crystallisation from the disentangled domains of the heterogeneous (non-equilibrium) polymer melt, whereas the low melting temperature endothermic peak was related to melting of crystals formed from entangled domains of the melt. It was further found that with increasing the annealing time in melt (160 °C), the enthalpy of the lower melting temperature peak increased at the expense of the higher melting temperature peak, confirming transformation of the non-equilibrium polymer melt to equilibrium melt state. The enthalpic relaxation process as a function of rGON showed that at the specific content of the filler, where the suppression of the transformation reached maximum, the high endothermic peak remained independent of the annealing time of the polymer melt at 160 °C. This observation strengthened the concept that in the presence of the filler, chain dynamics was arrested to an extent that the everlasting non-equilibrium melt state having lower entanglement density was retained facilitating crystal formation having high melting endothermic temperature. This unique property of the nanocomposites provokes potential in

facilitating their processability and making high demanding products in more complex dimensions.

List of Abbreviations and Symbols

Abbreviation/Symbol	Extended Names
DSC	Differential Scanning Calorimetry
FEG-SEM	Field Emission Gun-Scanning Electron Microscope
FI Catalyst	Bis[N-(*tert*-butylsalicylidene)pentafluoroanilinato]titanium (IV) Dichloride
FT-IR	Fourier Transform-Inferred Spectroscopy
GON	Graphene Oxide Nanoplatelets
HDPE	High Density Polyethylene
MAO	Methylaluminoxane
Min	Minute
M_n	Number-average Molecular Weight
M_w	Weight-average Molecular Weight (Molar Mass)
MWD/PDI:	Molecular Weight Distribution/Polydispersity Index
M_z	Higher Average Molecular Weights
NMR	Nuclear Magnetic Resonance
PE	Polyethylene
rGON	Reduced Graphene Oxide Nanoplatelets
SAXS	Small Angle X-ray Scattering
TEM	Transmission Electron Microscope
TGA	Thermogravimetric Analysis
UHMWPE	Ultra-high Molecular Weight Polyethylene
WAXS	Wide Angle X-ray Scattering
XPS	X-ray Photoelectron Spectroscopy
XRD	X-ray Diffraction
kg	Kilogram
cm	Centimetre
°C	Celsius/Centigrade
V	Volts

A	Ampere
$\boldsymbol{T_m}$	Endothermic Melting Peak
J	Joule
%	Percentage
Temp	Temperature
Pa	Pascale
wt	Weight
G'	Storage/Elastic Modulus
G''	Loss Modulus
$\boldsymbol{<M_e>}$	Molar Mass between Adjacent Physical Entanglements
$\boldsymbol{D_e}$	Deborah Number
s	Second

List of Figures

List of Tables

1 General Information

1.1 Disentangled UHMWPE

1.1.1 Ultra High Molecular Weight Polyethylene

Thermoplastic polymers are extensively used in a variety of applications due to their ease in processability, light weight, low cost and the possibility to modify their properties by suitable modifications of the molecular structure. Among this family, polyethylene, based on a simple structure of -CH_2CH_2- repeating units, is the most well studied polymer. The wide range of molecular architectures available, from linear to branched, from low to high molecular weight and the possibility to add a variety of fillers, make the polymer widely applied, not only in commodity applications, but also in high demanding ones such as ballistic protection, prostheses and high-strength light-weighted ropes where very high mechanical properties are required. For these high demanding applications, ultrahigh molecular weight polyethylene (UHMWPE), with molecular weight over 1 million g/mol, is usually the material of choice. The mechanical properties of the material are enhanced with increasing molecular weight but, an increase of the zero shear viscosity is also observed following the power law shown in equation 1- 1 when the molar mass exceeds a critical value [1],

$$\eta_0 = KM^{3.4} \qquad \text{(Equation 1-1)}$$

In the equation η_0 is the zero shear viscosity in the melt; K is the flow consistency index; M is the molecular weight. As we can estimate from the equation, when the molar mass is doubled, the zero shear viscosity increases by nearly 10 times, thus making the conventional melt-processing techniques unfeasible. In addition, the high viscosity also makes the homogeneous dispersion of filler to the polymer by melt-processing very challenging. The reason for the significant increment in viscosity has been explained by taking into account the chain dynamics in the molten state, mainly in terms of ‘reptation’, a concept introduced by P.G. de Gennes in 1971 [2,3]. In this model, a free chain in a polymer melt network is trapped in a virtual ‘tube’ having diameter of the same dimension of the average distance between adjacent entanglements [2,3], as shown in Figure 1-1. Within the tube, the polymer chains act as snake-like motion and ‘reptate’ along the tube axial.

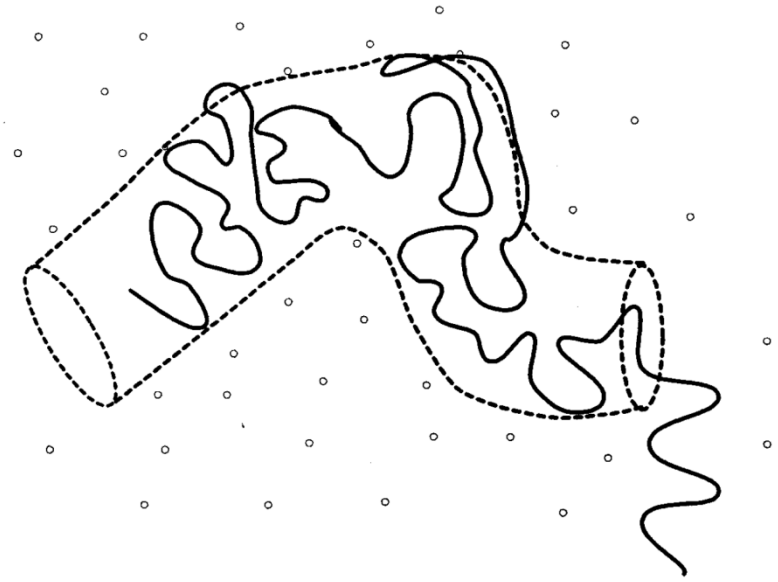

Figure 1-1 A virtual tube of a single chain in a polymer melt, caused by the topological constraints of its neighbourhood chains (small cycles); the diameter of the 'tube' has the same dimension of the average distance between adjacent entanglements [4].

The concept of entanglements has provided the basis for our understanding of the flow properties of thermoplastic polymer melts [2,3,5]. The virtual tube represent the sum of the constraints given by neighbouring chains and it supresses the motion perpendicular to the tube axis, but allows both curvilinear motion and centre-mass diffusion along the tube direction. The term 'reptation' is introduced to represent the snake-like wriggling of the polymer chains under Brownian motion. The characteristic timescale for a chain to 'escape' from its original position to the next one within a distance corresponding to the tube length, τ_d, is found to be proportional to the cube of the molecular weight of the restricted chain, M^3 (thereby the zero shear viscosity $\eta_0 \sim M^{3.0}$). The experimental discrepancy, that $\eta_0 \sim M^{3.4}$, is attributed to the contour length of the chain fluctuation that drives the chain contraction and stretching along the tube [2] for molar mass < $300 \times M_e$ g/mol [6] (M_e is molar mass between adjacent entanglements). Given the relationship between viscosity, molecular weight and entanglements, it has been postulated that, by reduction of either M or the entanglement density, it should be possible to reduce the viscosity of the polymer melt, thus providing potential for processing the high viscous polymer, incorporating nano-fillers homogeneously, and further widening its applications at lower cost.

Based on this hypothesis, a number of methods used to ease the processability of UHMWPE are discussed. Reducing the molecular weight would not achieve the required mechanical properties [7], and for this reason the second route (i.e. the reduction of entanglement density)

has been pursued by several research groups [8,9]. The decrease of the entanglement density with the consequent reduction of the zero shear viscosity can facilitate the processability even at temperatures lower than the equilibrium melting point (solid state processing). Three main routes have been successfully applied so far to achieve UHMWPE with a reduced number of entanglements, and they are: 1) solution spinning of UHMWPE (commonly known as wet spinning); 2) polymerisation using Ziegler-Natta catalysts at low temperatures; 3) polymerisation using a single-site, homogeneous catalyst under controlled conditions.

1.1.2 Disentanglement of Entangled UHMWPE by Wet-spinning

Commercially available UHMWPE is synthesised in slurry or gas phase using conventional Ziegler – Natta catalysts where the active sites responsible for the chain growth are spatially close [9]. The reaction is usually run in a temperature range of 60 and 80 ^{o}C and high pressures (monomer pressure: above 6-8 bars), resulting in a polymerisation rate (R_p) higher than the crystallisation rate (R_c). All these aspects contribute to the formation of a high number of entanglements between neighbouring polymer chains. Moreover, these catalysts usually produce UHMWPEs with a very large molecular weight distribution, where the low molecular weight component is responsible for reduction in the mechanical properties of the material.

The development of 'disentangled' UHMWPE using a physical method that could be applied to UHMWPE's post-production started with the preparation of solution-spun fibres with the so called 'wet-spinning process' in 1956 by Jurgenleit [8], and was first commercially produced by DSM in 1983 [9].

The general concept of this technique requires the dissolution of UHMWPE in a suitable solvent at very low concentrations, thereby realising the 'disentanglement' of chains, and the resultant gel is then spun into filaments, during which chains align and tend to crystallise with the removal of solvent. Following this method, it is possible to produce very strong fibres. Jurgenleit for example reported the method of spinning linear PE from solutions containing between 10 and 18 wt % of polymer in benzene or its homologues. Tensile strength up to 1.2 GPa was achieved after post drawing of the spun filaments [8]. Zwick conducted solution spun experiments of UHMWPE from naphthalene solutions [10]. In his patent [10], UHMWPE having molar mass between 1 and 3 million g/mol was used and three sub methods were performed to prepare the disentangled filaments with enhanced mechanical

properties. A modified technique of flash-spinning was introduced by Blades and White [11] who applied extrusions at high temperatures (at around 200 ºC) and high speeds using linear PE with low melt index (0.5) from a pressurised solution with solution concentration of 13 wt % in halogenated hydrocarbons. Fibrillated strands were then prepared by slow drawing, during which the spun filaments were precipitated on rapid cooling and solvent evaporated instantaneously. The achieved maximum values for modulus and tensile strength were reported as 120 GPa and 1.4 GPa, respectively. It may be important to notice that in the middle 1960s, Pennings and coworkers found that in a Couette apparatus, fibrous PE crystals formed when the inner cylinder exceeded a critical rotation rate coinciding with the onset of Taylor vortices [12]. However, the formation of fibrous crystal structures became less pronounced when HDPE was used, as discussed by Mitsuhashi, due to entanglement coupling [13]. Remarkably, at the end of the 1970s, Smith and Lemstra from DSM (in full Koninklijke DSM N.V.) invented the so called wet-spinning method, by which they obtained solution-spun UHMWPE fibres which could be ultra-drawn to ultra-high modulus and high strength fibres possessing modulus higher than 100 GPa and tensile strength over 3 GPa [14,15]; an apparatus for the wet spinning is schematically drawn in Figure 1-2.

The important aspect of this method is that UHMWPE obtained from this technique can be ultra-drawn even when the solvent is removed from the spun fibres. This enables the possibility of solid state processing of the intractable polymer. It has been possible to achieve modulus up to 150 GPa and tensile strength between 3 and 4 GPa through the optimization of the ultra-drawing procedure [13]. After the invention of the so called wet/gel-spinning process, a few variations of this technique have been patented and published [16,17]; however, the basic core principle still holds as the same.

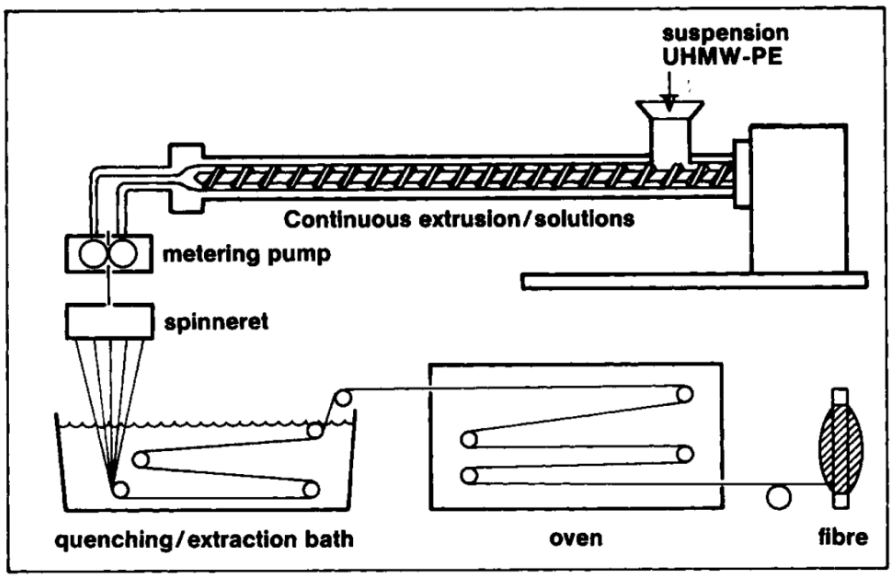

Figure 1-2 Wet spinning technique for preparation of ultra-high modulus and strength UHMWPE fibres [18], the oven dries the solvent off.

The method has made it possible to process the intractable UHMWPE into fibres by removing the entanglements and these fibres have shown enhanced mechanical properties and have attracted great attention for high demanding applications. However, this method involves consumption of large amount of organic solvents that have to be removed/recycled, and this is regarded as non-environmental friendly and possibly hazardous. Also, the dissolved UHMWPE can only be stretched uniaxially, i.e. the products are in fibrous shapes, and this limits the applications that require products having more complicated shapes.

Important to mention is that, in the 1970s, Kanamoto *et al.* and Zachariades *et al.* [19,20,21] showed that if nascent particles (particles that are taken directly from the reactor, and not subject to any heat treatment) of UHMWPE synthesised using Ziegler-Natta catalyst were compacted below the melting temperature of the material, the resulting material could be stretched to higher draw ratio compared to the maximum draw ratio attainable from melt-crystallised UHMWPE. The solid-state processed material resulted in higher values of tensile strength and modulus compared to the melt-crystallised material. They related this finding to the fact that the nascent UHMWPE had a relatively lower number of physical entanglements compared to the melt-crystallised material. Similar results were also reported later on by Zachariades *et al.* [22]. The results supported the idea that solid-state processing could be a possible processing method for UHMWPE, provided that the material has a low number of entanglements. The mechanical properties with modulus of 107 GPa and tensile strength of

1.4 GPa at maximum draw ratio of 77 were achieved [22]. However, the draw ratio was found to be much lower than that of solution-spun fibres, as well as the achieved tensile strength. The authors attributed these results to the fact that the solid state processing is strongly influenced by the narrow temperature window in which the drawing can be realised (a temperature window of only 2 °C close to the melting temperature of the material) and by the compaction stage, where no voids should be present in the material.

Further on, methods involving lower amount of solvents and enabling the high processability into more complicated shapes have been considered, for example, the synthesis of UHMWPE having lower entanglement density directly via polymerisation, followed by processing at temperatures lower than its melting point [23].

1.1.3 Disentangled UHMWPE: Heterogeneous Catalytic Systems

As discussed in the previous section, the entanglements can be reduced via solution spinning favouring the drawability of the material to produce high modulus fibres, but the amount of solvent that is required is large and the process is considered not very environmental friendly. In addition, the disentangled product is obtained as fibres and it is not feasible to produce film or other higher dimensional shapes.

The idea of realising disentangled UHMWPE directly via chemical synthesis has been then pursued. In order to achieve this goal, the reaction conditions need to be carefully controlled to allow a fast crystallisation during the polymerisation. On one side, polymerisation at low temperature could slow down the activity of catalytic system, *i.e.* polymerisation rate (R_p), and give the polymerised segments a chance to crystallise more quickly, i.e. $R_c > R_p$, where R_c is crystallisation rate, and subsequently produces UHMWPE with lower entanglement density. On the other side, using a single-site catalyst dissolved in the reaction medium at low concentration could space apart the active sites and hence reduce the possibility of the polymer chains to meet each other (and entangle) before crystallisation, also resulting in a less entangled polymer [40].

Chanzy and Smith [24,25] worked on the first concept using a heterogeneous Ziegler-Natta catalyst based on vanadium trichloride and aluminium triethyl, to synthesise UHMWPE at temperatures as low as -40 ^{o}C. At low temperatures, crystallisation happens faster than the polymerisation, thus resulting in a highly crystalline polymer with reduced entanglement

density [24,25,26]. The influence of polymerisation temperature on the entanglement is schematically shown in Figure 1-3.

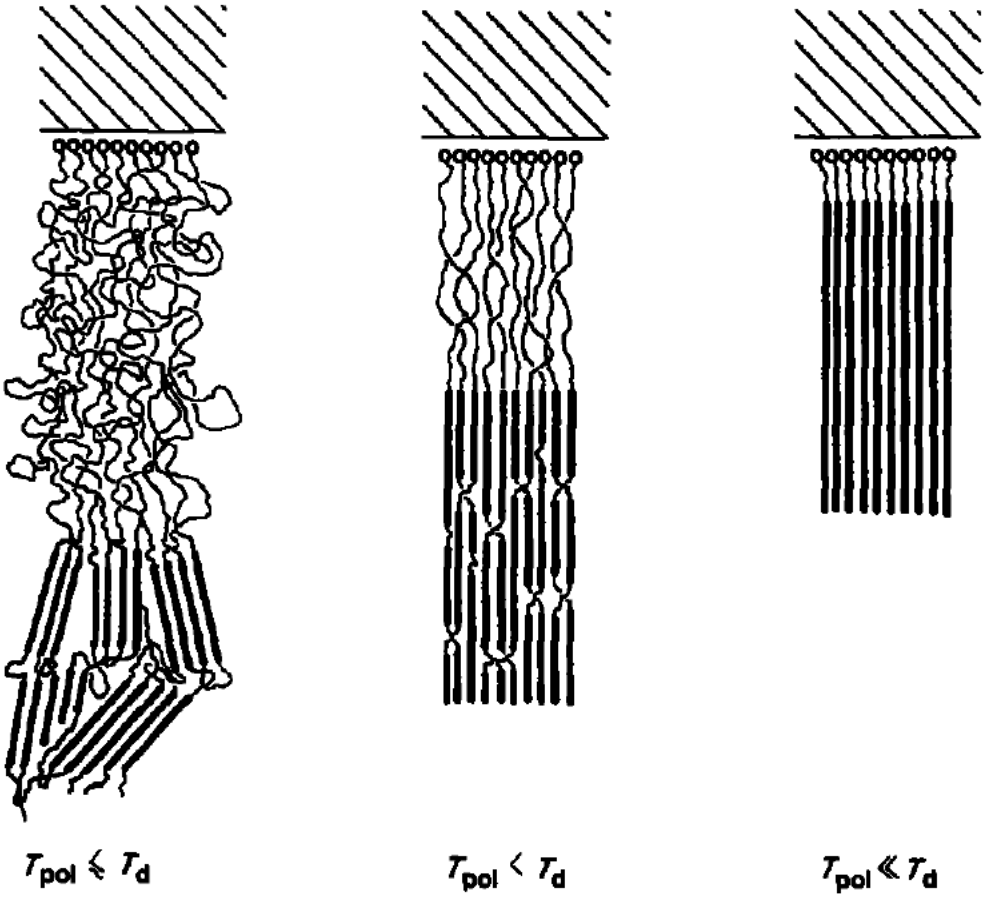

Figure 1-3 Schematic representation of influence of the reaction temperature on the morphology of the polymerised chains; T_{pol} represents the polymerisation temperature and T_d represents the temperature where a polymer molecule can be dissolved in the surrounding solution medium and crystallise with lower entanglement density [26].

As a result, the 'disentangled' PE samples synthesised feature a low entanglement density and this makes it possible to be stretched and drawn in the solid state to provide fibres with mechanical properties similar to that of solution spun fibres, but with a solvent-free processing. For instance, the authors reported modulus as high as ~100 GPa for the directly stretched UHMWPE powder [27,28]. However, as described by the authors [27,28], the mechanical properties and morphology of the nascent powder were highly dependent on the polymerisation conditions, and this brings variations to the polymer properties even if there is a small change in the polymerisation conditions. Important to notice is that, due to the very low catalytic activity of the system used at the low temperatures, the amount of polymer produced is very low and the industrial significance is thus very limited: this method was hence regarded as useful mainly for fundamental studies and not developed further.

1.1.4 Disentangled UHMWPE: Single-Site Homogeneous Catalytic Systems

The conventional Ziegler-Natta catalysts used for producing polyolefins at industrial scale are heterogeneous systems, where the term refers both to the insolubility of the catalysts in the polymerisation medium, and to their multi-sites structure. The resultant materials are complex polymer mixtures with widely varying molecular weights, molecular weight distribution and microstructures. Recently, breakthroughs in the development of homogeneous single-site catalysts have opened new possibilities in the synthesis of polyolefins [29]. Their definition highlights the fact that they can be dissolved in the reaction medium homogeneously and they are usually based on a single type of active site [29].

The exploration in homogeneous catalyst is dated back to 1957, within a few years of Ziegler's discovery of low pressure metal-catalysed alpha-olefin polymerisation, when two groups [30,31,32] reported the use of the first homogeneous catalyst for polymerisation of olefin. This catalyst was based on a complex of a group 4 transition metal, namely Cp_2TiCl_2 (dicyclopentadienyltitanium dichloride – shown in Figure 1-4) and it was activated by Et_2AlCl (diethylaluminium chloride). This catalytic system was able to polymerise olefins in conditions similar to that used for conventional Ziegler-Natta catalyst, but with the advantage that the catalytic site was well-defined ('single-site') and soluble in the reaction medium. The main drawback was the very low activity of this system. However, the breakthrough introduced by a novel type of co-catalyst, methylaluminoxane (MAO), in the 1980s caused the so called 'metallocene revolution' [33,34] that rejuvenated the interest in metallocene catalysts.

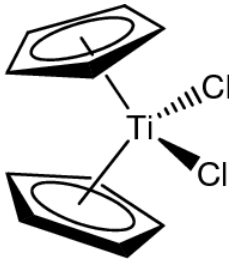

Figure 1-4 The first homogeneous catalyst for polymerisation, Cp_2TiCl_2, a metallocene catalyst [32]. This class of catalysts has the advantage of a better control of molar mass, molar mass distribution and stereo/regio-regularity of the polymer produced.

Remarkably, in 1997, a new generation of single-site catalysts composed of salicylaldimine (phenoxy-imine) compounds in combination with early and late transition metals, having unprecedented activity in olefin polymerisation, were independently discovered by three

groups, led by Fujita [35], Johnson [36] and Grubbs [37]. In particular, one of the system developed by Fujita showed high catalytic activity even at low temperature (~10 °C), and the ability to polymerise ethylene to UHMWPE with M_w higher than 2 million g/mol and a molecular weight distribution lower than 3 (compared to at least 10 of the heterogeneous systems). Using this catalytic system, Rastogi and co-workers demonstrated that it was feasible to obtain UHMWPE having significant low initial entanglement density (disentangled UHMWPE) directly from the synthesis by carefully controlling the reaction conditions [38,39,40], such as polymerisation temperature and catalyst concentration. In their studies, the bis[N-(3-tert-butylsalicylidene)pentafluoroanilinato]titanium (IV) dichloride catalyst, schematically represented in Figure 1-5, was used. In this thesis, for simplicity we will refer to this catalyst as FI catalyst. The authors addressed the influence of reaction conditions on the polymer properties, such as the polymerisation time, temperature, type of solvent, and cocatalyst-catalyst ratio, and they found that by carefully controlling all these parameters, samples of disentangled UHMWPE with desired molecular masses and molecular weight distributions could be obtained. The melting and crystallisation behaviours, mechanical properties as well as rheological properties of this disentangled UHMWPE have also been extensively studied by the same group [38,39,40].

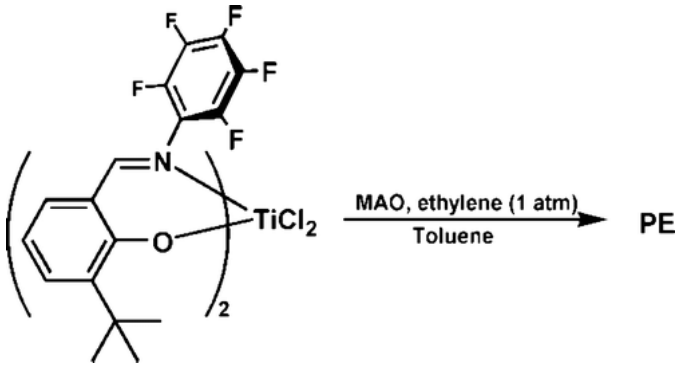

Figure 1-5 Schematic structure of single-site homogeneous FI catalyst that Rastogi and coworkers have used for direct synthesis of disentangled UHMWPE [39]. The catalyst activated by MAO shows a very high activity even at low temperature (~10 ^{o}C), and using this catalytic system, it is feasible to produce UHMWPE having low entanglement density and desired molar mass and molar mass distribution.

The comparison of the polymerisation mechanisms between conventional Ziegler-Natta heterogeneous catalytic systems and FI single-site catalytic system is schematically shown in Figure 1-6. In the heterogeneous system, active sites are spatially close and only exhibit high activity at relatively high temperature (70 °C for instance), and this causes the polymerised chains to entangle before crystallising and gives rise to high entanglement density; whereas in

the homogeneous system, a low concentration of the catalyst is coupled with low polymerisation temperature (10 °C for instance), to ensure that the growing chains start to crystallise before meeting each other and getting entangled, giving rise to a unique polymer with much lower entanglement density.

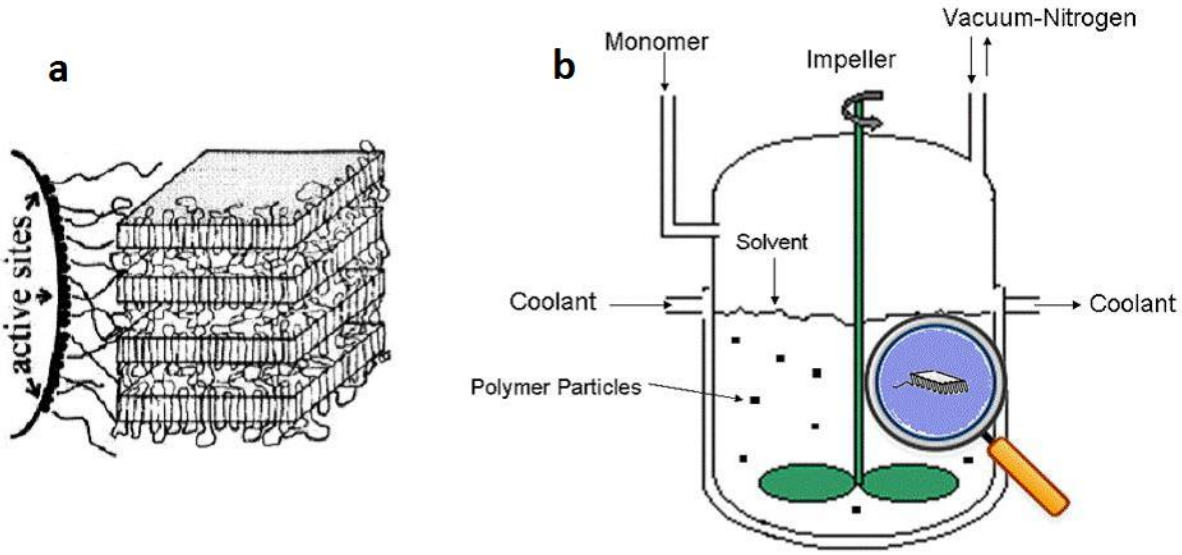

Figure 1-6 The difference between heterogeneous and homogeneous polymerisation systems [41,42]: **a)** heterogeneous polymerisation system in which the catalytic sites are very close to each other, and during the polymerisation, chains have chances to get entangled; **b)** homogeneous polymerisation in which the catalyst is well dispersed resulting in reduction of entanglements.

1.2 Properties of Disentangled UHMWPE

The disentangled UHMWPE, synthesised by single-site homogeneous catalyst in controlled conditions, has shown very unique behaviour compared to conventional UHMWPE, in terms of sintering properties, morphology, rheological properties, and mechanical properties. What follows is a brief overview of the most relevant findings.

1.2.1 Morphology, Molecular Weight and Molecular Weight Distribution

The disentangled UHMWPE that Rastogi's group obtained has shown a distinctive lamellar structure, where the lamellae having a thickness of below 20 nm are the results of the folding of few polymer chains. Figure 1-7 shows a comparison between disentangled UHMWPE obtained from the homogeneous catalyst and conventional (entangled) UHMWPE synthesised by heterogeneous Ziegler-Natta catalyst [39]. Different to the disentangled

UHMWPE, entangled UHMWPE powder shows strong intermolecular coherence-possibility when compressed below melting temperature. This is related to the high entanglement density.

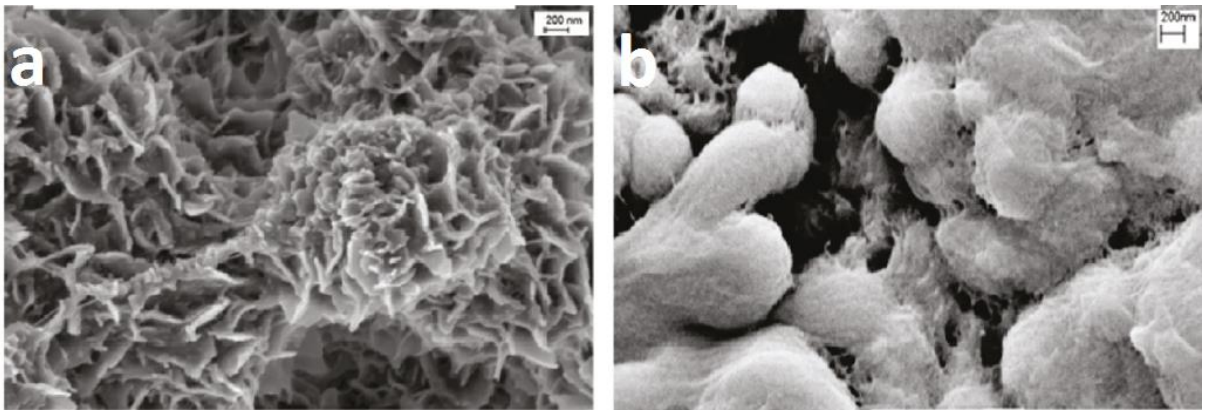

Figure 1-7 a) Morphology of disentangled UHMWPE synthesised via controlled synthesis, and **b)** morphology of entangled UHMWPE synthesised from Ziegler-Natta catalyst [39].

Molar mass (M_w) and molecular weight distribution (MWD or PDI) are main fundamental parameters that determine basic properties of polymeric materials. Methods to determine M_w and MWD of polymers include GPC and melt rheology; however standard GPC is not feasible to identify M_w and MWD of polyethylene once M_w exceeds 1 million g/mol [38], as the solubility of the material becomes very poor. Mead developed a method for M_w and MWD estimation using dynamic melt rheology [43,44] for polymers having molar mass up to a few million g/mol. This method has been commercialised by Rheometric Scientific by incorporation in their Orchestrator software. Tuminello [44], and Rastogi and coworkers [38] have demonstrated the applicability of this technique to estimate M_w and MWD of a range of polymers with molar mass up to 10 million g/mol, and reasonable results were achieved.

It has been reported that M_w and MWD of the disentangled UHMWPE can be well controlled by altering those polymerisation conditions that affect the activity of catalytic system, for instance polymerisation temperature, time and pressure [38,40,56], and their influences on M_w and MWD are shown in Figure 1-8. It shows that with increasing polymerisation time and pressure, M_n, M_w and MWD (PDI) all increase, and M_w increases much faster compared to M_n, as shown in Figure 1-8a and c. With increment of polymerisation temperature up to 20 °C, both M_n and M_w increase but M_n increases faster hence the MWD (PDI) decreases; however when the polymerisation temperature exceeds 20 °C [38], both M_n and M_w increase

but M_w increases faster and this makes MWD (PDI) increases [40], as shown in Figure 1-8b and Table 1-1.

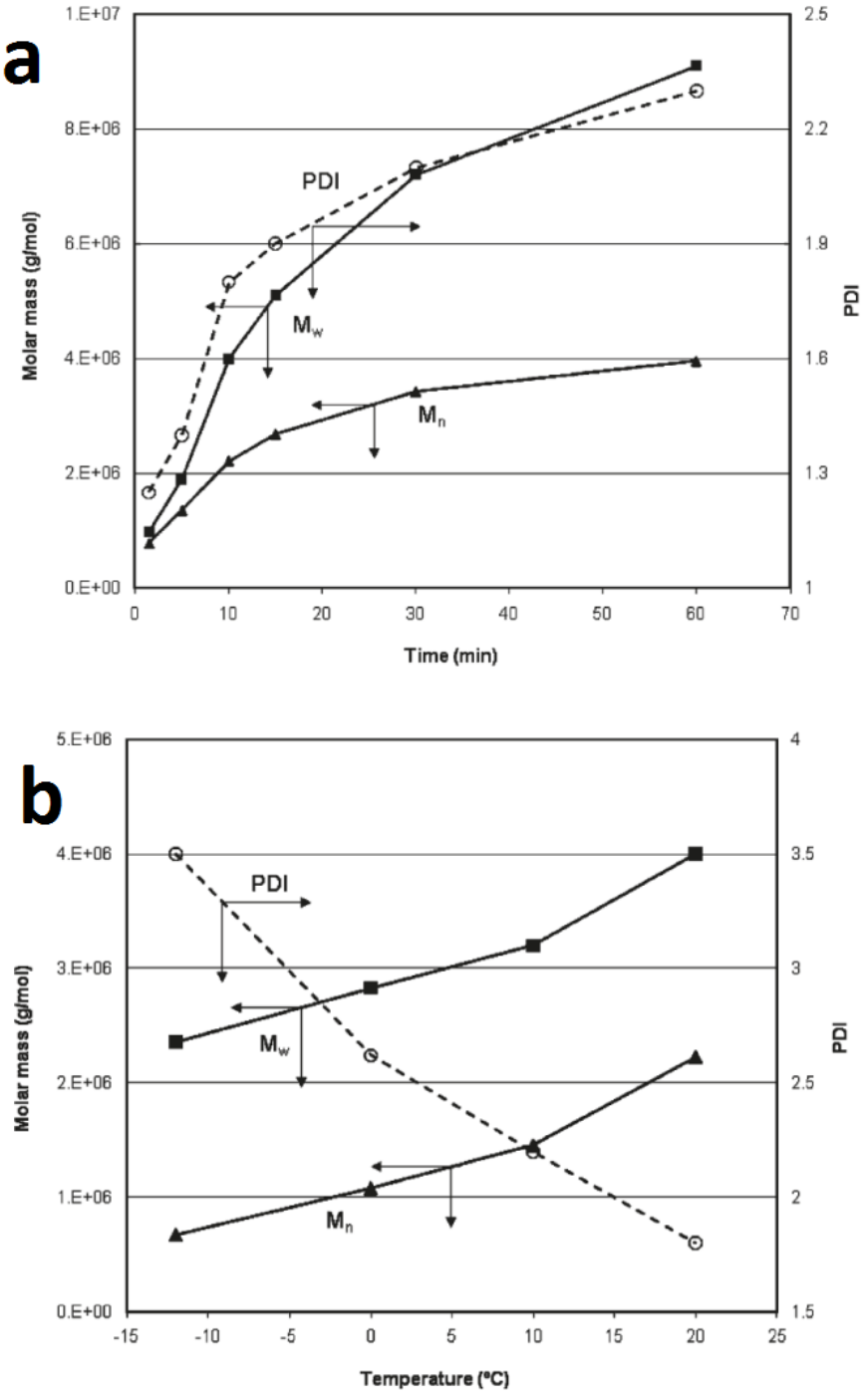

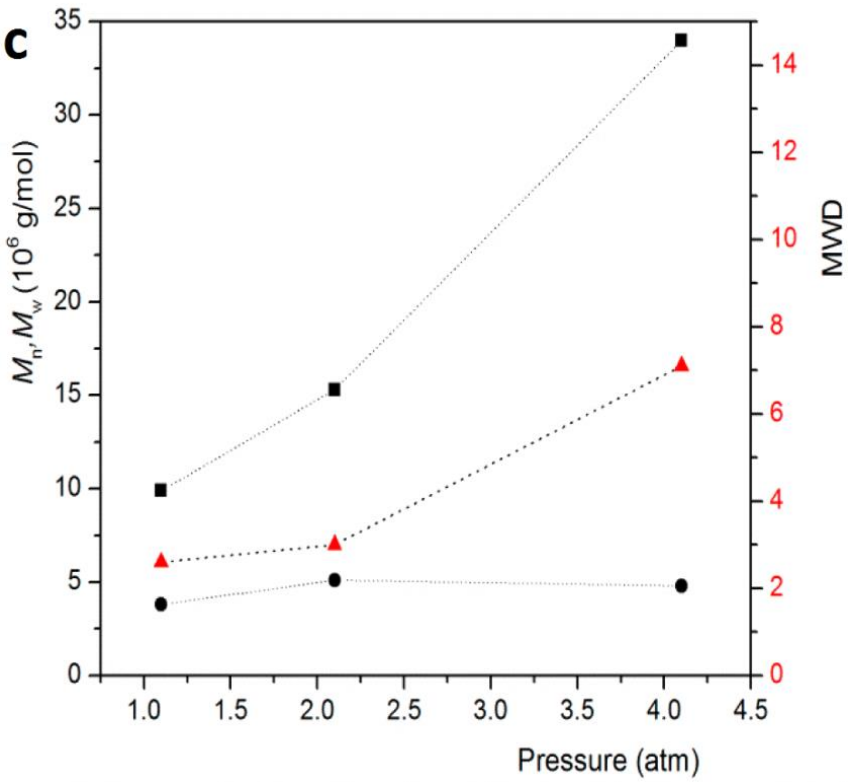

Figure 1-8 Influence of **a)** polymerisation time at fixed temperature and pressure, **b)** polymerisation temperature at fixed time and pressure, and **c)** polymerisation pressure at fixed times and temperatures on the M_w and MWD (marked as PDI in the figure) of disentangled UHMWPE synthesised by FI catalyst [38,40].

Table 1-1 M_w and MWD of samples synthesised at different temperature for a fixed polymerisation time of 30 min [40].

samples	M_w (million g/mol)	MWD	total entanglement time, t_m (s)
dPE_10C_30′	5.1	2.5	423 430
dPE_20C_30′	6.3	2.4	266 310
dPE_30C_30′	4.7	2.9	88 450
dPE_40C_30′	5.2	3.1	72 270

Polymerisation using the FI catalyst can provide UHMWPE with well controlled M_w and MWD. This provides potentials to tailor the properties of the polymers for different purposes.

1.2.2 Entanglement Formation upon Melting

Disentangled and entangled UHMWPE have shown different rheological responses, due to the differences in their initial entanglement density, as shown in Figure 1-9 [45]. Conventional UHMWPE synthesised using heterogeneous Ziegler-Natta catalyst, i.e. entangled UHMWPE, shows little build-up of storage modulus (*G'*) during dynamic time sweep and reaches equilibrium state (plateau region) in a very short time scale. The high starting value and little build-up have been attributed to the highly entangled state of the material after polymerisation.

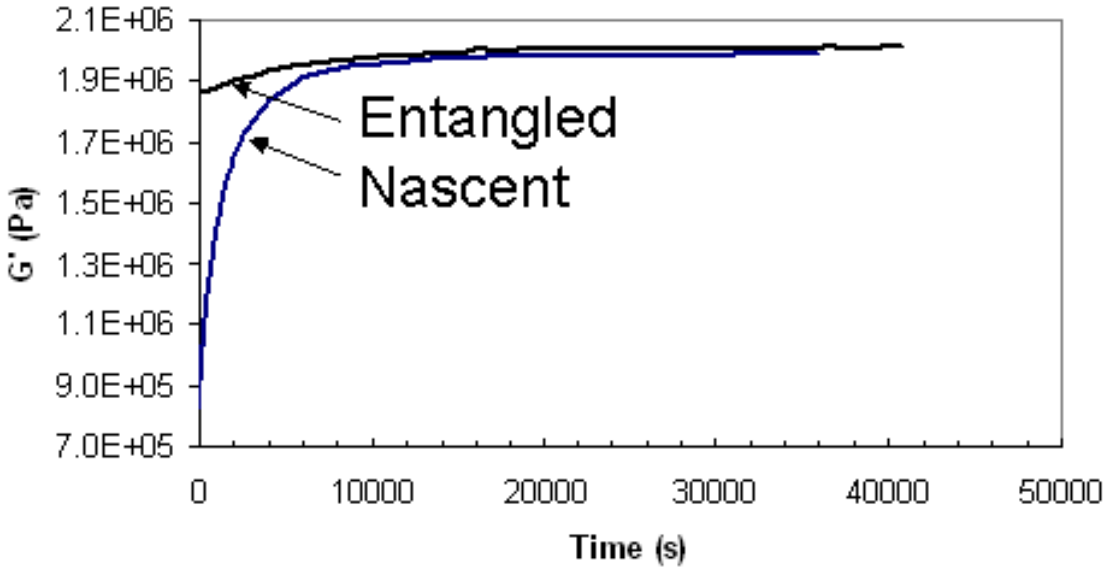

Figure 1-9 Storage modulus build-up as function of time (at 160 °C) of commercial/entangled UHMWPE (marked as entangled in the figure) and disentangled UHMWPE (marked as nascent in the figure) [45].

Disentangled UHMWPE polymerised using the FI catalyst has shown a very different rheological response. Pandey *et al.*[40], in their research, have observed a low starting value of storage modulus followed by significant increment with increasing annealing time, which ultimately reaches a plateau when reaching the thermodynamic equilibrium state, as shown in Figure 1-9 and Figure 1-10. The build-up of modulus is associated with the dynamic rearrangement of the chains in the melt from non-equilibrium to an equilibrium state with progressive formation of entanglements.

The *G'* build-up curve can be divided into two regions: Region 1 (R_1 in Figure 1.10), where a fast build-up is shown, attributed to fast chain explosion and mixing from single crystals; and

Region 2 (R_2 in Figure 1.10), where the slower build-up is attributed to further entanglement by chain reptation; eventually the polymer melt reaches its thermodynamic equilibrium state which is shown as a plateau in the plots. In the thermodynamic equilibrium state with homogeneous distribution of chain entanglements, the molar mass between adjacent entanglements (M_e) can be related to the storage modulus value at plateau, as mathematically described by equation 1-2 [46].

$$G_N^o = \frac{g_N \rho RT}{<M_e>} \qquad \text{(Equation 1-2)}$$

where G_N^o is the plateau modulus at thermodynamic equilibrium state; $<M_e>$ is the average molecular weight between adjacent entanglements and it is inversely proportional to the entanglement density; g_N is a numerical factor (could be 4/5 or 1 depending on convention); ρ is the density of the material at temperature T; R is gas constant and T is the absolute temperature.

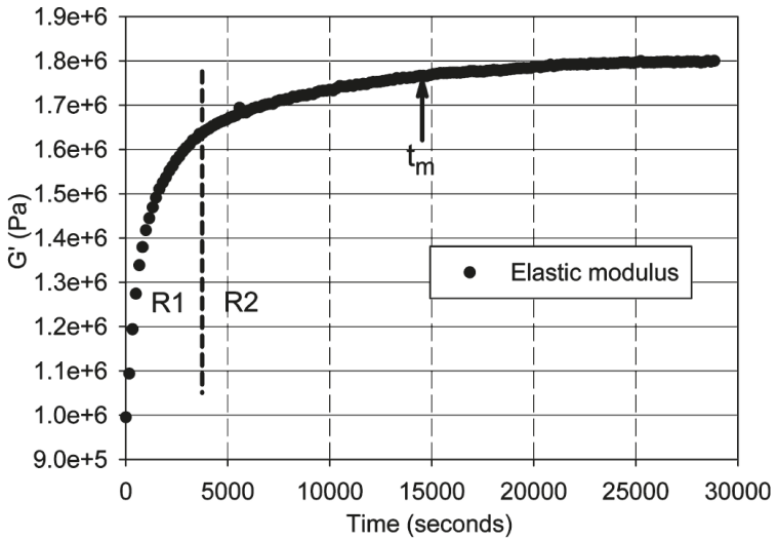

Figure 1-10 Storage modulus (*G'*) build-up of UHMWPE synthesised using FI catalyst [40].

The authors [40] reported that rheological analyses could be a reliable tool to identify the disentangled character of the UHMWPE. They have related the low starting point in the value of *G'* to the low density of entanglements present in the nascent disentangled polymer, corresponding to a larger value of $<M_e>$. The authors have also shown that the polymerisation time has an influence on the molecular weight of the resulting polymer and the initial

entanglement density, that in turn will influence the time required for reaching the fully entangled state (Figure 1-10) [40].

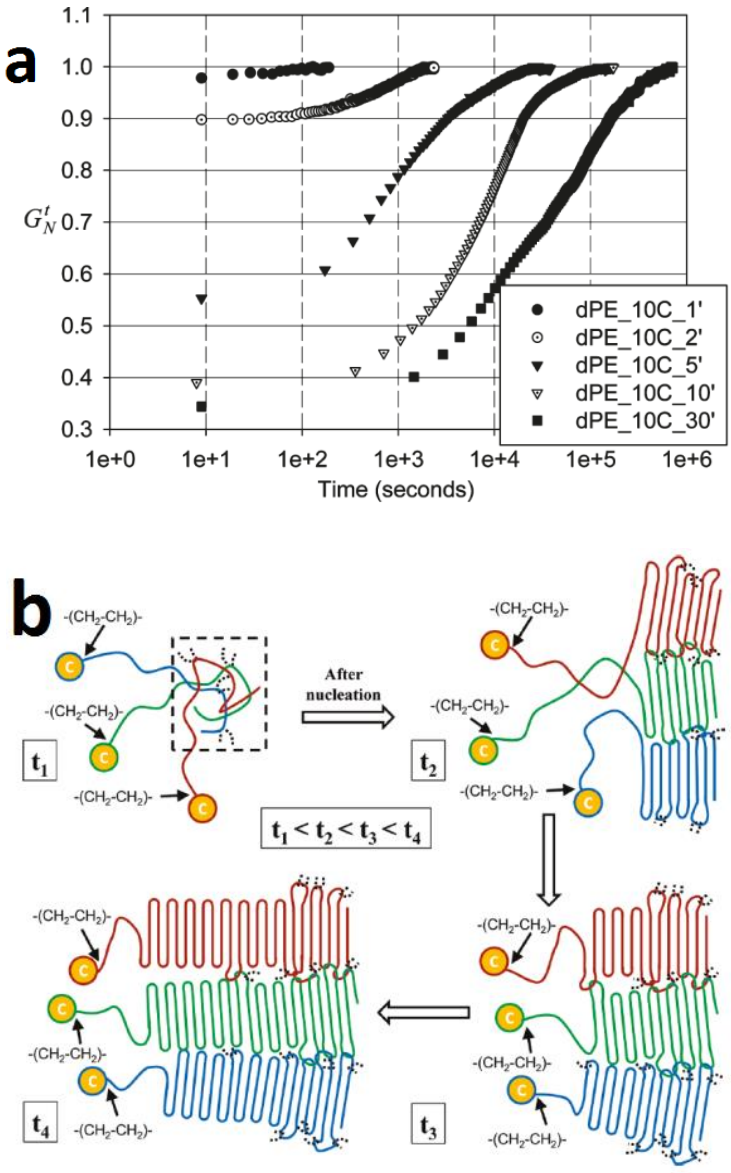

Figure 1-11 a) Normalised *G'* build-up at 160 °C of disentangled UHMWPE synthesised using FI catalyst at different reaction times (the build-up is normalised by the plateau value G_N^0 and shown as G_N^t in the figure) and **b)** schematic drawing of the relationship between entanglement density and polymerisation time [40]. At the beginning of the polymerisation, the entanglement density is relatively high due to the entanglement formation prior to crystallisation, but with increasing polymerisation time, the nucleation barrier is supressed and crystallisation starts to dominate, causing less entanglement formation, and hence UHMWPE having long chain length shows a lower starting value and slower modulus build-up.

Consistent decrease in the normalized modulus at the starting point with increasing molar mass, as shown in Figure 1-11a, demonstrates that the entanglement density decreases with increasing molar mass. The authors suggest that the number of entanglements that are formed in the early stage of polymerisation is higher, due to the entanglement prior to the crystallisation, and then it tends to decrease with increasing molar mass because of the suppression of the nucleation barrier that accelerates the crystallisation [40], as described in Figure 1-11b.

Another interesting feature of the disentangled UHMWPE that Rastogi and coworkers pointed out is that the disentangled UHMWPE could form a new meta-stable state by maintaining the disentangled state upon melt for a relatively long time scale, for instance a few hours [5,47]. The authors found that, through slow and well controlled melting, the disentangled crystals could form a heterogeneous melt with entangled region (due to chain mixing) at the near ends region of the chains and disentangled region at far end region of the chains as shown in Figure 1-12, while the fast melting gives homogeneous entanglement distribution across the melt. When the polymer is less entangled, it shows lower viscosity and this finding provides promising potential to process the otherwise intractable polymer.

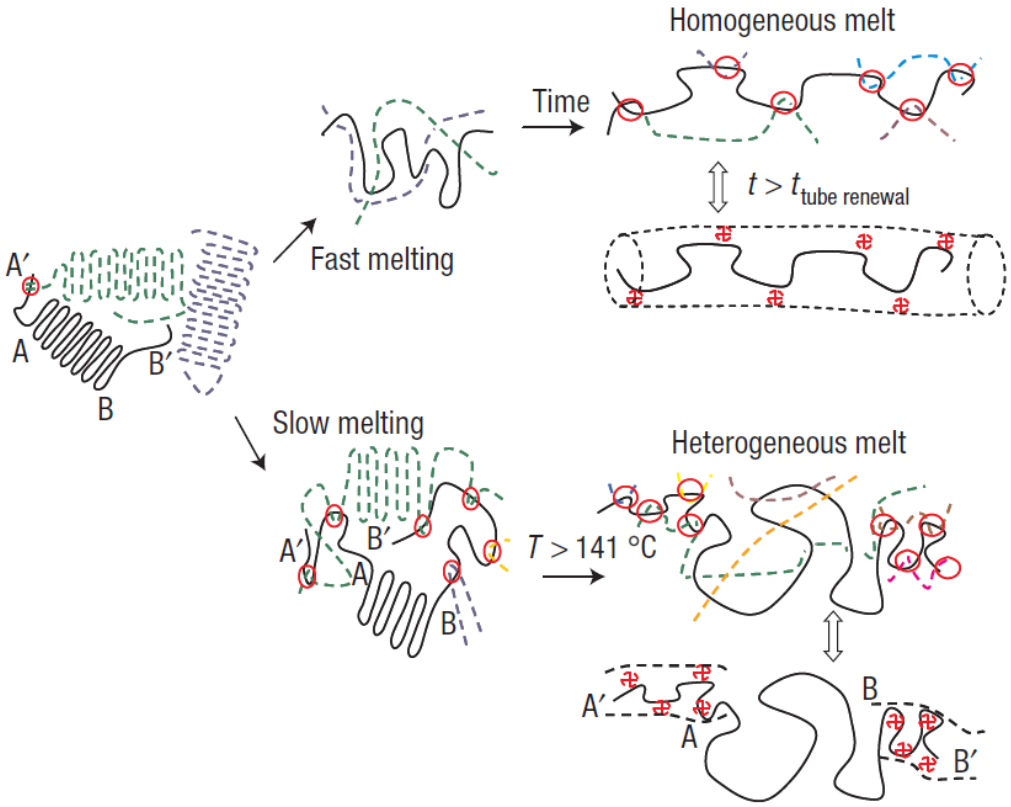

Figure 1-12 Melting kinetics of disentangled UHMWPE with fast and slow melting procedures (tube renewal is the time that a single chain needs to relax) [5]. Fast melting gives rise to homogeneous distribution of entanglements, whereas as a result of well-controlled slow melting, meta-stable melt with heterogeneous distribution of entanglements is obtained.

1.2.3 Melting Kinetics of Disentangled UHMWPE

Unlike small molecules that have sharp first order transitions at melt, a broad melting peak is normally observed during melting of semi-crystalline polymers, covering a wide range of crystal size and thickness. The melting temperature can be related to the crystal size and estimated by the Gibbs-Thomson equation, as shown in equation 1- 3 [48]:

$$\boldsymbol{T_m = T_m^{\infty}[1 - \frac{2\sigma}{l\rho\Delta H_m}]} \qquad \text{(Equation 1-3)}$$

Where T_m is the melting point determined experimentally; T_m^{∞} is the melting point at equilibrium state for crystals having infinite size (141.5 °C for polyethylene [49,50]); σ is the end surface free energy for the folded planes and l is crystal lamellae thickness, ρ is the crystal density and ΔH_m is the heat of fusion per unit mass. As observed by SEM, as-polymerised, nascent UHMWPE ($M_w > 1\times10^6$ g/mol), show a lamellae thickness up to 20 nm [5,51] and hence a melting point of c.a. 131 °C should be achieved according to the equation [52]; however, a higher melting point close to the equilibrium melting point of 141.5 °C is found by DSC analysis. The equilibrium melting value has been reported mainly on extended PE crystals, where 1 μm-thick lamella is achieved [50]. After crystallisation, the high melting peak disappears and a lower melting peak at around 136 °C is observed. These phenomena cannot be explained by the given equation or considering superheating. To understand the observed incongruence, it should be taken into account that not only the length of the stems in the crystals, but also the molecular conformation of chain segments residing in the amorphous region have implications on melting behaviour of the semi-crystalline polymer [53]. To elaborate, the transition zone between amorphous region and crystalline region has some topological constraints induced during polymerisation that will influence the first melting of the polymer. It has been suggested that the topological constraint from adjacent re-entrant chain folded crystals is governing the high melting point instead of lamellae thickness alone [54]. Both in the case of nascent entangled and nascent disentangled UHMWPE the first melting is close to the equilibrium value of 141.5 °C, and it

disappears once the sample is simply molten and re-crystallised from the melt, due to the loss of these topological constraints [47,55]. If the annealing experiments are performed on the nascent polymers, it is possible to recognise the difference between entangled and disentangled UHMWPE. In the transition zone between amorphous and crystalline regions, topological constrains caused by non-entangled adjacent or entangled non-adjacent re-entry lead to a different nature of chain folding resulting in different crystallisation behaviour [54]. Due to the near absence of structural coherence in the amorphous region, the quantification of entanglements is usually challenging. Recently with the help of DSC, Rastogi and coworkers have demonstrated the possibility to follow the formation of entanglements [54,56]. In the experimental protocol used (Figure 1-13a), the samples are first annealed for one hour at a temperature comprised between 137 and 138 °C, usually ~3.5 °C lower than the melting temperature of the high temperature peak. The subsequent heating run (cycle e-f) shows dual peaks with one at 140 °C and the other at 133 °C. The high melting peak is attributed to the remainder of nascent adjacent re-entrant crystals, and the low melting peak is due to the melt-crystallized component obtained on cooling during c-d. The measured enthalpy of the low melting peak normalised by the melting enthalpy of both peaks gives an indication on the heterogeneity of entanglement distribution in the amorphous region of the nascent powder.

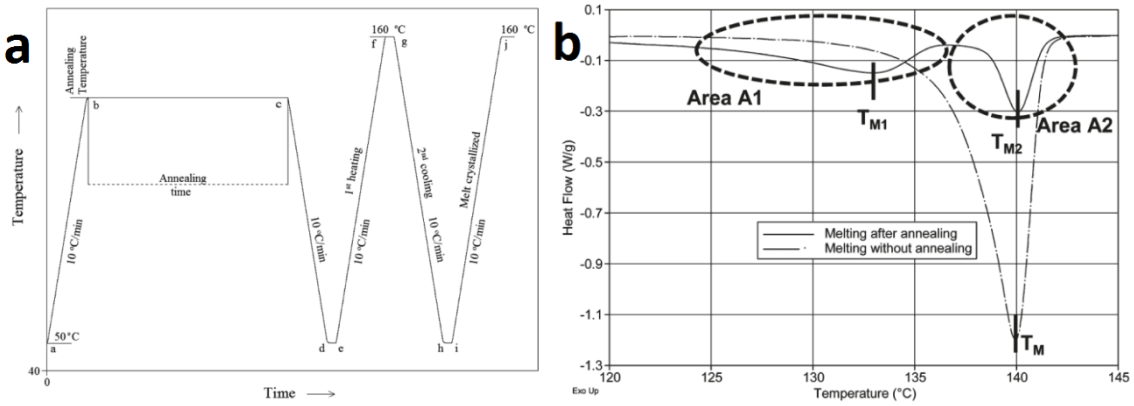

Figure 1-13 a) Protocol used by Rastogi and coworkers for the DSC annealing, where the annealing temperature is 3.5 °C below polyethylene's equilibrium melting point; **b)** the melting plots of the nascent powder with and without annealing [54,56].

Interestingly, the authors [54,56] found that with increasing the annealing time in the step b-c, the low melting peak area increases at the expenses of the high melting peak one, and the area ratio between A_1 (low melting peak area) and A_1+A_2 (total melting peak area) follows a trend similar to the dynamic time sweep of melt rheology, as can be seen by comparing Figure 1-10

and Figure 1-14. The low melting peak comes from the melt crystallised chains that entangled during isothermal crystallisation, i.e. the topological constraint from adjacent re-entrant crystals are released and the same chain is likely to be engaged in more than one crystal thus entangling with other chains in the amorphous region. The increase in A_1 represents entanglement formation of the disentangled chains during isothermal crystallisation. Similarly to what is observed in melt rheology, samples with low molecular weight show fast build-up of A_1 while the samples having high molar mass show a very slow A_1 build-up. Important to notice is that the melting peak of the nascent entangled or commercial samples almost shows no change in A_1 due to the suppression of the high entanglement density on the melting kinetics of the chains [56].

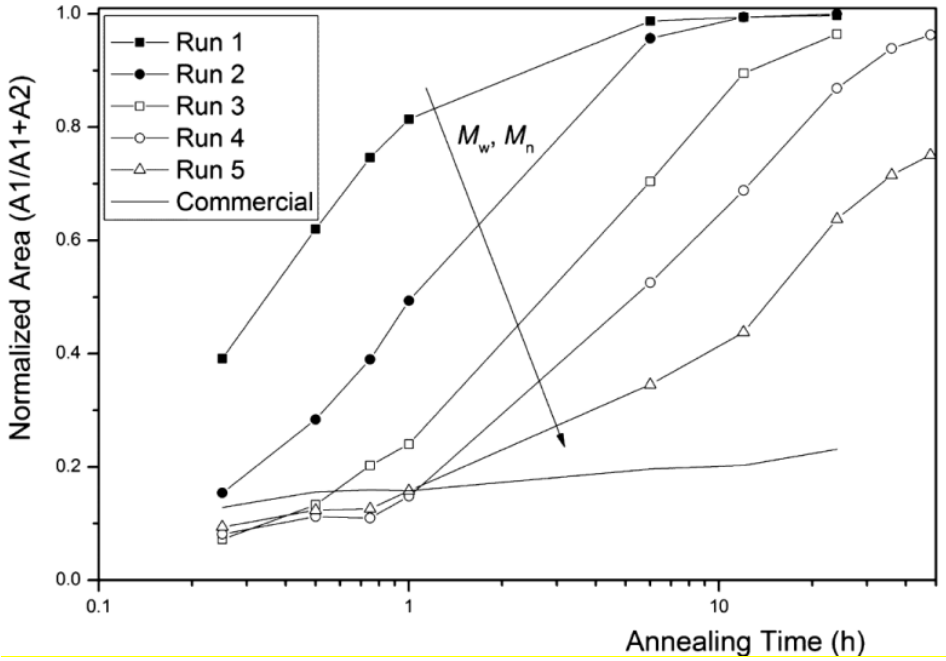

Figure 1-14 Build-up of A_1 with increasing annealing time for disentangled UHMWPE samples having different molar mass and molar mass distribution [56], shown as lines having symbols; as comparison, results of a commercial UHMWPE sample is also displayed, shown as the solid line. (The details for different runs are listed in **Table 1-3**)

In Rastogi and coworkers' studies [54,56], the high melting peak close to equilibrium melting peak may not attributed to be long extended chains but from the tight adjacent re-entrant topology which has high constraints at the near crystalline region and lifts the energy barrier for complete melting.

1.2.4 Processability and Mechanical Properties of Disentangled UHMWPE

Unprecedented ultra-high modulus and strength fibres and tapes have been achieved from the disentangled UHMWPE by solid-state processing. The possibility of solid-state processability is determined by the entanglement state of the polymer. It has been reported that the entanglement in amorphous region hinders the drawability of the polymer in the solid state [56]. Rastogi and coworkers reported that the disentangled UHMWPE can be drawn in solid state within a wide range of temperature (120 °C to 145 °C) in both uniaxial and biaxial directions; while the entangled UHMWPE can only be drawn in the uniaxial direction with a very narrow stretching temperature window of 2 °C around 142 °C.

The mechanical properties measured for the disentangled UHMWPE were much higher than that of the entangled UHMWPE at the same draw ratio as shown in Figure 1-15 [39]. Important to notice is that, compared to commercial UHMWPE, the disentangled UHMWPE samples can be easily stretched to high draw ratio, even to 300 or higher.

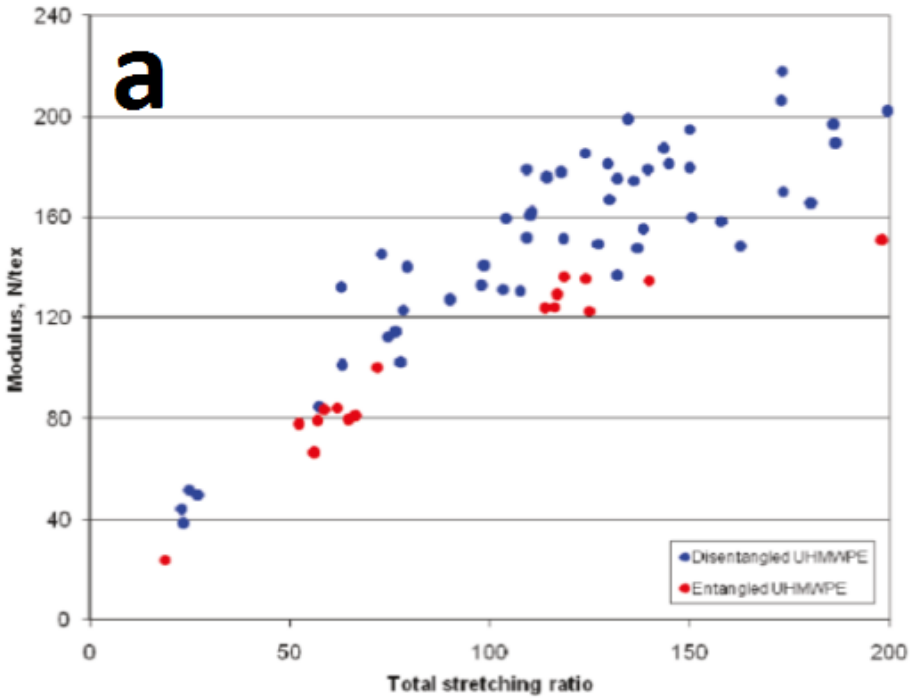

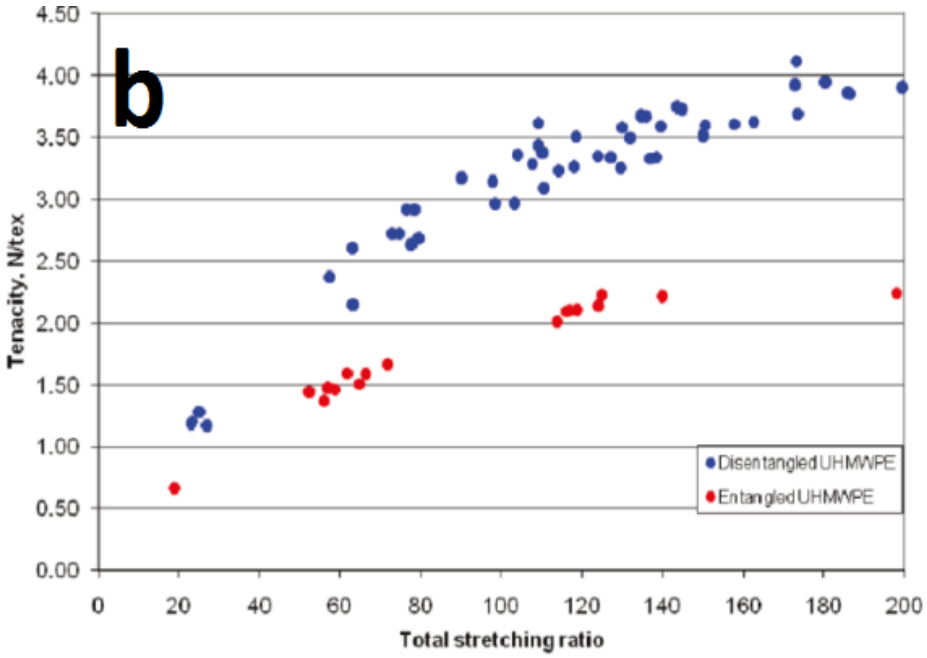

Figure 1-15 The comparison of strength and modulus between commercial/entangled UHMWPE and disentangled UHMWPE from controlled synthesis [39].

The authors [39]compared these samples with solution-spun Dyneema SK 75 twisted yarn which has a high modulus of 135 N/tex (132.3 GPa) and high tensile strength of 3.5 N/tex (3.43 GPa) and two high performance samples (Grade A and Grade B) from commercially available entangled UHMWPE; the results are shown in Table 1-2. It can be found that the disentangled samples obtained by the authors showed enhanced tensile strength over the solution spun fibres as well as modulus.

Table 1-2 Comparison of mechanical properties between the disentangled UHMWPE and commercially available UHMWPE [39].

	Tensile Strength [GPa]	Modulus [GPa]	$<\Phi_{\phi\theta}>$ [°]	C.P.O. peak ratio
Disentangled UHMWPE	3.75	157	1.1	7.1
Entangled UHMWPE Grade A	1.95	102	1.2	1.9
Entangled UHMWPE Grade B	2.30	165	1.1	6.0
Solution spun Fiber	3.50	135	2.2	0.3

The molar mass influence on mechanical properties of disentangled UHMWPE has also been recently investigated and it has been observed that mechanical properties are highly affected by the molar mass. Figure 1-16 shows the mechanical properties of disentangled UHMWPE having different molar mass at different draw ratios, carried out by Romano *et al.* [56]. The parameters of the different runs are listed in Table 1-3 [56].

Table 1-3 Ethylene Polymerisation results for different reaction times/pressures [56].

run	time (min)	pressure (atm)	yield (g)	Rp[b]	M_w[c]	M_n[c]	MWD
1	10	1.1	16.0	9738	2.3	1.0	2.3
2	30	1.1	32.4	6761	5.3	2.0	2.6
3	60	1.1	63.6	4599	9.9	3.8	2.6
4	60	2.1	51.8	3963	15.3	5.1	3.0
5	60	4.1	90.5	3547	34.0	4.8	7.1

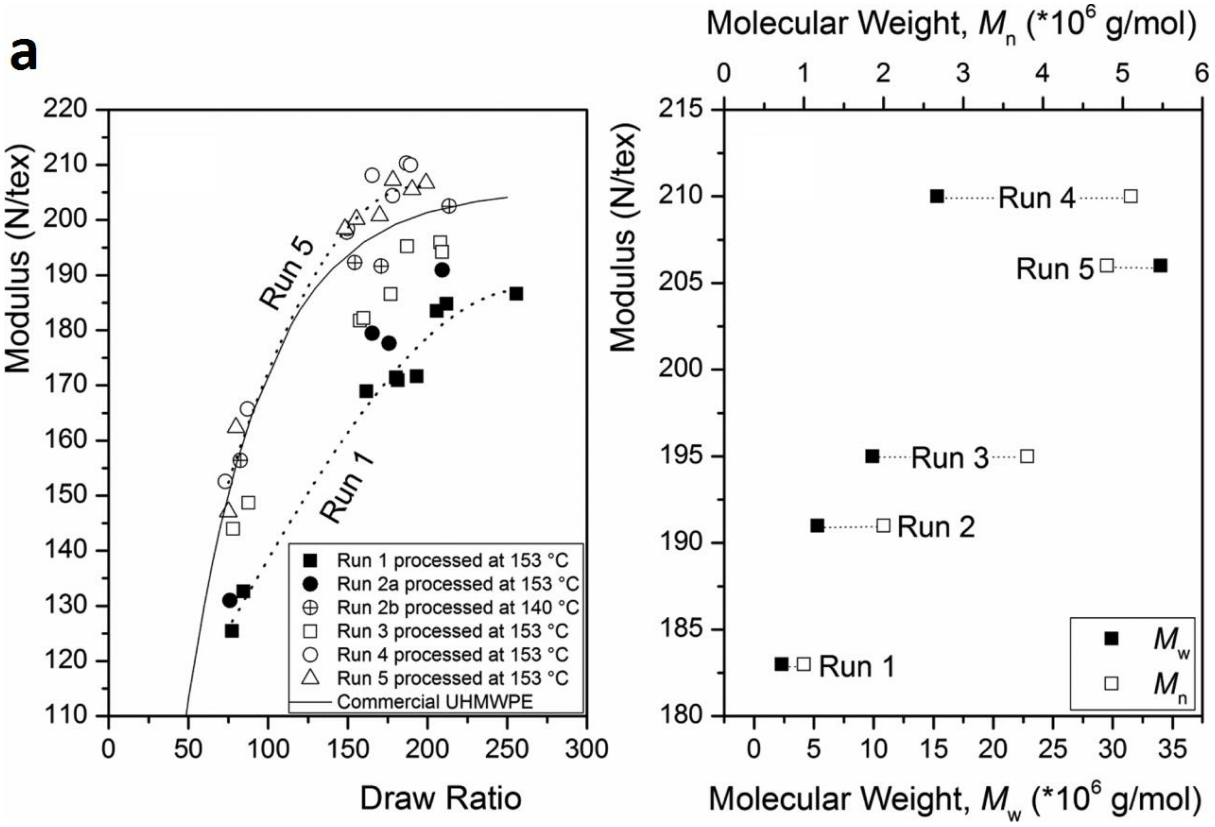

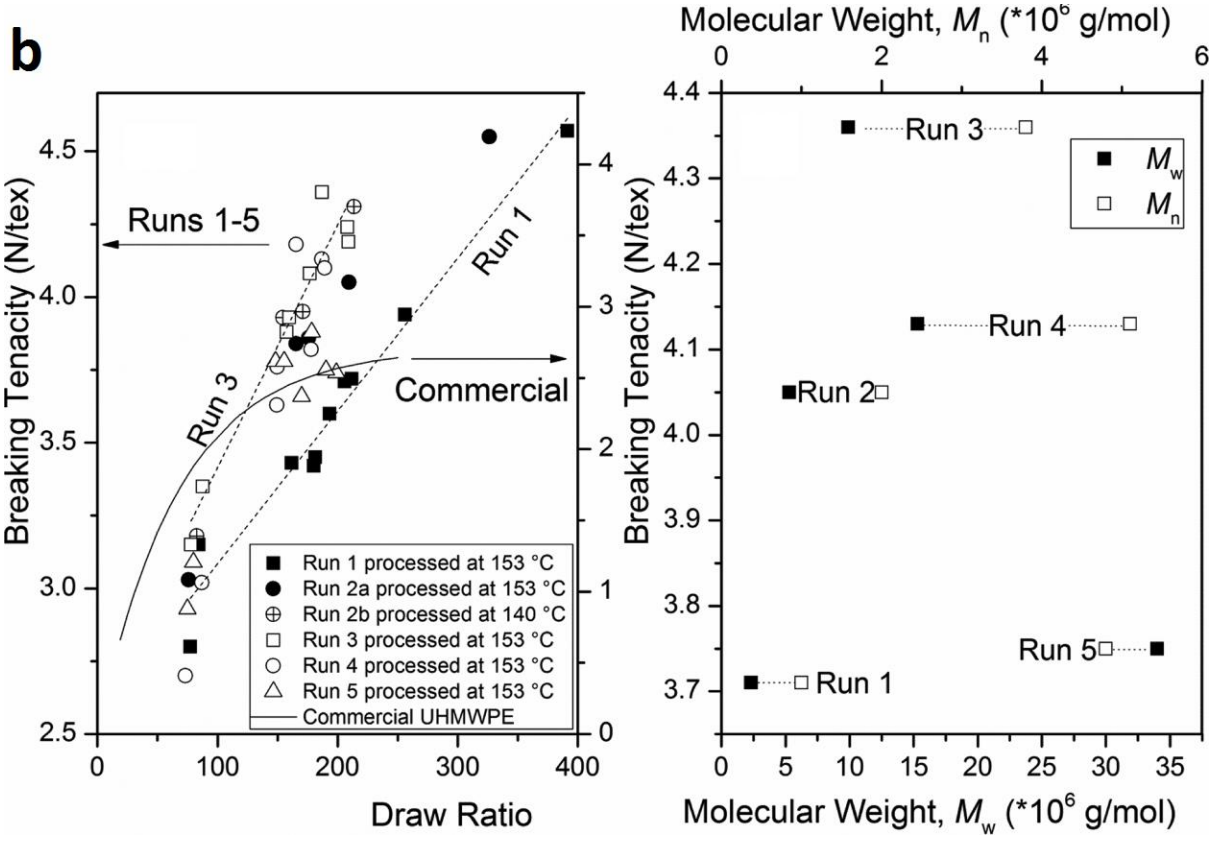

Figure 1-16 Molar mass influence on the mechanical properties of disentangled UHMWPE having different molar mass; **a)** modulus; **b)** tensile strength (breaking tenacity) [56].

Apart from the ease in processability and high values achieved in mechanical properties, this controlled route is both economically and environmentally more advantageous than the solution-spun because the disentangled UHMWPE does not need large amounts of solvent in the processing step.

1.3 Influence of Nanofiller on Polymer Properties

1.3.1 Graphene and Its Derivatives

Carbon based fillers, such as carbon fibres, carbon nanotubes (CNTs) and carbon black, have been largely used in composite materials, from day-to-day applications to high demanding materials. Carbon black for example has been used to enhance tyre properties. Carbon fibres have been found to have valuable mechanical properties, and they have been applied to light weight goods enhancements such as sport rackets, bicycle frames and for high temperature applications, such as aeroplane elements [57]. Recently, nano-sized carbon fillers with novel

mechanical properties, physical properties and biocompatibility have been added to the big family, such as CNTs, graphene and their derivatives [58,59]. The application of carbon based fillers has hence spread to other fields, including medical applications and electronics. More interestingly, the nanosize of these fillers has brought new properties to the composites realised, with a potential for important breakthroughs: for example, graphene with its extreme high specific area of 2630 m^2/g [60], provides the chance for enhanced interaction between polymeric matrix and filler, leading to unique physical properties, such as decrease in complex viscosity [61]. In this thesis focus is on graphene derivatives, and this section will give an overview of the current knowledge on graphene, its derivatives and their composites.

1.3.1.1 Pristine Graphene

Graphene in monolayer form was obtained for the first time using a simple mechanical exfoliation by Geim and Novoselov who were then awarded the 2010 Nobel Prize in physics for their discovery [62]. Since then, graphene has opened a new era for physics and given rise to new applications due to its combination of extraordinary physical properties and the ability of achieving good dispersion in various matrices due to the unparalleled properties graphene possesses [63]. Compared to other carbon based fillers in terms of structure, graphene is much less complicated. The graphene is a monolayer of honeycomb structured sp^2 hybridised carbon atoms. Each carbon atom participates in the formation of pi orbitals: the delocalised electrons present in these orbitals are responsible for the peculiar mechanical and electrical properties of graphene. Monte Carlo simulation and TEM studies have been used to predict and study the morphology of graphene monolayer [64,65]. The TEM studies provide evidence of the existence of corrugations which are around 9 nm in lateral dimension and 0.8 nm in height. Due to two ways of arrangement of the 6-atom ring at the edges, these can have two kinds of shapes: armchair and zigzag [66].

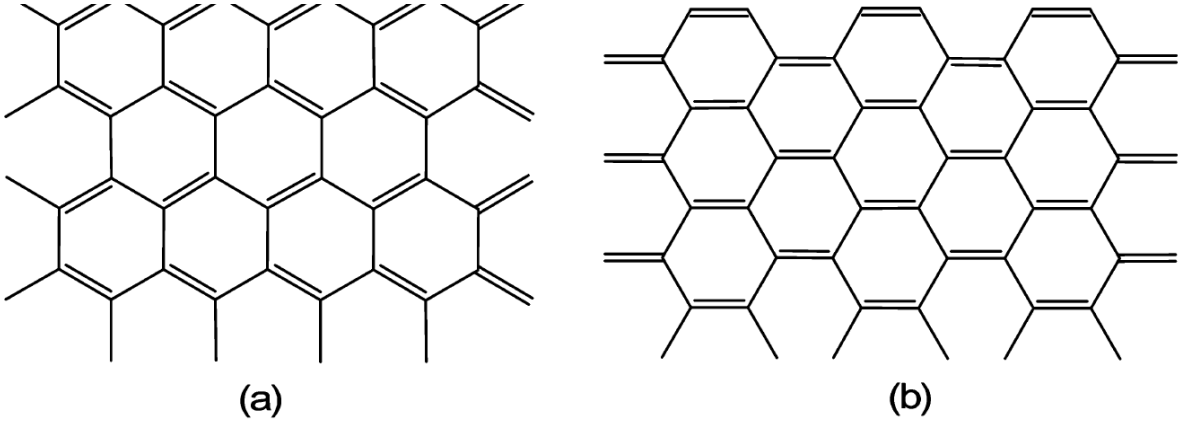

Figure 1-17 Graphene edges with **a)** zig-zag and **b)** armchair structures [66].

Several methods have been developed for the preparation of mono layered graphene and its derivatives. Three main methods will be considered in this literature review, with a particular focus on method b that will be used in this thesis:

a) Micromechanical exfoliation of graphite, giving graphene [62,67];
b) Chemical oxidation of graphite that could produce graphene oxide that can be further reduced to reduced graphene oxide [68,69];
c) Unzipping of carbon nanotubes that produces graphene nanoribbons [70];
d) Calcinations of SiC [71,72] and CVD growth on transition metals [73,74].

Micromechanical exfoliation is the first method that has been used to produce high quality defect-free graphene with large-size single layers, as shown in ref [62]. Fundamental studies of graphene's properties have been done on this novel single layer. The intrinsic strength had not been realistically measured before Lee *et al.* [75] used Novoselov's method [62] to suspend a monolayer of graphene. Lee *et al.* measured the Young's modulus and intrinsic breaking strength of a free standing monolayer of graphene [75]. They did nano-indentation using an atomic force microscope (AFM) to identify the mechanical properties of graphene membranes which were suspended on open holes [75]. Their experiments showed that a monolayer of graphene is the strongest material ever realistically measured with a Young's modulus of 1 TPa and an intrinsic strength of 130 GPa [75]. Extraordinary thermal conductivity and electrical conductivity of graphene have been reported and related to its structure. Balanbin *et al.* first reported the experimental investigation of the thermal conductivity in a suspended single layer of graphene, carried out using confocal micro-Raman spectroscopy [76,77]. Values in a range of 3080 WmK^{-1} to 5150 WmK^{-1} were measured from a single-layer graphene sheet from the dependence of the Raman G peak

frequency on the excitation laser power. Due to its distinctive electronic properties at room temperature graphene can be a very promising candidate for electronic applications. The mobility of pi-electrons in graphene is high also at low temperatures, compared to what happen to semi-conducting materials. Du *et al.* suspended graphene samples by bridging them over a SiO_2 substrate and fixed them by Au/Ti contacts at the two ends. These authors measured a low temperature carrier mobility of 200,000 $cm^2V^{-1}s^{-1}$, even when the charge carrier is at very low density [78]. These values correspond to the upper limit of thermal conductivity of CNTs, as shown in Table 1-4. Compared to other carbon based fillers, graphene is found to be a superior material that has combined novel physical and mechanical properties together. The table below summarises the comparison of thermal conductivities, electrical conductivities and mechanical properties among carbon based fillers.

Table 1-4 Comparisons of properties amongst carbon based fillers.

	Young's Modulus (GPa)	**Tensile Strength (GPa)**	**Thermal Conductivity (WmK^{-1})**	**Carrier Mobility ($cm^2V^{-1}s^{-1}$)**	**Refs**
Carbon Fibres	50~800	<7.0	1100	-	[79,80,81]
CNTs	1000	63	6000	>100,000	[82,83]
Graphene	1000	130	4840-5300	>200,000	[76,84,85,86,87]

Compared to other methods, this is so far the only method where the graphene obtained can be considered as 'nascent' graphene, and the mechanical and physical properties measured are close to the theoretical values. However, this mechanical method is limited in the amount of material that can be produced and it is only suitable for fundamental study, not for industrial interest.

1.3.1.2 Graphene Oxide Nanoplatelets and Reduced Graphene Oxide Nanoplatelets

Dating back to 19th century, methods to synthesise graphite oxide were first carried out in 1859 by a British chemist, B.C. Brodie, who was researching the graphite structure by investigating the reactivity of graphite [88,89]. After a few years Staudenmaier [90] and Hummers [91] independently reported their own methods for the preparation of graphite

oxide. All three methods involve oxidation of graphite in the presence of strong oxidants and concentrated acids. Recently after ultrasonication of graphite oxide in wtare or other polar solvents, monolayers are observed and they are referred to as graphene oxide nanosheets (GON) in this thesis. These researches form the first step of chemical reaction for GON preparation. Almost at the same time, reduction of graphene oxide using reducing agents or thermal degradation to restore thermal and electrical conductivities was carried out, and reduced graphene oxide nanosheets (rGON) were obtained. In general, there are 3 main steps involved to prepare graphene/rGON via the chemical oxidation method: 1) oxidation of graphite (to get graphite oxide); 2) ultrasonication of graphite oxide (to exfoliate the graphite oxide to graphene oxide nanosheets); 3) reduction of graphene oxide nanosheets. The chemical method is currently the most widely used for the preparation of graphene or reduced graphene oxide in large amounts.

Graphite oxide obtained from the first step is actually the graphite that is expanded by strong oxidation reaction. The layers still stack to each other forming a regular layered structure after oxidation. The oxidative agents that are used for graphite oxidations are usually a combination of very strong oxidants and acid, for instance, potassium permanganate, concentrated sulphuric acid or nitric acid. During the reaction, some small molecules, such as H_2SO_4, could penetrate into graphite layers and react with carbon atoms causing the expansion of layers [92,93]. At the same time, functional groups of hydroxyl, carboxyl and ketone groups are grafted on part of the carbon atoms in the planes or at the edges.

Graphene oxide obtained from the second step is a monolayer or few layer stacks that is obtained from graphite oxide via ultrasonication in suitable solvents. Because of the oxidation of graphite, part of the sp^2 hybridised C in the planes are changed to sp^3 hybridised, decreasing the number of pi electrons and modifying the pathway of free electrons, thus resulting in a decrement of both electrical and thermal conductivities. However, the following advantages still make GON very popular in the area of nano-composites.

1). GON is a monolayer which provides very high aspect ratio contributing to enhance the interaction between the filler and matrix;

2). Functional groups on the surface or edge of the layers, enhance the filler and functional groups of matrix interactions by chemical reactions or strong physical attractions;

3). GON is soluble in many polar solvents, which makes dispersion of GON in polymers possible via physical mixing or in situ polymerisation;

4). The preparation can be scaled up relatively easily.

Graphene oxide obtained from the second step and reduced graphene oxide obtained from the third step can be regarded as two kinds of graphene derivatives that possess very similar structure compared to graphene in the form of monolayer but with the added value that graphene oxide present functional groups which could be used to enhance the interfacial adhesion between fillers and matrix, thus resulting in higher mechanical properties. As expected, the thermal and electrical conductivities as well as the mechanical properties of these materials change according to the oxidation level of graphene oxide.

1.3.1.3 Structure of GON and rGON

Extensive research has been carried out to reveal the chemical nature of GON and rGON and a few models have been proposed, but the precise structural features are still a matter of debate. There are three main reasons that make difficult to find out the exact structure: 1) the exact position on the plane of the reactive carbons cannot be identified; 2) the level of oxidation varies depending on the species of oxidants, reaction conditions (reaction time and temperature) and the graphite precursor used; 3) for rGON, the level of reduction depend on both the oxidation level of the GON precursor and the reaction conditions in which the reduction takes place.

Earlier models on graphite oxide are presented in Figure 1-18. Holst and Hofmann [94] proposed a structure where epoxy groups spread across the entire basal planes without any hydrogen involved. In his model, the stereo-structure of the basal planes and the hydrogen was not considered. Ruess's model developed in 1946 incorporated hydroxyl groups on the surface of basal planes; he also took sp^3 tetrahedrally coordinated carbons into consideration, altering the sp^2 planar model from Holst and Hofmann. However, the C=O double bond that could influence the sp^3 structure was not taken into account [99].

In 1969, Scholz and Boehm [95] proposed a model in which the epoxide and ether groups are replaced by quinoidal species in a corrugated backbone. Another model proposed by Nakajima and Matsuo [96,97] was based on the assumption that the structure is lattice based and similar to $(C_2F)_n$ structure, and it formed a 2-stage intercalated graphite compound, as

shown in Figure 1-18. Apart from these models, studies based on development of the functional groups during the oxidation have also been carried out [98]. All these models made valuable contributions to the understanding of the nature of graphite oxide and GON.

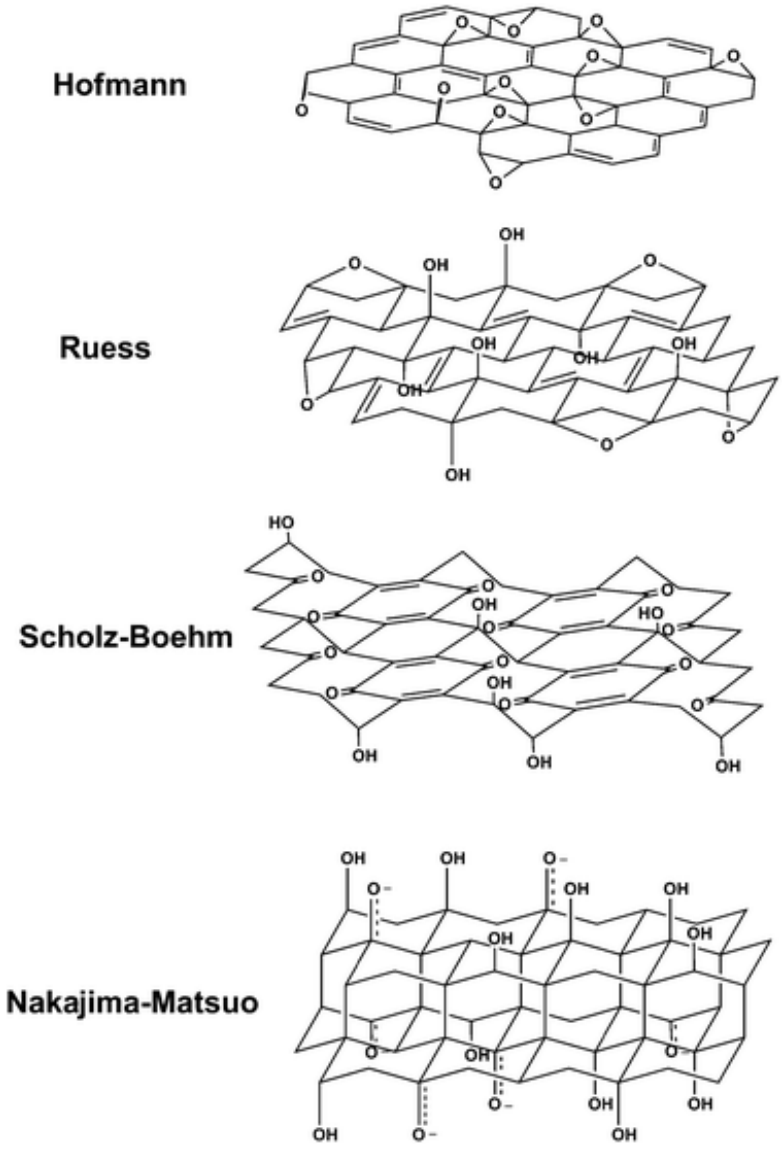

Figure 1-18 The models of graphite oxide/graphene oxide layer structure from previous work [99].

In the most recent GON models, the regular latticed model has been substituted by an amorphous and random alternative, the Lerf-Klinowski model proposed between 1996 and 1998 and supported by solid-state ^{13}C NMR magic-angle-spinning (MAS) spectroscopy of graphite oxide and ^{13}C-marked graphite oxide [100,101,102], and shown in Figure 1-20 (top) without –COOH groups and Figure 1-20 with –COOH groups. With the help of NMR, they suggested GON terminates with epoxide groups, while hydroxyl and carbonyl groups are randomly distributed on the GON planes. In their model, they considered the presence of un-

oxidised graphite portions of variable size as “islands” in a structure of aliphatic 6 atom ring on which hydroxyl and epoxide groups are grafted.

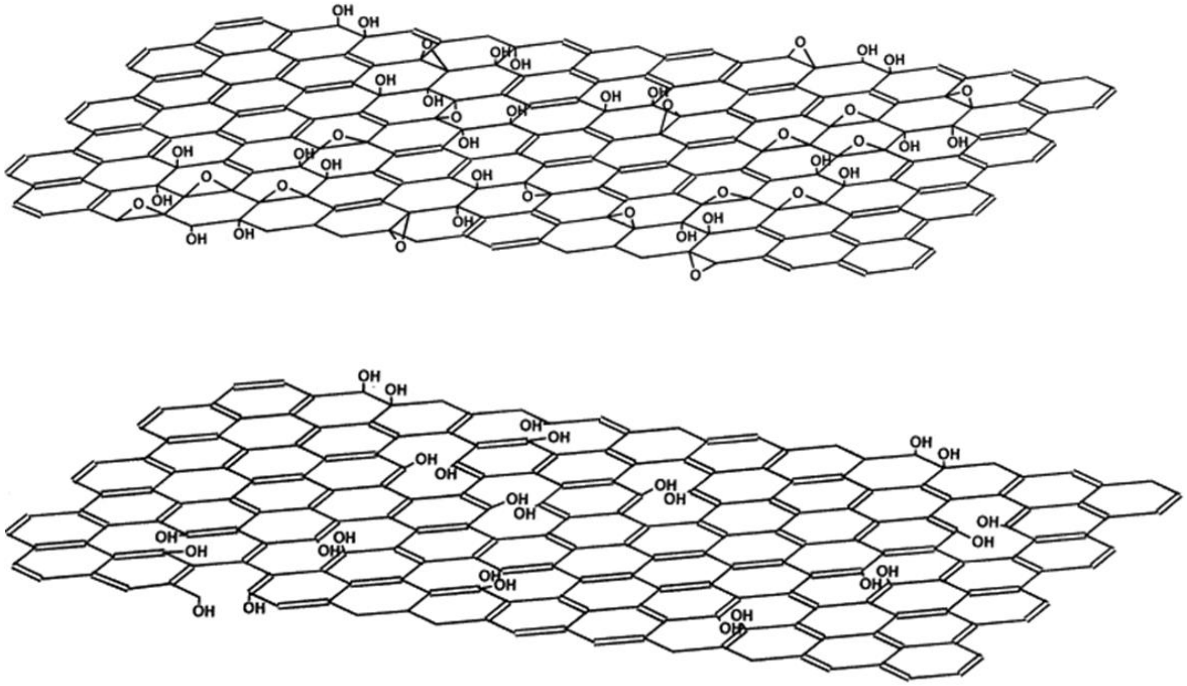

Figure 1-19 The most widely accepted GON structural model proposed by Lerf and his coworkers (Lerf-Klinowski model), top image; the structural model of thermally reduced GO, bottom image [102].

The authors proposed a model for the thermal reduced graphite oxide treated at 100 °C in vacuum for 24 hours, where a partial recovery of sp^2 hybridised carbon was believed to be achieved by removal of epoxide groups, as shown in Figure 1-19 (bottom) [102]. It is believed that during the thermal reduction, some of the functional groups are supposed to leave the surface of the filler, for instance, epoxide groups, whereas some other functional groups will still stay, for an example, hydroxyl groups.

Lerf and his group proposed a refined structure of graphite oxide by conducting reactions with a range of reagents and performing ^{13}C and ^{1}H NMR experiments: they determined that the existence of isolated double bonds is unlikely to be stable under strong oxidation states and most of them exist in aromatic rings or conjugated areas. They supposed that the opening of the rings containing epoxide groups at the edges of planes would bring carboxylic acid groups [101,102]. The Lerf-Klinowski model is currently the most widely accepted model.

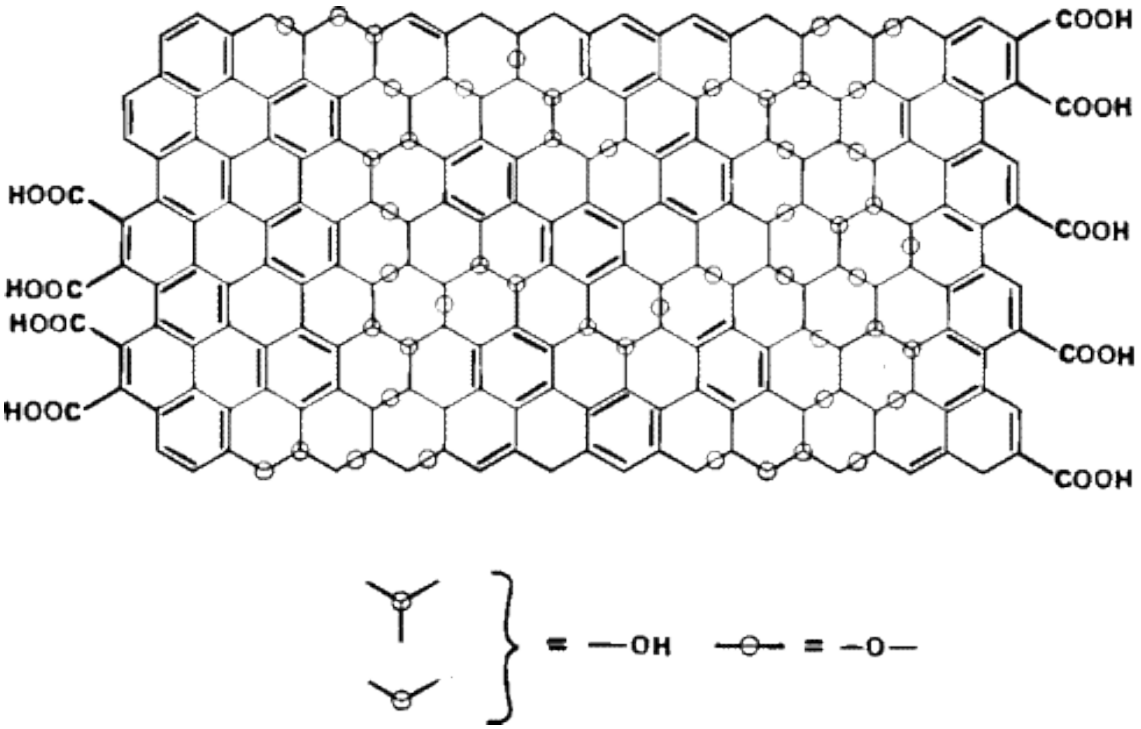

Figure 1-20 Lerf-Klinowski model of the GON sheets with –COOH groups at the edges [102].

However, it should be noted that Lerf-Klinowski model is related to the chemical connectivity, and the spatial orientation of functional groups is not taken into account, while during oxidation, a planar sp^2 network is transferred to a non-planar sp^3 structure disrupting the flatness of the graphene layers.

1.3.1.4 Suspension and Stability of GON in Solvents

Homogeneous colloidal suspensions of GON in a range of solvents are of remarkable interest for the formation of nanocomposites with well dispersed fillers as well as for further derivatisation reactions. The stability of graphene oxide dispersions in a range of solvents are shown in Figure 1-21.

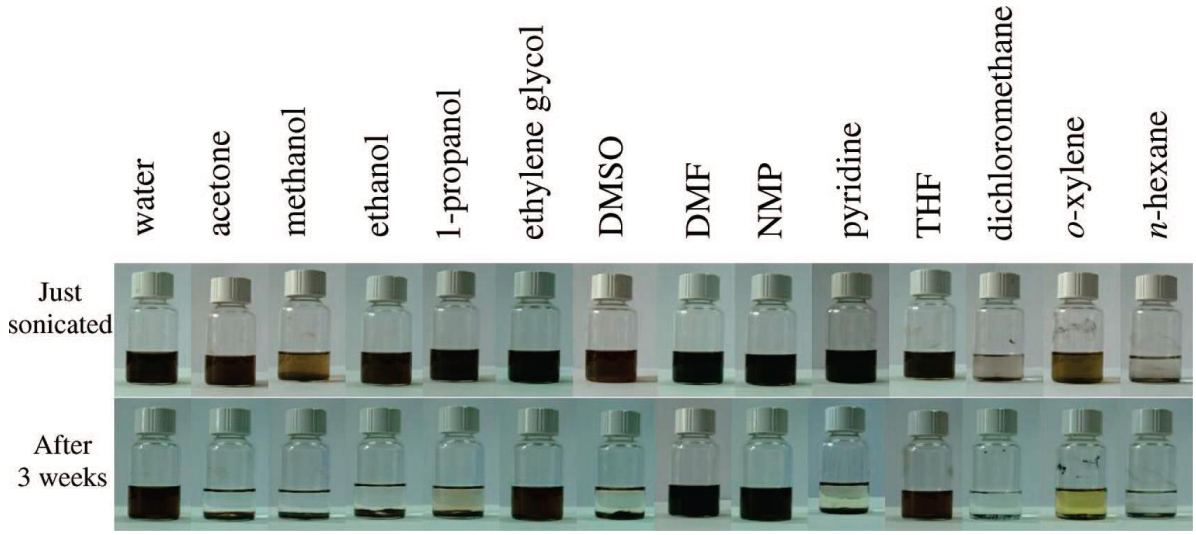

Figure 1-21 The dispersion of GON in different solvents [106].

It has been found that an efficient dispersion is dependent on both the extent of functional groups on the GON layers and the polarity of solvent, as polar solvents are more preferable to disperse oxidised GON. There are research groups that have achieved the homogenous dispersions of GON in a few aqueous media and in a range of organic solvents by sonication or ultrasonication. In water, the concentrations of GON could reach up to 3 mg/ml, and up to 0.5 mg/ml in a range of organic polar solvents, such as dimethylformamide (DMF), tetrahydrofuran (THF), N-methylpyrrolidone (NMP) and glycol [68,103,104,105,106].

1.3.2 The Influence of Nanofillers on Polymer Properties

1.3.2.1 Influence on Rheological Properties

Polymer nanocomposites with enhanced mechanical, electrical or thermal properties have been investigated intensively [107,108], and they have become one of the most important class of materials for high demanding applications. The modification in their properties is intimately related to the filler properties, for examples, aspect ratio, microscopic arrangement of the filler, chain-filler interaction, as well as the formation of filler-filler networks. It has been reported that the presence of filler could significantly influence the polymer chain dynamics, consequently influencing crystallisation during shear flow and ultimately mechanical properties of the polymer [109]. Linear oscillatory rheology is a well-established technique in the study of polymer-based nanocomposites [110,111,112]. The absolute values of loss (G'') and elastic (G') modulus, as well as their dependence on frequency could unveil

information on the structure of the dispersed phase and its interaction with the polymer matrix chains. Melt rheological studies have revealed that the presence of nanoparticles in polymers perturbs the microscopic inter-chain arrangement of the polymer network, influencing the linear rheological properties. Research on HDPE/CNTs composites have shown that the addition of nanofillers could influence the cross-over point between elastic and viscous components of the viscoelastic polymer melt and it has been reported that an increment of filler could hinder the chain relaxation in the terminal region (frequencies<*G', G''* cross-over frequency) resulting in an increase in *G'* values [111]. With further increment in filler concentration, a plateau normally appears in the terminal region, indicating a percolation of solid network [113,114,115,116]. However, decrease in *G'* with the addition of low concentration of nanofillers has been reported, which suggests a potential in the decrease of viscosity that is of high interest for processing in industry. Recently, Zhang *et al.* have observed that the presence of relatively low amount of CNT (<1.0 wt %) could decrease the storage modulus of commercial UHMWPE having a large molar mass distribution, as shown from dynamic frequency sweep experiments reported in Figure 1-22 [117].

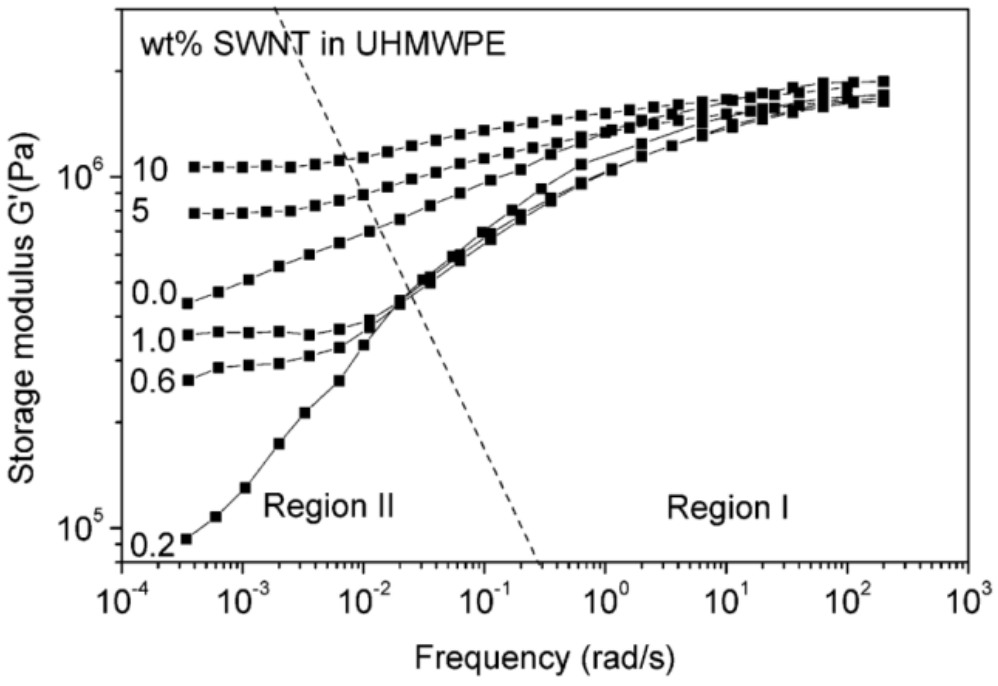

Figure 1-22 Behaviour of the storage modulus *G'* of UHMWPE composites having different loadings of CNTs as a function of frequency [117].

The authors suggested that the long molecular chains tend to be preferentially adsorbed on the surface of tubes due to van der Waals forces, whereas short chains are left in the matrix, resulting in fast relaxation compared to the pure polymer, leading to lower viscosities [117] at low frequencies. Similar phenomena have also been reported by several groups in different composite systems. Jain *et al.* observed a drop in polypropylene's viscosity at a specific concentration of silica [118]. Vega *et al.* have reported a drop in viscosity of HDPE/MWCNT composites compared to neat HDPE during extrusion and the authors have attributed the phenomenon to the adsorption of longest chains onto the nanotube surface through van de Waals interaction [119]. Other systems with similar results include PS/silica [120,121,122], UHMWPE/silica [123] and polystyrene filler with cross-linked polystyrenes [120] nanocomposites. The interaction of ethylene segments with carbon based filler has been conclusively demonstrated by Litvinov and co-workers on EPDM/carbon black composites by NMR , where the authors showed the adsorption of ethylene segments to the surface of carbon filler [124,125]. This suggests that the efficient dispersion of the filler across the polymer matrix resulting in a large contact area plays an important role in the change of rheological properties of the polymer matrix. Moreover, it has been also reported that graphene has the strongest interaction with PE matrix among all carbon-based nano inclusions, according to molecular dynamics simulations of PE nanocomposites with different carbon based fillers [126,127], and this is of paramount interest for this project, where graphene will be used for the preparation of UHMWPE composites followed by rheological analysis.

1.3.2.2 Electrical Conductivity

Saturated covalent bonds in polymers are non-conductive due to the absence of mobile electrons. In order to increase the conductivity of polymers for special applications, attempts of adding conductive fillers have been made. Significant increment in conductivity has been achieved, and at the same time a few models to predict and understand the conductivity mechanism have been developed. In general, the existing models can be based on percolation theory or non-percolation theory, where the latter includes the Bueche Model [128], Nielsen Mode [129], McCullough Model [130] and Ondracek Model [131], for example. In this literature review, we will focus mainly on the models based on the percolation theory.

The concept of 'percolation threshold' was first proposed by Broadbent and Hammersley in 1957 [132]. The basic idea is the formation of a continuous path going from a generic side A to a side B of an area, arising from the interaction of randomly or regularly distributed sites or bands. To apply the percolation threshold models to interpret the electrical conductivity of composites, an inhomogeneous conductor is needed [133], i.e. a mixture of a two-phase system having a conducting phase (the filler) and a non-conducting phase (the polymer). It has been found that, on increasing the amount of filler in the polymeric matrix, there is a sudden transition from insulating state to conductive state when the conductive filler's loading reaches a certain concentration: this concentration is indicated as percolation threshold. A simple power law relationship among composites conductivity, percolation threshold concentration and filler's loading has been developed for data interpretation [134,135], shown in equation 1-4:

$$\sigma_c = \sigma_o(\varphi_f - \varphi_{crit})^t \qquad \text{(Equation 1-4)}$$

Where σ_c is the volume electrical conductivity (S/cm); σ_0 is the conductivity of the filler (S/cm); φ_f is the filler's concentration; φ_{crit} is the critical concentration of the filler, *i. e.* the concentration at the percolation threshold; t is an experimental exponent dependent on the dimensions of the lattice that accommodate the conductive fillers. The equation is valid only for filler's concentrations higher than the critical concentration

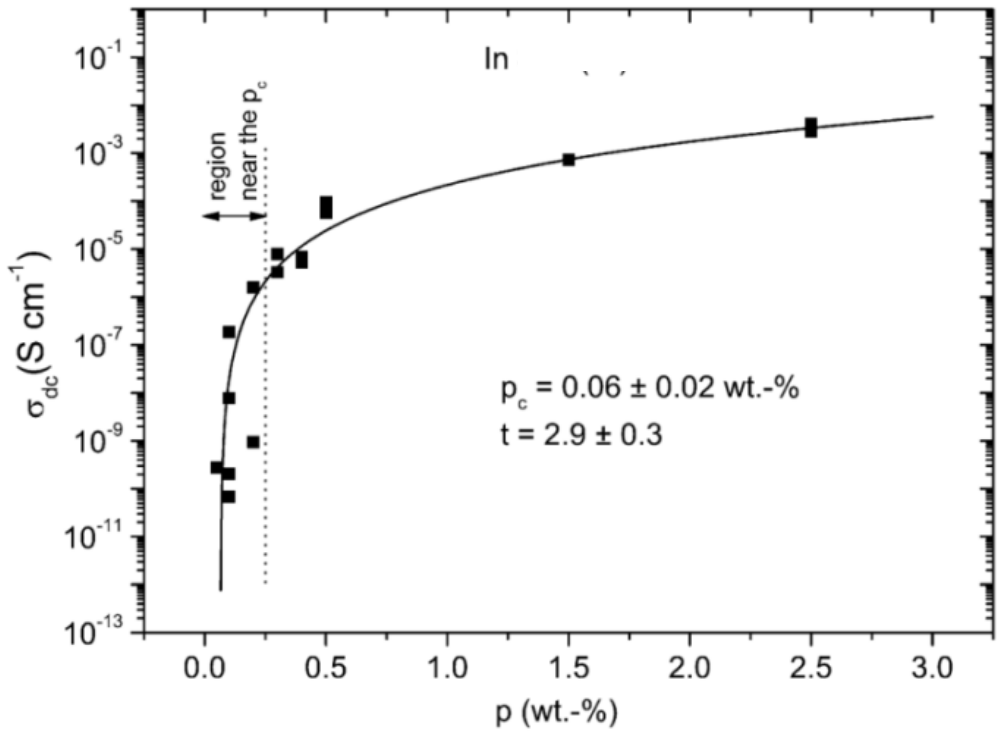

Figure 1-23 An example of percolation concentration of conductive fillers (ρ_c) in a non-conductive polymeric matrix [136].

The percolation threshold of different composite systems has been investigated, and it has been found that with the increase of the aspect ratio, the percolation threshold decreases [137,138,139]. Percolation threshold of over 5 wt % is normally reported for particles which have low aspect ratio, for instance, silver particles, carbon black and so on. Recently, much lower percolation thresholds have been reported for new generation fillers with ultra-high respect ratio: for example, percolation values down to 0.06 wt % have been achieved for CNTs added to UHMWPE [117,136, 140]. Realistically, the percolation threshold also depends on the dispersion of fillers, the processing method, the interaction between filler and matrix and the size and shape of the conductive phase. Due to the variation of dispersion techniques, reproducibility of the composites preparation, the types of matrix (non-conductive phase) etc., the percolation threshold values reported in the literature can vary considerably [141]. Sometimes, a low concentration of well-dispersed fillers is not able to form a physical way for the electron transport, while the same amount of fillers with local aggregation may enhance conductivity.

As mentioned above, in order to make insulating polymers conductive, a continuous path of conductive filler is usually necessary. Especially for commercial UHMWPE composites, the most used preparation technique is dry mixing followed by compression moulding, due to high entanglement density and high viscosity of the matrix. Most of the filler resides on the grain boundaries of the polymer particles, originated by the incomplete fusing of the nascent particles. The filler is then able to form a continuous path for electrons to travel from one side to the other, giving rise to very low percolation threshold of the composites, for instance Hu *et al.* have obtained UHMWPE/graphene composites having percolation threshold as low as 0.0028 vol % [142]. Other examples of low percolations of UHMWPE composites with carbon based fillers are listed in Table 1-5. Figure 1-24 shows an example of the formation of graphene conductive networks along the grain boundaries; at higher filler content, the filler still reside along the grain boundaries, giving rise to aggregation and resulting in a thicker conductive path [143].

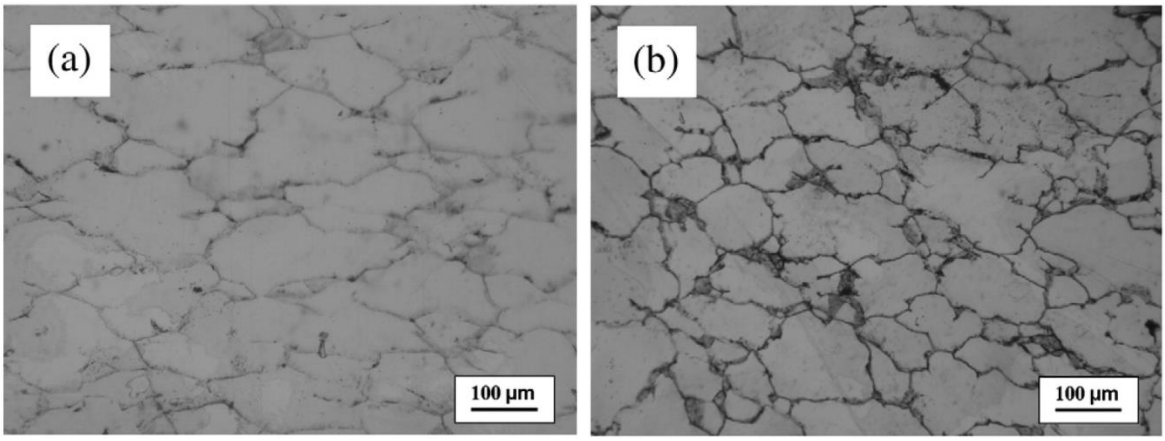

Figure 1-24 Optical microscope images of dispersion of graphene in UHMWPE matrix; **a)** 0.076 vol %; **b)** 0.15 vol % [143].

Table 1-5 Achieved conductivities and percolation thresholds of CNT/UHMWPE composites according to the different preparation methods.

CNT Type	Preparation Method	Percolation Threshold ρ_c (wt %)	Critical Component t	Refs.
MWCNT	Liquid dispersing-dry mixing, Sintering	0.045	2.63 ±0.12	[144]
MWCNT	Gelation/crystallization	3	1.86	[145]
MWCNT	Dry mixing&compression moulding	0.036	2.07	[146]
MWCNT	Dry mixing (raw power)	0.073	1.77	
MWCNT	Dry mixing&compression moulding	0.13	1.13 ±0.08	[147]
SWCNT	Liquid dispersing, dry mixing&sintering	0.09	2.25 ± 0.05	[145]
SWCNT	Spraying method, Solution casting	0.6	-	[117]
Graphene	Liquid dispersing and compression moulding	0.070	1.26±0.06	[143]
Graphene	Two-step process and compression moulding	0.028	-	[142]

However, as the filler segregates along the boundaries among grains, defects or weak interaction between chain and filler form along the boundaries, and this causes negative effect on the mechanical properties, for instance reduction in elongation and ultimate strength [144,148 ,149].

The enhancement in other properties, such as thermal conductivities and mechanical properties, have also been reported by adding nanofiller. For instance, Song *et al.* [150] have reported that with incorporation of a small amount of functionalised graphene in a nylon matrix, a significant increment in mechanical properties, such as tensile strength, elongation, impact strength and toughness, is achieved, due to the presence of strong chain-filler interaction between functional groups on the functionalised graphene surface and functional groups of nylon molecules. Shahil *et al.* reported that the addition of a small loading of 2.0 wt % of graphene could lead to a significant enhancement in the cross-plane thermal conductivity of epoxy/graphene composites. The authors attributed the increment to the high aspect ratio of graphene and lower Kapitza resistance at the graphene-matrix interface [151].

It has been previously reported that the blending of nanofiller into polymers could generate intrinsically non-equilibrium melts which could change the composites' properties with evolvement of the non-equilibrium state towards equilibrium state. Little studies on properties of polymer/graphene composites at non-equilibrium state at melt have been published. However, extensive investigation has been carried out on non-equilibrium polymer/CNTs composites at melt and change of properties during the equilibration has been reported [152,153,154,155]. A few groups have reported that the electrical conductivities of polymer/CNTs composites increased with increasing annealing time at temperatures higher than their melting points which pushes the equilibration of the non-equilibrium state [152,154]. Graphene with higher aspect ratio is expected to have more profound influence on the change of properties of non-equilibrium melts, and this topic will be of interest in this project.

The low initial viscosity and high particle porosity feature of non-equilibrium disentangled UHMWPE [156] could contribute to a better dispersion of the filler, leading to more effective chain-filler contact and refined filler-filler network. The consequent influence on rheological properties electrical conductivities, as well as mechanical properties, will be of interest in this project.

1.4 Thesis Scope

As mentioned above, disentangled UHMWPE, polymerised by single-site homogeneous FI catalyst in controlled conditions, possesses unique properties compared to commercially available one, such as highly porous particle morphology, low initial melting viscosity, heterogeneous melting behaviour, ease in processability, and high modulus/strength. This polymer provides unique opportunity to investigate the filler influence on the chain dynamics, entanglement formation, melt kinetics and crystallisation, especially when strong interactions between polyethylene chain and carbon based fillers are present [127,157], such as with reduced graphene oxide nanoplatelets (rGON) having very high aspect ratio. The investigation will give better insights on how the filler influences the transformation of the polymer melt from non-equilibrium state to equilibrium state, providing essential information on the processing of the intractable material. Both suspension mixing and in-situ polymerisation methods will be used for the preparation of the composites. Due to the homogeneous dispersion of the filler in various solvents, a homogeneous dispersion of the filler in the matrix can be realised using the suspension mixing method.

In the second method, the potential adhesion of the catalytic system onto the surface of the filler provides a possibility to achieve nanocomposites with homogeneous dispersion of filler having intimate contact with chains.

A better understanding of the processing features of the composite may open the way to the production, for example, of membranes or tapes or even higher dimensional shapes having the additional feature of enhanced mechanical properties and electrical conductivity.

Therefore the main objectives of this project are the following:

1) Preparation of the composites of reduced graphene oxide and polyethylene by both physical suspension mixing and in-situ polymerisation;

2) Investigation of the polyethylene chain-filler interaction followed by melt rheology, as well as time-resolved wide/small angle X-ray scattering performed at large-scale facility (European Synchrotron Radiation Centre);

3) Influence of reduced graphene oxide on the rheological properties of polyethylene samples having different entanglement densities;

4) Influence of reduced graphene oxide on the crystallisation kinetics and consequent melting behaviour of polyethylenes having different entanglement densities;

5) Influence of nascent powder morphology on the electrical conductivities of the composites;

6) Influence of reduced graphene oxide on the mechanical properties of the ultra-stretched tapes obtained via solid-state processing.

References

[1] Ferry, J. D. *Viscoelastic Properties of Polymers* 3rd ed. Wiley: New York, **1980**.

[2] Doi, M. Explanation for the 3.4-power law for viscosity of polymeric liquids on the basis of the tube model. *J. Polym. Sci.: Polym. Phys. Ed*. **1983**, 21, 667-684.

[3] De Gennes, P. G. *Scaling Concepts in Polymer Physics.* Cornell. Press, Ithaca, **1979**.

[4] Mcleish, T. C. B. Tube theory of entangled polymer dynamics. *Adv. Phys.* **2002**, 51(6), 1379-1527.

[5] Rastogi, S.; Lippits, D. R.; Peters, G. W. M.; Graf, R.; Yao, Y.; Spiess, H. W. Heterogeneous in polymer melts from melting of polymer crystals. *Nat. Mater.* **2005**, 4, 635-641.

[6] Milner, S. T.; McLeish, T. C. B. Reptation and contour-length fluctuations in melts of linear polymers. *Phys. Rev. Lett.* **1998**, 81(3), 725-728.

[7] Berry, G. C., Fox, T. G. The viscosity of polymers and their concentrated solutions. *Adv. Polym. Sci*. **1968**, 5, 261–357.

[8] Jurgenleit, W. Polyolefin wet spinning process. US patent 3048465, **1962**.

[9] Smith, P; Lemstra, P. J. Kirschbaum, R.; Laurentius, P.; Less, P. Process for the production of polymer filaments having high tensile strength and modulus. EP 0077590, **1983**.

[10] Zwick, M. NL Patent 6501248, **1965**.

[11] Baldes, H.; White, J. R. Fibrillated strand. US Patent 3081519, **1963**.

[12] Pennings, A. J.; Van Den Mark, J. M. A. A.; Booij, H. C. Hydrodynamically induced crystallization of polymers from solution. *Colloid. Polym. Sci*. **1970**, 236(2), 99-111.

[13] Ward, I. M. *Development in Oriented Polymers (Volume 2).* Elsevier Applied Science Publishers Ltd, New York, **1987**.

[14] Smith, P.; Lemstra, P. J. Process for making polymer filaments which have a high tensile strength and a high modulus. US Patent 4344908, **1982**.

[15] Kirschbaum, R., Lemstra, P. J.; Pijpers, J. P. L.; Paul, S. Process for the production of polymer filaments having high tensile strength. US Patent 4436689, **1984**.

[16] Tam, T. Y. T.; Zhou, Q.; Young, J. A.; Amett, C. R.; Hermes, J. E. Ultra high molecular weight (UHMW) polyethylene; tensile strength; passing through spinneret; continuous drawing; winding; rapidly cooling; desolventizing, relaxing, winding, unrolling, cooling. US Patent 7846363, **2010**.

[17] Kavesh, S. High tenacity, high modulus filament. US Patent 6448359, **2002**.

[18] Lemstra, P. J.; Bastiaansen, C. W. M.; Meijer, H. E. H. Chain-extended flexible polymers. *Macromol. Mater. Eng.* **1986**, 145(1), 343-358.

[19] Kanamoto, T.; Ohama, T.; Tanaka, K.; Takeda, M.; Porter, R. S. *Polymer* **1987**, 28, 1517–1520.

[20] Zachariades, A. E.; Watts, M. P. C.; Porter, R. S. Solid state extrusion of ultra high molecular weight polyethylene: processing and properties. *Polym. Eng. Sci.* **1980**, 20, 555–561.

[21] Kanamoto, T.; Tsuruta, A.; Tanaka, K.; Takeda, M.; Porter, R.S. On ultra-high tensile modulus by drawing single crystal mats of high molecular weight polyethylene. *Polymer. J.* **1983**, 15, 327-329.

[22] Zachariades, A. E.; Kanamoto, T. The effect of initial morphology on the mechanical properties of ultra-high molecular weight polyethylene. *Polym. Eng. Sci.* **1986**, 26 (10), 658-661.

[23] Rastogi, S.; Yao, Y.; Ronca, S.; Bos, J.; van der Eem, J. Unprecedented ultra-modulus high-strength tapes and films of ultrahigh molecular weight polyethylene via solvent-free route. *Macromolecules* **2011**, 44, 5558-5568.

[24] Chanzy, H. D.; Revol, J. F.; Marchessault, R. H.; Lamande, A. Nascent structures during the polymerization of ethylene I. Morphology and model of growth. *Colloid. Polym. Sci*. **1973**, 251, 563-576.

[25] Chanzy, H. D.; Bonjour, E.; Marchessault, R. H.; Lamande, A. Nascent structures during the polymerization of ethylene II. Calorimetric study. *Colloid. Polym. Sci*. **1974**, 252, 8-14.

[26] Smith, P.; Chanzy, H. D.; Rotzinger, B. P. Drawing of virgin ultrahigh molecular weight polyethylene: an alternative route to high strength/high modulus materials. *J. Mater. Sci.* **1987**, 22, 523-531.

[27] Rotzinger, B. P.; Chanzy, H. D.; Smith, P. High strength/high modulus polyethylene: synthesis and processing of ultra-high molecular weight virgin powders. *Polymer* **1989**, 30, 1814-1819.

[28] Smith, P.; Lemstra, P. J. Ultra-high-strength polyethylene filaments by solution spinning/drawing. *J. Mater. Sci.* **1980**, *15*, 505-514.

[29] Makio, H.; Fujita, T. Development and Application of FI catalysts for olefin polymerization: unique catalysis and distinctive polymer formation. *Acc. Chem. Res.* **2009**, 42(10), 1532-1544.

[30] Breslow, D. S.; Newburg, N. R. Bis-(clclopentadienyl)-titanium dichloride-alkylaluminum complexls as catalysts for the polymerization of ethylene. *J. Am. Chem. Soc.* **1957**, 79(18), 5072-5073.

[31] Breslow, D. S. Polymerization of ethylene. US Patent 2827446, **1955**.

[32] Natta, G.; Pino, P.; Mazzanti, G.; Giaannini U. A crystallizable organometallic complex containing titanium and aluminum. *J. Am. Chem. Soc*. **1957**, 79, 2975-2976.

[33] Makio, H.; Terao, H.; Iwanshita, A.; Fujita, T. FI catalysts for olefin polymerisation-a comprehensive treatment. *Chem. Rev.* **2011**, 111, 2363-2449.

[34] Kaminsky, W. Highly active metallocene catalysts for olyfin polymerization. *J. Chem. Soc., Dalton Trans.* **1998**, 1413-1418.

[35] Saito, J.; Mitani, M.; Matsui, S.; Sugi, M.; Tohi, Y.; Tsutsui, T.; Fujita, T.; Nitabaru, M.; Makio, H. Olefin polymerization catalysts, transition metal compounds, processes for olefin polymerization, and Alpha-olefin/conjugated diene copolymers. European Patent 0874005, **1998**.

[36] Johnson, L. K.; Bennett, A. M.; Ittel, S. D.; Wang, L.; Parthasarathy, A.; Hauptman, E.; Simpson, R. D.; Feldman, J.; Coughlin, E. B. *Polymerization of olefins*. WO Patent 1998030609, **1998**.

[37] Wang, C.; Friedrich, S.; Younkin, T. R.; Li, R. T.; Grubbs, R. H.; Bansleben, D. A.; Day, M. W. Neutral nickel (II)-based catalysts for ethylene polymerization. *Organometallics* **1998**, 17, 3149-3151.

[38] Talebi, S.; Duchateau, R.; Rastogi, S.; Kaschta, J.; Peters, G. M.; Lemstra, P. J. Molar mass and molecular weight distribution determination of UHMWPE synthesised using a living homogeneous catalyst. *Macromolecules* **2010**, 43 (6), 2780-2788.

[39] Rastogi, S.; Yao, Y.; Ronca, S.; Bos, J.; van der Eem, J. Heterogeneity in the distribution of entanglement density during polymerization in disentangled ultrahigh molecular weight polyethylene. *Macromolecules* **2011**, 44 (14), 5558-5568.

[40] Pandey, A.; Champouret, Y.; Rastogi, S. Heterogeneity in the distribution of entanglement density during polymerization in disentangled ultrahigh molecular weight polyethylene. *Macromolecules* **2011**, 44, 4952-4960.

[41] Tabebi, S. *Disentangled Polyethylene with Sharp Molar Mass Distribution; Implications for Sintering.* PhD thesis, Eindhoven University of Technology, **2008**.

[42] Loos, J.; Arndt-Rosenau, M.; Weingarten, U.; Kaminsky, W. Melting behavior of nascent polyolefins synthesized at various polymerizations conditions. *Bulletin* **2002**, 48, 191-198.

[43] Mead, D. Determination of molecular weight distributions of linear flexible polymers from linear viscoelastic material functions. *J. Rheol.* **1994**, 38, 1797-1827.

[44] Tuminello, W. H. Molecular weight and molecular weight distribution from dynamic measurements of polymer melts. *Polym. Eng. Sci.* **1986**, 26, 1339-1347.

[45] Lippits, D. *Controlling the Melting Kinetics of Polymers; A Route to A New Melt State*. PhD Thesis, Eindhoven University of Technology, **2007**.

[46] Ferry, J.D. *Viscoelastic Properties of Polymers 3rd Ed*, Wiley, New York, **1980**.

[47] Rastogi, S.; Lippits, D. R.; Höhne, G. W. H.; Mezari, B.; Magusin, C. M. M. The role of the amorphous phase in melting of linear UHMW-PE; implications for chain dynamics. *J. Phys.: Condens. Matter* **2007**, 19, 205122.

[48] Strobl, G. *The physics of polymers*. Springer, New York, **1997**.

[49] Tervoort-Engelen, Y. M. T.; Lemstra, P. J. Morphology of nascent ultrahigh-molecular-weight polyethylene reactor powder: chain-extended versus chain-folded crystals. *Polym. Commun.* **1991**, 32, 343-345.

[50] Wunderlich, B. Czornyj, G. A study of equilibrium melting of polyethylene. *Macromolecules* **1977**, 10 (5), 906-913.

[51] Rastogi, S.; Kurelec, L.; Lippits, D.; Cuijpers, J.; Wimmer, M.; Lemstra, P. J. Novel route to fatigue – resistant fully sintered ultrahigh molecular weight polyethylene for knee prosthesis. *Biomacromolecules* **2005**, 6, 942–947.

[52] Lippits, D.R.; Rastogi, S.; Höhne, W. H. Melting Kinetics in Polymers. *Phys. Rev. Lett.* **2006**, 96, 218303.

[53] Höhne, G. W. H. Another approach to the Gibbs-Thomson equation and the melting point of polymers and oligomers. *Polymer* **2002**, 43, 4689-4698.

[54] Pandey, A.; Toda, A.; Rastogi, S. Influence of amorphous component on melting of semicrystalline polymers. *Macromolecules* **2011**, 44, 8042-8055.

[55] Corbeij-Kurelec, L. *Chain Mobility in Polymer Systems; On the Borderline between Solid and Melt.* PhD Thesis, Eindhoven University of Technology, **2001**.

[56] Romano, D.; Tops, N.; Andablo-Reyes, E.; Ronca, S.; Rastogi, S. Influence of polymerization conditions on melting kinetics of low entangled UHMWPE and its implications on mechanical properties. *Macromolecules* **2014**, 47, 4750-4760.

[57] Donnet, J.; Bansal, R.C. *Carbon Fibres* **1984**, Chapter 5, 223-267.

[58] Chen, Y.; Qi, Y.; Tai, Z.; Yan, X.; Zhu, F.; Xue, Q. Preparation, mechanical properties and biocompatibility of graphene oxide/ultrahigh molecular weight polyethylene composites. *Eur. Polym. J.* **2012**, 48, 1026-1033.

[59] Lahiri, D.; Dua, R.; Zhang, C.; de Socarraz-Novoa, I.; Bhat, A.; Ramawamy, S.; Agarwal, A. Graphene nanoplatelet-induced strengthening of ultrahigh molecular weight polyethylene and biocompatibility in vitro. *ACS Appl. Mater. Interfaces* **2012**, 4, 2234-2241.

[60] Stoller, M. D.; Park, S.; Zhu, Y.; An, J.; Ruoff, R. S. Graphene-based ultracapacitors. *Nano. Lett.* **2008**, 8 (10), 3498-3502.

[61] Liu, K.; Ronca, S.; Andablo-Reyes, E.; Forte, G.; Rastogi, S. Unique rheological response of ultrahigh molecular weight polyethylene in the presence of reduced graphene oxide. *Macromolecules* **2014**, 48(1), 131-139.

[62] Novoselov, K. S.; Geim, A.K.; Morozov S.V.; Jiang, D.; Zhang, Y.; Dubonos, S.V.; Grigorieva, I. V.; Firsov, A. A. Electric field effect in atomically thin carbon films. *Science* **2004**, 306, 666–669.

[63] Geim, A. K.; Novoselov, K. S. The rise of graphene. *Nat. Mater.* **2007**, 6, 183–191.

[64] Meyer, J. C.; Geim, A. K.; Katsnelson, M. I.; Novoselov, K. S.; Booth, T. J.; Roth, S. The structure of suspended graphene sheets. *Nature* **2007**, 446, 60-63.

[65] Zhu, Y.; Murali, S.; Cai, W.; Li, X.; Suk, J. W.; Potts, J. R.; Ruoff, R. S. Graphene and graphene oxide: synthesis, properties, and applications. *Adv. Mater.* **2010**, 22, 3906-3924.

[66] Xu, K.; Ye, P. D. Theoretical study of atomic layer deposition reaction mechanism and kinetics for anuminum oxide formation at graphene nanoribbon open edges. *J. Phys. Chem. C* **2010**, 114, 10505-10511.

[67] Lu, X.; Yu, M.; Huang, H.; Ruoff, R. S. Tailoring graphite with the goal of achieving single crystals. *Nanotechnology* **1999**, 10, 269-272.

[68] Stankovich, S.; Piner, R.D.; Nguyen, S. T. Ruoff, R. S. Synthesis and exfoliation of isocyanate-treated graphene oxide nanoplatelets. *Carbon* **2006**, 44(15), 3342-3347.

[69] Stankovich, S.; Piner, R.D.; Chen, X.; Wu, N.; Nguyen, S. T.; Ruoff, R. S. Stable aqueous dispersions of graphitic nanoplatelets via reduction of exfoliated graphite oxide in the presence of poly(sodium 4-styrenesulfonate). *J. Mater. Chem.***2006**, 16, 155-158.

[70] Kosynkin, D. V.; Higginbotham, A. L.; Sinitskii, A.; Lomeda, J. R.; Dimiev, A.; Price, B. K.; Tour, J. M. Longitudinal unzipping of carbon nanotubes to form graphene nanoribbons. *Nature* **2009**, 458, 872-876.

[71] Berger, C.; Song, Z.; Li, X.; Wu, X.; Brown, N.; Naud, C.; Mayou, D.; Li, T.; Hass, J.; Marchenkov, A. N.; Conrad, E. H.; First, P. N.; de Heer, W. A. Electronic confinement and coherence in patterned epitaxial graphene. *Science*, **2006**, 312, 1191–1196.

[72] Zhou, S. Y.; Gweo, G. H.; Fedorov, A. V.; First, P. N.; de Heer, W. A.; Lee, D. H.; Guinea, F.; Neto, A. H.; Lanzara A. Substrate-induced bandgap opening in epitaxial graphene. *Nat. Mater.* **2007**, 6, 770–775.

[73] Marchini, S.; Gunther, S.; Wintterlin, J. Scanning tunnelling microscopy of graphene on Ru(0001). *J. Phys. Rev. B* **2007**, 76, 075429.

[74] Pan, Y.; Zhang, H.; Shi, D.; Sun, J.; Du, S.; Liu, F.; Gao H. Highly ordered, millimetre-scale, continuous, single-crystalline graphene monolayer formed on Ru (0001). *Adv. Mater.* **2009**, 21, 2777–2780.

[75] Lee, C.; Wei, X.; Kysar, J. W.; Hone, J. Measurement of the elastic properties and intrinsic strength of monolayer graphene. *Science* **2008**, 321, 385-388.

[76] Balandin, A. A.; Ghosh, S.; Bao, W.; Calizo, I.; Teweldebrhan, D.; Miao, F.; Lau, C. Superior thermal conductivity of single-layer graphene. *Nano Lett.* **2008**, 8 (3), 902-907.

[77] Ghosh, S.; Calizo, I.; Teweldebrhan, D.; Pokatilov, E. P.; Nika, D. L.; Balandin, A. A.; Bao, W.; Miao, F.; Lau, C. N. Extremely high thermal conductivity of graphene: prospects

for thermal management applications in nanoelectronic circuits. *Appl. Phys. Lett.* **2008**, 151911.

[78] Du, X.; Skachko, I.; Duerr, F.; Luican, A.; Andrei, E. Y. Fractional quantum hall effect and insulating phase of dirac electrons in graphene. *Nature* **2009**, 462, 192–195.

[79] Gallego, N. C.; Edie, D. D.; Nysten, B.; Issi, J. P.; Treleaven, J. W.; Deshpande, G. V. The thermal conductivity of ribbon-shaped carbon fibres. *Carbon* **2000**, 38, 1003-1010.

[80] Chand, S. Review carbon fibres for composites. *J. Mate. Sci.* **2000**, 35, 1303-1313.

[81] Lavin, J. G.; Boyington, D. R.; Lahijani, J.; Nysten, B.; Issi, J. P. The correction of thermal conductivity with electrical resistivity in mcsophase pitch-based carbon fiber. *Carbon* **1993**, 31, 1001–1002.

[82] Tang, Z.; Zhang, L.; Wang, N.; Zhang, X.; Wen, G.; Li, G. D.; Wang, J. N.; Chan, C. T.; Sheng, P. Superconductivity in 4 anstrom single-walled carbon nanotubes. *Science,* **2001**, 292, 2462–2465.

[83] Kelly, B. T. *Physics of Graphite.* London: Applied Science, **1981**.

[84] Chen, S.; Moore, A. L.; Cai, W.; Suk J. W.; An, J.; Mishra, C.; Amos, C.; Magnuson, C. W.; Kang, J.; Shi, L.; Ruoff, R. S. Raman measurements of thermal transport in suspended monolayer graphene of variable sizes in vacuum and gaseous environments. *ACS Nano* **2011**, 5, 321–328.

[85] Faugeras, C.; Faugeras, B.; Orlita, M.; Potemski, M.; Nair, R. R.; Geim, A. K. Thermal conductivity of graphene in corbino membrane geometry. *ACS Nano* **2010**, 4, 1889–1892.

[86] Lee, J.; Kim, D.; Lee, S. W.; Cheong, H. Thermal conductivity of suspended pristine graphene measured by Raman spectroscopy. *Phys. Rev. B* **2011**, 83, 081419.

[87] Bolotin, K. I.; Sikes, K. J.; Jiang, Z.; Klima, M.; Fudenberg, G.; Hone, J.; Kim, P.; Stormer, H. L. Ultrahigh electron mobility in suspended graphene. *Solid State Communications* **2008**, 146, 351-355.

[88] Brodie, B. C. *Ann. Chim. Phys.* **1860**, 59**,** 466.

[89] Marcano, D. C.; Kosynkin, D. V.; Berlin, J. M.; Sinitskii, A.; Sun, Z.; Slesarev, A;Alemany, L. B.; Lu, W.; Tour, J. M. Improved synthesis of graphene oxide. *ACS Nano* **2010**, 4, 4806-4814.

[90] Staudenmaier, L.; *Ber. Deut. Chem. Ges; 1898;* **31,** 1481.

[91] Hummers, W. S.; Offeman, R. E. Preparation of graphitic oxide. *J. Am. Chem. Soc.* 1958, **80,** 1339.

[92] Sun, L.; Fugetsu, B. Mass production of graphene oxide from expanded graphite. *Mater. Lett.* **2013**, 109, 207-210.

[93] Hong, Y.; Wang, Z.; Jin, X. Sulfuric acid intercalated graphite oxide for graphene preparation. *Sci. Rep.* **2013**, 3, 3439.

[94] Hofmann, U.; Holst, R. *Ber. Dtsch. Chem. Ges.* **1939**, 72, 754.

[95] Scholz, W.; Boehm, H. P.; *Z. Anorg. Allg. Chem.* **1969**, 369, 327.

[96] Nakajima, T.; Mabuchi, A.; Hagiwara, R. A new structure model of graphite oxide. *Carbon*, **1988**, 26, 357-361.

[97] Nakajima, T.; Matsuo, Y. Formation process and structure of graphite oxide. *Carbon* **1994**, 32 (3), 469-475.

[98] Hontoria-Lucas, C.; Lopez-Peinado, A. J.; Lopez-Gonzalez, J. D.; Rojas-Cervantes, M. L.; Martin-Aranda, R. M. Study of oxygen-containing groups in a series of graphite oxides: physical and chemical characterization. *Carbon* **1995**, 33 (11), 1585-1592.

[99] Szabo, T.; Berkesi, O.; Forgo, P.; Josepovits, K.; Sanakis, Y.; Petridis, D.; Dekany, I. Evolution of surface functional groups in a series of progressively oxidized graphite oxides. *Chem. Mater.* **2006**, 18(11), 2740-2749.

[100] He, H.; Riedl, T.; Lerf, A.; Klinowski, J. Solid-state NMR studies of the structure of graphite oxide. *J. Phys. Chem.* **1996**, 100(51), 19954-19958.

[101] Lerf, A.; He, H.; Riedl, T.; Forster, M.; Klinowski J. 13C and 1H MAS NMR studies of graphite oxide and its chemically modified derivatives. *Solid State Ionics* **1997**, 101-103(2), 857-862.

[102] Lerf, A.; He, H.; Forster, M.; Klinowski, J. Structure of graphite oxide revisited. *J. Phys. Chem. B* **1998**, 102(23), 4477-4482.

[103] Park, S.; Lee, K.; Bozoklu, G.; Cai, W.; SonBinh, T. N.; Ruoff R. S. Graphene oxide papers modified by divalent ions-enhancing mechanical properties via chemical cross-linking. *ACS Nano* **2008**, *2*(3), 572-578.

[104] Stankovich, S.; Piner, R.; Nguyen, S. T.; Ruoff, R. S. Synthesis and exfoliation of isocyanate-treated graphene oxide nanoplatelets. *Carbon* **2006**, 44(15), 3342–3347.

[105] Stankovich, S. ; Dikin, D. A.; Piner, R. D.; Kohlhaas, K. A.; Kleinhammes, A.; Jia, Y.; Wu, Y.; Nguyen, S. T.; Ruoff, R. S. Synthesis of graphene-based nanosheets via chemical reduction of exfoliated graphite oxide. *Carbon* **2007**, 45(7), 1558–1565.

[106] Paredes, J. I.; Villar-Rodil, S.; Martinez-Alonso, A.; Tascon, J. M. D. Graphene oxide dispersion in organic solvents. *Langmuir* **2008,** 24(19), 10560–10564.

[107] Paul, D. R.; Robeson, L. M. Polymer nanotechnology: nanocomposites. *Polymer* **2008**, 49, 3187-3024.

[108] Sahoo, N. G.; Rana, S.; Cho, J. W.; Li, L.; Chan, S. H. Polymer nanocomposites based on functionalized carbon nanotubes. *Prog. Polym. Sci.* **2010**, 35, 837-867.

[109] Patil, N. *Flow Induced Crystallisation of Polyethylene in Presence of Nanoparticles.* PhD Thesis, Loughborough University, **2010**.

[110] Dealy J. M.; Larson, R. G. *Structure and Rheology of Molten Polymers: from Structure to Flow Behavior and Back Again.* Hanser Publishers, Munch; 2005.

[111] Song, Y.; Zheng, Q. Linear rheology of nanofilled polymers. *J. Rheol.* **2015**, 59(1), 155-191.

[112] Cassagnau, P. Melt rheology of organoclay and fumed silica nanocomposites. *Polymer* **2008**, 49, 2183-2196.

[113] McNally, T.; Potschke, P.; Halley, P.; Murphy, M.; Martin, D.; Bell, S. E. J.; Brennan, G. P.; Bein, D.; Lemoine, P.; Quinn, J. P. Polyethylene multiwalled carbon nanotube composites. *Polymer* **2005**, 46, 8222-8232.

[114] Zhang, Q.; Rastogi, S.; Chen, D.; Lippits, D.; Lemstra, P. J. Low percolation threshold in single-walled carbon nanotube/high density polyethylene composites prepared by melting processing technique. *Carbon* **2006**, 44, 778-785.

[115] Xiao, K.; Zhang, L.; Zarudi, I. Mechanical and rheological properties of carbon nanotube reinforced polyethylene composites. *Compos. Sci. Technol.* **2007**, 67, 177-182.

[116] Kim, H.; Abdala, A. A.; Macosko, C. W. Graphene/polymer nanocomposites. *Macromolecules* **2010**, 43, 6515-6530.

[117] Zhang, Q.; Lippits,.; D. R.; Rastogi, S. Dispersion and rheological aspects of SWNTs in ultrahigh molecular weight polyethylene. *Macromolecules* **2006**, 39, 658-666.

[118] Jain, S.; Goosens, G. W. M.; van Duin, M.; Lemstra, P. J. Strong decrease in viscosity of nanoparticle-filled polymer melts through selective adsorption. *Soft Matter* **2008**, 4, 1848-1854.

[119] Vega, J. F.; Martinez-Salazar, J.; Trujillo, M.; Arnal, M. L.; Muller, A. J.; Bredeau, S.; Dubois, Ph. Rheology, processing, tensile properties, and crystallization of polyethylene/carbon nanotube nanocomposites. *Macromolecules* **2009**, 42, 4719-4727.

[120] Mackay, M. E.; Dao, T. T.; Tuteja, A.; Ho, D. L.; Horn, B. V.; Kim, H. C.; Hawker, C. J. nanoscale effects leading to non-Einstein-like decrease in viscosity. *Nat. Mater.* **2003**, 2, 762-766.

[121] Tuteja, A.; Mackay, M. E.; Hawker, C. J.; Van Horn, B. Effect of ideal, organic nanoparticles on the flow properties of linear polymers: non-Einstein-like behavior. *Macromolecules* **2005**, 38, 8000-8011.

[122] Li, Y.; Kroger, M.; Liu, W. K. Nanoparticle effect on the dynamics of polymer chains and their entanglement network. *Phys. Rev. Lett.* **2012**, 109, 118001.

[123] Maurer, F. H. J.; Schoffeleers, H. M.; Kosfeld, R.; Uhlenbroich, T. Analysis of polymer filler interaction in filled polyethylene. *Prog. Sci. Eng. Compos.* **1982**, 803.

[124] Litvinov, V. M.; Steeman, P. A. M. Vulcanized siloxane chains swollen by polymer chains: NMR investigations into free-chain dynamics. *Macromolecules* **1999**, 32, 8476-8490.

[125] Litvinov, V. M.; Orza, R. A.; Klüppel, M.; van Duin, M.; Magusin, P. C. M. M. Rubber-filler interaction and network structure in relation to stress-strain behavior of vulcanized, carbon black filled EPDM. *Macromolecules* **2011**, 44, 4887-4900.

[126] Cheng, S.; Chen, X.; Hsuan, G. Y.; Li, C. Y. Reduced graphene oxide-induced polyethylene crystallization in solution and nanocomposites. *Macromolecules* **2011**, 45, 993-1000.

[127] Li, Y. Effect of nano inclusions on the structural and physical properties of polyethylene matrix. *Polymer* **2011**, 52(10), 2310-2318.

[128] Bueche, F. Electrical resistivity of conducting particles in an insulating matrix. *J. Appl. Phys.* **1972**, 43(11)**,** 4837-4838.

[129] Nielsen, L. E. The thermal and electrical conductivity of two-phase systems. *Ind. Eng. Chem Fundam.* **1974**, 13(1), 17-20.

[130] McCullough, R. L. Generalized combining rules for predicting transport properties of composites materials. *Compos. Sci. Technol.* **1985**, 22(1), 3-21.

[131] Ondracek, G. The quantitative microstructure-field property correlation of multiphase and porous materials. *Rev. Powder Metall. Phys. Ceram.* **1987**, 3, 205-322.

[132] Broadbent, S. R.; Hammersley, J. M. Percolation process. *Proc. Camb. Philos. Soc.* **1957**, 53(3), 629-641.

[133] Kirkpatrick, S. Percolation and conduction. *Rev. Mod. Phys.* **1973**, 45, 574-588.

[134] Katsura, T.; Kamal, M. R.; Utracki, L. A. Electrical and thermal properties of polypropylene filled with steel fibres. *Adv. Polym. Tech.* **2003**, 5(3), 193-202.

[135] Weber, M.; Kamal, M. R. Estimation of the volume resistivity of electrically conductive composites. *Polymer Composites* **2004**, 18(6), 711-725.

[136] Logakis, E.; Pissis, P.; Pospiech, D.; Korwitz, A.; Krause, B.; Reuter, U.; Potschke, P. Low electrical percolation threshold in poly(ethylene terephthalate)/multi-walled carbon nanotube nanocomposites. *Euro. Polym. J.* **2010**, 46(5), 928-936.

[137] Balberg, I.; Anderson, C. H.; Alexander, S.; Wagner, N. Excluded volume and its relation to the onset of percolation. *Phys. Rev. B* **1984**, 30, 3933–3943.

[138] Garboczi, E. J.; Snyder, K. A.; Douglas, J. F.; Thorpe M. F. Geometrical percolation threshold of overlapping ellipsoids. *Phys. Rev. E* **1995**, 52, 819–828.

[139] Saar, M. O.; Manga, M. Continuum percolation for randomly oriented soft-core prisms. *Phys. Rev. E* **2002**, 65, 056131.

[140] McAllister, M. J.; Li, J.; Adamson, D. H.; Schniepp, H. C.; Abdala, A. A.; Liu, J.; Herrera-Alonso, M.; Milius, D. L.; Car, R.; Prud'homme, R. K.; Aksay, I. A. Single sheet functionalized graphene by oxidation and thermal expansion of graphite. *Chem. Mater.* **2007**, 19(18), 4396-4404.

[141] Vavouliotis, A.; Fiamegou, E.; Karapappas, P.; Psarras, G.; Kostopoulos, V. Electrically conductive epoxies using multiwall carbon nanotubes. *Society of Plastics Engineers Plastics Research Online* **2010**.

[142] Hu, H.; Zhang, G.; Xiao, L.; Wang, H.; Zhang, Q.; Zhao, Z. Preparation and electrical conductivity of graphene/ultrahigh molecular weight polyethylene composites with a segregated structure. *Carbon* **2012**, 50 (12), 4596-4599.

[143] Pang, H.; Chen, T.; Zhang, G.; Zeng, B.; Li, Z. M. An electrically conducting polymer/graphene composite with a very low percolation threshold. *Mater. Lett.* **2010**, 64(20), 2226-2229.

[144] Mierczynska, A.; Mayne-L'Hermite, M.; Boiteux, G.; Jeszka, J. K. J. Electrical and mechanical properties of carbon nanotube/ultrahigh-molecular-weight polyethylene composites prepared by a filler prelocalization method. *Appl. Polym. Sci.* **2007**, 105(1), 158-168.

[145] Ciselli, P.; Zhang, R.; Wang, Z.; Reynolds, C. T.; Baxendale, M.; Peijs, T. Oriented UHMW-PE/CNT composites tapes by a solution casting-drawing process using mixed solvent. *Euro. Polym. J.* **2009**, 45(10), 2741-2748.

[146] Lisunova, M.; Mamunya, Y.; Lebovka, N.; Melezhyk, A. Percolation behaviour of ultrahigh molecular weight polyethylene/multiwalled carbon nanotubes composites. *Euro. Polym. J.* **2007**, 43(3), 949-958.

[147] Gao, J.; Li, Z.; Meng, Q.; Yang Q. CNTs/UHMWPE composites with a two-dimensional conductive network. *Mater. Lett.* **2008**, 62(20), 3530-3532.

[148] Zhang, C.; Ma, C.; Wang, P.; Sumita, M. Temperature dependence of electrical resistivity for carbon black filled ultra-high molecular weight polyethylene composites prepared by hot compaction. *Carbon*, **2005**, 43(12), 2544-2553.

[149] Bakshi, S. R.; Tercero, J. E.; Agarwal, A. Synthesis and characterization of multiwalled carbon nanotube reinforced ultra high molecular weight polyethylene composite by electrostatic spraying technique. *Composites Part A* **2007**, 38(12), 2493-2499.

[150] Rafiq, R.; Cai, D.; Jin, J.; Song, M. Increasing the toughness of nylon 12 by the incorporation of functionalized graphene. *Carbon* **2010**, 48, 4309-4314.

[151] Shahil, K. M.; Balandin, A. A. Graphene-multilayer graphene nanocomposites as highly efficient thermal interface materials. *Nano. Lett.* **2012**, 12(2), 861-867.

[152] Palza, H.; Kappers, M.; Hennrich, F.; Wilhelm, M. Morphological changes of carbon nanotubes in polyethylene matrices under oscillatory tests as determined by dielectrical measurements. *Compos. Sci. Technol.* **2001**, 71, 1361-1366.

[153] Cipriano, B. H.; Kota, A. K.; Gershon, A. K.; Laskowski, C. J.; Kashiwagi, T.; Bruck, H. A.; Raghaven, S. R. Conductivity enhancement of carbon nanotube and nanofiller-basedpolymer nanocomposites by melt annealing. *Polymer* **2008**, 49, 4846-4851.

[154] Skipa, T.; Lellinger, D.; Saphiannikova, M.; Alig, I. Shear-stimulated formation of multi-wall carbon nanotube net works in polymer melts. *Phys. Status. Solidi.* **2009**, 246, 2453-2456.

[155] Obrzut, J.; Douglas, J.; Kharchenko, S.; Migler, K. Shear-induced conductor-insulator transition in melt-mixed polypropylene-carbon nanotube dispersions. *Phys. Rev. B* **2007**, 76, 195420.

[156] Romano, D. *Influence of Catalytic Systems on the Synthesis of (Dis)entangled UHMWPE and Its Implication on Mechanical Properties.* PhD Thesis, Loughborough University, **2014**.

[157] Cheng, S.; Chen, X.; Hsuan, G. Y.; Li, C. Y. Reduced graphene oxide-induced polyethylene crystallization in solution and nanocomposites. *Macromolecules* **2011**, 45(2), 993-1000.

2 Rheological Response of High Density Polyethylene/Reduced Graphene Oxide Nanosheets Composites

Abstract

In this chapter, the rheological and electrical aspects of high density polyethylene/reduced graphene oxide nanoplatelets (HDPE/rGON) nanocomposites, and the influence of rGON on chain orientation and crystallisation behaviour after shear flow are investigated. Melt rheology reveals the presence of strong interaction between polymer chains and filler. Above 4.0 wt % of the filler concentration, the terminal region of frequency sweep shows changes in the linear viscoelastic properties of the composites. In particular, at these concentrations the G',G'' cross-over frequency at which the transition from predominantly elastic to viscous occurs is significantly displaced to lower values, indicating the formation of a solid-like percolated network. Electrical conductivity measurements suggest that, in the solid state, a continuous filler network forms at a filler concentration of approximately 4.5 wt %, slightly higher than the rheological percolation. The influence of chain-filler interaction on chain orientation and its influence on the crystallisation is followed by time resolved WAXS/SAXS. The orientation of the crystalline domains, quantified by the Herman's orientation factor, supports the presence of strong chain-filler interaction, an observation in accordance with the melt rheology. The Deborah numbers of reptation and retraction suggests that during the applied non-linear shear the composites experienced mild stretch which is not significant enough to induce crystallisation at high temperature (136 °C). However, restriction imposed by the filler on the chain mobility is pronounced enough to preserve the oriented state that could cause anisotropy in crystallisation upon cooling.

2.1 Introduction

Polymer nanocomposites with enhanced mechanical, electrical or thermal properties have been investigated intensively [1,2], and they have become one of the most important class of materials. The change in their properties is intimately related to the aspect ratio, microscopic arrangement of the disperse phase, chain-filler interaction, as well as the formation of filler-filler networks. For an example, the presence of filler could significantly influence the polymer chain dynamics consequently influencing crystallisation during shear flow and ultimately mechanical properties of the polymer [3,4]. Melt rheological studies have revealed that the presence of nanoparticles in polymers perturbs the microscopic inter-chain arrangement of the polymer network, influencing the matrix's rheological properties. Understanding the influence of nanofillers on polymer dynamics is crucial for the design and process of nanocomposites with desired properties, for example decrease in entanglement density and ease in processability by incorporating nanofillers [5,6,7,8,9]. It has also been reported that a strong shear flow, with *De* ($\tau_{retraction} \times \dot{\gamma}$) > 1, plays a crucial role in the polymer chain stretching and orientation, resulting in the formation of highly anisotropic, oriented structures upon crystallisation [10,11], for instance, shish-kebab composing two distinctive structures have been observed under flow condition [10]: a shish structure, formed by extended chains, and a kebab structure originating from polymer chains attached to the shish. Important to notice is that, in the presence of nanoparticle, the shish-kebab structure that arises from the significant chain stretch and orientation can be enhanced [10]. However, the influence of the filler on the enhancement at mild shear flow stays unclear, especially for the fillers which have significant interaction to PE chains, graphene for instance [5]. Recently, graphene has attracted considerable attention due to its remarkable electrical, thermal and mechanical properties [12,13,14,15] and its potential in developing high performance nanocomposites. Due to its very high aspect ratio [16] and theoretical specific surface area – 2630 m^2/g [17], graphene is capable of modifying the material properties at very low loadings. For example, 0.028 vol % of graphene in UHMWPE is reported to produce a composite having electrical conductivity [18]. In addition, low graphene concentration could hinder polyethylene chain dynamics causing drop in complex viscosity [5].

In this chapter, following a two-step preparation method, the HDPE/rGON composites are prepared [5]. To recall, combination of the stability of GON dispersion in water and the ease in reduction of GON by heat treatment allows the homogeneous dispersion of the nanosheets

in the polymer matrix. The influence of rGON on chain orientation during shear deformation and subsequent crystallization is investigated by time-resolved WAXD/SAXS studies. These findings are linked with rheological response of the composites.

2.2 Experimental

2.2.1 Materials

Graphene oxide nanosheets (GON) were prepared using a modified Hummers method [19] followed by further modifications [5]. Materials for the synthesis of GON were purchased from Sigma-Aldrich: fine graphite powder (diameter of c.a. 25 μm), 98 wt % concentrated sulphuric acid, distilled water, potassium permanganate, and 30 wt % hydrogen peroxide. HDPE (in the form of fine powder) was purchased from Dow Chemicals. All the reagents were used as received. The estimation of molar mass (*M*w) and molar mass distribution (MWD) of HDPE was carried out by melt rheology using an Advanced Rheometrics Expansion System (ARES) rheometer. The molar mass parameters were calculated using an Orchestrator software based on refs [20,21,22] and the results are shown in Figure 2-1.

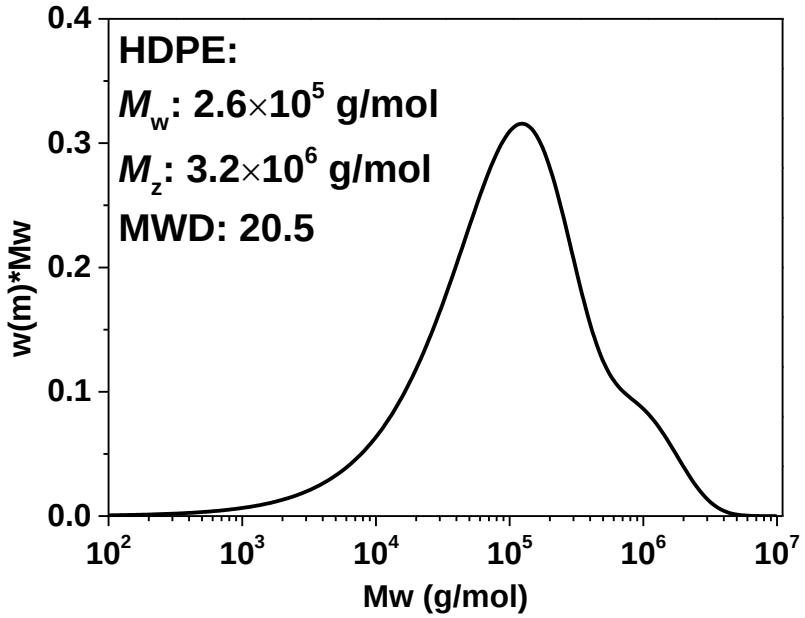

Figure 2-1 Estimation of M_w and MWD of HDPE by melt rheology; M_w: molar mass, M_z: higher average molecular weights, MWD: molar mass distribution.

2.2.2 Preparation of Graphene Oxide Nanoplatelets (GON) and Reduced Graphene Oxide Nanoplatelets (rGON)

2.2.2.1 Preparation of GON

The synthesis of graphene oxide has been performed according to a modified Hummers method [23,24], combined with further modifications, described as follows. A 1.5 l jacketed reactor was equipped with a magnetic stirrer, a temperature probe, and the two inlets were connected with a separating funnel and a reflux tube, respectively. The temperature was controlled by a chiller through oil circulation in the jacket. 300 ml of 98 wt % concentrated sulphuric acid was transferred to the reactor followed by the addition of 10 g of graphite powder. 40 g of $KMnO_4$ was then slowly added in, keeping the exothermic reaction at a temperature comprised between 25 and 30 ºC. Once the addition was completed, the system was heated up to 40 ºC and kept under stirring for 40 min. Subsequently, 600 ml of distilled water were slowly added to the reactor through a separating funnel and the mixture was maintained at 100 ºC under stirring for 90 min. The reaction was quenched using 50 ml of 30 % H_2O_2 in 200 ml of distilled water.

After the oxidation reaction, the resultant material was repeatedly vacuum-filtered and washed, 3 times with 5 wt % HCl and a few times with distilled water, until the upper liquid became dark. The suspension became darker with the increasing number of washing steps, suggesting progressive extraction of GON from the bottom layer to the upper suspension. The average number of water washing steps applied was approximately ten, until the pH of the suspension changed from ~ 2 to ~ 7. The dark-liquid portions were combined and dried in a petri dish at 50 ºC for 2 days. Films of GON were obtained by peeling them off from the petri dish.

2.2.2.2 Preparation of rGON

The GON films having dimensions of approximately 5 cm × 1 cm × 20 cm were reduced to rGON using a combination of temperatures and pressures: 83 bars for 1 min, 415 bars for 5 min, 1245 bars for 15 min and 1660 bars for 5 min at temperatures of 160 ºC, 180 ºC, 200 ºC and 230 ºC, respectively.

2.2.3 Preparation of HDPE/rGON Nanocomposites

HDPE/rGON nanocomposites were obtained by a two-step preparation method: step 1) the required amount of GON was weighed and re-dispersed in 40 ml of water followed by 15 min ultrasonication, while the required amount of HDPE powder was suspended in acetone and kept under magnetic stirring. The ultrasonicated GON water suspension was added to the acetone-suspended HDPE. The mixture was kept under magnetic stirring in a fume cupboard until most of the solvent evaporated and the resultant solid was further dried in a vacuum oven at 40 ºC for at least 12 hours. During step 2), the powders prepared in step 1) were compression-moulded at 160 ^{o}C with the pressure reaching 1660 bars in a hydraulic press to simultaneously achieve the reduction of the GON to rGON and prepare suitable specimens for rheology, WAXD/SAXS and electrical conductivity measurements. To all the samples, 1.0 wt % anti-oxidant (Irganox 1010, Ciba) was added to avoid possible oxidation or thermal degradation of polymer matrices during compression moulding, rheological analysis or X-ray characterisation. Composites having 0.0 wt %, 0.1 wt %, 0.3 wt %, 0.5 wt %, 0.8 wt %, 2.0 wt %, 4.0 wt %, 4.5 wt %, 5.0 wt % and 6.0 wt % of rGON in HDPE were prepared using this method.

2.2.4 Characterisation

A JEOL-2000FX Transmission Electron Microscope (TEM) was used to observe the exfoliation state of GON in water with an applied voltage of 200 kV. A bench top D2 X-ray Diffraction (XRD) with a radiation wavelength of CuKα 0.154 nm was used to characterise the oxidation state of the GON and 2θ angles from 1º to 30º were scanned.

Electrical conductivities of HDPE/rGON composites were measured with a Keithley instrument composed of a 6220 precision current source and a 2182A nanovoltmeter; the geometry of the samples was corrected by taking into account the geometric factors according to ref [25].

All linear rheological characterisations were performed in an ARES-LS2 rheomoter (TA instruments) using a 25 mm parallel plate geometry. Melt state measurements were performed at an isothermal temperature of 160 °C under nitrogen atmosphere inside a convection oven. A short dynamic time sweep with strain of 0.1 % was performed to reach

equilibrium state of the sample and then followed by dynamic frequency sweep test with angular velocities ranging from 0.001 to 100 rad/s at a constant strain of 0.5 % within the linear viscoelastic regime of the samples.

Time-resolved wide angle X-ray diffraction and small angle X-ray scattering (WAXD/SAXS) experiments were performed on the beamline BM26/DOUBBLE at the European Synchrotron Radiation Facility (ESRF) in Grenoble, France. WAXD patterns were recorded by a Frelon detector placed approximately 89 cm away from the sample. The wavelength of the X-ray applied was 0.103 nm. Background of dark current was subtracted from each WAXD pattern before analysis. SAXS patterns were recorded by a Pilatus detector placed approximately 6.07 m from the sample. A vacuum chamber was placed in between the detector and sample to minimise the absorption and scatter of X-rays from air or dust. The wavelength of the X-ray applied was 0.103 nm. A Linkam Shear Cell (CSS-450) equipped with diamond windows was applied to carry out the shear flow experiments followed by the time resolved WAXD/SAXS. The shear cell was placed perpendicular to the beamline direction. Two protocols were applied to investigate the influence of shear on the polymer chains in the presence of rGON, as schematically shown in Scheme 2-1 and Scheme 2-2.

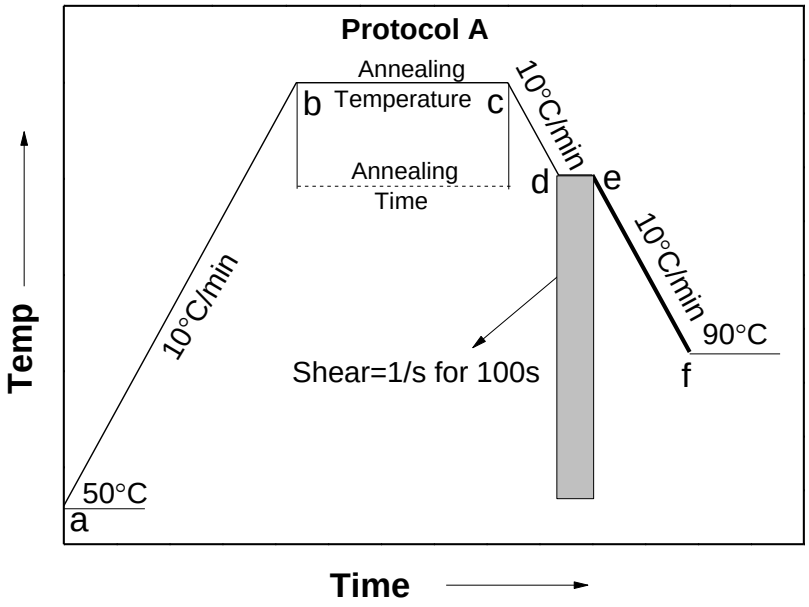

Scheme 2-1 The schematic representation of shear and temperature profiles during the WAXD/SAXS experiments of Protocol A.

(a-b) Heating from 50 °C to the annealing temperature 160 °C at 10 °C/min, higher than the equilibrium melting point 141.5 °C of linear polyethylene [26];

(b-c) Annealing at 160 ^{o}C for 5 min with the aim to remove the sample's thermo-mechanical history;

(c-d) Cooling from 160 ^{o}C to the shear temperature of 136 °C at 10 °C/min;

(d-e) Once the set shear temperature is reached, shear for 100 s at a fixed rate of 1 /s;

(e-f) Cooling from 136 °C to 90 °C at 10 °C/min and recording WAXD/SAXS images every 15 s.

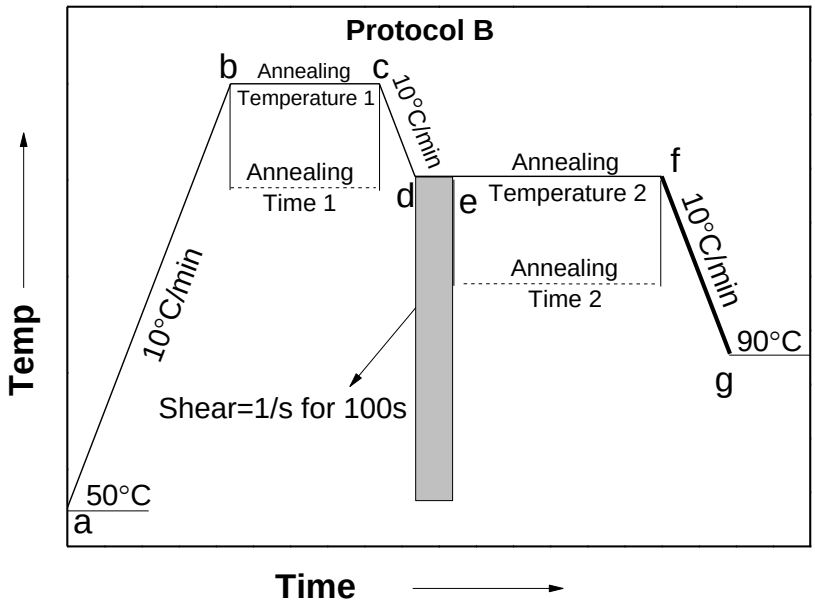

Scheme 2-2 The schematic representation of shear and temperature profiles during the WAXD/SAXS experiments of Protocol B.

(a-b) Heating from 50 °C to the annealing temperature 160 °C at 10 °C/min;

(b-c) Annealing at 160 °C for 5 min with the aim to remove the sample's thermo-mechanical history;

(c-d) Cooling from 160 °C to the shear temperature of 136 °C at 10 °C/min;

(d-e) Once the set shear temperature is reached, shear for 100 s at a fixed rate of 1 /s;

(e-f) Isothermal annealing at 136 °C for 10 min after cycle (d-e) finishes;

(f-g) Cooling from 136 °C to 90 °C at 10 °C/min and recording 2D WAXD/SAXS images every 15 s.

The orientation of polymer crystals are estimated by calculating Herman's orientation factor f_h using equation 2-1 [27],

$$f_h = \frac{1}{2}\{3 < cos^2\emptyset > -1\} \qquad \text{(Equation 2-1)}$$

where f_h is the Herman's orientation factor, $< cos^2\emptyset >$ is the average cosine squared weighted by the intensity as a function of the radial angle for the oriented plane for WAXD and it can be calculated from equation 2-2 [27],

$$< cos^2\emptyset > = \frac{\int_0^{90} I(\theta) cos^2\theta sin\theta d\theta}{\int_0^{90} I(\theta) sin\theta d\theta} \qquad \text{(Equation 2-2)}$$

where $I(\theta)$ is the intensity of the planes normal to *c*-axis and θ is the azimuthal angle. Herman's orientation factors give a good qualitative estimation of the average crystal orientation. The value of f_h may vary between -0.5 and 1.0 for perpendicular and parallel crystal plane orientation with respect to the flow direction, respectively.

2.3 Results and Discussion

2.3.1 Characterisation of GON

The modification of Hummers' method hereby presented for the synthesis of GON has two main advantages compared to other methods reported in the literature. First, the oxidation does not produce toxic gases [28], as no HNO_3, $NaNO_3$ or $KClO_3$ are used, while all the three methods of Brodie [29, 30], Staudenmaier [31] and Hummers [32] involve the liberation of gases such as NO_2, N_2O_4 or ClO_2 [35]. The possibility of avoiding the use of $NaNO_3$ has been reported by Liu *et al.* [33] as a possible route to prepare graphene oxide. Different to their method, we have decided to perform additional washing steps of the oxidised material using distilled water. After several washing, the separation of different layers was observed; the top layer constitutes of graphene oxide was well dispersed in water, forming a stable suspension,

whereas the bottom layer contained big lumps of both oxidised and un-oxidised material. Figure 2-2 shows the comparison between the filtered bottom layer and the dried top layer (see experimental section) re-suspended in water at concentrations similar to that before drying. The re-suspended solutions are subsequently ultrasonicated at room temperature for 15 minutes. The material coming from the top layer can be easily re-dispersed in water and it shows retention of a homogeneous suspension even after 3 days without aggregation, while the bottom layer even on ultrasonication tends to quickly aggregate and precipitate. The presence of a stable suspension suggests that oxidation and exfoliation of graphite are comparable to the observations reported in the literature for GON made by the Hummers method [34, 35]. After the analysis of the layers with the methods described in the experimental section, it becomes apparent that the stable suspension obtained from the top layer contains well exfoliated nanosheets of graphene oxide, as observed by TEM (Figure 2-2b) while the bottom layer mainly contains lumps (Figure 2-2c). The vast majority of the sheets from the top layer have dimensions in the range of hundreds of nanometres to a few micrometres and from the edges we can appreciate a number of stacked layers comprised between 2 and 5 [36]. A mono-layer was captured and is shown in Figure 2-2d.

This procedure allows the removal of big sized, un-oxidised graphite or un-exfoliated graphite oxide and direct access to a homogeneous exfoliated suspension of GON in water, making the dispersion of GON in other matrices more environmentally friendly. The GON film obtained after the drying process appears to be brownish, as viewed by direct visual observation and shown in Figure 2-2e. The darker regions correspond to a thickness of approximately 6 μm and the lighter regions to ~1 μm. As expected, the film thus obtained is electrically insulating due to disruption of pi-pi bonds after oxidation [37]. The film after reduction (Figure 2-2f) turns dark, becomes brittle, and electrical conductive, as expected by the partial restoration of the pi-pi bonds.

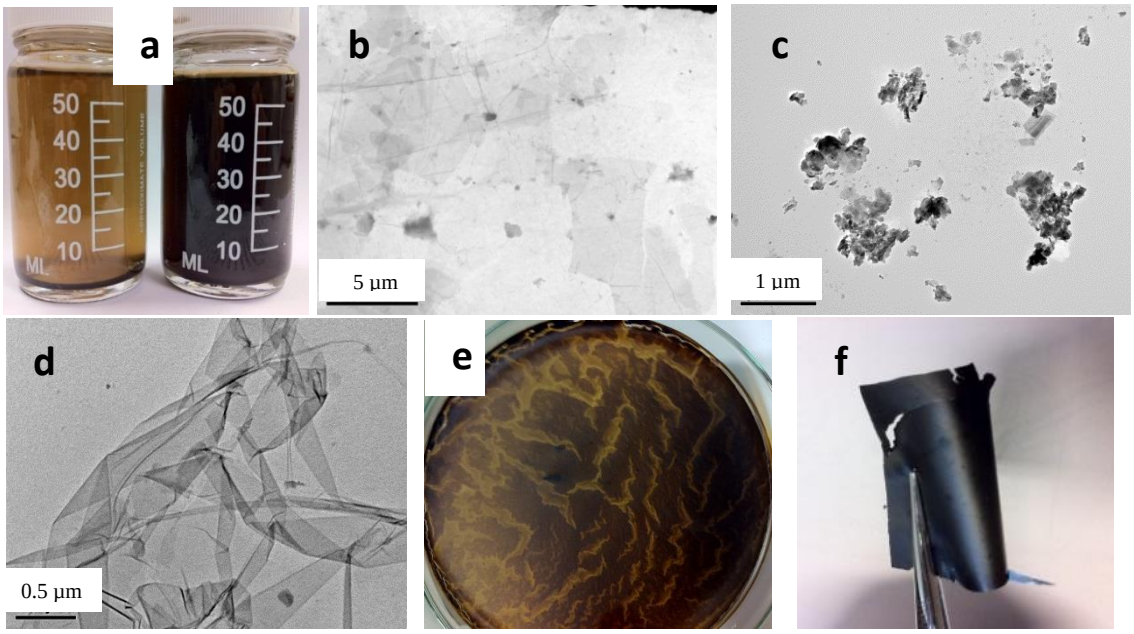

Figure 2-2 (a) Ultrasonicated bottom layer (on the left) and top layer (on the right) in distilled water after 3 days of re-dispersion; TEM images of **(b)** top layer and **(c)** bottom layer in water after ultrasonication; **(d)** few layers stacked GON; **(e)** GON film obtained from static evaporation of solvent; **(f)** rGON film after thermal reduction.

The XRD spectrum of the GON film shown in Figure 2-3a, in red, clearly shows that the sharp intense peak of graphite at $2\theta = 26.28º$, referring to X-ray diffraction from the (002) planes, has disappeared and a broader, shorter peak is now found at $2\theta = 11º$, indicating the disruption of the regular stacked structure and expansion of layer distance due to oxidation. The basal spacing between GON layers increases from 0.335 nm to 0.749 nm, and is comparable to the values reported in the literature: following the Hummers method, the spacing between GON layers was found to be in between 0.691 nm [38] and 0.840 nm [39,40]. Further insight on the nature and relative abundance of the bonds formed after oxidation was obtained with FT-IR and XPS. From the FT-IR spectrum shown in Figure 2-3b it is possible to attribute the peak at 3400 cm^{-1} to O-H stretching (due to OH groups or absorbed water), the peak at 1730 cm^{-1} to the stretching of carbonyl groups, the peak at 1620 cm^{-1} to C=C stretching, and peaks at 1222 and 1053 cm^{-1} to C-O stretching vibration of C-OH and C-O-C [41,42,43], respectively. In the spectrum of pure graphite, no peaks at 1730 cm^{-1} 1222 cm^{-1}, and 1053 cm^{-1} are observed [44], indicating the success in oxidising graphite using the modified Hummers method.

From the XPS spectrum shown in Figure 2-3c the presence of carbon-oxygen bonds is confirmed and it is possible to get the C/O atomic ratio by fitting the peaks located at 284.58

eV, 286.68 eV and 289.24 eV, and attributed to C-C/C-H, C=O and O-C=O bonds, respectively. A value of 2.09 for the C/O atomic ratio is calculated from the fitting and it is in accordance with previously reported values [45]. As comparison, only sp^2 C-C/C=C peak is observed in pure graphite/graphene [46].

The thermal stability of GON is studied by thermo-gravimetric analysis (TGA): the spectrum, as shown in Figure 2-3d, and the corresponding first derivative show a fast weight loss at 231 ºC and 565 ºC. The loss at 231 ºC is attributed to the liberation of oxygen in the form of CO and CO2 [47,48,49] while the loss at 565 ºC is due to decomposition of the basal carbon layers. These results are in line with those previously reported by Stankovich *et al.* [50], Marcano *et al.* [51] and Some *et al.* [52]. In the case of graphite, there is only one step of weight loss commencing from high temperature of c.a. 750 °C [53].

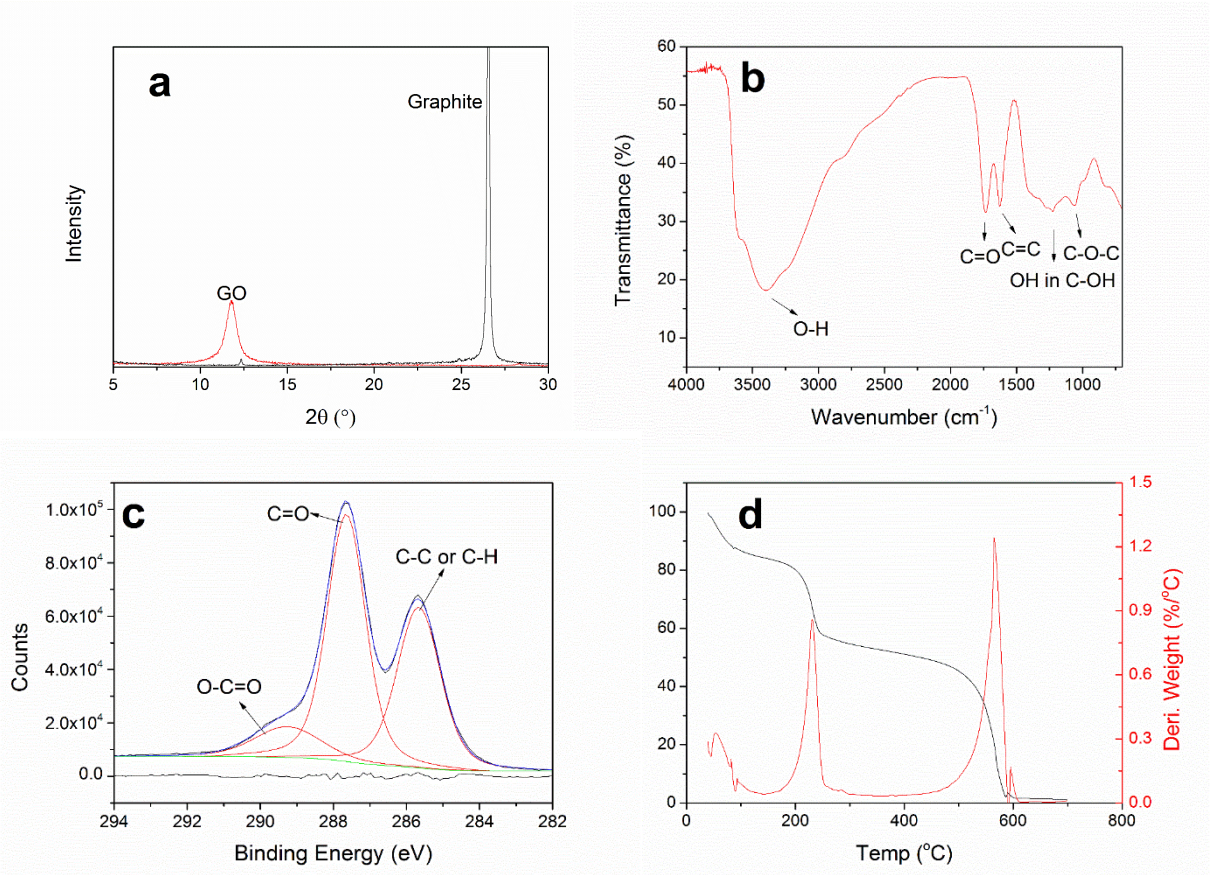

Figure 2-3 **(a)** XRD spectra of graphite powder and GON; **(b)** FTIR spectrum of GON film; **(c)** C1s high resolution XPS spectrum of GON; **(d)** TGA spectrum and first derivative of TGA spectrum of GON.

These results conclusively demonstrate the successful exfoliation and oxidation of graphite attained with the proposed method.

To achieve electrical conductivity, it is essential that the GON should be reduced to restore the pi-pi bonds. However, reducing the GON prior to its addition to the polymer prevents its homogeneous dispersion in water. For this reason, the GON is added to the polymer in its oxidised form first and the resulting composite is subjected to the desired heat treatment under pressure, with the advantage that in one step the filler is reduced and composite sheets with enhanced filler dispersion for further testing are prepared. In order to get an indication of the degree of reduction obtained with the heat treatment, the plain GON film was pressed at different temperatures for 26 min under variable pressures. The electrical conductivity of reduced GON (rGON) is measured with the four-point probe technique, and a plot of the conductivity of rGON against the reduction temperature is shown in Figure 2-4, together with the TGA curve of GON. The average electrical conductivity of rGON on heat treatment at 160 ºC is 76.1 ± 19.2 S/m, and the conductivity increases with increasing the reduction temperature. rGON reduced at 230 ºC reaches the highest value of 532.0 ± 5.7 S/m and is in trend with the TGA curve, in which the fastest weight loss due to reduction occurs at 231 ºC. For comparison, Tour and coworkers found conductivities of 210 ± 140 S/m for rGON synthesised from Hummers method when the sample was reduced at 300 ºC for 30 min [54]. To avoid oxidation or degradation of the polymer matrix, 160 ºC is initially chosen for the preparation of PE/rGON composites. The absence of oxidation or degradation became apparent on investigating the rheological and thermal response of the composites that were treated at and above 160 °C.

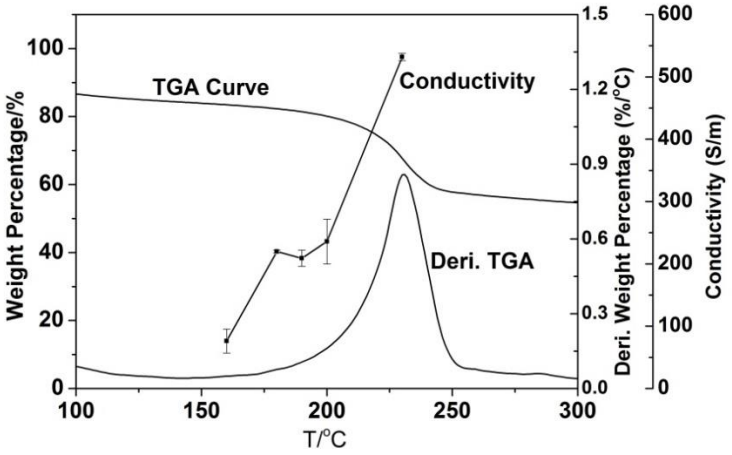

Reduction Temperature (°C)	Conductivity (S/m)
160	76.±19.2
180	219.8±2.4
190	209.2±13.1
200	235.9±35.9
230	532.0±5.7

Figure 2-4 On the left it shows electrical conductivities of reduced graphene oxide against reduction temperatures, together with the TGA curve. On the right, the table summarises electrical conductivity versus the reduction temperature.

2.3.2 Rheological Response and Electrical Conductivity

Linear oscillatory rheology is a well-established technique in the study of polymer-based nanocomposites [55]. Absolute values of the storage (*G'*) and loss (*G''*) moduli, as well as their frequency dependence, reveal details of the structure of the disperse phase and its interaction with the polymer matrix.

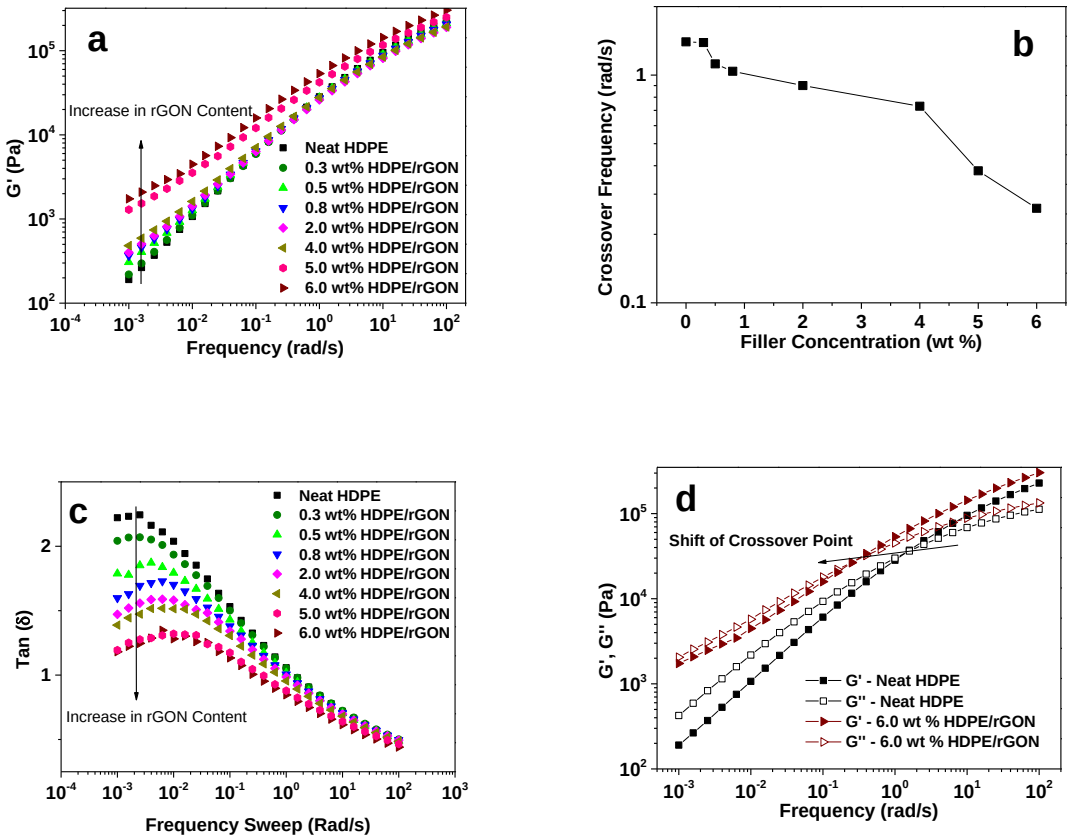

Figure 2-5 (a) Storage modulus (*G'*) of HDPE/rGON composites as a function of frequency; **(b)** *G'*/*G''* cross-over frequencies of HDPE/rGON composites having different filler content; **(c)** corresponding damping factor tan (δ), as a function of frequency for HDPE/rGON composites. The phase angle is obtained from the frequency sweep data in **(a)**; **(d)** shift of cross-over point from plain HDPE to 6.0 wt % HDPE/rGON nanocomposite. The measurements were carried out in isothermal conditions at 160 ºC.

Figure 2-5a shows storage modulus (*G'*) of the samples with different filler concentrations as a function of angular frequency. Due to the higher elastic modulus of rGON compared to the polymer melt, the absolute value of *G'* increases progressively with increasing filler content,

up to 6.0 wt % in the terminal region (frequency<1.0 rad/s). The increase of *G'* is evident at the lower frequencies where a distinct change in both *G'* values and the slope is observed once the filler content increases from 4.0 to 5.0 wt %. Similar changes have been reported in an earlier study where carbon nanotubes (CNT) composites were investigated [56]. Another indication concerning influence of the filler on the polymer matrix is the *G'/G"* cross-over frequency, which reflects the transition from predominantly elastic to viscous behaviour in the visco-elastic polymer melt. In a plain polymer melt at equilibrium state, this point is related to the chain constraint renewal time by the so-called reptation dynamics [57]. In Figure 2-5b, a gradual shift in cross-over point to lower frequencies with the increasing filler content up to 4.0 wt % is observed. Beyond 4.0 wt %, significant shift in the cross-over frequency to lower values occurs, suggesting that the presence of the filler restrains the relaxation of polymer chains by arresting the chain segments. The dramatic shift in the cross-over frequency from 4.0 wt % to 5.0 wt % is attributed to the formation of a solid-like network arising from the close connectivity of rGON, considered as rheological percolation. Similar results from HDPE/CNTs composites have also been reported in earlier studies [56,58,59]. It is further noticed that by increasing the filler concentration, Figure 2-5c, the decrease in the absolute value of the damping factor (tan (δ) = *G"/G'*) becomes more evident at the low frequency range (<0.1 rad/s). It is noticeable that at low frequencies, composites having high filler concentration tends to form a second cross-over point, corresponding to the presence of a weak network arising from the percolation of rGON sheets, as supported from the frequency sweep of 6.0 wt % HDPE/rGON sample shown in Figure 3d. Similar observations have been reported in the composites of polycarbonate/CNTs [60], where the authors reported significant increase in *G'* at low frequencies as the CNT content increases and consequently causes the appearance of a second cross-over point at low frequencies.

Figure 2-6 shows change in the elastic modulus recorded at different frequencies of the composites having different filler concentrations. For comparison, two frequencies above (1.6 and 10 rad/s) and two frequencies below (0.01 and 0.001 rad/s) the cross-over point (0.2-1.0 rad/s) of elastic and viscous moduli have been chosen. From the data, it is apparent that for the frequencies above the cross-over point the elastic modulus is nearly independent of the filler concentration, whereas the strong influence of filler concentration on modulus at frequencies below the cross-over point, close to the terminal region is observed. The dependence of the elastic modulus on the filler concentration, below the cross-over point, suggests that due to the interaction of polyethylene chains with rGON, the chain dynamics is

influenced by the interaction of polyethylene chains to rGON to an extent that the viscous response of the visco-elastic polymer melt is significantly increased.

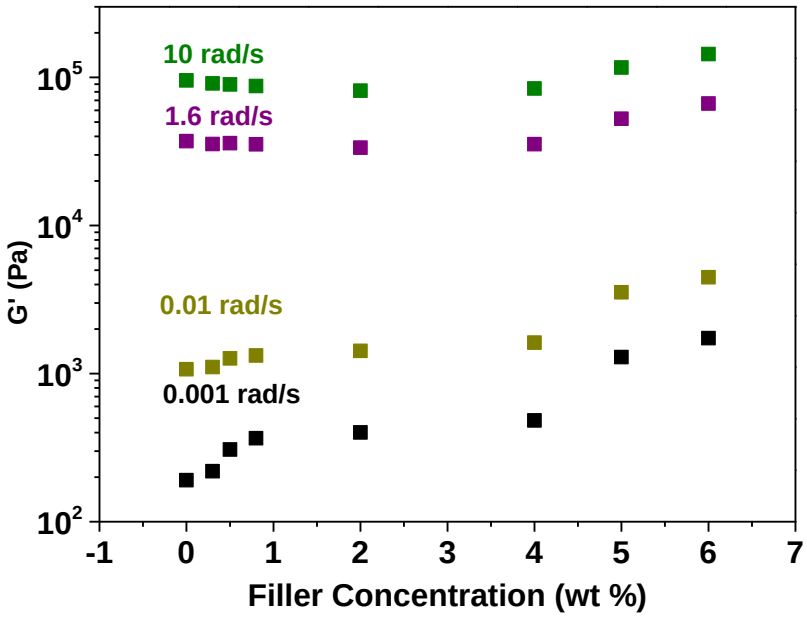

Figure 2-6 Storage modulus (*G'*) of HDPE/rGON nanocomposites recorded at different frequencies for a range of filler concentrations. Two frequencies of 10 rad/s and 1.6 rad/s are chosen above the cross-over frequencies (0.2-1.0 rad/s), whereas the other two frequencies of 0.01 rad/s and 0.001 rad/s are chosen below cross-over frequencies. From the data, plotted on the logarithmic scale, it is apparent that the elastic modulus at low frequencies increases with the increase in filler content at low concentrations (<1.0 wt %).

The electrical conductivity percolation found at c.a. 4.5 wt % of filler concentration, as shown in Table 2-1, is close to rheological percolation, at 4.0 wt %. The small difference between the two values of percolation thresholds can be attributed to the different percolation mechanisms. The electrical percolation threshold is defined as the minimal concentration of the conductive filler at which a sudden increase in conductivity of the insulating matrix appears. This requires a continuous filler-filler network. It is to be noted that network facilitates the tunnelling/hopping effect of electrons, contributing to the electrical conductivity [61]. However, the tunnelling/hopping effect itself is not significant enough to make a remarkable increment. Assuming the electron hopping mechanism in graphene/polymer composites is similar to that of CNT/polymer, the connectivity between

neighbouring rGON should be less than 5 nm for the hopping to occur [56]. Whereas for the rheological percolation, the connecting distance between the neighbouring rGON has to be less than 10 nm, that is the average diameter of Gaussian coil in polymer melt, (*i. e.* it is a combined filler-polymer-filler network rather than a continuous filler-filler network, that dominates the rheological properties [62,63]): this implies the possibility for the rheological percolation to appear at slightly lower loading of the filler. A similar difference was also observed and reported in earlier studies on CNT/HDPE composites [56,63].

Table 2-1 Electrical conductivity of the samples.

Filler concentration (wt %)	**Semi-Conductivity (S/m)**
Plain (0 wt %)	1×10^{-18} [64]
≤ 4.0	N/A
4.5	**4.5×10^{-6}**
5.0	6.4×10^{-3}
6.0	3.6×10^{-3}

2.3.3 Wide Angle X-ray Scattering on HDPE/rGON Composites under Flow

It is well established that flow plays a crucial role in the extension and orientation of polymer chains, resulting in the formation of highly anisotropic, oriented structures upon crystallisation [65,66]. Nanofillers are known to have a noticeable influence on chain extension and orientation influencing relaxation dynamics. The non-equilibrium, constrained melt serves as precursors for crystallisation. To have insight on the influence of rGON on the polymer melt after application of non-linear shear, we monitored the Herman's orientation factor of the samples by WAXD following Protocols A and B depicted in Scheme 2-1 and Scheme 2-2, respectively. The calculation is mentioned in the experimental part. The difference in the schemes is on the annealing time after the application of shear in melt.

Figure 2-7a and Figure 2-7b illustrate the Herman's orientation factor for diffraction planes (110) and (200) of polyethylene crystals. These values are determined by integrating the diffraction patterns recorded on following the Scheme 2-1, where the samples were cooled

immediately after the application of shear. From figures it is apparent that the diffraction planes (110) and (200) exhibit the flow induced orientation for both neat polymer and the composites. However, the absolute value of the orientation factor in the composites is higher than that in the neat sample and it becomes more pronounced with increasing rGON concentration, indicating that the presence of rGON enhances the orientation during flow.

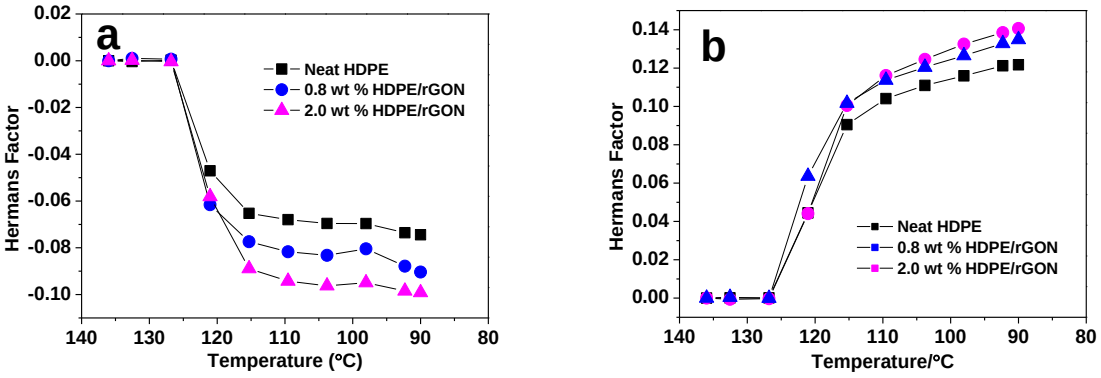

Figure 2-7 Herman's orientation factor f_h of polyethylene's diffraction planes, (110) **(a)** and (200) **(b)** as a function of temperature recorded on cooling, with and without rGON, after application of shear (**Scheme 2-1**).

In the neat sample the cause of the orientation can be attributed to higher relaxation time of the higher molar mass component compared to the low molar mass component in the sample having broad polydispersity. The reptation time determined from the cross-over point of the sample is approximately 1 s, Figure 2-5b. After shear, most of the low molar mass polymer chains in the neat sample tend to relax; however the long chain components stay oriented, resulting in anisotropic structure of the crystallised material. However, the enhancement of anisotropy in the composites is dependent on the filler content. After shear, the mobility of chains is highly restricted by the filler-chain interaction. With increasing filler concentration, more polymer chains are hindered and hence the orientation becomes more pronounced. The corresponding WAXD patterns of the samples recorded at 90 °C after cooling are illustrated in Figure 2-8 where anisotropic rings of (110) and (200) diffraction planes are observed in neat as well as its composite samples. The inner (110) diffraction plane, shows equatorial arcs representing chain orientation along the flow direction. The outer (200) diffraction plane shows meridian arcs indicating crystal plane orientation perpendicular to the flow direction.

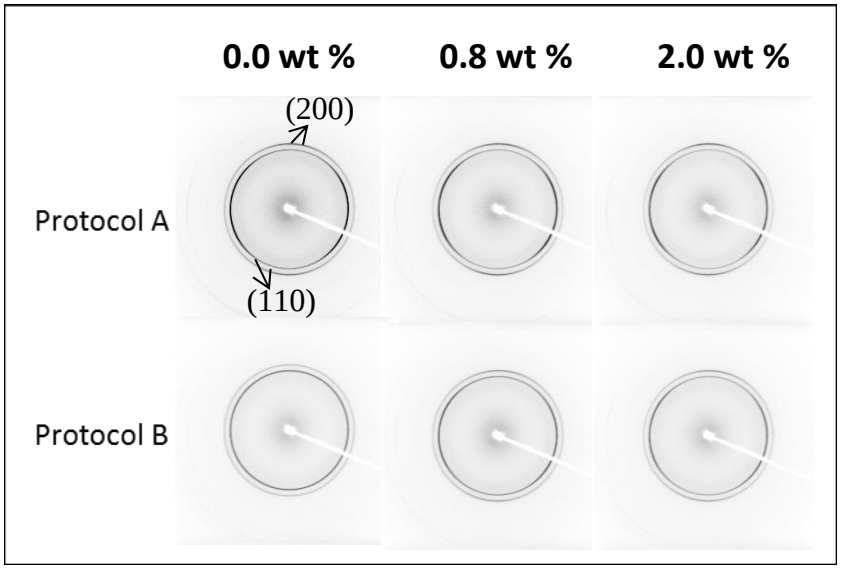

Figure 2-8 WAXD patterns of the HDPE samples recorded at 90 °C following protocols depicted in **Scheme 2-1** and **Scheme 2-2**, respectively.

To follow the influence of annealing time on relaxation after the application of shear, Protocol B depicted in Scheme 2-2 is followed. The samples are left to anneal under isothermal condition, at 136 °C for 10 min, after the application of shear. Figure 2-9a and Figure 2-9b depict the Herman's orientation factors of neat HDPE and its composites. It is evident from the figures that the orientation factor for neat HDPE is close to zero, which represents the isotropic state, whereas the composites show non-zero values that become more pronounced with increasing the filler concentration.

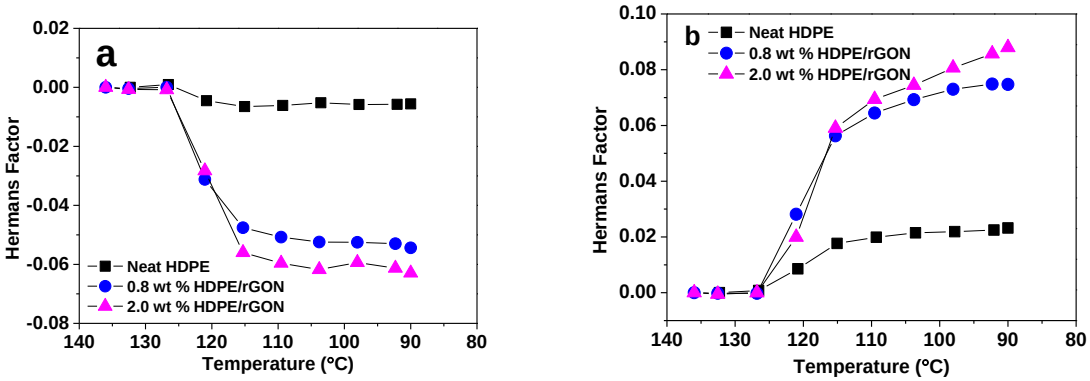

Figure 2-9 Herman's orientation factor (*f*h) of polyethylene's (110) diffraction plane **(a)**, and (200) diffraction plane **(b)** as a function of temperature during cooling, with and without rGON, obtained on following the Protocol B depicted in **Scheme 2-2**.

Figure 2-5b shows the cross-over point for neat HDPE from elastic to viscous behaviour at ~1.0 rad/s, *i.e.* the relaxation time for most of the chains is approximately 1s. Thus the 10 min of the isothermal annealing time after application of shear at 136 ºC is likely to be long enough for the relaxation of chains in neat HDPE, as supported by Figure 2-9a. On the contrary, using the same protocol in the presence of the filler, considerable orientation is maintained. This observation is in line with the shift in the cross-over point reported in Figure 3b. The experiments suggest the idea that chains having interaction with the filler are unable to adopt the random coil conformation and maintain orientation even after isothermal annealing in melt for 10 min. These unrelaxed oriented chains contribute to the formation of non-equilibrium oriented domains, which enhances crystallisation followed by the development of highly anisotropic structure. The influence of the filler concentration on chain orientation is evident. Their corresponding 2D patterns recorded at 90 °C, after the shear, isothermal treatment and crystallization, are shown in Figure 2-8 where the neat sample shows an isotropic pattern whereas the composites show orientation for both (110) and (200) diffraction planes, indicating chain orientation due to strong chain-filler interaction that hinders the relaxation of chains.

2.3.4 The Deborah Numbers

To quantify the effect of flow on the microscopic chain conformation and to understand whether there is significant chain stretch occurring during applied shear that could cause flow induced crystallisation [66], the Deborah number accounting for the chain stretch relaxation and reorientation processes is calculated. Chain stretching refers to configurations where the length of the occupied tube departs from its equilibrium state [67], while reorientation occurs by reptation dynamics.

The Deborah number proposed by Reiner, describes a non-dimensional number that distinguishes how a particular material behaves within a given time scale [68], as shown in equation (3).

$$De = \frac{t_{rel}}{t_{obs}} \qquad \text{(Equation 2-3)}$$

where t_{rel} refers to time required for material to relax and t_{obs} refers to the time of observation. *De* has been applied in shear flow to investigate the crystallisation behaviour of stretched chains in flow induced crystallisation (FIC) [66]. For this purpose, two time scales, τ_{rep} and τ_s,

where τ_{rep} refers to reptation time associated with the reptation process and orientation and τ_s refers to chain retraction time associated with the relaxation time of the chain retraction, have been proposed to quantify the orientation and stretch using two Deborah numbers described in equations 2-4 and 2-5, respectively, for the applied shear rate.

$$De_{rep}=\tau_{rep}\times\dot{\gamma} \quad \text{(Equation 2-4)}$$

$$De_{s}=\tau_{s}\times\dot{\gamma} \quad \text{(Equation 2-5)}$$

In the equation, τ_{rep} is the longest reptation time (terminal relaxation time), recently, proposed by Likhtman and McLeish [69], displayed as equation 2-6.

$$\frac{\tau_{rep}}{\tau_d} = 1 - \frac{3.38}{Z^{0.5}} + \frac{4.17}{Z} - \frac{1.55}{Z^{1.5}} \quad \text{(Equation 2-6)}$$

where τ_d is the reptation time or disengagement time in the absence of fluctuations, given by $3Z^3\tau_e$ and Z is the number of entanglements per chain, $Z=M_z/M_e$, of high molecular weight chains (HMW) with M_e=828 g/mol [70] and $M_z=3.2\times10^6$ g/mol, Figure 1. The retraction time, τ_s, is obtained by $Z^2\tau_e$ [57]. Equilibrium time at 136 °C, $\tau_e=1.75\times10^{-8}$ s, is extrapolated from the equilibrium state at 190 °C (7×10^{-9} s) using time-temperature superposition principle of Arrhenius dependence empirical expression with activation energy, E_a=26.7 kJ/mol at 160 °C [71]. The values of Z, τ_d are given below:

$$Z = \frac{M_z}{M_e} = \frac{3.2\times10^6}{828} \approx 3854$$

$$\tau_d = 3\times Z^3\times\tau_e = 3\times3854^3\times1.75\times10^{-8} \approx 3000\ s$$

The calculated values of τ_{rep}, τ_s and their *De*, at 136 °C, are reported in Table 2-2. The details for the calculation are attached in Appendix 2.

Table 2-2 The calculated relaxation times and the Deborah numbers of HMW chains.

Shear Rate (/s)	τ_{rep} **(s)**	τ_s **(s)**	$De_{(rep)}$	$De_{(s)}$
1	2.8×10^3	0.26	2.8×10^3	0.26

As reported in literature, in principle, significant chain stretch should occur when $\tau_s\times\dot{\gamma}>1$ [67], and this is considered as essential condition for the formation of shish-kebab precursor and thus shish-kebab structure after crystallisation [66,72]. In the case of shear rate of 1/s, $De_{(s)}$ <

1, thus only insignificant stretch can occur during shear. These results explain the absence of shish-kebab structure formation during the applied mild shear of 1/s. In Figure 2-10, 2D SAXS patterns of plain HDPE and its composites, recorded at 136 °C after application of shear and 90 °C after crystallisation following Scheme 2-1, are shown.

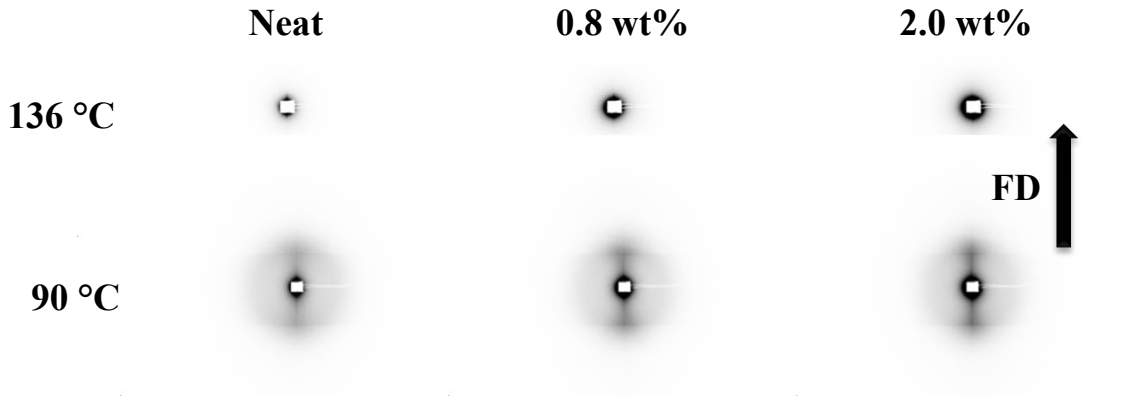

Figure 2-10 2D SAXS patterns of samples recorded at 136 ºC (after application of shear) and 90 ºC (after dynamic cooling) following the Protocol A described in **Scheme 2-1**. The samples measured are neat sample, 0.8 wt % and 2.0 wt% HDPE/rGON composites. The samples were prepared at 160 ºC by compression moulding. The 1/s shear was applied for 100 s at 136 ºC. Just after shear the sample was cooled down to 90 °C, at 10 ºC/min.

From SAXS patterns recorded at 136 ºC, no clear shish structure is observed, suggesting that the sample experienced mild stretch during shear. The SAXS data recorded at 90 ºC **,** following the Scheme 2-1, is in accordance with WAXD data, confirming enhancement in oriented structure with increasing filler concentration, as shown in Figures 2-8 and 2-10. These findings are further in agreement with the rheological response of the materials depicted in Figure 3b where shift in cross-over point to lower frequencies with increasing filler content is observed, indicating the increase in the effective reorientation time with the increasing concentration of the filler.

It is important to notice that the quantitative calculation of the Deborah number is strictly valid for the neat polymer, as the τ_e used for calculation is based on the polymer without any filler. The presence of graphene might influence the chain dynamics at different frequencies. However, the relaxation moduli *G'* and *G''* shown in Figure 2-5 and Figure 2-6 for the composites with the filler concentration lower than 4.0 wt % show insignificant changes in

the high frequency range (≥ 0.1 rad/s – *i.e.* higher than the cross-over frequencies), indicating that for the low filler concentrations, chain stretch relaxation is little influenced, and hence the Deborah number calculation for the composites should not have significant departure from the true values.

2.4 Conclusions

In this chapter, reduced graphene oxide nanoplatelets (rGONs)/high density polyethylene (HDPE) nanocomposites were prepared using a two-step solution/suspension method. The rheological percolation measured by linear oscillatory rheology reveals a slightly lower threshold (4.0 wt %) compared to the electrical percolation measured using a 4-point probe (4.5 wt %). The difference is ascribed to the different mechanisms acting in the two cases: for electrical conductivity, a continuous filler phase is required for the conduction of electrons, whereas the rheological response is influenced by the chain-filler interaction evident from changes in the storage and loss moduli that could be affected by the formation of filler-chain network. Time resolved WAXD/SAXS investigation on the HDPE/rGON samples subjected to shear flow depicts the strong chain-filler interaction that maintains strong chain orientation. On immediate cooling after the application of shear, following Scheme 2-1, polymer chains in the composites show stronger orientation compared to the neat sample. Remarkable to notice is that while the composite samples, following the protocol depicted in Scheme 2-2, left for 10 mins under isothermal condition after the application of shear, maintain obvious orientation whereas the orientation in the neat sample is lost. These findings, supported by the rheological response of the neat and the composite samples, demonstrate strong interaction between GON and polyethylene chains. The Deborah number is calculated to understand the influence of applied shear on chain stretching, which suggests that in the applied shear conditions the investigated samples experienced mild chain stretch – resulting in the absence of shish formation. Thus the orientation observed in composites is attributed to the interaction of rGON with chain segments primarily.

References

[1] Paul, D. R.; Robeson, L. M. Polymer nanotechnology: nanocomposites. *Polymer* **2008**, 49, 3187-3024.

[2] Sahoo, N. G.; Rana, S.; Cho, J. W.; Li, L.; Chan, S. H. Polymer nanocomposites based on functionalized carbon nanotubes. *Prog. Polym. Sci.* **2010**, 35, 837-867.

[3] Medellin-Rodriguez, F. J.; Burger, C.; Hsiao, B. S.; Chu, B.; Vaia, R.; Philips, S. Time-resolved shear behavior of end-tethered nylon 6-clay nanocomposites followed by non-isothermal crystallization. *Polymer* **2001**, 42 (21), 9015-9023.

[4] Fu, B. X.; Yang, L.; Somani, R. H.; Zong, S. X.; Hsiao, B. S.; Philips, S.; Blanski, R.; Ruth, P. *J. Polym. Sci. Part B Polym. Phys.* **2001**, 39 (22), 2727-2739.

[5] Liu, K.; Ronca, S.; Andablo-Ryes, E.; Forte, G.; Rastogi, S. Unique rheological response of ultrahigh molecular weight polyethylenes in the presence of reduced graphene oxide. *Macromolecules* **2014**, 48(1),131-139.

[6] Li, Y.; Kroger, M.; Liu, K. W. Nanoparticle effect on the dynamics of polymer chains and their entanglement network. *Phys. Rev. Lett.* **2012**, 109, 118001.

[7] Rastogi, S.; Lippits, D. R.; Peters, G. W. M.; Graf, R.; Yao, Y.; Spiess, H. W. Heterogenety in polymer melts from melting of polymer crystals. *Nat. Mater.* **2005**, 4, 635-641.

[8] Kharchenko, S. B.; Douglas, J. F.; Obrzut, J.; Grulke, E. A.; Migler, K. B. Flow-induced properties of nanotube-filled polymer materials. *Nat. Mater.* **2004**, 3, 564-568.

[9] Jain, S.; Goosen, G. W. M.; Van Duin, M.; Lemstra, P. J. Strong decrease in viscosity of nanoparticle-filled polymer melts through selective adsorption. *Soft Matter* **2008**, 4, 1848-1854.

[10] Patil, N.; Balzano, L.; Portale, G.; Rastogi, S. Influence of shear in the crystallization of polyethylene in the presence of SWNTs. *Carbon* **2010**, 48, 4116-4128.

[11] Balzano, L. *Flow Induced Crystallization of Polyolefins.* PhD Thesis. Eindhoven University of Technology, **2008**.

[12] Novoselov, K. S.; Geim, A.K.; Morozov S.V.; Jiang, D.; Zhang, Y.; Dubonos, S.V.; Grigorieva, I. V.; Firsov, A. A. Electric field effect in atomically thin carbon films. *Science* **2004**, 306, 666–669.

[13] Nilsson, J.; Neto, A. H. C.; Guinea, F.; Peres, N. M. R. Electronic properties of graphene multilayers. *Phys. Rev. Lett.* 2006, 97, 266801.

[14] Balandin, A. A.; Ghosh, S.; Bao, W. Z.; Calizo, I.; Teweldebrhan, D.; Miao, F.; Lau, C. N. Superior thermal conductivity of single-layer Graphene. *Nano Lett.* **2008**, 8 (3), 902-907.

[15] Lee, C. G.; Wei, X. D.; Kysar, J. W.; Hone, J. Measurement of the elastic properties and instrinsic strength of manolayer graphene. *Science* **2008**, 231, 385-388.

[16] Krompiewski, S. Electronic transport through side-contacted graphene nanoribbons: effects of overlap, aspect ratio and orientation. *Nanotechnology* **2011**, 22, 445201.

[17] Stoller, M. D.; Park, S.; Zhu, Y.; An, J.; Ruoff, R. S. Graphene-Based Ultracapacitors. *Nano Lett.* **2008**, 8 (10), 3498-3502.

[18] Hu, H. L.; Zhang, G.; Xiao, L.; Wang, H.; Zhang, Q.; Zhao, Z. Preparation and electrical conductivity of graphene/ultrahigh molecular weight polyethylene composites with a segregated structure. *Carbon* **2012**, 12, 4596-4599.

[19] Liu, P.; Gong, K.; Xiao, P.; Xiao, M. Preparation and characterization of poly(vinyl acetate)-intercalated graphite oxide nanocomposite. *J. Mater. Chem.* **2000**, 10, 933-935.

[20] Mead, D. Determination of molecular weight distributions of linear flexible polymers from linear viscoelastic material functions. *J. Rheol.* **1994**, 38, 1797-1827.

[21] Talebi, S.; Duchateau, R.; Rastogi, S.; Kaschta, J.; Peters, G. W. M.; Lemstra, P. J. Molar mass and molecular weight distribution determination of UHMWPE synthesised using a living homogeneous catalyst. *Macromolecules* **2010**, 43, 2780-2788.

[22] Tuminello, W. H. Molecular weight and molecular weight distribution from dynamic measurements of polymer melts. *Polym. Eng. Sci.* **1986**, 26, 1339-1347.

[23] Hummers, W. S.; Offeman, R. E. Preparation of graphitic oxide. *J. Am. Chem. Soc.* **1958**, 80, 1339.

[24] Rafiq, R.; Cai, D.; Jin, J.; Song, M. Increasing the toughness of nylon 12 by the incorporation of functionalized graphene. *Carbon* **2010**, 48, 4309-4314.

[25] Topsoe, H. Geometric factors in four point resistivity measurement. 2nd revised ed. Bulletin No. 472-13. Vedbaek: **1968**;

[26] Tervoort-Engelen, Y. M. T.; Lemstra, P. J. Morphology of nascent ultrahigh-molecular-weight polyethylene reactor powder: chain-extended versus chain-folded crystals. *Polym. Commun.* 1991, 32, 343-345.

[27] Alexander, L. E. X-ray diffraction methods in polymer science. Wiley–Interscience, New York: **1969**.

[28] Dreyer, D. R.; Park, S.; Bielawski, C. W.; Ruoff, R. S. The chemistry of graphene oxide. *Chem. Soc. Rev.* **2010**, 39, 228-240.

[29] Brodie, B. C. *Ann. Chim. Phys.* **1860**, 59**,** 466.

[30] Marcano, D. C.; Kosynkin, D. V.; Berlin, J. M.; Sinitskii, A.; Sun, Z.; Slesarev, A;Alemany, L. B.; Lu, W.; Tour, J. M. Improved synthesis of graphene oxide. *ACS Nano* **2010**, 4, 4806-4814.

[31] Staudenmaier, L. *Ber. Deut. Chem. Ges,* **1898**, 31, 1481.

[32] Hummers, W. S.; Offeman, R. E. Preparation of graphitic oxide. *J. Am. Chem. Soc.* 1958, **80,** 1339.

[33] Liu, P.; Gong, K.; Xiao, P.; Xiao, M. Preparation and characterization of poly(vinyl acetate)-intercalated graphite oxide nanocomposite. *J. Mater. Chem.* **2000**, 10, 933-935.

[34] Guo, J.; Ren, L.; Wang, R.; Zhang, C.; Yang, Y.; Liu, T. Water dispersible graphene noncovalently functionalized with tryptophan and its poly(vinyl alcohol) nanocomposite. *Composites: Part B* **2011**, 42, 2130-2135.

[35] Paredes, J. I.; Villar-Rodil, S.; Amrtinez-Alonso, A.; Tascon, J. M. D. Graphene oxide dispersions in organic solvents. *Langmuir* **2008**, 24, 10560-10564.

[36] Lotya, M.; Hernandez, Y.; King, P. J.; Smith, R. J.; Nicolosi, V.; Karlsson, L. S.; Blighe, F. M. De S.; Wang, Z.; McGovern, I. T.; Duesberg, G. S. Coleman, J. N. Liquid phase production of graphene by exfoliation of graphite in surfactant/water solutions. *J. Am. Chem. Soc.* **2009**, 131 (10), 3611-3620.

[37] Park, S.; An, J.; Suk, J. W.; Ruoff, R. S. Graphene-Based Actuators. *Small* **2010**, 6 (2), 210-212.

[38] Szabo, T.; Berkesi, O.; Forgo, P.; Josepovits, K.; Sanakis, Y.; Petridis, D.; Dekany, I. Evolution of Surface Functional Groups in a Series of Progressively Oxidized Graphite Oxides. *Chem. Mater.* **2006**, *18*, 2740-2749.

[39] Pu, L.; Ma, Y.; Zhang, W.; Hu, H.; Zhou, Y.; Wang, Q.; Pei, C. Simple method for the fluorinated functionalization of graphene oxide. *RSC Adv.* **2013**, 3, 3881-3884.

[40] Collins, W. R.; Schmois, E.; Swager, T. M. Graphene oxide as an electrical for carbon nucleophiles. *Chem. Commun.* **2011**, *47*, 8790-8792.

[41] Wang, X.; Dou, W. Preparation of graphite oxide (GO) and the thermal stability of silicone rubber/GO nanocomposites. *Thermochimica Acta* **2012**, 529, 25-28.

[42] Bradder, P.; Ling, S.; Wang, S.; Liu, S. Dye adsorption on layered graphite oxide. *J. Chem. Eng. Data* **2011**, 56, 138–141.

[43] Steurer, P.; Wissert, R.; Thomann, R.; Mulhaupt, R. Functionalized graphenes and thermoplastic nanocomposites based upon expanded graphite oxide. *Macromol. Rapid Commun.* **2009**, *30*, 316–327.

[44] Tan, L. L.; Ong, W. J.; Chai, S. P.; Mohamed, A. R. Reduced graphene oxide-TiO2 nanocomposite as a promising visible-light-active photocatalyst for the conversion of carbon dioxide. *Nanoscale Res. Lett.* **2013**, 8, 465.

[45] Park, S.; Suk, J. W.; An, J.; Oh, J.; Lee, S.; Lee, W. The effect of concentration of graphene nanoplatelets on mechanical and electrical properties of reduced graphene oxide papers. *Carbon* **2012**, *50*, 4573-4578.

[46] Liu, X.; Zheng, M.; Xiao, K.; Xiao, Y.; He, C.; Dong, H.; Lei, B.; Liu, Y. Simple, green and high-yield production of single- or few layer graphene by hydrothermal exfoliation of graphite. Nanoscle 2014, 6, 4598-4603.

[47] He, H.; Klinowski, J.; Forster, M.; Lerf, A. The new structural model of graphene oxide. *Chem. Phys. Lett.* **1998**, *287*, 53-56.

[48] Lerf, A.; He, H.; Forster, M.; Klinowski, J. Structure of graphite oxide revisitied. *J. Phys. Chem. B* **1998**, 102, 4477-4482.

[49] Wang, G.; Yang, Z.; Li, X.; Li, C. Synthesis of poly(aniline-co-o-anisidine)-intercalated graphite oxide composite by delamination/reassembling method. *Carbon* **2005**, 43, 2564-2570.

[50] Stankovich, S.; Dikin, D. A.; Piner, R. D.; Kohlhaas, K. A.; Kleinhammes, A.; Jia, Y.; Wu, Y.; Nguyen, S. T.; Ruoff, R. S. Synthesis of graphene-based nanosheets via chemical reduction of exfoliated graphite oxide. *Carbon* **2007**, 45, 1558-1565.

[51] Marcano, D. C.; Kosynkin, D. V.; Berlin, J. M.; Sinitskii, A.; Sun, Z.; Slesarev, A;Alemany, L. B.; Lu, W.; Tour, J. M. Improved synthesis of graphene oxide. *ACS Nano* **2010**, *4*, 4806-4814.

[52] Some, S.; Kim, Y.; Hwang, E. H.; Yoo, H. J.; Lee, H. Binol salt as a completely removable graphene surfactant. *Chem. Commun.* **2012**, 48, 7732-7734.

[53] Yang, H.; Li, F.; Shan, C.; Han, D.; Zhang, Q.; Niu, L.; Ivaska, A. Covalent functionalization of chemically converted graphene sheets via silane and its reinforcement. *J. Mater. Chem.*, **2009**, 19, 4632-4638.

[54] Marcano, D. C.; Kosynkin, D. V.; Berlin, J. M.; Sinitskii, A.; Sun, Z.; Slesarev, A.; Alemany, L. B.; Lu, W.; Tour, J. M. Improved synthesis of graphene oxide. *ACS Nano* **2010**, 4, 4806-14.

[55] Krishnamoorti R, Chatterjee T. Rheology and processing of polymer nanocomposites, in applied polymer rheology: polymer fluids with industrial applications (ed M. Kontopoulou). John Wiley&Sons, inc, Hoboken, NJ, USA **2011**.

[56] Zhang, Q.; Rastogi, S.; Chen, D.; Lipptis, D.; Lemstra, P. J. Low percolation threshold in single-walled carbon nanotube/high density polyethylene composites prepared by melting processing technique. *Carbon* **2006**, 44, 778-785.

[57] Doi, M.; Edwards, S. F. The theory of Polymer Dynamics. Clarendon Press, Oxford: **1986**

[58] Valentino, O.; Sarno, M.; Rainone, N. G.; Nobile, M. R.; Ciambelli, P.; Neitzert, H. C.; Simon, G. P. Influence of the polymer structure and nanotube concentration on the conductivity and rheological properties of polyethylene/CNT composites. *Physica E* **2008**, 40, 2440-2445.

[59] McNally, T.; Potschke, P.; Halley, P.; Murphy, M.; Martin, D.; Bell, S. E. J.; Brennan, G. P.; Bein, D.; Lemoine, P.; Quinn, J. P. Polythylene multiwalled carbon nanotube composites. *Polymer* **2005**, 46, 8222-8232.

[60] Mun, S. C.; Kim, M.; Prakashan, K.; Jung, H. J.; Son, Y.; Park, O. O. A new approach to determine rheological percolation of carbon nanotubes in microstructured polymer matrices. *Carbon* **2014**, 67, 64-71.

[61] Feng, C.; Jiang, L. Micromechanics modelling of the electrical conductivity of carbon nanotube (CNT)-polymer nanocomposites. *Composites: Part A* **2013**, 47, 143-149.

[62] Potschke, P.; Abdel-Goad, M.; Alig, I.; Dudkin, S.; Lellinger, D. Rheological and dielectrical characterization of melt mixed polycarbonate-multiwalled carbon nanotube composites. *Polymer* **2004**, 45, 8863-8870.

[63] Du, F.; Scogna, R. C.; Zhou, W.; Brand, S.; Fischer, J. E.; Winley, K. I. Nanotube networks in polymer nanocomposites: rheology and electrical conductivity. *Macromolecules* **2004**, 37, 9048-9055.

[64] Brydson, J. A. Plastics Materials, 4th ed. Butterworth-Heinemann, London: **1982**.

[65] Somani, R. H.; Hsiao, B. S.; Nogales, A.; Srinivas, S.; Tsou, A. H.; Sics, I.; Balta-Calleja, F. J.; Ezquerra, T. A. Structure development during shear flow-induced crystallization of i-PP: in-situ small-angle X-ray scattering study. *Macromolecules* **2000**, 33(25), 9385-9394.

[66] Balzano, L.; Kukalyekar, N.; Rastogi, S.; Peters, G. W. M.; Chadwick, J. C. Crystallization and dissolution of flow-induced precursors. *Phys. Rev. Lett.* **2008**, 100, 048302.

[67] Graham, R. S.; Likhtman, A. E.; Mcleish, T. C. B.; Milner, S. T. Microscopic theory of linear, entangled polymer chains under rapid deformation including chain stretch and convective constraint release. *J. Rheol.* **2003**, 47 (5), 1171-1200.

[68] Reiner, M. The Deborah number. *Physics Today* **1964**, 62.

[69] Likhtman, A. E.; McLeish, T. C. B. Quantitative theory for linear dynamics of linear entangled polymers. *Macromolecules* **2002**, 35, 6332-6343.

[70] Fetters, L.J.; Lohse, D. J.; Richter, D.; Witten, T. A.; Zirkel, A. Connection between polymer molecular weight, density, chain dimensions, and melt viscoelastic properties. *Macromolecules* **1994**, 27(17), 4639-4647.

[71] Ngai, K. L.; Plazek, D. J. Relation of internal rotational isomerism barriers to the flow activation energy of entangled polymer melts in the high-temperature Arrhenius region. *J. Polym. Sci.: Polym. Phys.* **1985**, 23, 2159-2180.

[72] Patil, N.; Balzano, L.; Portale, G.; Rastogi, S. A study on the chain-particle interaction and aspect ratio of nanoparticles on structure development of a linear polymer. *Macromolecules* **2010**, 43 (16), 6749-6759.

3 Unique Rheological Response of UHMWPE in the Presence of rGON

Abstract

In the previous chapter, it has been discussed how the strong polyethylene chain and filler (reduced graphene oxide nanoplatelets-rGON) interaction could hinder the chain dynamics of HDPE. In this chapter the study has been extended to both commercial (entangled) and disentangled UHMWPE/rGON composites prepared by a same suspension-mixing method, to investigate the influence that rGON has on the chain dynamics and chain entanglement formation, as well as the electrical conductivities of the resulting composites. It has been found that composites made with disentangled UHWMPE can reach conductivities at least 100 times higher than those with the same composition made with commercial UHWMPE, if the thermal reduction treatment is done at lower temperatures. However, the difference in the electrical conductivity diminishes when both sets of samples are given a high temperature treatment. This phenomenon is attributed to the difference in morphology of the polymer matrices, in particular related to the presence/absence of particle boundaries after compression moulding. Furthermore, rheological analyses of the two sets of UHMWPE/rGON nanocomposites conclusively demonstrate differences in the interaction between polyethylene chain segments of the disentangled UHMWPE and rGON, compared to the entangled commercial UHMWPE. Both composites show minima in the storage modulus at a specific graphene composition. The strong interaction of polyethylene chains with the filler inhibits disentangled UHMWPE to achieve the thermodynamic equilibrium melt state, whereas in the commercial sample, having a broader molar mass distribution, the higher adhesion probability of the long chains to the graphene surface lowers the elastic modulus of the polymer melt. Correlation between the percolation threshold for electrical conductivity and rheological response of the composites has also been discussed.

3.1 Introduction

In Chapter 1 it has been discussed how the mechanical properties of UHMWPE enhance when increasing the molecular weight, but this happens at the expense of the processability of the material. To recall, very high molecular weights correspond to high melt viscosities due to the increasing number of entanglements along chains [1]. Because of the high entanglement density, the most common method reported for the composites preparation is hot press of a dried UHMWPE-filler mixture [2], where a segregated structure of filler residing along the grain boundaries of the polymer particles is observed [3,4]. Outstanding electrical conductivities have been reported using this method [5]. However a difficulty in sintering of the grain boundaries reduces the contact area between filler and chains, thus negatively influencing their interaction and consequently also reducing the mechanical properties of the composites, for example, elongation at break and ultimate strength [6,7]. Recently, it has been reported that when UHMWPE is synthesised in suitable controlled conditions, a reduced number of entanglements can be achieved [8]. The resultant low entangled UHMWPE or disentangled UHWMPE provides ease in solid-state processing and higher tensile strength and tensile modulus of the uniaxially drawn tapes and the biaxially drawn films [8,9]. The morphology of the nascent powders of disentangled UHWMPE is significantly different from the commercially available UHMWPE. For instance, disentangled UHWMPE powders have a more "porous" structure, as shown in Figure 3-1.

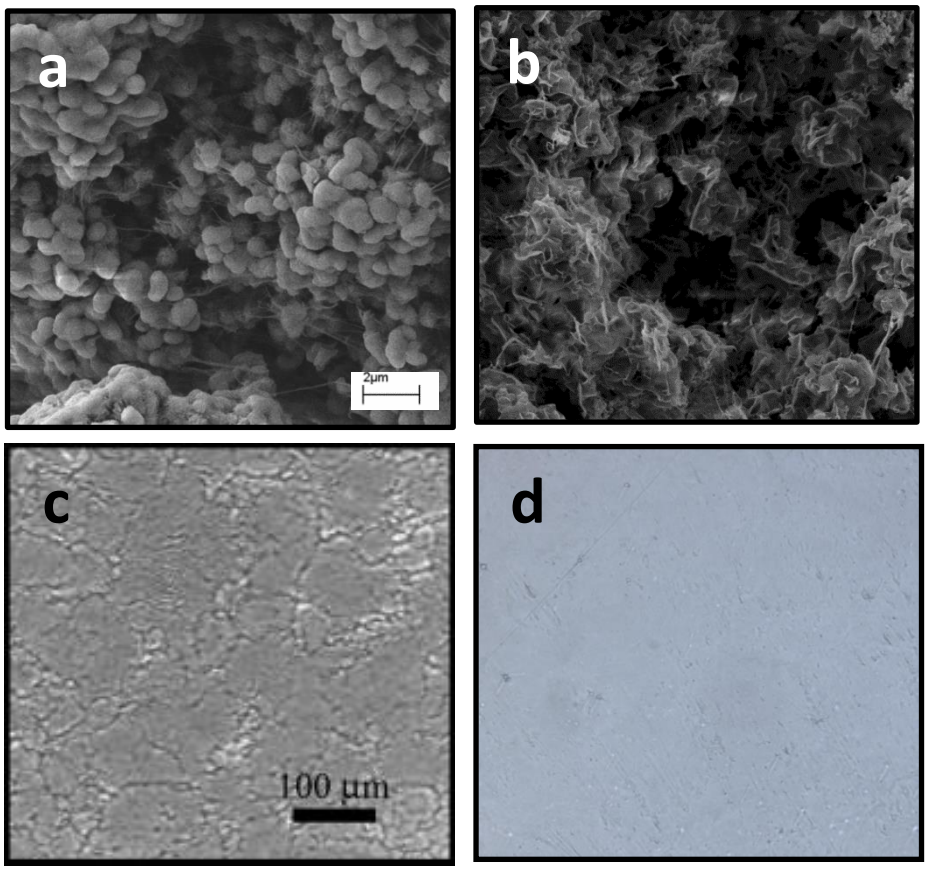

Figure 3-1 The figure depicts electron (**a, b -** same scale, 2 microns) and optical micrographs (**c, d** – same scale, 100 microns) of the commercial (**a, c**) and disentangled (**b, d**) UHMWPEs. The commercial UHMWPE powder is synthesised using a Ziegler-Natta catalyst. The commercial sample shows presence of grain boundaries after compression moulding **(c)**, whereas the disentangled UHMWPE powder does not show any grain boundaries. The absence of grain boundaries in the disentangled sample is attributed to low bulk density and low entangled state of the sample, the latter enhancing the local chain dynamics. The difference in the bulk density in the two samples is also evident from the dense and the porous structure of the commercial **(a)** and **(b)** disentangled UHMWPEs observed by electron micrograph.

The porosity in the powder facilitates the penetration of nano-sized filler into pores and eases the filler dispersion during compression moulding in the melt. The high porosity of the nascent disentangled UHWMPE sample also facilitates compression of the powder below its melting temperature, thus ensuring that the disentangled state is maintained and solid-state processing is possible [8]. Considering these advances in morphology control of UHMWPE, we expect the nanofillers to be more homogeneously distributed in the disentangled matrix, and the resulting composite to be solid-state processable.

In order to get a better insight on the difference that the entanglement density can make on the electrical conductivity and rheological response of UHMWPE/rGON composites, in this chapter we have studied and compared composites of commercial UHWMPE/rGON and

disentangled UHWMPE/rGON at different composition, after compression moulding. A significant difference in electrical conductivities, measured at room temperature, is observed in the two sets of composites made from the two types of PEs. The observed difference in electrical conductivity after given the same thermal treatment at 160 °C is associated with differences in particle morphology and melting behaviour of the two polymers. For more details on the melting behaviour of the two polymers, the readers are referred to ref [10]. The dissimilarity in electrical conductivity diminishes when the materials are subjected to high temperature treatment at 230 °C, where the local chain dynamic in the commercial UHMWPE is enhanced. Considering what was observed in the previous chapter for HDPE/rGON, a strong interaction between the long polyethylene molecules and GON is anticipated. Such an interaction is investigated and its implications on the rheological response of the polymer have been followed by plate-plate rheometry, in the linear viscoelastic region.

3.2 Experimental

3.2.1 Materials

GON was synthesised using a modified Hummers method [11], as described in Chapter 2. Materials for the GON synthesis were purchased from Sigma-Aldrich and used as received. Commercial UHMWPE powder having molecular characteristics reported in Table 3-1 was also purchased from Sigma-Aldrich. Disentangled UHMWPE with a significantly reduced number of entanglements was synthesised in our lab following the procedures: all manipulations of polymerisation with respect to air and moisture-sensitive compounds were performed in an argon glove box or under nitrogen flow atmosphere using standard high-vacuum Schlenk technique. A Büchi 1.5 l jacketed reactor sealed with a stainless steel lid that is equipped with gas gauge, a thermometer probe, ethylene feeding tube, a gas inlet/outlet, a rubber septum for catalyst injection, a mechanical stirrer having three 4-bladed propellers, are kept at 125 °C under vacuum overnight controlled by a feedback loop controller Huber Unistat 425 thermo-regulator. The reactor was then backfilled with nitrogen and purged to vacuum for three cycles. After that, the temperature of the reactor was brought to 25 °C and anhydrous toluene was then pumped into the reactor through a sealed pipe from toluene tank by applying high pressure nitrogen. The temperature of the reactor was then set at 10 °C. The desired amount of of scavenger (MAO) was injected into the reactor to remove any possible

contaminations and then the nitrogen atmosphere is replaced by ethylene and the pressure is fixed at 1.2 absolute bars by a gas flow meter Büchi BPC 6002. A stirring speed of 1250 rpm was then set to mix and saturate the reaction medium with ethylene. After the pressure stabilize again at 1.2 bars, 9 mg of the catalyst bis[N-(*tert*-butylsalicylidene)pentafluoroanilinato]titanium (IV) dichloride (FI catalyst) activated by MAO in toluene was injected into the reactor to initiate the polymerisation. After reaching the time, the reaction was then quenched by injection of methanol.

The obtained polymers were then filtered, and further washed with copious amount of methanol/acetone. To achieve good dispersion of antioxidant, 0.7-1.0 wt % antioxidant was then added to the polymers suspended in acetone and stirred in a fuming hood. After acetone evaporated, the left mixture was then placed in a vacuum oven at 40 °C for 12 hours. Similar procedures can also be found in elsewhere [8, 9].

Table 3-1 summarises some molecular and physical characteristics that are of interest for the present work. Entanglement density estimation in the disentangled nascent sample has been done by measuring the initial value of the storage modulus obtained on melting of the sample. Table 3-1 shows the initial storage modulus of the disentangled (0.56 MPa) and the commercial entangled (1.58 MPa) samples recorded at 10 rad/s, 160 °C, in the linear viscoelastic region. Under isothermal melt condition, at 10 rad/s, the storage modulus of the disentangled sample increases from 0.56 MPa to 2.0 MPa (approximately), where the time required for modulus build-up shows molar mass dependence [10]. On the contrary, the commercial UHMWPE sample does not show any substantial increase in the modulus build up.

Table 3-1 Overview of physical properties of the two samples of PE investigated in this study.

Polymer	**Particle diameter (μm)**	**Particle Morphology (Nascent Powder)**	***M*w (10^6 g/mol)**	**MWD**	**Entanglement density (starting storage modulus at 10 rad/s)**
Commercial UHMWPE	~ 50	0.3 g/cm^3 [12]	4.4	31.1	High (1.58 MPa)
Disentangled UHMWPE	~ 500	0.1 g/cm^3 [12]	4.8	3.1	Low (0.56 MPa)

3.2.2 Determination of Molecular Weight and Molecular Weight Distribution

Molar mass, M_w, and molecular weight distribution (MWD) of both polymers were estimated by rheology using Advanced Rheometrics Expansion System (ARES) as described in the literature [13,14,15] and the results are shown in Figure 3-2.

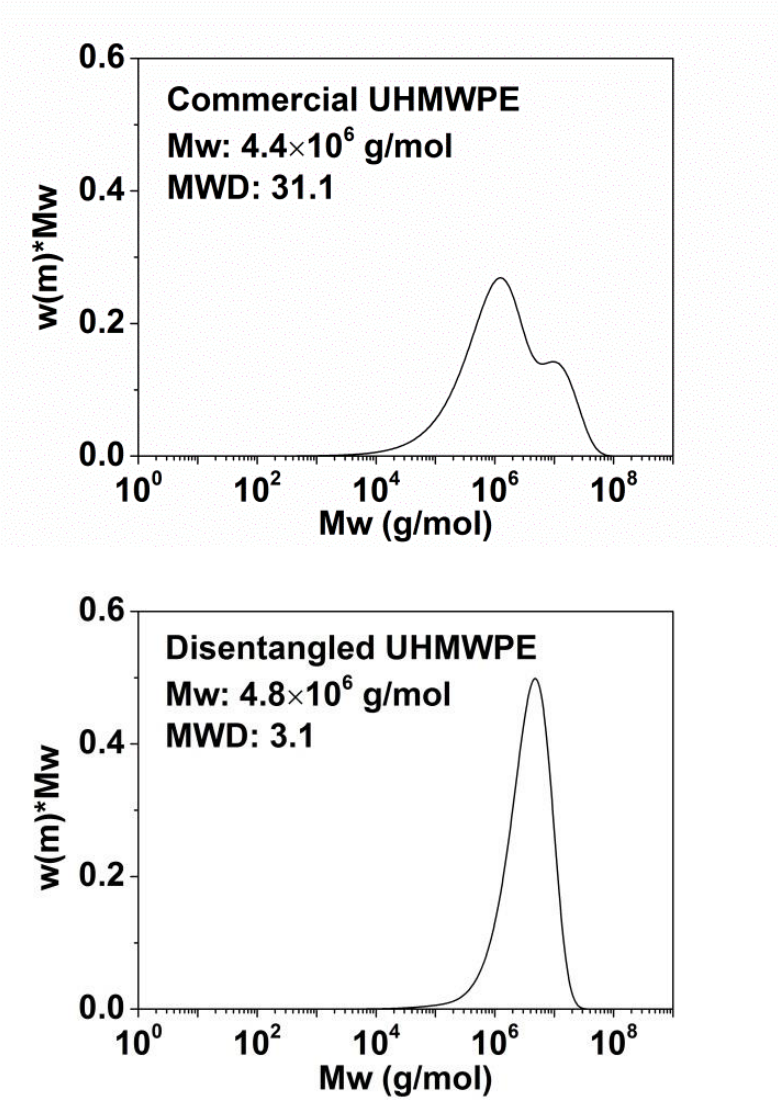

Figure 3-2 Characterisation of molar mass and molar mass distribution as obtained from rheology: (top) commercial PE and (bottom) disentangled PE.

3.2.3 Preparation of GON, rGON and PE/rGON Composites

The synthesis of GON was done following a modified Hummers Method [11] with additional modifications, as described in Chapter 2.

A two-step procedure, used for preparation of HDPE/rGON composites, was also employed to prepare the electrically conductive composites with the two types of UHMWPEs: first, the required amount of dried GON was weighed and re-dispersed in 40 ml of water by 15 min ultrasonication, while the required amount of PE was suspended in acetone and stirred for 10 min. In the second step, the ultrasonicated homogeneous GON suspension was added to the acetone-suspended PE under stirring. The mixture was stirred in a fume hood until most of the solvent evaporated and the resulting solid was further dried at 40 ºC for 12 hours to remove any residual solvent. The residue, a UHMWPE/rGON composite, was obtained in the form of powder.

To achieve the reduction of the dispersed GON for electrical conductivity, the dried composite powders were compressed in a hydraulic press at 160 ºC (or 230 ºC), following the same protocol used for the reduction of GON films, as described in Chapter 2. Following this procedure, composites films of PE/rGON were prepared. In all samples, 0.7 wt % antioxidant (Irganox 1010, Ciba) was added to avoid oxidation or degradation of UHMWPE during the hot press procedure. WAXD recorded in the transmission mode, on the compressed samples, did not show any orientation.

For rheological studies ~ 0.7 g of disentangled UHMWPE/GON powder was compression moulded into discs of 50 mm diameter and 0.6 mm thickness by compression moulding at a constant temperature of 125 °C and average force of 20 tons. Similarly, commercial UHMWPE/GON powder was moulded at a constant temperature of 160 °C. From the compressed powder films smaller discs of 12 mm diameter were punched.

3.2.4 Characterisation of GON, rGON and Composites

A JEOL-2000FX Transmission Electron Microscope (TEM) was used to observe the exfoliated single or few-stacked-layers of GON in water with an applied voltage of 200 kV. The morphology of the composites after compression moulding was observed with a Leica DM RX transmitted light microscope. Field Emission Gun-Scanning Electron Microscope (FEG-SEM) was used for morphological analysis of PE powders. For the analysis, the samples were coated with gold by a sputtering technique. The electrical conductivities of the UHMWPE/rGON composites were measured with a Keithley instrument composed of a 2182A nanovoltmeter and a 6220 precision current source. The shape and thickness of the samples were corrected by taking into account the geometric factors according to ref [16].

All rheological measurements were performed in an ARES-LS2 rheometer (TA, Instruments) using a 12 mm diameter parallel plate geometry. In order to avoid polymer degradation during long time measurements, the samples were kept under a nitrogen atmosphere inside a convection oven. The 12 mm polymer disc was placed in the rheometer at 110 °C and the temperature was increased to 160 °C (approximately 18 °C above the equilibrium melting temperature of polyethylene, 141.5 °C [17]) with a heating rate of 10 ºC/min. Along this process, an average normal load of 4.0 N was applied to maintain appropriate contact between the sample and plates. Once the temperature (160 °C) was reached, a small amplitude oscillatory test at a constant frequency of 10 rad/s and strain 0.1% (within the linear viscoelastic region) was performed to follow the storage modulus (*G'*) build-up. Data acquisition was started 60 seconds after reaching the experimental temperature of 160 ºC. On the fully equilibrated melt state, dynamic frequency sweep with angular velocity from 0.001 rad/s to 100 rad/s was performed with a constant 0.5 % strain in the linear viscoelastic region on both of the commercial UHMWPE/rGON and disentangled UHMWPE/rGON samples. More detailed description of the rheological procedures can be found elsewhere [10].

3.3 Results and Discussion

3.3.1 Electrical Conductivities of Composites

Figure 3-3 depicts 1 g samples of the plain polymers and their corresponding composites at different filler concentrations. Due to the low bulk density of disentangled UHMWPE powder, for the same mass, the volume of the disentangled UHMWPE composite is much higher.

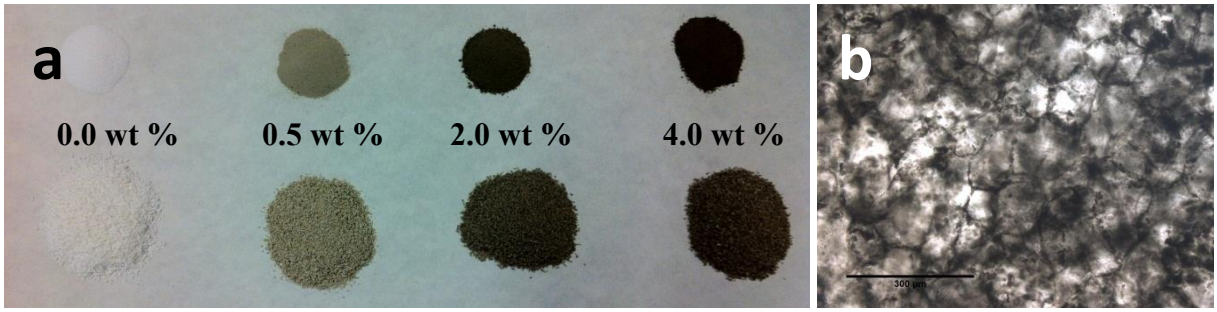

Figure 3-3 a) Pure UHMWPEs and GON-filled PE particles (top series: commercial UHMWPE; bottom series: disentangled UHMWPE). All samples weigh 1 g. Plates for rheological and electrical conductivity measurements were made by compressing these powders at 160 °C or 230 °C; **b)** rGON

can be observed along the grain boundaries after compression moulding of the commercial UHMWPE having 0.5 wt % of the filler. This sample was compressed at 160 °C.

After thermal reduction of the GON during the compression moulding step, the electrical conductivities of commercial UHMWPE/rGON and disentangled UHMWPE/rGON composites were measured using a 4-point probe technique and the resulting values are shown in Figure 3-4 and listed in Table 3-2 (the conductivity value of pure PE is taken from ref [18]). The conductivity of the samples containing 0.1 wt % of rGON could not be measured as it was outside the sensitivity of the equipment.

The different conductivity behaviours observed for the two sets of the samples suggest differences in the formation of the filler network. The percolation threshold, defined as the minimal concentration of conductive filler at which a sudden increase in conductivity of the insulating matrix appears, is observed for both matrices to be just below 0.3 wt % (Figure 3-4). The percolation threshold of the UHMWPE/rGON composites is much higher than that of HDPE/rGON composites, which is at ~4.5 wt %, as reported in Table 2-1. This can be attributed to the very low viscosity of HDPE in the melt, where the chains can move more freely and embed the graphene layers thus reducing the connecting points between the fillers.

The conductivities of polymer composites have been investigated based on the modified classical percolation threshold power law [19,20], equation 1-4, as mentioned in Chapter 1.

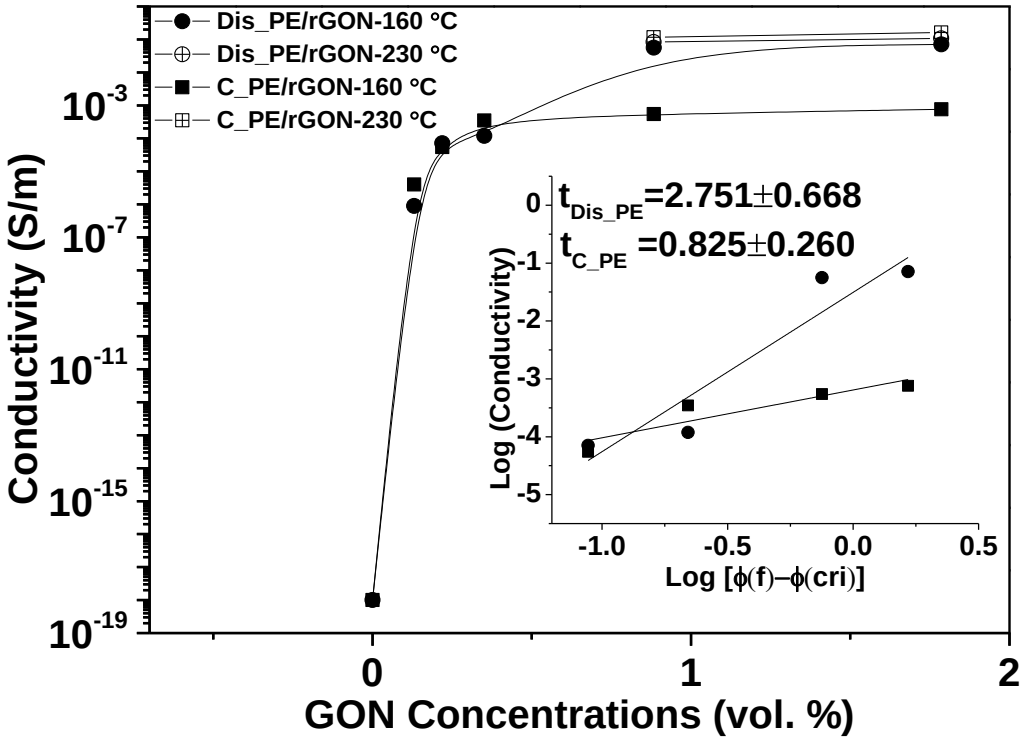

Figure 3-4 Electrical conductivities of commercial UHMWPE/rGON composites (C_PE/rGON (square)) and disentangled UHMWPE/rGON composites (Dis_PE/rGON (circle)) as function of rGON content. The insert shows the log-log plot of electrical conductivity with [$\varphi(f)$ - $\varphi(cri)$]. (the conversion between wt % and vol % of rGON in the composites are shown in Appendix I)

Table 3-2 Conductivity values from **Figure 3-4** of commercial UHMWPE/rGON and disentangled UHMWPE/rGON composites compressed at 160 °C and 230 °C.

Sample	Compression Temp (◦C)	Conductivity (S/m)
Commercial UHMWPE/rGON 0.3 wt %	160	4.00×10^{-6}
Commercial UHMWPE/rGON 0.5 wt %	160	5.46×10^{-5}
Commercial UHMWPE/rGON 0.8 wt %	160	3.48×10^{-4}
Commercial UHMWPE/rGON 2.0 wt %	160	5.47×10^{-4}
Commercial UHMWPE/rGON 4.0 wt %	160	7.55×10^{-4}

Disentangled UHMWPE/rGON 0.3 wt %	160	8.93×10^{-7}
Disentangled UHMWPE/rGON 0.5 wt %	160	7.07×10^{-5}
Disentangled UHMWPE/rGON 0.8 wt %	160	1.19×10^{-4}
Disentangled UHMWPE/rGON 2.0 wt %	160	5.60×10^{-2}
Disentangled UHMWPE/rGON 4.0 wt %	160	7.10×10^{-2}
Commercial UHMWPE/rGON 2.0 wt %	230	1.17×10^{-1}
Commercial UHMWPE/rGON 4.0 wt %	230	1.62×10^{-1}
Disentangled UHMWPE/rGON 2.0 wt %	230	0.83×10^{-1}
Disentangled UHMWPE/rGON 4.0 wt %	230	1.08×10^{-1}

From Figure 3-4 it can be appreciated that the conductivities measured for the two composites, compressed at 160 °C, at concentrations after the percolation threshold are rather different and considerably higher in the case of disentangled UHMWPE/rGON composites. It is observed that the conductivities of disentangled UHMWPE/rGON become at least 100 times higher than that of commercial UHMWPE/rGON with filler concentrations ≥ 2.0 wt %. The critical exponent value of commercial UHMWPE/rGON samples is around 0.83 and more interestingly a much higher critical exponent of about 2.75 is determined for disentangled UHMWPE/rGON samples. At low loadings of GON (close to the percolation threshold), the filler is homogeneously dispersed in both commercial and disentangled PE composites, thus similar conductivity values in the two composites are observed [21,22], as

shown in Figure 3-5a and c. For higher loadings of GON in the commercial UHMWPE, the filler is likely to stack along the grain boundaries of the powder particles, thus resulting in just a slight increase of conductivity when the filler content is increased from 0.8 to 4.0 wt %, as described in Figure 3-5b.

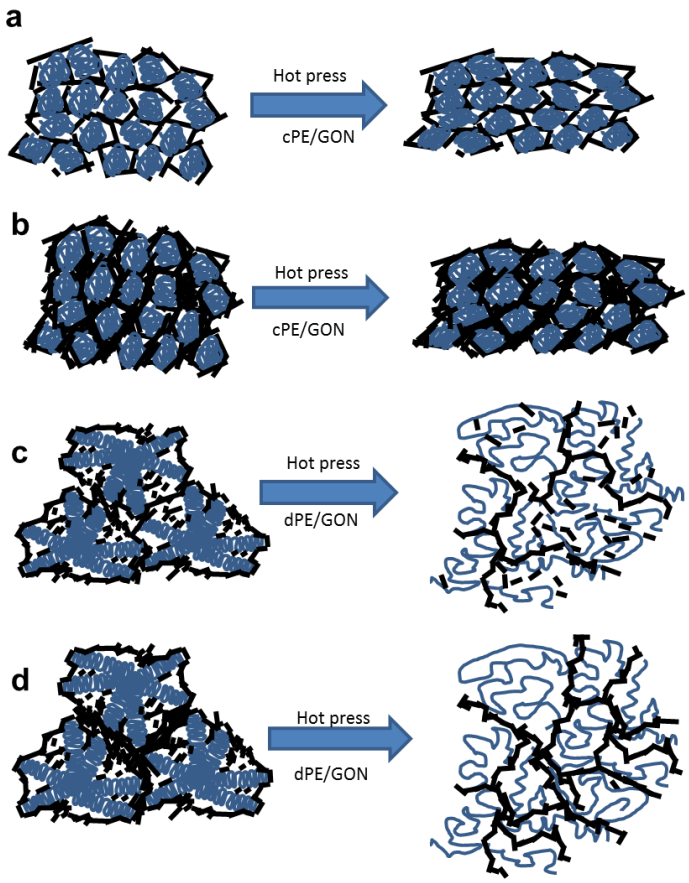

Figure 3-5 A schematic representation of our hypothesis on the influence that the polymer melting behaviour has on the filler network formation during melt; **(a)** c-UHMWPE/rGON and **(c)** dis-UHMWPE/rGON at or near the threshold; **(b)** c-UHMWPE/rGON and **(d)** dis-UHMWPE/rGON at high concentrations, at or over, 2.0 wt %.

On the contrary in disentangled UHMWPE because of the porous structure and the lower initial melt viscosity [9,23] of the polymer, the penetration of the filler into the porous polymer powders is facilitated. This results into homogeneous dispersion of rGON platelets without their aggregation, as shown in Figure 3-5d. Thus, compared to commercial UHMWPE, the same concentration of GON in disentangled UHMWPE forms a more efficient filler-filler network, as shown in Figure 3-6a and b. The resultant effect is that for the same concentration of GON the conductivity increases by more than 100 times in disentangled UHMWPE compared to commercial UHMWPE composites, on increasing the filler content from 0.8 wt % to 2.0 wt %. The difference in the electrical conductivity

vanishes when both samples are heat treated at a higher temperature, 230 °C. The loss in the difference is attributed to the enhanced chain mobility for the commercial entangled UHMWPE at the higher temperature and enhanced dispersion of the rGON filler, as shown in Figure 3-6c.

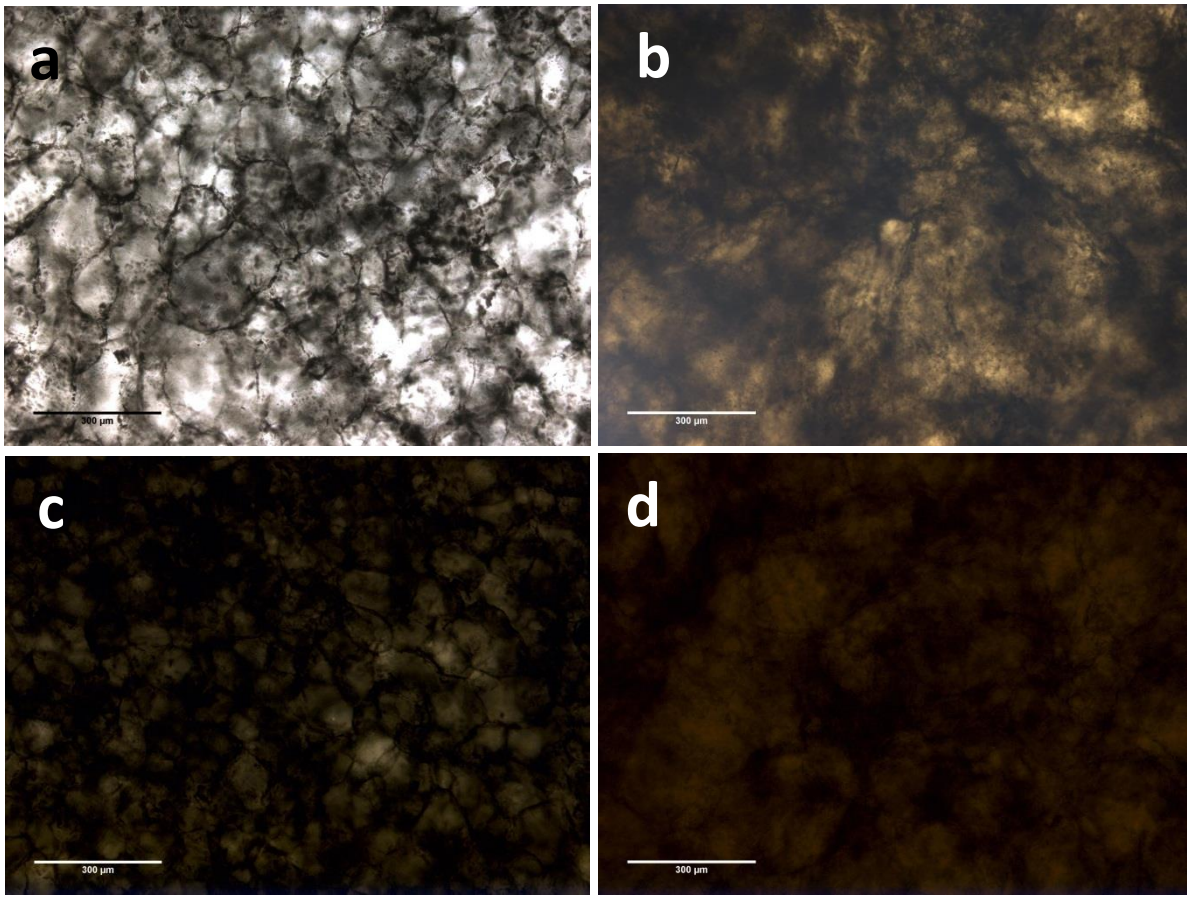

Figure 3-6 Optical microscopic images of commercial UHMWPE/rGON samples compressed at 160 °C **(a)** and 230 °C **(c)**, and disentangled UHMWPE/rGON samples compressed at 160 °C **(b)** and 230 °C **(d)**.

From electrical conductivity measurements it is evident that the presence of grain boundaries and the chain dynamics have strong implications on the interaction between methylene chain segments and graphene. To have further insight on the difference in the chain-filler interactions, rheological studies on the composites have been performed in the two sets of samples at 160 °C. At this 'low' temperature the commercial sample maintains the grain boundary arising from the nascent powder morphology, whereas the disentangled sample loses its initial particle morphology.

3.3.2 Rheological Analysis

3.3.2.1 Rheological Analysis of Commercial UHMWPE/rGON and Disentangled UHMWPE/rGON Composites

The elastic modulus (*G'*) build-up curves for commercial UHMWPE/rGON and disentangled UHMWPE/rGON composites are shown in Figure 3-7a and Figure 3-7b, respectively. The corresponding curves obtained for the polymers without any filler are also shown for comparison. The lower value of the initial storage modulus in the disentangled UHMWPE compared to commercial UHMWPE suggests that the molar mass between entanglements (M_e) achieved on melting of the disentangled nascent powder is much larger. In accordance with the earlier findings, the commercial sample hardly shows any modulus build-up with time, whereas the disentangled sample shows modulus build-up with the transformation of melt from its non-equilibrium to equilibrium state i.e. decrease in $<M_e>$ till it reaches the equilibrium value. We would like to mention that though metastable crystalline states in polymer science have been studied extensively [24] the non-equilibrium melt states have not been investigated in detail.

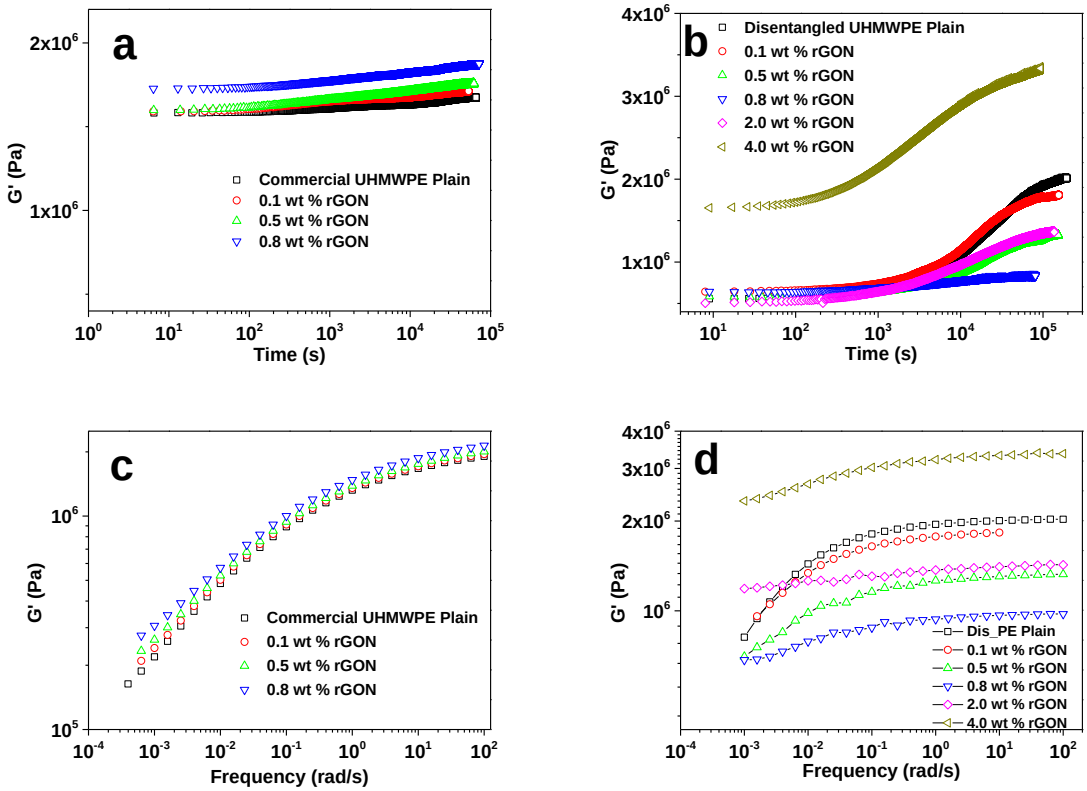

Figure 3-7 a) *G'* build-up of commercial UHMWPE/rGON composites; **b)** *G'* build-up of disentangled UHMWPE/rGON composites; **c)** dynamic frequency sweep of commercial UHMWPE/rGON composites; and **d)** dynamic frequency sweep of disentangled UHMWPE and its composites. The commercial UHMWPE samples were compressed at 160 °C, whereas the disentangled UHMWPE samples were compressed at 125 °C. The low compression temperature for the disentangled UHMWPE sample was used to follow the entanglement formation in time sweep experiments (Figure b). Followed by the time sweep experiments (**a** and **b**), on the same samples, the frequency sweep experiments were performed (Figures c and d). All rheological studies were done at 160 °C in the linear viscoelastic region.

In Figure 3-7a, the increase in elastic modulus build-up of commercial UHMWPE/rGON composites is closer to the plain commercial polymer. The slight increase in the final value of *G'*, which increases with the filler concentration, can be attributed to mechanical enhancement from the high modulus graphene. The increase in the modulus with the addition of filler is in accordance with the earlier findings reported in literature [19,25,26]. Contrary to the commercial polyethylene, the modulus build-up time of disentangled UHMWPE/rGON composites shows a strong dependence on the rGON content in the polymer matrix. Though the initial value of *G'*, observed on melting of the crystals, is independent of the rGON content (at least for rGON < 4.0 wt %), the modulus build-up time is strongly influenced by the content of the filler in the polymer matrix. For example, the polymer having no filler shows the fastest modulus build-up compared to the samples having fillers. Among the samples with fillers, the sample with 0.8 wt % of the rGON shows the slowest modulus build-up. This further strengthens the hypothesis discussed in the previous chapter of a strong molecular interaction between the polyethylene chain segments and the filler, that in the case of disentangled UHMWPE inhibits the transformation of melt from its non-equilibrium to the equilibrium state. The gradual increase in the modulus build-up time occurs with the increasing amount of rGON from 0.1 wt % to 0.8 wt %. On increasing the filler content from 0.8 wt % to 2.0 wt % the modulus build-up time tends to decrease. This decrease in the modulus build-up time suggests that the filler is more homogeneously distributed for 0.8 wt %. On increasing the filler concentration, beyond 0.8 wt %, the filler tend to aggregate causing increase in the storage modulus, as shown in Figure 3-7b.

Important to notice is that unlike the commercial sample composites, where the final plateau modulus value on the addition of filler is higher, in the disentangled UHMWPE composites the final plateau modulus reaches a minimum followed by an increase, as shown in Figure

3-8a. The minimum achieved in the final value of the plateau modulus of the composite (0.8 wt % of GON) can be attributed to the maximum interaction of the rGON network with the polyethylene chains in disentangled UHMWPE, which forbids the chains from further entanglement formation resulting in higher molar mass between entanglements M_e; hence reduces the plateau values in accordance with equation 1-2, reported in Chapter 1 [27]:

$$G_N^0 = \frac{g_N \rho RT}{M_e} \qquad \text{(Equation 1-2)}$$

The disappearance of the terminal region for the composite having 0.8 wt % of GON suggests maximum interaction between polyethylene chain segments and rGON, Figure 3-8. For the same concentration of rGON, 0.8 wt %, the increase in electrical conductivity for the disentangled UHMWPE/rGON composite is also observed, Figure 3-4. This suggests that at the specific concentration of 0.8 wt % the rGON is well dispersed, and forms an efficient continuous network, which provides enhanced electrical conductivity and high surface to volume ratio for maximum number of chain segments to attach on the surface of rGON. From Figure 3-7b, Figure 3-7d and Figure 3-8a it is evident that at and above 2.0 wt %, the plateau value of disentangled UHMWPE samples increases with increase in the filler content, suggesting aggregation of the rGON layers, contributing to the increase in the storage modulus. The aggregation retards an increase in the electrical conductivity with the increasing filler concentration (Figure 3-4).

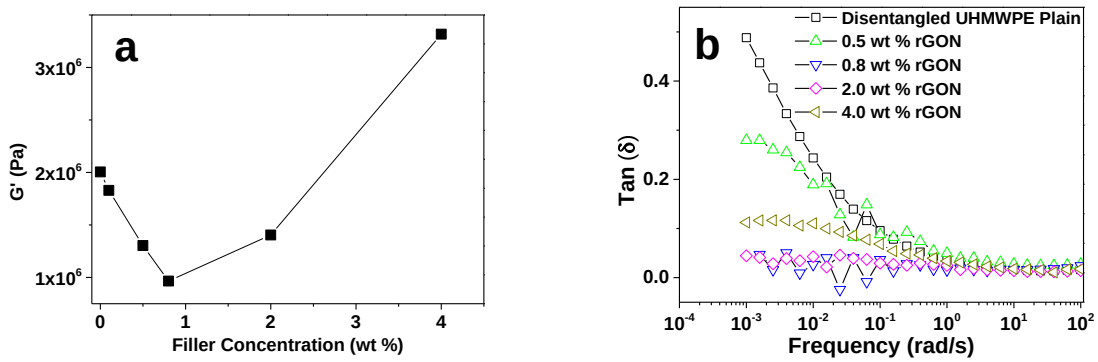

Figure 3-8 a) Storage modulus of disentangled UHMWPE/rGON composites at plateau (10 rad/s) of frequency sweep, shown in **Figure 3-7d**. **b)** Corresponding changes in phase angle, tan δ, as a function of frequency for different disentangled UHMWPE/rGON composites. The phase angle is obtained from the frequency sweep data shown in **Figure 3-7d**. All experiments were performed under isothermal condition, 160 °C in the linear viscoelastic region.

Similar trend in the drop of *G'* in HDPE/rGON composites is also observed from Figure 2-5a, Chapter 2 at high frequencies (>*G'*, *G''*cross-over frequency). The *G'* at 100 rad/s versus filler concentration is plotted and shown in Figure 3-9. Unlike UHMWPE, the decrease in HDPE samples is less significant and only appears at high frequencies above cross-over frequency. Due to the strong chain-filler interaction and short chain reptation time of HDPE chains, the presence of the filler could disturb the polymer melt network, and hinder chain dynamics by arresting some of the chain segments. At the high frequency region, the disturbed polymer melt exhibits a high M_e, estimated according to equation 1-2, causing a non-equilibrium state, and the state is maintained by the chain-filler interaction, resulting in lower plateau value. Similar to UHMWPE samples, at the filler content of c.a. 2 wt %, a most efficient chain-filler contact is reached, resulting in a minima in the *G'*. With further increment of the filler, aggregation of the filler starts to appear and gives rise to significant mechanical enhancement, which is shown as increase in *G'*. In the low frequency region (<*G'*,*G''* cross-over frequency), the reptation of the chains are hindered, hampering the chain relaxation of both short and long chains; at the same time the mechanical enhancement is more significant due to the low *G'* values of HDPE melt, and thsi results in a significant increment of *G'* in the low frequency region. Similar results in HDPE composites have also been reported in earlier work, where Vega and coworkers [28] observed a drop in viscosity and shear modulus of HDPE when mixed with MWCNT filler at a concentration of 0.52 wt %, during extrusion. The authors have attributed the drop to the adhesion of longest polymer chains onto the nanotube surface by van de Waals force.

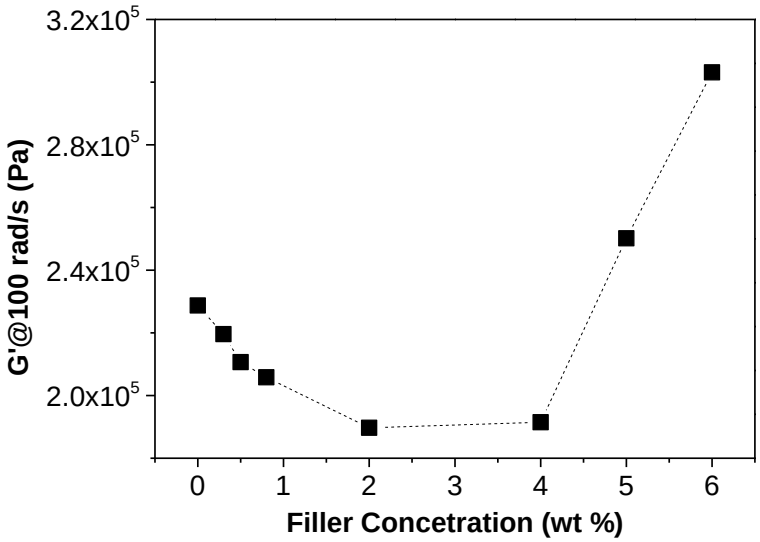

Figure 3-9 Storage modulus versus filler concentration of HDPE/rGON composites at high frequency of 100 rad/s. The values are collected from **Figure 2-5a**.

3.3.2.2 Dynamic Crystallisation and DSC Heating Run of Isothermally Crystallised Samples after Reaching Their Equilibrium States

Dynamic crystallisation of the samples after they reached the equilibrium states (after dynamic time and frequency sweeps) is shown in Figure 3-10a. It demonstrates that the crystallisation of composites upon cooling is hindered; especially at concentration of 0.8 wt % of rGON, it shows the maximum chain hindering effect from the filler, which is consistent with the dynamic frequency sweep as shown in Figure 3-7d. A quick DSC heating run is carried out on the samples that isothermally crystallised at 128 °C after dynamic time and frequency sweep, and the plots are shown in Figure 3-10b. Dual peaks are observed from the DSC plots, with the low melting peak at 134 °C and high melting peak at 141.5 °C which is close to polyethylene's equilibrium melting point. As discussed previously [29], the low melting peak can be attributed to melting of melt-crystallised crystals from entangled domains and the high melting peak can attributed to the disentangled domains in the heterogeneous melt. More detailed results and discussion are given in the following chapter. This indicates that even after long time annealing of dis-UHMWPE at 160 °C, the polymer chains are not fully entangled and during the isothermal crystallisation, the disentangled chain segments retrieve the non-entangled adjacent re-entrant crystals and this also supports the heterogeneous distribution of the entanglement during melting; however, with increasing filler concentration, the entanglement formation is highly hindered, and this can be attributed to the strong chain-filler interaction as discussed previously.

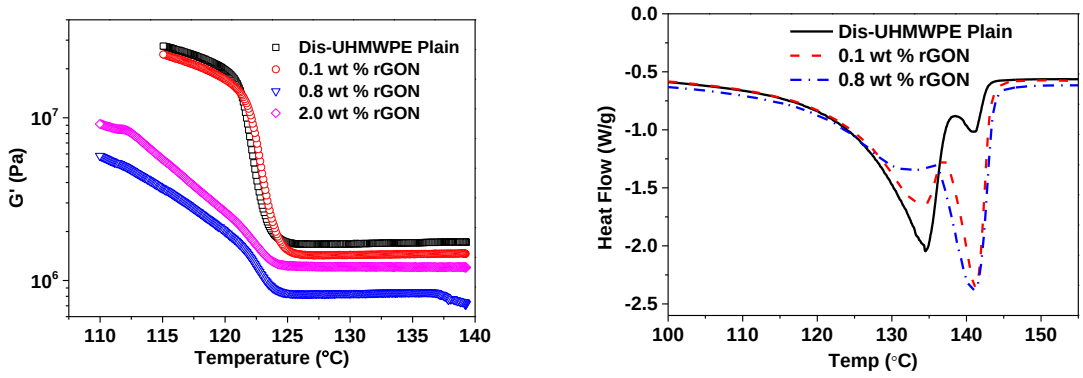

Figure 3-10 a) Dynamic crystallisation of the disentangled UHMWPE after the samples reached thermodynamic equilibrium state from 160 °C to 115 °C with a cooling rate of 0.5 °C/min; **b)** heating

run after dynamic cooling of isothermal crystallisation at 128 °C for 3 hrs with cooling and heating rate of 10 °C/min.

The commercial samples show increment of storage modulus with increasing filler content at low frequencies, Figure 3-7c, suggesting contribution of fillers in the mechanical enhancement mainly. On the contrary, similar to the modulus build-up, the frequency response of disentangled UHMWPE composites shows strong influence of rGON concentration (Figure 3-7d). The elastic to viscous transition of the polymer melt diminishes with the increasing concentration of graphene from 0.1 wt % to 2.0 wt %. The composite having 2.0 wt % of rGON shows a plateau stretching over a broad frequency range – indicating inhibition of chain reptation within the experimental time scale. The difference in the rheological behaviours between the two sets of samples, commercial UHMWPE and disentangled UHMWPE, is attributed to the entanglement density of the polymer having different powder morphology, which holds the key to the dispersion of the filler as well as the level of interaction between the filler and the polymer chains. This means that by suppressing the influence of grain boundaries between the nascent particles - that could be achieved by enhancing the chain dynamics at higher temperatures- the commercial samples shall also show a trend similar to the disentangled UHMWPE samples. The results for this case are reported in the next paragraph.

With increasing concentration of rGON, in the measured frequency region, the response of the phase angle (Figure 3-8b) combined with the storage modulus (G') (Figure 3-7a, Figure 3-7c and Figure 3-7d) rules out any possibility of thermo-oxidative degradation. The chain-scission or cross-linking would have excluded the observed decrease in the terminal region, or plateau in the elastic region, in the sample having higher concentration (4.0 wt %) of rGON. Thus the rheological response of the commercial UHMWPE and the disentangled UHMWPE, Figure 3-7c, Figure 3-7d and Figure 3-8b, in the frequency sweep experiments strongly suggests the absence of thermal oxidative degradation in the presence of rGON. The absence becomes more evident while analysing the rheological response of the commercial sample compressed at a higher temperature of 230 °C.

3.3.2.3 Rheological Analysis of Commercial UHMWPE/rGON Composites Compressed at 230 °C

In order to suppress the grain boundaries effect in the commercial UHMWPE, the samples are heated to a higher temperature, 230 °C. The increase in temperature enhances the chain dynamics thus providing greater interaction between polymer chains and the filler. Rheological experiments in the conditions same as disentangled UHMWPE composites are performed at 160 °C. Similar to disentangled UHMWPE, Figure 3-11a and Figure 3-11c, composites from the commercial sample also show decrease in the plateau modulus with the increasing filler content, where the minimum in the storage modulus is observed at 2.0 wt % of graphene loading. Frequency response of the composites is summarized in Figure 3-11b. The drop in the storage modulus and parallel shift in the frequency response with the increasing concentration of rGON suggests decrease in the melt viscosity. These findings, combined with those from the disentangled UHMWPE composites, conclusively suggest that, upon suppression of the grain boundaries influence at high temperature, it is feasible to disperse fillers more homogeneously in the matrix of the commercial sample, thus providing better interaction between polymer chains and graphene that hinders the chain mobility. Similar trends have been also reported in earlier works of commercial UHMWPE/SWCNTs nanocomposites, showing that selective physicoabsorption of the high molar mass fraction onto the filler surface promotes appreciable decrease in the storage modulus and dynamic complex viscosity at low frequencies of the composites [30]. The drop in viscosity is in agreement with the other recent findings reported elsewhere with different composites systems, as mentioned in Chapter 1, polystyrene filler with cross-linked polystyrenes [31] and UHMWPE/silica nanocomposites [32]. Jain and coworkers also reported drop in polypropylene's viscosity at a specific concentration of silica particles [33]. Recently, influence of molecular weight and chain branching on melt viscosity of PE/CNTs has been addressed by Vega and coworkers [34]. In this publication the authors have investigated rheological response of low density polyethylene, having molar mass ranging between 100K to 300K g/mol, in the presence of CNTs. The authors have conclusively shown that, with the increasing molar mass, influence of CNTs on nucleation of polyethylenes decreases, which suggests higher interaction of CNTs with the longer polymerchains. The interaction of ethylene segments with carbon black has been conclusively shown by Litvinov and co-workers while investigating EPDM/Carbon black composites by NMR , where the authors reported the adsorption of EPDM to the surface of carbon black [35,36].

It has to be noted that the maximum decrease of plateau value of commercial UHMWPE samples is observed at 2.0 wt % while for disentangled samples, the maximum decrease in the modulus is observed at 0.8 wt %. The difference is attributed to the dispersion of the filler and the molar mass distribution. Although the commercial samples were heat-treated at higher temperatures, the initial high entanglement density still restricts the chain mobility. Thus the entangled chains in the commercial samples cannot move as freely as the disentangled PE chains. This chain mobility refrains from homogeneous dispersion of the filler and its interaction with the chains in the entangled polymer melt.

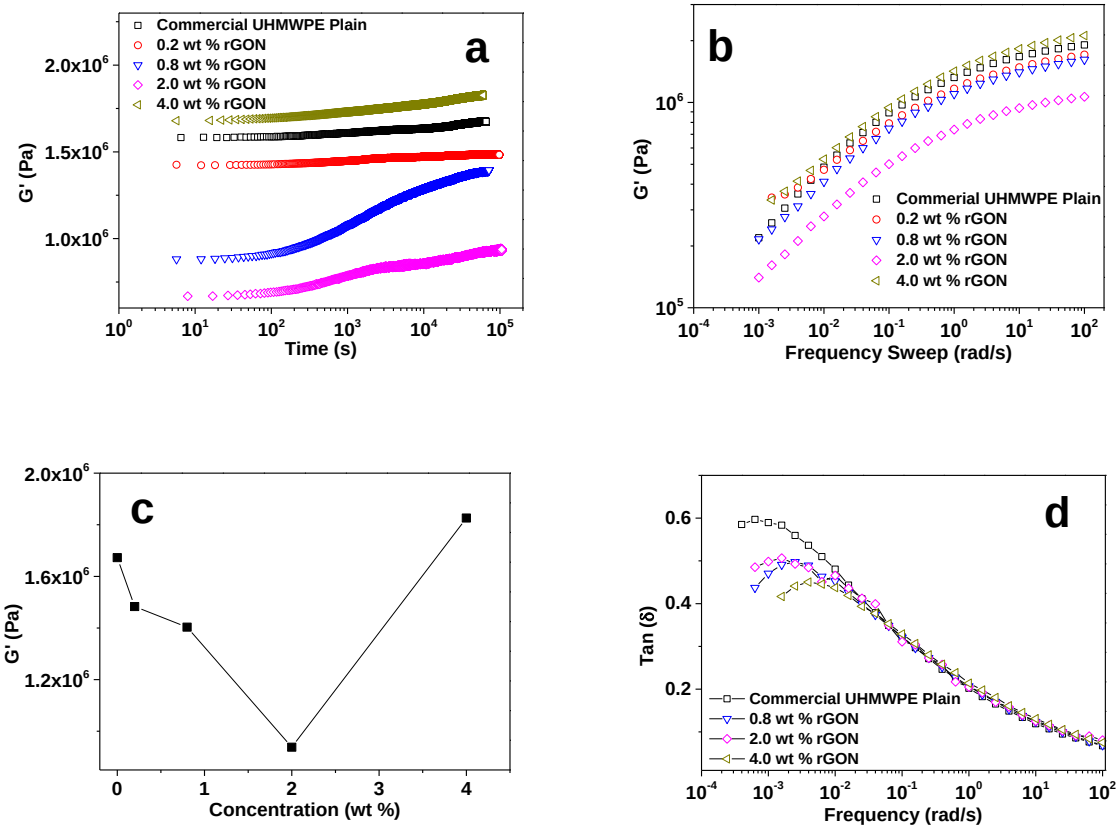

Figure 3-11 a) Storage modulus (*G'*) build-up of commercial UHMWPE/rGON composites; **b)** frequency sweep of commercial UHMWPE/rGON composites; **c)** Storage modulus of commercial UHMWPE/rGON composites at plateau of frequency sweep (10 rad/s); **d)** corresponding changes in phase angle, tan δ as a function of frequency for different commercial UHMWPE/rGON composites. All experiments were performed under isothermal condition at 160 °C in the linear viscoelastic region though these samples were previously subjected to heat treatment of 230 °C for suppression of the grain boundaries influence in dispersion of the filler. The difference in phase angle (**Figure 3-8b** to **Figure 3-11d**) can be attributed to the difference in molar mass distribution, as it is apparent from the terminal region of the two polymers (**Figure 3-7b** and **Figure 3-11b**), respectively.

These rheological findings will be discussed in more details in the next chapter, where the influence of rGON on chain configuration and associated crystallisation behaviour [37] will be further discussed by coupling solid state NMR studies and DSC analysis. The reduced melt viscosity at a specific concentration of the filler opens the new possibility of mixing UHMWPE/rGON composites to low molar mass polyolefins thus opening the prospects of enhancing mechanical properties such as tensile modulus and strain hardening of the easily processable polyolefins. This subject will be also addressed in the following chapters.

3.4 Conclusions

This chapter reports the difference in electrical conductivities and rheological response of disentangled UHMWPE/rGON and commercial UHMWPE/rGON composites. A tentative explanation of the observed difference in the electrical conductivity is attributed to (a) the difference in the bulk density of the commercial and the disentangled UHMWPE nascent powders, and (b) the different chain dynamics of the two polymers. The ease in dispersion of the filler in disentangled UHMWPE is attributed to the porous matrix and low melt viscosity of the polymer, influencing the electrical conductivity. However, the difference in the electrical conductivity between the commercial and the disentangled UHMWPE vanishes when both sets of samples are subjected to a high temperature treatment, where the grain boundary difference in the nascent powder particles is suppressed. The rheological analyses of the two sets of UHMWPE/rGON nano-composites conclusively demonstrate differences in the interaction between the chains and rGON, mainly caused by the grain boundaries present in the nascent powder morphology of the entangled polymer. After suppressing the grain boundary differences in the nascent powders, the disentangled PE samples show minima in the storage modulus at 0.8 wt % graphene content and commercial samples show minima at 2.0 wt % graphene content. The minimum value appears when the chain mobility is arrested by the strong interaction between polymer chains and graphene. The strong interaction of the polyethylene chains with the filler inhibits the disentangled UHMWPE to achieve the thermodynamic equilibrium melt state, within the experimental time scale. In the commercial sample, having a larger molar mass distribution, the higher adhesion probability of the long chains to the graphene surface lowers the elastic modulus of the polymer melt. These findings further confirm that the contact surface area of molecular chain segments of polyethylene and rGON becomes similar in the disentangled UHMWPE and the commercial samples once the difference in the grain boundaries is decreased thus resulting in similar electrical conductivity

and rheological behaviors of the two sets of nanocomposites. At the GON concentration of 0.8 wt % in the disentangled UHMWPE composite, the electrical conductivity starts increasing significantly and also the plateau reaches a minimum in the storage modulus; this demonstrates that at this specific concentration, an effective continuous filler-filler network is formed where the maximum surface to volume ratio, for the adhesion of ethylene segments in the homogeneously dispersed GON in UHMWPE matrix, is achieved.

References

[1] De Gennes, P. G. *Scaling concepts in polymer physics*. Cornell University Press: Ithaca and London, **1979**.

[2] Sturzel, M.; Kempe, F.; Thomann, Y.; Mark, S.; Enders, M.; Mulhaupt R. Novel graphene UHMWPE nanocomposites prepared by polymerization filling using single-site catalysts supported on functionalized graphene nanosheet dispersions. *Macromolecules* **2012**, 45, 6878-6887.

[3] Hu, H.; Zhang, G.; Xiao, L.; Wang, H.; Zhang, Q.; Zhao, Z. Preparation and electrical conductivity of graphene/ultrahigh molecular weight polyethylene composites with a segregated structure. *Carbon* **2012**, 50 (12), 4596-4599.

[4] Zhang, C.; Ma, C. A.; Wang, P.; Sumita, M. Temperature dependence of electrical resistivity for carbon black filled ultra-high molecular weight polyethylene composites prepared by hot compaction. *Carbon* **2005**, 43, 2544-2553.

[5] Pang, H.; Xu, L.; Yan, D. X.; Li, Z. M. Conductive polymer composites with segregated structures. *Prog. Polym. Sci.* **2014**, 39(11), 1908-1933.

[6] Mierczynska, A.; Mayne-L'Hermite, M.; Boiteux, G.; Jeszka, J. K. J. Electrical and mechanical properties of carbon nanotube/ultrahigh-molecular-weight polyethylene composites prepared by a filler prelocalization method. *Appl. Polym. Sci.* **2007**, 105, 158-168.

[7] Bakshi, S. R.; Tercero, J. E.; Agarwal, A. Synthesis and characterization of multiwalled carbon nanotube reinforced ultrahigh molecular weight polyethylene composites by electrostatic spraying technique. *Composites Part A* **2007**, 38, 2493-2499.

[8] Rastogi, S.; Yao, Y.; Ronca, S.; Bos, J.; van der Eem, J. Unprecedented ultra-modulus high-strength tapes and films of ultrahigh molecular weight polyethylene via solvent-free route. *Macromolecules* **2011**, 44, 5558-5568.

[9] Rastogi, S.; Kurelec, L.; Lippits, D. R.; Cuijpers, J.; Wimmer, M.; Lemstra, P. J. Novel route to fatigue – resistant fully sintered ultrahigh molecular weight polyethylene for knee prosthesis. *Biomacromolecules* **2005**, 6, 942-947.

[10] Pandey, A.; Champouret, Y.; Rastogi S. Heterogeneity in the distribution of entanglement density during polymerization in disentangled ultrahigh molecular weight polyethylene. *Macromolecules* **2011**, 44(12), 4952-4960.

[11] Liu, P.; Gong, K.; Xiao, P.; Xiao, M. J. Preparation and characterization of poly(vinyl acetate)-intercalated graphite oxide nanocomposite. *Mater. Chem.* **2000**, 10, 933-935.

[12] Rastogi, S.; Ronca, S. Ultra-high molecular weight polyethylene comprising refractory particles. WO 079173A1, **2010**.

[13] Mead, D. Determination of molecular weight distributions of linear flexible polymers from linear viscoelastic material functions. *J. Rheol.* **1994**, 38, 1797-1827.

[14] Talebi, S.; Duchateau, R.; Rastogi, S.; Kaschta, J.; Peters, G. W. M.; Lemstra, PJ. Molar mass and molecular weight distribution determination of UHMWPE synthesized using a living homogeneous catalyst. *Macromolecules* **2010**, 43 (6), 2780-2788.

[15] Tuminello, W. H. Molecular weight and molecular weight distribution from dynamic measurements of polymer melts. *Polym. Eng. Sci.* **1986**, 26, 1339-1347.

[16] Topsoe, H. *Geometric factors in four point resistivity measurement.* 2nd revised ed. Topsoe Haldor: Vedbaek, **1968**.

[17] Tervoort-Engelen, Y. M. T.; Lemstra, P. J. Morphology of nascent ultrahigh-molecular-weight polyethylene reactor powder: chain-extended versus chain-folded crystals. *Polym. Commun.* **1991**, 32, 343-345.

[18] Brydson, J. A. *Plastics Materials*, 4th ed. Butterworth-Heinemann: London, **1982**.

[19] Pang, H.; Chen, T.; Zhang, G.; Zeng, B.; Li, Z. M. An electrically conducting polymer/graphene composite with a very low percolation threshold. *Mater. Lett.* **2010**, 64, 2226-2229.

[20] Long, G. C.; Tang, C. Y.; Wong, K. W.; Man, C. Z.; Fan, M. K.; Lau, W. M.; Tao, Xu.; Wang, B. Resolving the dilemma of gaining conductivity but losing environmental friendliness in producing polystyrene/graphene composites via optimizing the matrix-filler structure. *Green Chem.* **2013**, 15(3), 821-828.

[21] Stauffer, D.; Aharnoy, A. *Introduction to Percolation Theory*. Taylor & Francis: London, 1991.

[22] Li, J.; Kim, J. K. Percolation threshold of conducting polymer composites containing 3D randomly distributed graphite nanoplatelets. *Compos. Sci. Technol.* **2007**, 67, 2114-2120.

[23] Rastogi, S.; Lippts, D. R.; Peters, G. W. M.; Graf, R.; Yao, Y.; Spiess, H. W. Heterogeneity in polymer melts from melting of polymer crystals. *Nat. Mater.* **2005**, 4, 635-641.

[24] Cheng, S. Z. D. *Phase transition in polymers: the role of metastable states*. Elsevier: Oxford, **2008**.

[25] Wang, B.; Li, H.; Li, L.; Chen, P.; Wang, Z.; Cu, Q. Electrostatic adsorption method for preparing electrically conducting ultrahigh molecular weight polyethylene/graphene nanosheets composites with a segregated network. *Compos. Sci. Technol.* **2013**, 89, 180-185.

[26] Chatterjee, T.; Krishnamoorti, R. Rheology of polymer carbon nanotubes composites. *Soft Matter* **2013**, 9, 9515-9529.

[27] Ferry, J. D. *Viscoelastic Properties of Polymers* 3rd ed. Wiley: New York, **1980**.

[28] Vega, J. F.; Martinez-Salazar, J.; Trujillo, M.; Arnal, M. L.; Muller, A. J.; Bredeau, S.; Dubois, Ph. Rheology, processing, tensile properties, and crystallization of polyethylene/carbon nanotube nanocomposites. *Macromolecules* **2009**, 42, 4719-4727.

[29] Pandey, A.; Toda, A.; Rastogi, S. Influence of amorphous component on melting of semicrystalline polymers. *Macromolecules* **2011**, 44 (20), 8042-8055.

[30] Zhang, Q.; Lippits,.; D. R.; Rastogi, S. Dispersion and rheological aspects of SWNTs in ultrahigh molecular weight polyethylene. *Macromolecules* **2006**, 39, 658-666.

[31] Mackay, M. E.; Dao, T. T.; Tuteja, A.; Ho, D. L.; Brooke van, H.; Kim, H. C.; Hawker, C. Nanoscale effects leading to non-Einstein-like decrease in viscosity. *Nat. Mater.* **2003**, 2, 762.

[32] Maurer, F. H. J.; Schoffeleers, H. M.; Kosfeld, R.; Uhlenbroich, T. H. Analysis of polymer filler interaction in filled polyethylene. *Prog. Sci. Eng. Compos.* **1982**, 803.

[33] Jain, S.; Goosens, G. W. M.; van Duin, M.; Lemstra, P. J. Strong decrease in viscosity of nanoparticle-filled polymer melts through selective adsorption. *Soft Matter* **2008**, 4, 1848-1854.

[34] Vega, J. F.; da Silva Y.; Vicente-Alique, E.; Nunez-Ramirez, R.; Trujillo, M.; Arnal, M. L.; Muller, A. J.; Dubois, P.; Martinez-Salazar, J. Influence of chain branching and molecular weight on melt rheology and crystallization of polyethylene/carbon nanotube nanocomposites. *Macromolecules* **2014**, 47, 5668-5681.

[35] Litvinov, V. M.; Steeman, P. A. M. EPDM-carbon black interactions and the reinforcement mechanisms, as studied by low-resolution ^{1}H NMR. *Macromolecules* **1999**, 32, 8476-8490.

[36] Litvinov, V. M.; Orza, R. A.; Klüppel, M.; van Duin, M.; Magusin, P. C. M. M. Rubber-filler interactions and network structure in relation to stress-strain behavior of vulcanized, carbon black filled EPDM. *Macromolecules* **2011**, 44, 4887-4900.

[37] Xu, J. Z.; Zhong, G. J.; Hsiao, B. S.; Fu, Q.; Li, Z. M. Low-dimensional carbonaceous nanofiller induced polymer crystallization. *Prog. Polym. Sci.* **2014**, 39, 555-593.

4 Heterogeneous Distribution of Entanglements and Their Influence on Crystallisation in Disentangled UHMWPE/rGON Composites

Abstract

In Chapter 3, the influence of reduced graphene oxide nanoplatelets (rGON) on rheological response of disentangled UHMWPE was studied. The study provided insight in the influence of the filler on chain dynamics having implications on entanglement formation. The chain-filler interaction in the composite lead to the suppression in the build-up of elastic shear modulus, to an extent that non-equilibrium melt state is retained within the experimental time. In this chapter, a thermal protocol is used to follow the influence of non-equilibrium polymer melt on crystallisation kinetics of disentangled UHMWPE with and without rGON. The analysis is carried out by means of differential scanning calorimetry (DSC) and the results are supported by rheology. The changes in enthalpic relaxation process are found in good agreement with the rheological response of the material during shear modulus build-up. For an example, thermal analysis shows the presence of two endothermic peaks in a sample that is left to crystallise under isothermal condition after melting. The high temperature endothermic peak (141.5 °C) is related to melting of crystals obtained on crystallisation from the disentangled domains of the heterogeneous (non-equilibrium) polymer melt, whereas the low melting temperature endothermic peak is related to melting of crystals formed from entangled domains of the melt. It is found that with increasing the annealing time in melt (160 °C), the enthalpy of the lower melting temperature peak increases at the expense of the higher melting temperature peak, confirming transformation of the non-equilibrium polymer melt to equilibrium melt state. The enthalpic relaxation process as a function of rGON has been also investigated. The observations are that at the specific concentration of the filler, where the plateau value of elastic shear modulus at 10 rad/s is at the minimum, the high endothermic peak remains independent of the annealing time of the polymer melt at 160 °C. This observation strengthens the concept that in the presence of the filler, chain dynamics is arrested to an extent that the everlasting non-equilibrium melt state having lower entanglement density is retained facilitating crystal formation having high melting endothermic temperature.

4.1 Introduction

Topology of methylene segments in the non-crystalline region of the semi-crystalline polymer, UHMWPE, has profound influence on mechanical deformation either uniaxially or biaxially. The topology can be tailored by controlling crystallisation kinetics either by dissolution or controlled polymerisation [1,2,3,4]. The influence of molar mass on the topology of non-crystalline phase has been a subject of interest where the abstract nature of the mobile phase is probed by solid state NMR [5]. Yao *et al.* showed the influence of polymerisation conditions on the non-crystalline phase [6]. To recall, the authors demonstrated that the non-crystalline region in the polymer synthesised using Ziegler-Natta deferred from the polymer synthesised using the single-site catalytic system.

The absence of structural order in the non-crystalline region of semi-crystalline polymers imposes challenges to an extent that the issue of adjacent or non-adjacent re-entry remains unsolved even today after the discovery of chain folded crystals in 1957 [7,8]. Recently, in UHMWPE, it is shown that melting temperature of the as synthesised polymer (nascent) approaches equilibrium melting temperature because of the restricted mobility of the methylene segments in the non-crystalline region [9]. Differentiation between the nano-crystalline regions of the polymer synthesised using Z-N and single site catalytic systems can be made by following kinetics in melting of the crystals [6,9]. To recall, when the nascent sample is left to anneal at the onset of the melting temperature of the endothermic peak, having peak temperature close to 141.5 °C, crystals tend to melt via consecutive detachment of chains from the crystal surface followed by reeling-in of the chain stems into melt [9]. The rate at which the consecutive detachment occurs is suggested to be dependent on the polymerization conditions i.e. topological constraints, entanglements, present in the non-crystalline region. Combining the NMR observations on segmental mobility in the non-crystalline region and melting kinetics of crystals, the high temperature melting peak of the nascent crystals is shown to be related with the restriction imposed by the non-crystalline region. Combining the mechanical deformation characteristics of the nascent UHMWPE crystals in solid-state with the melting kinetics, it is well understood that the number of entanglements or entanglement density in the non-crystalline region phase can be tailored by controlling crystallisation kinetics.

The nascent crystals, having reduced number of entanglements, on melting, result into the non-equilibrium polymer melt where the initial low elastic shear modulus increases with time

till the melt reaches the equilibrium state. Time required in build-up of the shear elastic modulus is shown to be dependent on the molar mass following the power law $t_{\text{build-up}} \sim M^{2.6}$ [28]. The non-equilibrium polymer melt is suggested to have heterogeneous distribution of entanglements, with domains having low and high density of entanglements [4]. This heterogeneity, in the distribution of entanglements, will have implications on crystallisation kinetics. For an example, methylene segments in the low density entanglement domain are likely to have lower nucleation barrier compared to the segments in the high density entanglement domain [21,22,23,24].

In this chapter we aim to investigate the influence of heterogeneous melt on crystallisation kinetics. Nascent UHMWPE, synthesised using a single-site catalytic system, provides unique opportunity to investigate the influence of heterogeneity in entanglements on crystallisation – in the same polymer. For the purpose a specific thermal protocol is applied where the residence time of the polymer in its non-equilibrium melt state is varied. Thus by increasing the residence time at melt, with increasing elastic shear modulus, the overall entanglement density of the polymer melt is increased. Crystallisation kinetics of the heterogeneous melt has been pursued by annealing the sample below equilibrium melting temperature. At a critical crystallisation temperature (128 °C), where the nucleation rate dependence on supercooling is suppressed, the influence of heterogeneous entanglement distribution is realised in the form of two endothermic peaks on heating the annealed sample to melt. The high temperature endothermic peak (141.5 °C) is found to be close to the equilibrium melting temperature, whereas the low temperature endothermic (135 °C) peak is related to the component that did not crystallise under isothermal condition. These observations will be related to the elastic shear modulus build-up of the polymer, reflecting the homogenisation of the heterogeneous distribution of entanglements in melt state. At the end of the chapter the conclusions drawn will be strengthened by investigating composites of polyethylene with rGON. What follows are the experimental findings on the nascent disentangled polymer, where a commercial UHMWPE having entangled nascent crystals, synthesised using a Z-N catalyst is used as a comparative example.

In this Chapter, the results suggest presence of heterogeneous melt having two domains/regions: a more entangled region and a less entangled region, obtained from disentangled UHMWPE after annealing at 160 °C and isothermal crystallisation at 128 °C. The two regions are found to be crystallizing differently in kinetics and the change in the melting enthalpies of the two regions during the subsequent heating reflects a continuous

transformation of the heterogeneous melt from non-equilibrium state to equilibrium state. This is found in line with rheological behaviour of the sample. Furthermore, we also investigated the influence of reduced graphene oxide nanofiller on the crystallisation behaviour of the heterogeneous melt, to support our recent claim that the entanglement formation is prohibited due to the presence of strong chain-filler interaction [10]. The chain-filler interaction is further characterized by solid state NMR, and related back to the thermal analysis and rheological analysis.

4.2 Experimental

4.2.1 Materials

Toluene (99.8%, anhydrous) and methyaluminoxane solution (MAO, 10 wt % solution in toluene) were purchased from Sigma-Aldrich; ethylene (grade 3.0) was purchased from BOC, and FI catalyst was purchased from MCat. Materials for the synthesis of graphene oxide were purchased from Sigma-Aldrich: fine graphite powder (diameter of c.a. 25 μm), 98 wt % concentrated sulphuric acid, distilled water, potassium permanganate, and 30 wt % hydrogen peroxide. Commercial UHMWPE powder was purchased from Sigma-Aldrich. Antioxidant Irganox 1010 is purchased from Ciba. All reagents are used as received.

4.2.2 Synthesis of Disentangled UHMWPE

The disentangled UHMWPE samples are synthesized using the same polymerisation method described in Chapter 3 using FI Catalyst. Two reactions with different reaction times were carried out for the study, 10 min and 30 min reaction respectively.

The obtained polymers were then filtered, and further washed with copious amount of methanol/acetone. To achieve a good dispersion of antioxidant, 0.7-1.0 wt % antioxidant was then added to the polymers suspended in acetone and stirred under a fume hood. After all the acetone has evaporated, the polymer was further dried in a vacuum oven at 40 °C for 720 min. The disentangled UHMWPE with 30 min reaction is the same as the one used in Chapter 3.

4.2.3 Synthesis of GON and Preparation of Composites

The GON was synthesized in accordance to a modified Hummers Method [11] with further modifications as described in Chapter 3 [10]. To recall, after the oxidation reaction was finished, the resultant material was repeatedly vacuum-filtered and washed of 3 times with 5 wt % HCl followed by a few times of distilled water wash, until the upper liquid became dark. The suspension became darker with the increasing number of washing steps, suggesting progressive extraction of GON from the bottom layer to the upper suspension. The average number of water washing steps applied was approximately ten, until the pH of the suspension changed from ~2 to ~7. The previously collected dark-liquid portions were combined and dried in a petri dish at 50 ºC for 2 days. Films of GON were obtained by peeling them off from the petri dish.

The composites of 30 min-reaction disentangled UHMWPE and GON were then prepared using a two-step preparation method, as described in Chapter 3 [10]: composites having GON content of 0.1 wt % and 0.8 wt % were prepared using the same method. GON reduces to rGON when the composites reach high temperatures, such as 160 °C.

4.2.4 Determination of Molar Mass and Molar Mass Distribution

Weight averaged molecular weight M_w and molecular weight distribution (MWD) of the synthesized UHMWPE was estimated by melt rheology using Advanced Rheometrics Expansion System (ARES) of TA instruments, and the results are shown in Table 4-1, and the method for calculation is described earlier in Chapter 3 and elsewhere [3,12 ,13].

Table 4-1 Molecular characteristics of the UHMWPE samples; C-PE refers to commercial UHMWPE and Dis-PE represents disentangled UHMWPE.

Samples	M_w **(×10^6 g/mol)**	M_w/M_n	G_N^0**@100 rad/s (MPa)***
C-PE	4.5	31.1	2.0
0.8 wt % C-PE/rGON	4.5	31.1	2.0
Dis-PE-1 (30 min-reaction)	4.8	3.1	2.0
0.1 wt % Dis-PE-1/rGON	4.8	3.1	1.8
0.8 wt % Dis-PE-1/rGON	4.8	3.1	0.8
Dis-PE-2 (10 min-reaction)	2.0	2.3	2.0

*G_N^0 is obtained from dynamic frequency sweep after the samples plateau in elastic shear modulus build-up.

4.2.5 Thermal Analysis

A Q-2000 MDSC from TA instruments was used to follow the crystallisation kinetics and subsequent melt enthalpies. High precision T-Zero pans with lids were used for the experiments. To minimize the thermal lag caused by the samples, the sample weight is kept within 1.5±0.1 mg for each sample. During the measurement, nitrogen is continuously purged at 50 mL/min. Temperature and enthalpy calibrations were conducted using certified indium at the heating rate used for the samples. A thermal protocol has been devised to obtain samples having different entanglement densities and to follow the crystallisation kinetics and enthalpies. The protocol is given in Scheme 4-1.

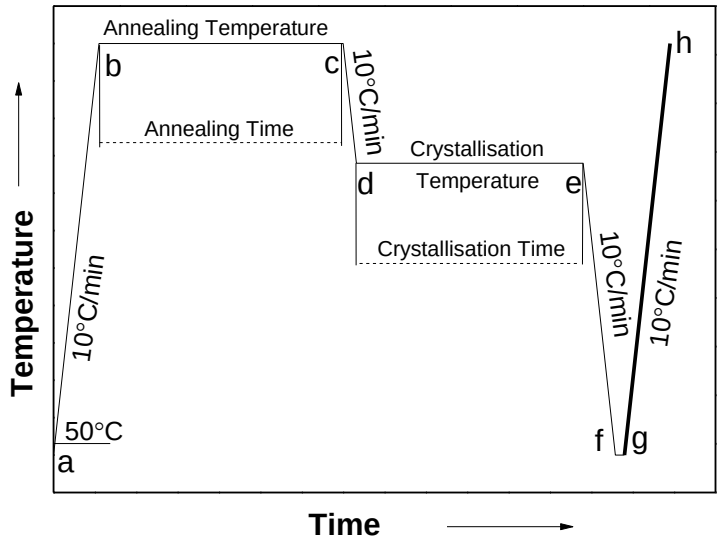

Scheme 4-1 Thermal analysis protocol; different annealing times are chosen to vary entanglement density; isothermal crystallisation at different temperatures, where 128 °C differentiates crystallisation from entangled and disentangled domains.

(a-b) Heating from 50 °C to an annealing temperature which is higher than PE's equilibrium temperature (141.5 °C) at 10 °C/min, for instance 160 °C;

(b-c) Annealing for a fixed time (5, 30, 60, 180, 360, 720, 1440 min, respectively);

(c-d) Cooling to an isothermal crystallisation temperature, for example 128 °C, at 10 °C/min;

(d-e) Isothermal crystallisation at the isothermal crystallisation temperature for a fixed time, for instance, 60, 180, 300 min;

(e-f) Cooling to 50 °C at 10 °C/min;

(g-h) Second heating from 50 ºC to 160 °C at 10 °C/min.

The DSC plots shown in the Results and Discussion section were obtained during the ramp **g-h**.

4.2.6 Rheology Measurements

The nascent powders were compressed into a plate having diameter of 50 mm and thickness of c.a. 0.7 mm at a fixed temperature of 125 °C, combined with pressures of 510 bars for 5

min, 1020 bars for 10 min and 2040 bars for 5 min. Disks with 12 mm diameter were cut from the compressed plate using a hollow punch for the rheology measurements.

The rheological measurements are performed using the protocol described in Chapter 3.

4.3 Results and Discussion

4.3.1 Crystallisation of Heterogeneous Polymer Melt

Disentangled UHMWPE used in this study has unique features, for instance, significant low initial entanglement density and well-tailored molar mass and molar mass distribution. Extensive studies on chemistry and physics of the UHMWPE have been carried out [1,3, 14,15,16]. To recall, due to the high solubility of the catalyst in the polymerisation medium, toluene for instance, a uniform distribution of active sites across the medium becomes feasible and their concentration is kept low in order to achieve a reasonable distance between growing chains, so to lower the possibility of entanglement formation during the synthesis. In addition, the activity of the catalyst stays high even at relatively low polymerisation temperature (10 °C for instance), and it is important to notice that at this temperature the crystallisation rate is high enough for the polymer to start crystallising within the first few seconds of polymerisation. As a result, the polymer has a very low entanglement density as well as well-controlled molar mass and molar mass distribution. However, the chains start entangling as soon as the melting point is reached, and the change in entanglement density has been successfully monitored by rheology [1,14]. In rheology, it has been shown that the disentangled UHMWPE has a significant elastic shear modulus build-up with increasing annealing time at 160 °C, associated with transformation of the polymer melt from non-equilibrium to equilibrium state, whereas the commercially available, entangled UHMWPE (usually synthesised by Ziegler-Natta catalyst), shows little increase in its modulus. Figure 4-1a shows the elastic shear modulus build-up of a disentangled sample, Dis-PE-1, and an entangled UHMWPE sample, C-PE and the results are plotted in normal scale.

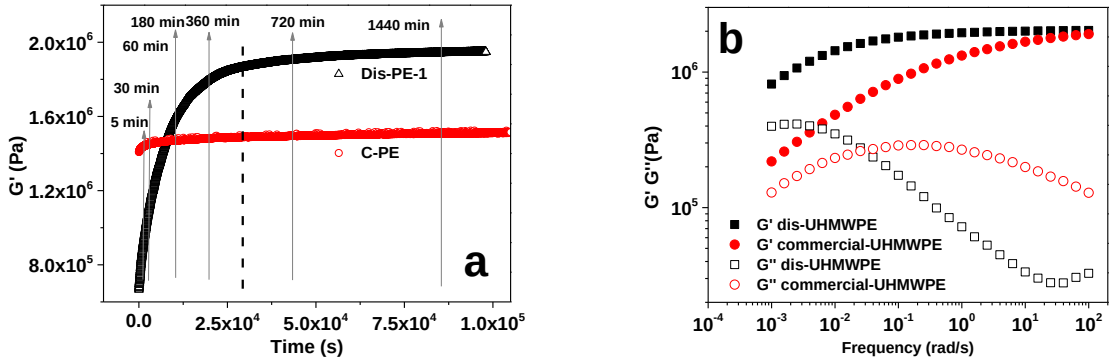

Figure 4-1 a) Elastic shear modulus build-up of disentangled (open triangle) and entangled UHMWPE (open cycle); the measurements were carried out at 160 °C, at a constant frequency of 10 rad/s and constant strain of 0.5 % (well within the linear viscoelastic regime); the arrows show a selection of annealing time at 160 °C that have been used in the DSC measurements, in order to create samples with different entanglement density; **b)** Frequency sweep of the polymers after reaching plateau as shown in **a)**.

The near absence of elastic shear modulus build-up in the entangled UHMWPE, compared to the disentangled UHMWPE, suggests that the sample synthesised using Ziegler-Natta catalyst approaches equilibrium melt state much faster than the sample synthesised using single-site FI catalytic system, Figure 4-1a. The continuous shear modulus build-up of disentangled sample indicates that before reaching the thermodynamic equilibrium state, the polymer melt stays in a non-equilibrium state, where M_e (the molar mass between entanglements) is considerably higher than the equilibrium value (we should recall that M_e can be mathematically related to the elastic shear modulus at rubbery plateau as described in Chapter 1, equation (1-2) [1,17]). G_N^t, obtained by normalizing the absolute value of G' after time t in the melt by the plateau value G_N^0, can be used to estimate the change in entanglement density (or M_e).

To obtain UHMWPE with different entanglement densities, the nascent disentangled UHMWPE samples are melted and kept for different annealing times at 160 °C. The annealing times are chosen by referring back to the modulus build-up, as shown in Figure 4-1a. After annealing, the samples are cooled to 128 °C where they are subjected to isothermal crystallisation for 180 min. Prior to the second heating, g-h, the samples are cooled to 50 °C at 10 °C/min, e-f, Scheme 4-1. The DSC curves of heating ramp, g-h, are plotted in Figure 4-2a, and for comparison, the entangled commercial C-PE was subjected to the same thermal protocol and the results are plotted in Figure 4-2b.

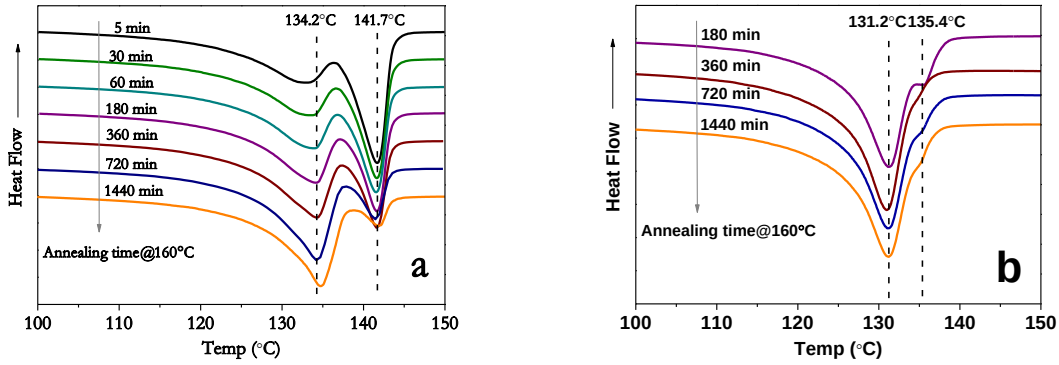

Figure 4-2 DSC plots, obtained from cycle g-h of **Scheme 4-1**, of **a)** Dis-PE-1 samples annealed at 160 ºC for different times selected according to **Figure 4-1a**; **b)** C-PE samples.

The disentangled UHMWPE samples show two separate melting peaks after annealing and isothermal crystallisation, Figure 4-2a, with a lower temperature melting peak at 134.5 °C and a higher temperature melting peak close to 141.5 °C, indicating crystallisation from entangled and disentangled domains of the heterogeneous polymer melt, respectively. Remarkable fact is that the melting peak of 141.5 °C is close to the equilibrium melting temperature, which following the Gibbs-Thomson equation refers to extended chain crystals or the nascent crystals having restricted mobility in the non-crystalline region. The ratio between the low and the high melting temperature peaks changes with the annealing time of the melt at 160 °C. Considering that the elastic shear modulus build-up with the annealing time at 160 °C and transformation of the heterogeneous melt into more homogeneous state, the increase in the heat of fusion of the low melting temperature peak is likely to be influenced by the entangled state of the material that causes increase in the nucleation barrier [21].

The absence of the prominent double-peak and the inversion process in the comparative commercial sample, as shown in Figure 4-2b, further strengthens the hypothesis that entanglement density has influence on the kinetics of the enthalpic increase in the low temperature peak, as observed in the case of disentangled samples of UHMWPE.

To have insight into the origin of the double-peak in the disentangled UHMWPE the samples were left to crystallise at different temperatures at d-e in the Scheme 4-1 for a fixed isothermal crystallisation time of 180 min after being annealed in melt, b-c, for 60 min. The observations are that the endothermic peak observed on heating from g-h shows gradual shift from 135 °C to 141.5 °C with increasing crystallisation temperature from 120 °C to 126 °C,

Figure 4-3a. The shift to the higher temperature with increasing the crystallisation temperature is in good agreement with the earlier findings and can be explained by the increase in crystal thickness and/or crystal perfection [18,19]. However, the increase in the high endothermic peak to 141.5 °C is rather unique and appears to be a property of disentangled UHMWPE that requires further consideration. Above the annealing temperature of 126 °C, Figure 4-3a, the appearance of low temperature endothermic peak together with the high temperature endothermic peak, on heating the sample along g-h, is observed. The enthalpy of the low temperature endothermic peak increases with the crystallisation temperature. The presence of the low temperature peak and the associated heat of fusion can be explained by the higher nucleation barrier at lower supercoolings. Thus the origin of the low temperature endothermic peak is from the melt crystallised component of the sample on cooling from e-f, whereas the high temperature endothermic peak is related to the crystalline component obtained during isothermal crystallisation. The comparative example of commercial sample also shows the presence of two peaks on crystallisation at lower supercoolings, in Figure 4-3b. However, unlike disentangled sample the high temperature endothermic peak is found to be around 134 °C which is not surprising and is along with the expected earlier reported findings on linear polyethylenes [20].

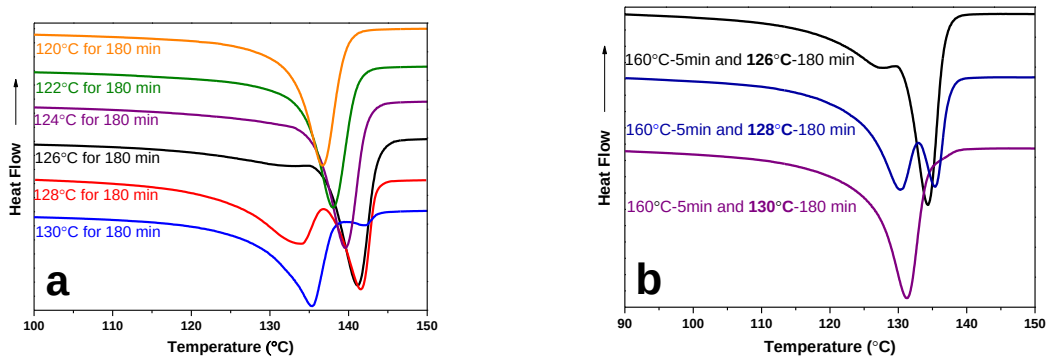

Figure 4-3 DSC plots, obtained from ramp g-h of **Scheme 4-1**, of **a)** Dis-PE-1 samples annealed at 160 ºC for a fixed time and isothermally crystallised for 180 min at different temperatures, and **b)** C-PE samples annealed at 160 ºC for a fixed time and isothermally crystallised for 180 min at different temperatures.

To have further insight on the origin of the double peaks in disentangled UHMWPE the sample of Dis-PE-2 was left to crystallise at 128 °C for different times, ranging from 60 min to 300 min. With increasing isothermal crystallisation time the high temperature endothermic peak increases in enthalpy at the expense of the low temperature endothermic peak, as

observed in Figure 4-4. This result further confirms that the enthalpy related to the high temperature endothermic peak is dependent on the supercooling that influences the nucleation density of the polymer.

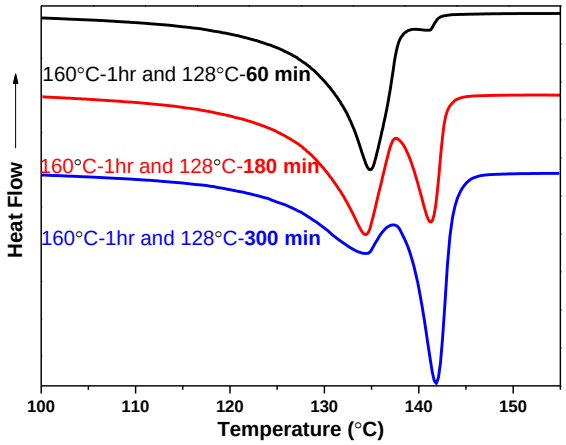

Figure 4-4 DSC plots, obtained from cycle g-h of Scheme 4-1, of Dis-PE-1 samples annealed at 160 ºC for a fixed time and isothermally crystallised at 128 °C for different times.

To rule out the possibility of formation of crystals giving low temperature endothermic peak during isothermal crystallisation, one sample is annealed at 160 ºC for 60 min and isothermal crystallisation at 128 ºC for 180 min and then heated to 160 ºC without cooling to 50 ºC. As expected, only high temperature endothermic peak is observed.

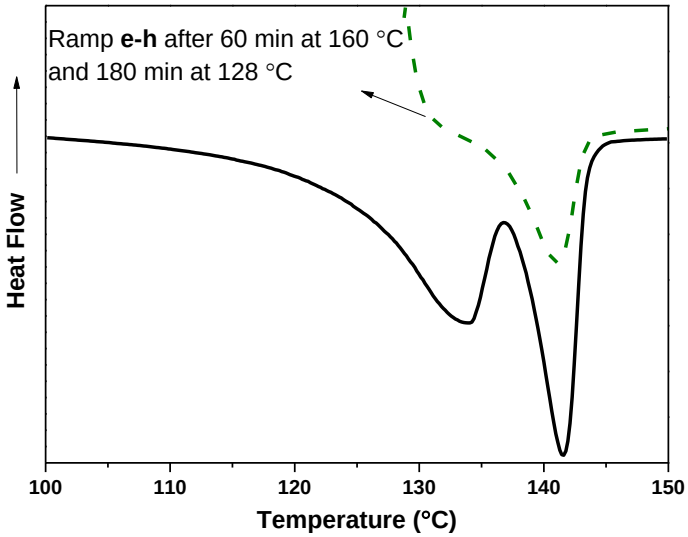

Figure 4-5 Dash line is DSC plot obtained from ramp e-h of **Scheme 4-1**, of the disentangled UHMWPE samples annealed at 160 ºC for 60 min and isothermally crystallised at 128 °C for 180 min. As a comparison, ramp g-h of **Scheme 4-1** of a same disentangled sample, after the same heat treatment (160 ºC for 60 min and 128 ºC for 180 min), but with cooling, is also displayed in the figure.

This further confirms that crystals responsible for high melting endothermic peak are formed at 128 ºC, whereas the crystals that give low temperature endothermic peak crystallise during dynamic cooling.

The influence of entanglements on nucleation density is in agreement with the earlier findings where Hikosaka and co-workers demonstrated that, with the increasing entanglements nucleation density decreases [21,22,23,24]. To recall, for their study the authors also created disentangled state but in a low molar mass high density polyethylene either by polymerisation or by crystallising the sample from melt in the hexagonal phase at high pressure and temperature. The sample in disentangled state showed higher nucleation density compared to its entangled state, which was achieved on annealing the sample in melt.

On summing up the findings above it can be conclusively stated that in disentangled UHMWPE the inversion in peak ratio arises from the entanglement formation, i.e. with the increasing entanglement density or increasing elastic shear modulus. The enthalpy of the high temperature endothermic peak decreases with annealing time at 160 °C for the samples crystallised at 128 °C for the same isothermal crystallisation time. However, when the disentangled sample after reaching the equilibrium melt state is left to the isothermal crystallisation temperature of 126 °C, Figure 4-6, the high temperature endothermic peak at 141.5 °C becomes pronounced. Independent of the annealing times in melt state, of the samples having different entanglement density, no difference in enthalpy of the high temperature endothermic peak could be observed. These findings do question the nature of entanglements, interaction between the neighbouring chains and their influence in packing during crystallisation.

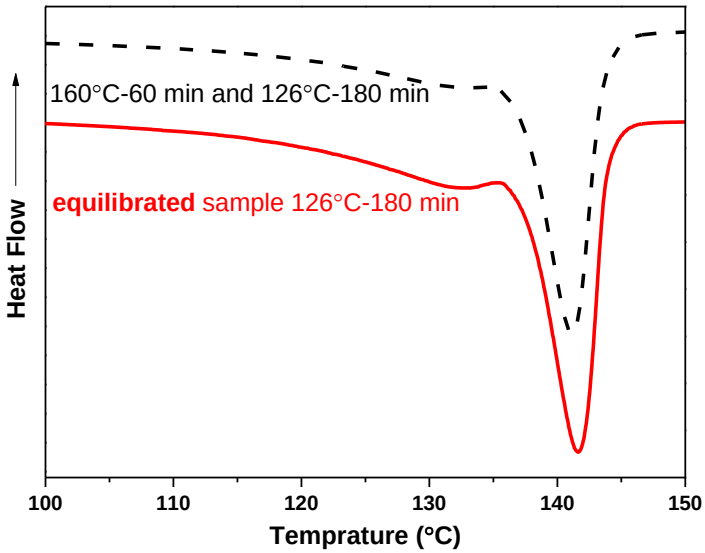

Figure 4-6 DSC plots, obtained from ramp g-h of **Scheme 4-1**, of the disentangled UHMWPE samples annealed at 160 ºC for different times and isothermally crystallised at 126 °C for 180 min. The dash line represents a sample that was annealed for 60 min, and the continuous line represents a sample that was equilibrated which was annealed at 160 ºC for over 1440 min (24 hrs).

The low temperature endothermic peak, when normalised by the total enthalpy of the two endothermic peaks, shows increase with increasing annealing time in melt. The rate at which the low temperature endothermic peak increases shows strong dependence on the molar mass. For example, the time required for the increase in the enthalpy of the low temperature peak is longer for the higher molar mass. Such an example is depicted in Figure 4-7. The observed trend is in agreement with the modulus build-up of the disentangled UHMWPE by rheology. The figure shows good correlation between the thermal and rheological response of the non-equilibrium polymer melts having different molar masses. The increase confirms the influence of entanglement formation on crystallisation. Any melt memory effect is ruled out by the studies performed on the entangled polymer melt, especially on the fully entangled polymer synthesised using the single-site catalytic system, as shown in Figure 4-6. To clarify this point, the sample prior to its cooling to the crystallisation temperature was left in melt for transformation from non-equilibrium to equilibrium state for more than 1440 min. Thus the appearance of the high melting temperature peak (141.5 °C) at 126 °C reflects the differences in the entangled nature achieved in the sample synthesised using the single-site catalytic system, compared to the Z-N catalyst. Similar high temperature endothermic peak, under similar crystallisation conditions, is observed in polymer synthesised using the Z-N catalyst

but at lower temperature (134.5 °C). Thus important to realise is that the inversion in enthalpy during transformation of non-equilibrium melt to equilibrium state is an intrinsic property of the polymer synthesised using the single-site catalytic system, Figure 4-6. To follow the influence of melt temperature on the rate of entanglement formation thermal analysis experiments are performed. These are summarised in **Figure 4-8**a, where as anticipated the observations are that the time required for reaching the equilibrium melt state decreases with the increasing annealing temperature.

What follows is a more detailed analysis on Figures 4-6 and 4-7.

In rheology, as observed from the modulus build-up in Figure 4-1a, and Figure 3-7b in Chapter 3, there is continuous entanglement formation of the disentangled polymer in the melt, which suggests that with increasing annealing time, more entangled region will form at the expense of disentangled domains. This is found to be in agreement with our DSC measurements, Figure 4-2a, where it shows low temperature endothermic peak increases at the expense of high temperature endothermic peak. To see a clear trend of the change in enthalpies of both low and high melting peaks with annealing time of the disentangled PE, the ratio between the areas of low temperature endothermic peak to the whole melting peak versus the annealing time is plotted and shown in Figure 4-7 (open symbols). As a comparison, the corresponding modulus build-up from rheology is added (filled symbols).

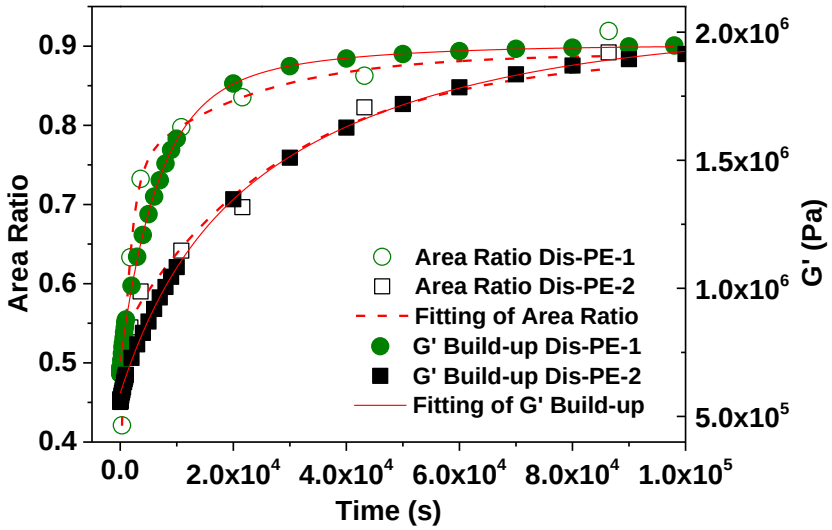

Figure 4-7 Area ratio of the the low temperature endothermic peak to the overall endothermic peak, versus annealing time at 160 °C, of Dis-PE-1 (open squares) and Dis-PE-2 (open cycles), and storage modulus build-up of Dis-PE-1 (filled squares) and Dis-PE-2 (filled cycles); the measurement is

carried out at 160 °C, at frequency of 10 rad/s and strain of 0.5 % (within linear viscoelastic regime). Both the area ratio and build-up curves are fitted with equation (4-1) to understand chain dynamics at different stages and the influence of the molar mass, with dotted red lines for area ratio fitting and the red continuous lines for elastic shear modulus build-up fitting.

A proper overlay between the area ratio and *G'* build-up is observed, indicating that the crystallisation kinetics is dominated by the change in entanglement density. This further confirms the transformation of the heterogeneous melt from non-equilibrium polymer melt to equilibrium state. Similar to elastic shear modulus build-up, a low initial value, a consecutive increase with annealing time, and achievement of a stable value at the time when the high temperature endothermic peak almost vanishes are apparent in the area ratio. The low initial value, at the beginning of the annealing, represents high enthalpy of the high temperature endothermic peak that corresponds to a high amount of chains in a low entanglement state. The subsequent increase of the ratio, related to the increase of low temperature endothermic peak enthalpy and decrease of high temperature endothermic peak, is due to the formation of entanglement, and further followed by a plateau value which represents its equilibrium state.

The influence of the molar mass on the entanglement formation of disentangled UHMWPE has been investigated using rheology by Pandey *et al.* [1], and it has shown that polymer with longer chains takes longer time for the modulus to reach the thermodynamic equilibrium. This is also seen in the crystallisation behaviour of the polymer melts having different molar mass chains and thus different entanglement density, as shown in Figure 4-7, together with their corresponding modulus build-up (open and filled symbols respectively).

Dis-PE-1, having the higher molar mass of 5.0 x 10^6 g/mol, takes longer time to reach its equilibrium state, so the non-equilibrium heterogeneous melt survives for longer time. As a result, the increase in the low melting peak area is delayed compared to that of Dis-PE-2 having low molar mass, as shown in the figure. This is in line with their modulus build-up, which also shows faster modulus build-up for Dis-PE-2 than Dis-PE-1.

The modulus and area ratio build-up can be divided into two regions: region I, a quick build-up at short times due to chain explosion and mixing; region II, a slow build-up at long times due to chain reptation and further entanglement. To have a quantitative estimation of the chain entanglement and relaxation in the two different regions, equation (4-1) is applied to fit both the rheology and area ratio, which was first proposed by Teng *et al.* [25].

$$A(t) = A_N^0 - \sum_{i=1}^{N} \mathrm{A}_i \exp\left(\frac{-t}{\tau_i}\right) \qquad (4\text{-}1)$$

where A(t) is the modulus or the area ratio at time t, A_N^0 is the plateau value of storage modulus build-up or the plateau value of the area ratio, A_i is the increment in elasticity in modulus build-up or area ratio in crystallisation, corresponding to the relaxation mode with characteristic time τ_i. Two modes are used to properly fit the curves, in order to match the two-step build-up behaviour defined for disentangled UHMWPEs. The first mode at short times, τ_1, can be attributed to entropic mixing of the disentangled chains and the second mode at longer times of τ_2 is related to the further chain diffusion. For details of the fitting using two modes for disentangled UHMWPE, readers are referred to an article from Andablo-Reyes *et al.* [26]. The fitting curves are shown in Figure 4-7, where the fitting lines for the area ratio are dotted and the fitting lines for the modulus build-up are continuous. The fitting parameters for Dis-PE-1 and Dis-PE-2 in both cases of modulus build-up and area ratio are shown in Table 4-2.

Table 4-2 Fitting parameters of the polymers (Dis-PE-1 and Dis-PE-2) investigated in this work: from modulus build-up and area ratio respectively (A_1 and A_2 are normalised by their plateau values of area ratio (crystallisation) or elastic shear modulus build-up (rheology)).

Polymer	A_1	A_2	τ_1 (s)	τ_2 (s)
Dis-PE-1 (Rheology)	0.21	0.50	9579	40528
Dis-PE-1 (Crystallisation)	0.11	0.39	853	29346
Dis-PE-2 (Rheology)	0.51	0.12	6461	25139
Dis-PE-2 (Crystallisation)	0.44	0.17	1470	21206

Good agreement is observed in fitting parameters between the rheological and thermal data of both polymers, suggesting that the change in enthalpic area ratio is indicative of the entanglement formation in the same way as the elastic modulus build-up. It is apparent that the modulus build-up and area ratio of Dis-PE-1, having higher molar mass, show lower A_1 compared to that of Dis-PE-2. The lower A_1 can be attributed to low initial entanglement density of the polymer. Pandey *et al.* also reported similar trend in their research, where the authors show a continuous decrease in starting value of modulus build-up with increase of molecular weight that can be associated with the initial entanglement density formed during polymerisation [27]. Both fittings of the area ratio and the modulus build-up show that τ_1 and τ_2 of Dis-PE-2 are lower than or close to that of Dis-PE-1. The low τ_1 suggests disentangled UHMWPE with low molar mass have faster entropic mixing reaching melt, and the low τ_2

indicates that for the sample having shorter chains, it takes shorter time to reach equilibrium state.

4.3.2 Annealing Temperature Influence on the Crystallisation Kinetics

The influence of annealing temperature at melt on the entanglement formation and its influence on crystallisation kinetics are also investigated, as we carried out the annealing at different temperatures: 160 °C, 170 °C, 180 °C and 190 °C for 60 min and then isothermal crystallisation at 128 °C for 180 min. We see from Figure 4-8 that with increasing the annealing temperature at melt, the high temperature endothermic peak, related to the crystals that form from disentangled domains, decreases. This indicates the acceleration of entanglement formation with increasing annealing temperature, and it is attributed to the higher chain mobility at higher annealing temperature. This is also supported by earlier reported rheological studies on these polymers, where the elastic shear modulus build-up time for the non-equilibrium melt to reach the equilibrium melt state is shown to be shorter at higher annealing temperatures [28].

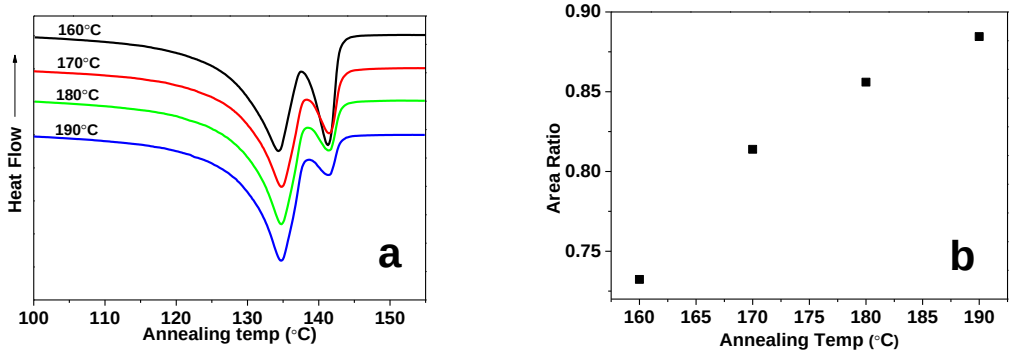

Figure 4-8 a) DSC heating runs, plotted from ramp g-h of Scheme 4-1, after annealing at 160, 170, 180 and 190 °C for 60 min, respectively and followed by 180 min isothermal crystallisation at 128 °C; b) area ratio of the enthalpy of low temperature endothermic peak to the overall endothermic peak, as a function of annealing temperature at melt.

4.3.3 Entanglement Hindering of Disentangled UHMWPE in the Presence of Graphene

The correlation between the rheological and thermal response of disentangled polymer melt is further strengthened by exploring the chain filler interaction. To recall, it is shown in Figure 4-9d, and Figure 3-7b in Chapter 3 that in the presence of a specific concentration of rGON,

the elastic shear modulus build-up is restricted to an extent that within the experimental time scale, at 160 °C, little increase in modulus is observed reflecting the survival of everlasting non-equilibrium melt. In this section we aim to investigate the thermal response of the everlasting non-equilibrium melt on crystallisation in the presence of rGON. The experimental protocols are the same as that for the Figure 4-2a and Figure 4-3.

The nascent powder mixed with rGON, after drying, is directly used for the thermal analysis. The heating runs after annealing at 160 °C for different times followed by 180 min isothermal crystallisation at 128 °C are summarised in Figure 4-9, where Figure 4-9a and Figure 4-9b show the results of 0.1 wt % and 0.8 wt % composites, respectively. The normalised low temperature endothermic peak, for both composites and the pure polymer are shown in Figure 4-9c, whereas Figure 4-9d shows the corresponding rheological response of the samples.

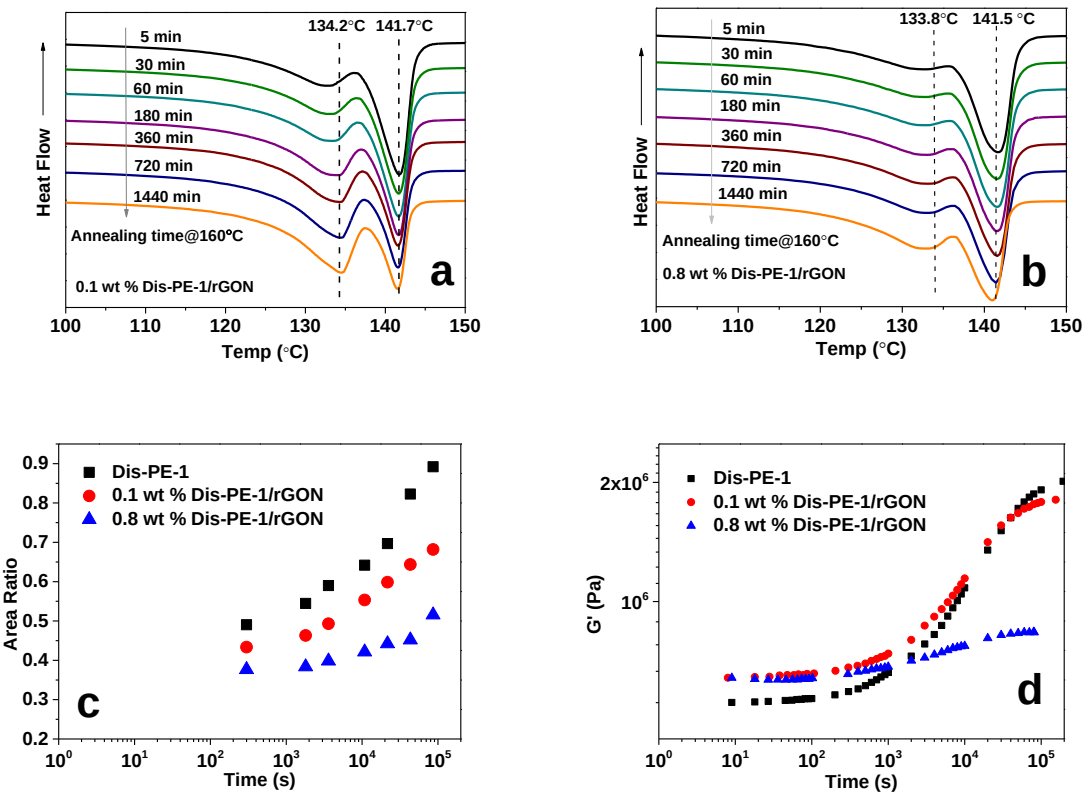

Figure 4-9 DSC heating runs after different annealing times at 160 °C followed by 180 min isothermal crystallisation at 128 °C of **a)** 0.1 wt % Dis-PE-1/rGON and **b)** 0.8 wt % Dis-PE-1/rGON composites; **c)** normalised low temperature endothermic peak as a function of annealing time at 160 °C, of Dis-PE-1, 0.1 wt % Dis-PE-1/rGON and 0.8 wt % Dis-PE-2/rGON, and **d)** elastic shear modulus build-up of Dis-PE-1, 0.1 wt % Dis-PE-1/rGON and 0.8 wt % Dis-PE-1/rGON samples.

It is apparent, from Figure 4-9a and b, that the decrease in the enthalpy of high temperature endothermic peak with increasing annealing time in melt is suppressed in the presence of rGON. The suppression becomes more pronounced when the filler concentration increases. At rGON concentration of 0.8 wt %, both low and high temperature endothermic peak areas are found to be nearly independent of the annealing time at 160 °C, suggesting that the heterogeneous melt state having heterogeneity in the distribution of entanglements survives for a very long time. In Figure 4-9c and d, it is found that the changes in the area ratio follows trend similar to the elastic shear modulus build-up, starting from low values. The modulus build-up is the slowest at the 0.8 wt % of the filler concentration. In both thermal and rheological studies, the inhibition in enthalpic and shear elastic modulus build-up is attributed to the strong chain-filler interaction that arrests the dynamic of the disentangled chains, keeping them less entangled for longer times. In the case of crystallisation, the survival of less entangled regions, at filler concentration of 0.8 wt %, accelerates the nucleation rate and thus facilitates the overall crystallisation rate during isothermal crystallisation at 128 ºC, giving rise to little change in high temperature endothermic peak. It is important to mention that the presence of rGON could also enhance the nucleation rate of the less entangled chains by enhancing the nucleation efficiency and further accelerating the crystallisation rate of the chains during the isothermal crystallisation [29].

To have insight into the influence of the presence of the filler on the double peaks in the disentangled UHMWPE, the protocol for Figure 4-3 is also applied to the composite sample having 0.8 wt % rGON, and the results are shown in Figure 4-10. Similar to the plain sample in Figure 4-3a, it is observed, in the composite, that the endothermic peak on heating of g-h shows gradual shift from 135 °C to 141.5 °C with increasing crystallisation temperature from 120 °C to 126 °C. Above the annealing temperature of 126 °C, a low temperature endothermic peak, on heating the sample along g-h, starts to appear, but not as obvious as that shown in plain sample, Figure 4-3. The presence of the small low temperature endothermic peak of the composite, compared to that of plain sample in Figure 4-3 at 128 ºC, can be attributed to the same reason for suppression of the change in both low and high endothermic peaks with annealing time at 160 °C as described in Figure 4-9b.

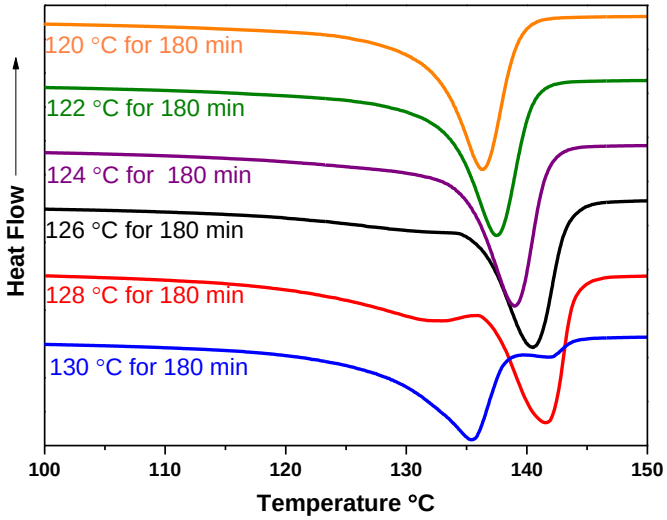

Figure 4-10 DSC plots, obtained from ramp g-h of **Scheme 4-1**, of 0.8 wt % Dis-PE-1/rGON sample annealed at 160 ºC for a fixed time and isothermally crystallised for 180 min at different temperatures.

To strengthen the response of enthalpic relaxation specific to the polymer synthesised using the single-site catalytic system, a comparative study of commercial sample in the presence of rGON is also performed. The same thermal protocol for Figure 4-9b is applied to 0.8 wt % C-PE/rGON composites, no high temperature endothermic peak is observed, Figure 4-11. The observations are similar to Figure 4-2b where no rGON was used. Thus the influence of rGON on the observed changes in the disentangled sample Figure 4-9b, synthesised using the single-site catalytic system, are attributed to the intrinsic nature of the heterogeneous melt state.

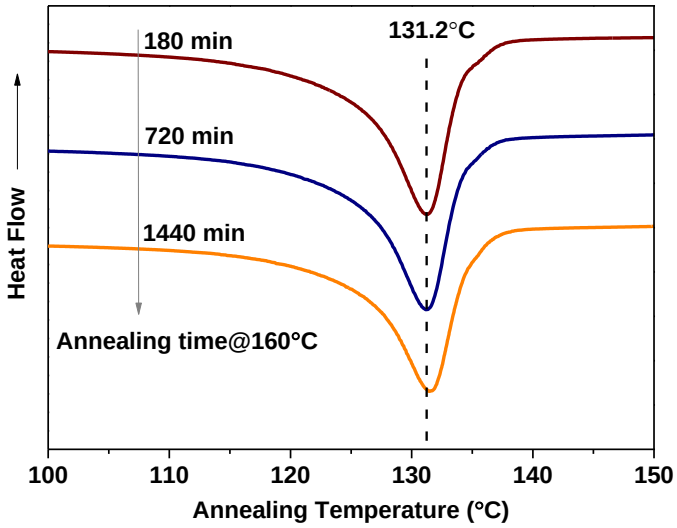

Figure 4-11 DSC heating runs of C-PE/0.8 wt % rGON sample after different annealing times (180 min, 720 min and 1440 min) followed by 180 min isothermal crystallisation at 128 °C.

Figure 4-12 summarises the total melting enthalpies of the samples with increasing annealing time. A significant decrease in the enthalpy of plain sample is observed, compared to that of entangled UHMWPE samples, and it can be attributed to the entanglement process. However in the presence of rGON, the suppression in entanglement formation causes presence of disentangled domains that favours nucleation and no change in overall enthalpy is observed, Figure 4-12. Furthermore, these results also rule out the possibility of any thermal oxidation of the samples in the presence of rGON.

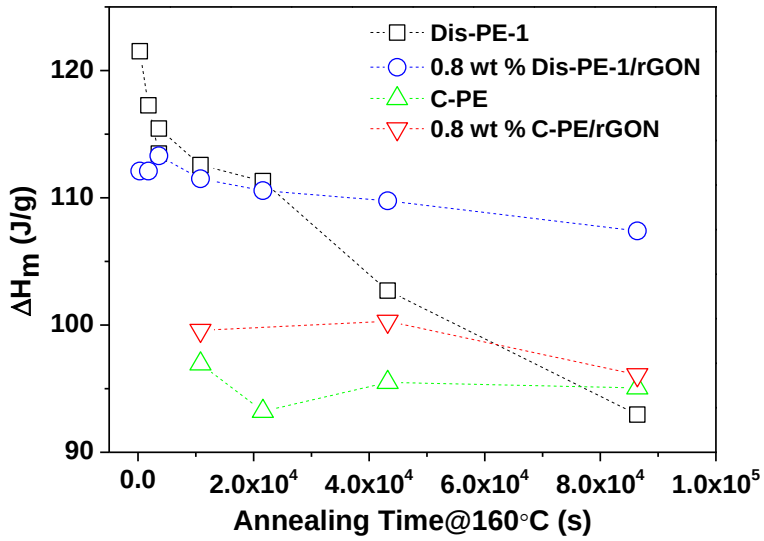

Figure 4-12 Total melting enthalpies versus increasing annealing time at 160 ºC of both disentangled and commercial entangled UHMWPE samples with and without rGON. The enthalpies are calculated from **Figure 4-2a**, **Figure 4-2b**, **Figure 4-9b** and **Figure 4-11**, which are obtained from ramp g-h of **Scheme 4-1**.

4.3.4 Interaction between Graphene Oxide and the Disentangled UHMWPE

To have further insight between the interaction of rGON with disentangled UHMWPE chains, NMR studies have been performed. Figure 4-13a shows one-dimensional (1D) ^{1}H NMR spectrum of PE (at chemical shift 0-3 ppm) and the filler (5-7 ppm). The assignment of the interaction between PE and the filler was made tentatively on the Dis-PE-1/rGON sample having good dispersion of the filler. The 2D exchange spectrum with exchange time τ=40 ms exhibits strong cross peaks that connect protons from functional groups of the filler with protons of the polyethylene. These cross-peaks arise from the exchange of nuclear magnetization via intramolecular spin diffusion during exchange process, τ, indicating existence of strong physical interaction between the filler and the matrix.

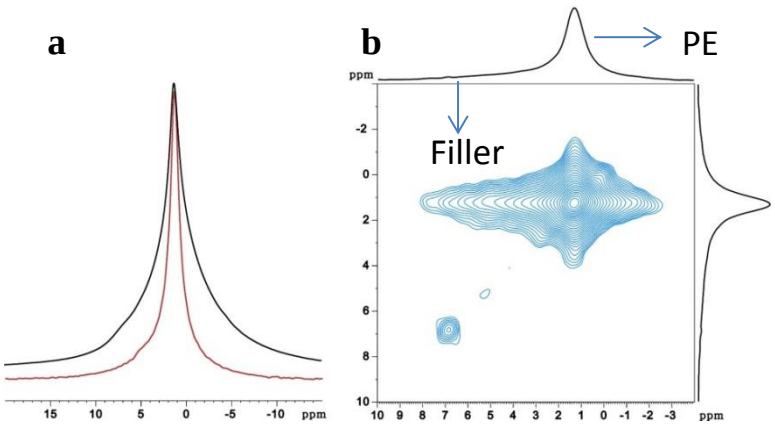

Figure 4-13 a) 1D spectrum (out line is the sp, inner line is Hahn Echo L1=1), and **b)** Carbonyl region of the 2D exchange spectrum ^{1}H NMR (Hahn-Echo-NOSEY L1=1 d6=40ms) of 0.8 wt % Dis-PE-2/rGON (right).

The interaction of ethylene segments with carbon based filler has also been conclusively demonstrated by Litvinov and co-workers in the studies on ethylene propylene diene rubber (EPDM)/carbon black composites by NMR , where the authors showed the interaction is due to the adsorption of ethylene segments to the large surface of carbon filler [30,31]. Moreover, it is reported that among all carbon based nano fillers, graphene has the strongest interaction

with PE matrix interpreted by the molecular dynamic simulations of PE nanocomposites with different carbon based fillers [32,33]. In summary, the strong chain-filler interaction supported by NMR studies strengthens our findings on thermal and rheological response of the composites.

4.4 Conclusions

We have investigated the crystallisation kinetics and associated melt enthalpies of isothermally crystallised disentangled UHMWPE samples that have different entanglement density. The two peaks observed on annealing the polymer at 160 °C and isothermal crystallisation are attributed to the heterogeneous distribution of entanglements having different response to crystallisation. The less entangled domains, having higher nucleation rate, form crystals that on melting correspond to high temperature endothermic peak. Whereas, the entangled domains having higher nucleation barrier that requires higher supercooling for crystallisation, crystallises mainly on cooling below the chosen isothermal crystallisation temperature. It is also found that the low temperature endothermic peak increases at the expense of high temperature endothermic peak with annealing time at 160 °C, following the trend similar to the increase in elastic shear modulus with entanglement formation. The molar mass also shows an influence on the entanglement formation and consequently on crystallisation. The annealing temperature of non-equilibrium melt is found of importance to the entanglement formation, which progresses faster with increasing annealing temperature. We also demonstrate that in the presence of rGON, high temperature endothermic peak, i.e. less entangled domains, is less influenced by annealing time in melt, and at the filler concentration of 0.8 wt %, the peak is almost independent of the annealing time. We have attributed this phenomenon to strong chain-filler interaction that arrests chain dynamics and thus supresses the chain entanglement formation. The chain-filler interaction is further investigated and supported by NMR characterisation.

The thermal analysis on disentangled UHMWPE in this chapter do question the nature of the entanglement formation in melt, and the presence of high temperature endothermic peak which is observed to be close to PE's equilibrium melting point, 141.5 °C, after melt and isothermal crystallisation.

References

[1] Organ, S. J.; Keller, A. Fast growth rates of polyethylene single crystals grown at high temperatures and their relevance to crystallization theories. *J. Polym. Sci.: Part B: Polym Phys.* **1986**, 24, 2319-2335.

[2] Yin, L.; Chen, J.; Yang, X.; Zhou, E. Structure image of single crystal of polyethylene. *Polymer* **2003**, 44, 6489-6493.

[3] Talebi, S.; Duchateau, R.; Rastogi, S.; Kaschta, J.; Peters, G. W. M.; Lemstra, P. J. Molar mass and molecular weight distribution determination of UHMWPE synthesized using a living homogeneous catalyst. *Macromolecules* **2010**, 43 (6), 2780-2788.

[4] Rastogi, S.; Lippits, D. R.; Peters, G. W. M.; Graf, R.; Yao, Y.; Spiess, H. W. Heterogeneous in polymer melts from melting of polymer crystals. *Nat. Mater.* **2005**, 4, 635-641.

[5] Tapash, A.; DesLauriers, P. J.; White, J. L. Simple NMR experiements reveal the influence of chain and chain architecture on the crystalline/amorphous interface in polyethylene. *Macromolecules* **2015**, 48(9), 3040-3048.

[6] Yao, Y.; Jiang, S.; Rastogi, S. 13C solid state NMR characterization of structure and orientation development in the narrow and broad molar mass disentangled UHMWPE. *Macromolecules* **2014**, 47, 1371-1382.

[7] Peterlin, A. Chain folding in lamellar crystals. Macromolecules 1980, 13(4), 777-782.

[8] Sadler, D. M. New explanation for chain folding in polymers. Nature 1987, 326, 174-177.

[9] Pandey, A.; Toda, A.; Rastogi, S. Influence of amorphous component on melting of semicrystalline polymers. *Macromolecules* **2011**, 44, 8042-8055.

[10] Liu, K.; Ronca, S.; Andablo-Reyes, E.; Forte, G.; Rastogi, S. Unique rheological response of Ultrahigh Molecular Weight Polyethylenes in the presence of reduced graphene oxide. *Macromolecules* **2015**, 48(1), 131-139.

[11] Liu, P.; Gong, K.; Xiao, P.; Xiao, M. Preparation and characterization of poly(vinyl acetate)-intercalated graphite oxide nanocomposite. *J. Mater. Chem.* **2000**, 10, 933-935.

[12] Mead, D. Determination of molecular weight distributions of linear flexible polymers from linear viscoelastic material functions. *J. Rheol.* **1994**, 38, 1797-1827.

[13] Tuminello, W. H. Molecular weight and molecular weight distribution from dynamic measurements of polymer melts. *Polym. Eng. Sci.* **1986**, 26, 1339-1347.

[14] Rastogi, S.; Lippits, D. R.; Peters, G. W. M.; Graf, R.; Yao, Y.; Spiess, H. W. Heterogeneous in polymer melts from melting of polymer crystals. *Nat. Mater.* **2005**, 4, 635-641.

[15] Romano, D.; Tops, N.; Andablo-Reyes, E.; Ronca, S.; Rastogi, S. Influence of polymerization conditions on melting kinetics of low UHMWPE and its implications on mechanical properties. *Macromolecules* **2014**, 47(14), 4750-4760.

[16] Saito, J.; Mitani, M.; Matsui, S.; Sugi, M.; Tohi, Y.; Tsutsui, T.; Fujita, T.; Nitabaru, M.; Makio, H. Olefin polymerization catalysts, transition metal compounds, processes for olefin polymerization, and Alpha-olefin/conjugated diene copolymers. European Patent 0874005, 1997.

[17] Ferry, J. D. *Viscoelastic Properties of Polymers*, 3rd ed. Wiley: New York, 1980.

[18] Kovacs, A. J.; Gonthier, A.; Straupe, C. Isothermal growth, thickening, and melting of poly(ethylene oxide) single crystals in the bulk. *J. Polym. Sci.: Symp.* **1975**, 50, 283-325.

[19] Weeks, J. J. Melting temperature and change in lamellar thickness with time for build polyethylene. Journal of research of the national bureau of standards-A. *Phys. Chem.* **1963**, 67A(5), 441-451.

[20] Gopalan, M.; Mandelkern, L. The effect of crystallization temperature and molecular weight on the melting temperature of linear polyethylene. *J. Phys. Chem.* **1967**, 71(12), 3833-3841.

[21] Yamazaki, S.; Hikosaka, M.; Gu, F.; Ghosh, S. K.; Arakaki, M.; Toda, A. Effect of entanglement on nucleation rate of polyethylene. *Polymer J.* **2001**, 33 (11), 906-908.

[22] Yamazaki, S.; Hikosaka, M.; Toda, A.; Wataoka, I.; Gu, F. Role of entanglement in nucleation and ‘melt relaxation’ of polyethylene. *Polymer* **2002**, 43, 6585-6593.

[23] Yamazaki, S.; Gu, F.; Watanabe, K.; Okada, K.; Toda, A.; Hikosaka, M. Two-step formation of entanglement from disentangled polymer melt detected by using nucleation rate. *Polymer* **2006**, 47, 6422-6428.

[24] Hikosaka, M.; Watanabe, K.; Okada, K.; Yamazaki, S. Topological mechanism of polymer nucleation and growth-the role of chain sliding diffusion and entanglement. *Adv. Polym. Sci.* **2005**, 191, 137-186.

[25] Teng, C.; Gao, Y.; Wang, X.; Jiang, W.; Zhang, C.; Wang, R.; Zhou, D.; Xue, G. Reentanglement kinetics of freeze-dried polymers above the glass transition temperature. *Macromolecules* **2012**, 45, 6648-6651.

[26] Andablo-Reyes, E.; de Boer, E.; Romano, D.; Rastogi, S. Stress relaxation in the nonequilibrium state of a polymer melt. *J. Rheol.* **2014**, 58(6), 1981-1991.

[27] Pandey, A.; Champouret, Y.; Rastogi, S. Heterogeneity in the distribution of entanglement density during polymerization in disentangled ultrahigh molecular weight polyethylene. *Macromolecules* **2011**, 44(12), 4952-4960.

[28] Pandey, A. V. *Nonlinear viscoelastic response of a thermodynamically metastable polymer melt*. PhD Thesis **2011**. Loughborough University.

[29] Xu, J. Z.; Zhong, G. J.; Hsiao, B. S.; Fu, Q.; Li, Z. M. Low-dimensional carbonaceous nanofiller induced polymer crystallisation. *Prog. Polym. Sci.* **2014**, 39, 555-593.

[30] Litvinov, V. M.; Steeman, P. A. M. Vulcanized siloxane chains swollen by polymer chains: NMR investigations into free-chain dynamics. *Macromolecules* **1999**, 32, 8476-8490.

[31] Litvinov, V. M.; Orza, R. A.; Klüppel, M.; Van Duin, M.; Magusin, P. C. M. M. Rubber-filler interaction and network structure in relation to stress-strain behavior of vulcanized, carbon black filled EPDM. *Macromolecules* **2011**, 44, 4887-4900.

[32] Cheng, S.; Chen, X.; Hsuan, G. Y.; Li, C. Y. Reduced graphene oxide-induced polyethylene crystallisation in solution and nanocomposites. *Macromolecules* **2011**, 45, 993-1000.

[33] Li, Y. Effect of nano inclusions on the structural and physical properties of polyethylene matrix. *Polymer* **2011**, 52(10), 2310-2318.

5 Rheological Aspects and Melt kinetics of Disentangled UHMWPE Polymerised in the Presence of Reduced Graphene Oxide Nanoplatelets

Abstract

In Chapters 3 and 4, the rheological response and the crystallisation behaviour of the disentangled UHMWPE/rGON composites prepared via a two-step physical mixing method were studied. In this chapter, disentangled UHMWPE synthesised in the presence of rGON has been investigated by means of rheology and Differential Scanning Calorimetry (DSC). The synthesis in the presence of rGON allows homogeneous dispersion of the filler in the intractable matrix of UHMWPE. These polymers on melting could form a non-equilibrium melt that transforms into the equilibrium state with homogeneous distribution of entanglements by increasing the number of entanglements with annealing time. The rheological analysis suggests that in the presence of rGON chain dynamics in the melt state could be influenced to the extent that the homogenisation of entanglement distribution and concurrent increase in the entanglement density is inhibited, which is indicative of strong chain-filler interaction. The long lasting non-equilibrium polymer melt, having low entanglement density, influences polymer crystallisation. The crystallisation kinetics is investigated by DSC. The findings are that crystallisation from non-equilibrium or disentangled domains in the melt, under quiescent conditions, result into crystals having high temperature endothermic peak at 141.5 ºC, i.e. PE's equilibrium melting temperature which is related to the extended chain crystals or folded chain crystals having constrained amorphous region. DSC performed on a series of *in-situ* polymerised composites supports the rheological response of UHMWPE in the presence of rGON at different concentrations. The disentangled state of UHMWPE achieved after polymerisation is further confirmed by uniaxial deformation in solid state. The influence of rGON on uniaxial deformation of UHMWPE and its influence on mechanical properties have been also a subject of this study.

5.1 Introduction

As mentioned in Chapter 1, efforts have been made to synthesise UHMWPE with lower entanglement density for the purpose of increasing processability of the intractable materials. To recall, three methods have been explored so far, and they are 1) solution-spinning, 2) synthesis using Ziegler-Natta catalyst at low temperatures, and 3) synthesis using single site homogeneous catalytic system, among which 3) has shown the most promising advantages in terms of processability and mechanical properties. For instance, the obtained disentangled UHMWPE can be processed in the solid-state within a processing window of more than 20 °C below its equilibrium melting point of 141.5 ºC [1,2] and into more complicated shapes, such as 2D thin films. In addition, control of the molecular weight (M_w) and molecular weight distribution (MWD) of the disentangled UHMWPE can be realized by tailoring the polymerisation conditions [3]. The materials show substantial ease in processability and enhanced mechanical properties compared to the commercially available UHMWPE grades [2]. It should be pointed out that the disentangled UHMWPE chains start to entangle once they are in melt thus increasing the viscosity and affecting the processability and drawability on crystallisation in solid state. In order to control the entanglement formation in melt, and maintain its processability, we have explored the application of fillers that could alter or arrest chain dynamics and further inhibit entanglement formation. As discussed in the studies presented in the previous chapters on physically mixed disentangled UHMWPE/rGON composites, the results suggest the presence of strong interaction between polyethylene chain segments and reduced graphene oxide (rGON) that inhibits the transition of the polymer melt from non-equilibrium to equilibrium state [4] thus maintaining the low entanglement state. The results have motivated us to carry on with the composites prepared by *in-situ* polymerisation which could provide more uniform filler dispersion and more effective chain-filler contact. This study is also of interest to compare the dispersion differences by two methods of physical mixing and *in-situ* polymerisation.

In this chapter, disentangled UHMWPE was synthesised in polymerisation conditions described in Chapter 3, with the notable difference that rGON was introduced in the reactor prior to the start of the polymerisation. The idea behind this set of experiments was to compare the differences between the disentangled UHMWPE composites prepared by physical mixing and *in-situ* polymerisation, which provide different filler dispersion and filler-chain interactions, and further confirm the filler influence on the rheological response

and crystallisation behaviours of disentangled UHMWPE. It is believed that, when using the *in-situ* polymerisation method, the filler would be embedded in the polymer matrix, instead of residing on the surf ace of the polymer particles. This difference has been found to be crucial in earlier studies, where the composites obtained via *in-situ* polymerisation have shown enhanced features in term of filler-polymer interaction [5]. Moreover, the rGON filler could constitute a valid substrate for anchoring the homogeneous catalytic system, thus resulting in a supported catalytic system that may be of interest for the industrial upscaling of the polymerisation process [6]. In addition, the filler influence on the mechanical properties of ultra-drawn tapes is also investigated.

5.2 Experimental

5.2.1 Polymerisation Procedures

All manipulations of air and moisture-sensitive compounds were performed in an argon glove box or under nitrogen flow using standard high-vacuum Schlenk techniques. Toluene (99.8%, anhydrous) and methyaluminoxane (MAO, 10 wt % solution in toluene) were purchased from Sigma-Aldrich. Ethylene (grade 3.5) was purchased from Air Products, and the single site catalyst, bis[N-(*tert*-butylsalicylidene)pentafluoroanilinato]titanium (IV) (referred to FI catalyst in this thesis), was purchased from MCat. Materials for the synthesis of graphene oxide nanoplatelets (GON) were purchased from Sigma-Aldrich: fine graphite powder (average diameter of about 25 μm), 98 wt % concentrated sulphuric acid, potassium permanganate, distilled water and 30 wt % hydrogen peroxide. Irganox 1010, added as antioxidant to the plain polymer and composites after synthesis, was purchased from Ciba. All reagents were used as received.

5.2.1.1 Preparation of rGON Suspension in Toluene

GON was synthesised using a modified Hummers Method [7], with further modifications as described in Chapter 2, and rGON was obtained via compression moulding. To recall, the GON films were thermally reduced by compression at 160 °C with loadings of 415 bars for 5 min, 830 bars for 15 min and 1660 bars for 5 min, followed by further drying in a vacuum oven at a temperature of 50 °C for 24 hours. Prior to the synthesis of the nanocomposites, the

rGON was suspended in toluene. The rGON was removed from the vacuum oven and immediately transferred to a glove box where it was weighed, placed into a 100 ml Shlenck tube, added of 20 ml of toluene and then sealed with a glass lid. The mixture was then taken out of the glove box and alternatively magnetically stirred and sonicated 2 times, with 30 min each time. Subsequently 50 ml more of toluene were added to the mixture under nitrogen flow and the suspension was kept sonicating for 4 hrs.

5.2.1.2 In-situ Polymerisation of Disentangled UHMWPE in the Presence of rGON

The polymerisation procedure that uses single site catalyst to synthesise disentangled UHMWPE is described in Chapter 3 [8], based on which we carried out the polymerisations in the presence of rGON: a wall-mounted, 2 l jacketed Büchi reactor sealed with a stainless steel lid equipped with a double plane propeller blade mechanical stirrer, a temperature probe, a gas inlet/outlet, a rubber septum for catalyst injection, and an ethylene feeding pipe, were kept overnight at 125 ºC by means of applying a feedback loop control Huber Unistat 425 thermo-regulator. The reactor was then prefilled with nitrogen and purged three times of vacuum/nitrogen cycles. After that, the reactor temperature was brought to 25 °C and the required amount of toluene (750 ml) was then transferred into the vessel under a nitrogen flow. The vessel temperature was then set at 10 ºC using a thermostat probe connected to the thermo-regulator. When the desired temperature was reached, the prepared rGON/toluene suspension was injected into the reactor. The amount of rGON was adjusted in each run to achieve composites with filler contents of 0.0 wt %, 0.1 wt %, 0.5 wt % and 1.0 wt %.

After that, a certain amount of 10 wt % MAO/toluene solution was injected as scavenger to remove possible contaminants, and the ethylene pressure was set at 1.2 bar, by a Büchi press flow gas controller BPC 6002. After the solution was saturated with ethylene at the desired pressure of 1.2 bar, 9 mg of the FI catalyst activated by MAO was injected into the reactor to initiate the polymerisation. After the consumption of ethylene reached 28.6 l, the reaction was quenched by injection of methanol.

The polymerised materials were then filtered and washed with copious amount of methanol/acetone mixture. Irganox 1010 (0.7-1.0 wt %) was added to the resultant materials to avoid degradation in the long rheological measurements at high temperature (160 °C).

5.2.2 Characterisation of GON and rGON

X-ray photoelectron spectroscopy (XPS), using Al $K_{\propto}$ micro-focused monochromator as X-ray source, was used to characterise the elemental composition of GON and rGON, respectively. The XPS spectra were fitted using Thermo Scientific Avantage data system and origin software. A field emission gun-scanning electron microscope (FEG-SEM) was used to investigate the morphology and distribution of rGON in the composites. The composites were compression moulded, frozen in liquid nitrogen and snapped to make fractured surface for SEM measurements. The samples were coated with gold by a sputtering technique before the analysis.

5.2.3 Rheological Characterisation Procedures

The same protocol for the rheological measurements, described in Chapter 3, was used to characterise the rheological properties of the *in-situ* synthesised composites. To recall, samples for rheology measurements were compressed into plates having diameter of 50 mm and thickness of 0.6-0.7 mm, using a hydraulic press at average pressure of 1020 bar. 12 mm diameter disks were cut from the compressed plate using a punching tool. Low compression temperature of 125 °C was used, at which the disentangled samples can be well sintered and at the same time avoid significant entanglement formation before rheological measurement.

Rheological measurements were performed in a strain controlled rheometer ARES G2 (TA, Instruments) using a 12 mm diameter parallel plate geometry. The protocol used for the measurements was the same as described in Chapter 3. To summarise, dynamic time sweep at frequency of 10 rad/s was carried out, followed by dynamic frequency sweep after the storage modulus reaches a plateau; frequencies in a range from 100 rad/s to 0.001 rad/s are applied.

5.2.4 Thermal Characterisation Procedures

The thermal analysis was carried out by means of differential scanning calorimetry (DSC), in accordance with the thermal protocol described in Scheme 4-1, Chapter 4. To recall, all DSC experiments in this work were performed using a Q-2000 MDSC from TA instruments. High precision T-Zero pans with lids were used in all experiments. An amount comprised between

1.4 and 1.6 mg was used for the analyses. A dynamic nitrogen flow of 50 mL/min was continuously purged through the DSC cell during the measurement. Temperature and enthalpy calibrations were conducted using certified indium at the same heating rate used in the measurements. The data for the results and discussion were collected from ramp **g-h,** in Scheme 4-1, after annealing and isothermal crystallisation treatments.

5.2.5 Mechanical Characterisation Procedures

5.2.5.1 Uniaxially Oriented Tapes

The plain polymer and the polymer composites were processed into uniaxially oriented tapes at temperatures below the UHMWPE melting point. A general description of the method used to prepare uniaxially oriented tapes is reported elsewhere [9] and summarized as follows: 25 g of nascent powder was uniformly distributed into a mould with a cavity of 620 mm in length and 30 mm in width and then compressed at 129 ºC and 130 bar for 10 min. A 1.42 mm thick sheet was obtained and then preheated for at least 1 min at a constant temperature of 136 ºC and rolled with a Collin calender (with rolls having 250 mm in diameter; 0.15 mm of slit distance and 0.5 m/min of inlet speed). While rolling at a speed of 2.5 m/min, the sheet was partially stretched. The rolled and stretched sheet was further stretched on a 50 cm-long, oil heated hot plate. The draw ratio was obtained by dividing the specific weight of the sheet prior to deformation by the specific weight of the tape after stretching. A typical processing temperature of polyethylene in the stretching steps ranged between 130 to 154 ºC. The higher stretching temperature, above 140 ºC, was used for the partially stretched samples, as the melting temperature of linear uniaxially stretched UHMWPE can be increased under external constraints [10]. The sample was stretched to the desired initial draw ratio in the first stretching step. Parts of the drawn samples were then used to measure the mechanical properties, whereas the remaining samples were drawn to the final draw ratio and the mechanical properties were determined subsequently.

5.2.5.2 Determination of the Mechanical Properties

Tensile properties of the samples were characterised using an Instron 5566 tensile tester at room temperature (25 ºC) in accordance with ASTM D7744-2011. Side action grip clamps

with flat draw faces were used to avoid the possible slippage and samples with nominal gauge length of 100 mm were tested at a constant extension speed of 50 mm/min (crosshead travel speed). The breaking tenacity (or tensile strength) and Young's modulus were determined from the measured force and elongations.

5.3 Results and Discussion

5.3.1 Atomic Composition of GON and rGON

The atomic composition and bonding information of GON and rGON were measured by X-ray photoelectron spectroscopy (XPS). This analysis provides elemental information of the filler that affects performance of the catalytic system. The high oxygen content of GON can be detrimental to the polymerisation catalyst due to the tendency of this catalyst to interact with oxygen groups and loose activity. On the other hand, a certain number of functional groups, such as -COOH and –OH are desired on the filler surface in order to act as 'anchoring sites' for the co-catalyst, thus promoting the exfoliation of the filler and embedding them into the growing polymer chains [11]. As a compromise, we reduced the GON under mild conditions as described in the experimental section and the information of the elemental analysis is reported in Figure 5-1, Table 5-1 and Table 5.2.

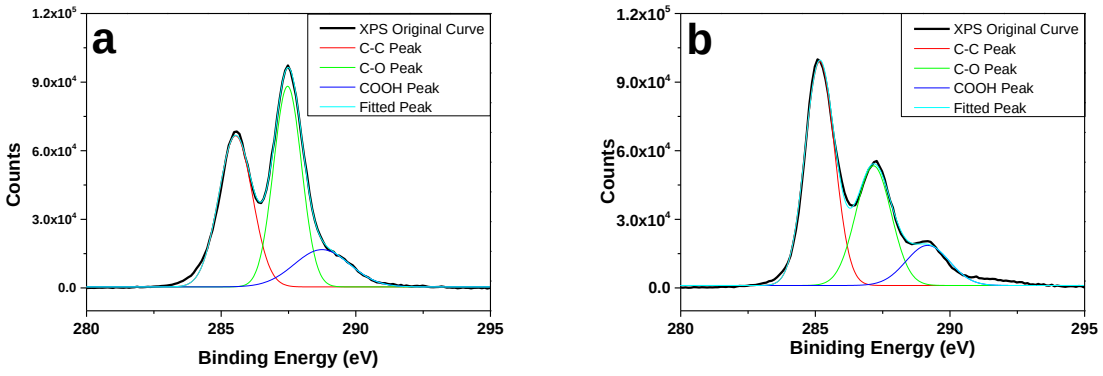

Figure 5-1 a) high resolution XPS spectra of C1s for GON, and **b)** high resolution XPS spectra of C1s for rGON; the measurements were carried out on dried GON and rGON films, respectively.

Table 5-1 XPS data of GON

GON	Peak BE (eV)	At. %	Bond
C1s	285.08	39	C-C and C=C
	287.16	43	C-O (epoxy, hydroxyl groups)
	289.16	18	carbonyl groups

Table 5-2 XPS data of rGON

GON	Peak BE (eV)	At. %	Bond
C1s	285.08	49	C-C and C=C
	287.16	34	C-O (epoxy, hydroxyl groups)
	289.16	17	carbonyl groups

Figure 5-1a shows the C1s spectra of GON and Figure 5-1b presents the C1s of rGON prepared by thermal reduction, and the original peak is split into 3 sub-peaks that correspond to different functional groups. The binding energies and atomic percentage of each group of GON and rGON are given in

Table 5-1 and Table 5-2, respectively. The C1s spectra indicate the successful oxidation of graphite into GON, as suggested by the presence of epoxy, carbonyl and hydroxyl groups. The analysis of rGON C1s spectra suggests a partial removal of oxygen: the CC/CO intensity area ratio for rGON is much higher (~1) than that of GON (~0.6), where CC represents the sum of C-C and C=C bonds and CO refers to all combination of carbon/oxygen bonds.

5.3.2 Polymerisation Parameters

The rGON was added to the polymerisation medium prior to the addition of the catalyst/cocatalyst. The presence of rGON is found to have influence on the catalyst performance, as appreciated from Table 5-3 and Figure 5-2. To have the same amount of polymer produced in each run, all polymerisation experiments were stopped after reaching the same ethylene consumption.

Table 5-3 Reaction parameters of the disentangled UHMWPE and its composites polymerised in the presence of rGON.

Samples	Amount of Catalyst/MAO	Amount of rGON (g)	Time of Reaction (s)	Yield (g)	R_p ($kg_{PE} \bullet mol_{cat}^{-1} \bullet atm^{-1} \bullet h^{-1}$)
Plain disentangled UHMWPE	9 mg/9 ml	0	1220	38.5	8764
0.1 wt % disentangled UHMWPE/rGON	9 mg/11 ml	0.04	3136	41.0	3825
0.5 wt % disentangled UHMWPE/rGON	9 mg/12 ml	0.23	3995	41.8	3057
1.0 wt % disentangled UHMWPE	9 mg/14 ml	0.40	3753	39.6	3083

*Other conditions: reaction temperature = 10 °C; ethylene pressure = 1.2 bar; toluene = 0.75 l

MAO acts not only as cocatalyst to activate the catalyst, but also as scavenger to reduce the possible contaminants from rGON. For this reason, 1 ml extra MAO is added for each increase of 0.1 g rGON. In order to control the composition of the composites, in the reaction, the ethylene consumption is fixed at 28.6 l (corresponding to ~ 40 g of polymer production).

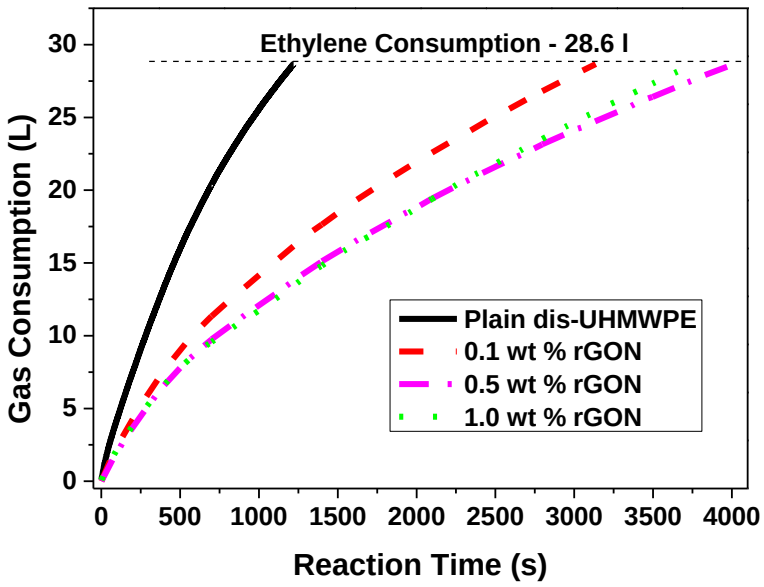

Figure 5-2 The ethylene uptake for polymerisation of disentangled UHMWPE and its composites.

Figure 5-2 shows the ethylene uptake for the polymerisation of disentangled UHMWPE and its rGON composites. It is apparent that the presence of rGON reduces the activity of the catalyst. The reduction can be attributed either to the poisoning of part of the catalyst (after thermal reduction at 160 °C, some of the functional groups on the surface of the filler still survive, for instance –OH groups which can normally be thermally removed at 650 °C according to Gao *et al.* research [12], and this is also confirmed by XPS results), or to a decreased accessibility of the ethylene molecules to the active sites (the permeability of ethylene gas through rGON to reach catalyst may be highly reduced, as single layer graphene has been reported to be able to act as a molecular barrier [13]), or even a combination of both. As a consequence, the polymers synthesised in the presence of rGON may have longer chain component and their influence on the rheological properties are discussed in the rheology section.

Figure 5-3 shows the SEM image of the 0.5 wt % rGON/polymer composite after being compression moulded at 160 °C, and then frozen in liquid nitrogen and snapped. It is apparent that the filler is exfoliated and well dispersed across the composite fracture surface.

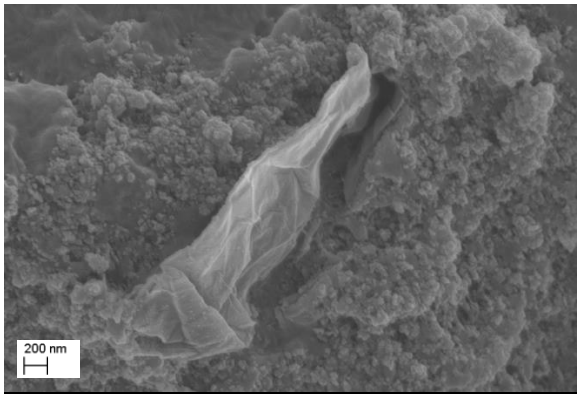

Figure 5-3 SEM image of rGON dispersed in polymer matrix after compression moulding at 160 ºC and frozen in liquid-nitrogen and snapped.

5.3.3 Rheological Properties of *in-situ* Polymerised Disentangled UHMWPE/rGON Nanocomposites

Linear rheology is a well-established method to study structural and dynamic properties of polymers and polymer nanocomposites [14]. The time- and frequency-dependent absolute values of the storage (*G'*) and loss (*G''*) moduli are rich in information of structural dispersion of filler and its interaction with the polymer matrix. Figure 5-4a shows *G'* build-up

curves obtained under isothermal condition at 160 °C for the nascent UHMWPE and *in-situ* polymerised UHMWPE/rGON composites. Data acquisition was started 60 s after the isothermal temperature was reached. The lower initial values of the storage modulus (elastic shear modulus) build-up curves compared to the elasticity of the plain polymer in equilibrium, confirms the disentangled characteristic of the polymer matrix [15]. The relatively high initial value of *G'* for 1.0 wt % rGON sample is attributed to the mechanical enhancement from the filler. Though the starting value of *G'* is independent on the rGON content (when rGON<1.0 wt %), the storage modulus build-up time is strongly affected by the concentration of the filler in the polymer matrix. For example, the plain sample shows the fastest elastic shear modulus build-up compared to that of the composites, as identified by the slope of the curves. The slowed modulus build-up is attributed to the presence of the filler that arrests the chain dynamics and hence inhibits the entanglement formation.

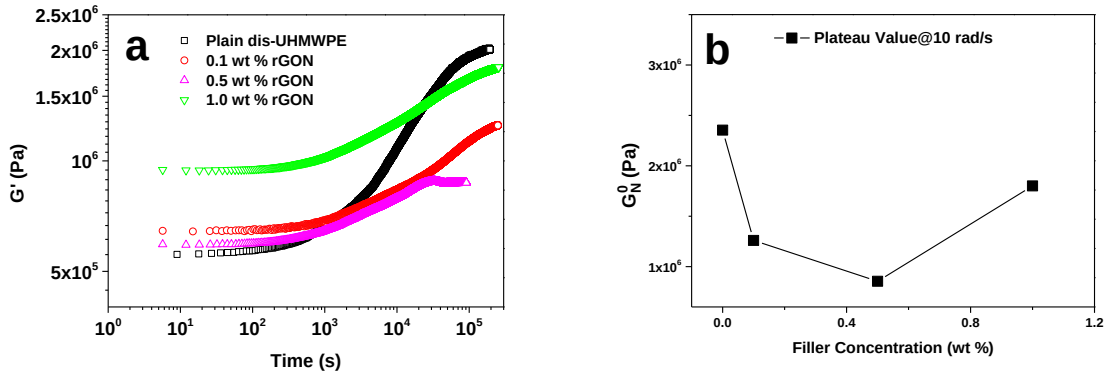

Figure 5-4 a) shear elastic modulus (*G'*) build-up of plain disentangled UHMWPE polymer and its composites synthesised in the presence of rGON. **b)** summary of plateau values of *G'* reached after the end of the modulus build-up shown in **a)**.Tests were performed at constant temperature of 160 °C within the linear viscoelastic region.

It is important to notice that unlike many of the reported rheological response of entangled polymer composites, where the equilibrium plateau modulus value increases continuously with increasing the amount of filler [16,17,18,19], the *in-situ* polymerised disentangled UHMWPE composites show gradual decrease in plateau value with filler concentration increasing from 0.0 to 0.5 wt %, and on further increasing filler to 1.0 wt %, the plateau value tends to increase again. At filler concentration of 0.5 wt %, a minimum in the plateau appears, suggesting that a more homogeneous distribution is achieved and results in a more effective contact between polymer chains and the filler at this concentration. For higher content, the further increase in the plateau value is attributed to the aggregation of rGON that reduces the

effective contact area with the polymer chains and contributes to the increase in the absolute values of storage modulus, as shown in Figure 5-4.

According to the early shown equation (1-2) [20], M_e (the molar mass between entanglements) can be related to the plateau value of the elastic modulus (G_N^0) at thermodynamic equilibrium state of entangled polymer melts:

$$G_N^0 = \frac{g_N \rho RT}{<M_e>} \quad (1\text{-}2)$$

where g_N is a numerical factor (1 or 4/5 [21]), ρ is the density, R is the gas constant and T is the absolute temperature. Given that the melt density does not change significantly with the additions of small amount of the filler (up to 1.0 wt %), we can infer that the average M_e of the 0.5 wt% composite is twice that of the plain polymer, supporting the presence of a long-lasting less entangled state. It is important to point out that in rheological experiments, all the samples, if given enough time, should reach an equilibrium state with homogeneously distributed entanglements and a fixed M_e.

It is noted that a similar behaviour has been observed in the previous chapters for the physically mixed composites, but the minima of the *G'* plateau in that case was found at 0.8 wt %. At the filler content of 0.5 wt % of physical mixed sample, the plateau modulus is above 1 MPa, whereas in the case of the *in-situ* polymerised samples the plateau modulus drops below 1 MPa, further strengthening the hypothesis that in the *in-situ* polymerised composites the filler is more homogeneously dispersed.

In early research, similar trend of decrease in modulus in the polyethylene-carbon based filler systems has also been reported and the phenomenon has been attributed to van der Waals forces. Zhang *et al.* reported a considerable decrease in the modulus for a series of UHMWPE/SWCNT nanocomposites and the authors explained the findings as a consequence of the selective adsorption of the longest chains of the UHMWPE onto the filler's surface [17]. As mentioned in Chapter 1, Vega *et al.* also observed a drop in viscosity of HDPE/MWCNT composites compared to neat HDPE in extrusion, and they attributed the phenomenon to the adsorption of longest chains onto the nanotube surface also via van der Waals interactions [22]. The interaction of ethylene segments with carbon based filler has been conclusively demonstrated by Litvinov and co-workers working on EPDM/carbon black composites by NMR , where the authors showed the adsorption of ethylene segments to the surface of carbon filler [23,24]. Moreover it has been also reported that, according to

molecular dynamics simulations of PE nanocomposites with different carbon based fillers, graphene shows the strongest interaction with PE matrix among all carbon-based nano inclusions, [25,26]. Also in Chapter 3, we have observed a similar trend in both disentangled and commercial UHMWPE/rGON composites prepared via a simple physical mixing method, where we attributed the decrease to strong chain-filler attraction provided by efficient filler-chain contacts that are achieved by successful removal of grain boundaries [4].

Figure 5-5a shows the viscoelastic moduli *G'* and *G"* as a function of angular frequency ω covering a range from 100 to 0.001 rad/s. Frequency sweep tests are performed after the modulus build-up reaches its stable value in Figure 5-4a. The time dependent relaxation modulus function (*G(t)*) (or equivalently its frequency dependent Fourier components known as elastic (*G'(ω)*) and viscous (*G"(ω)*) moduli) contains information on the tube renewal time [27].

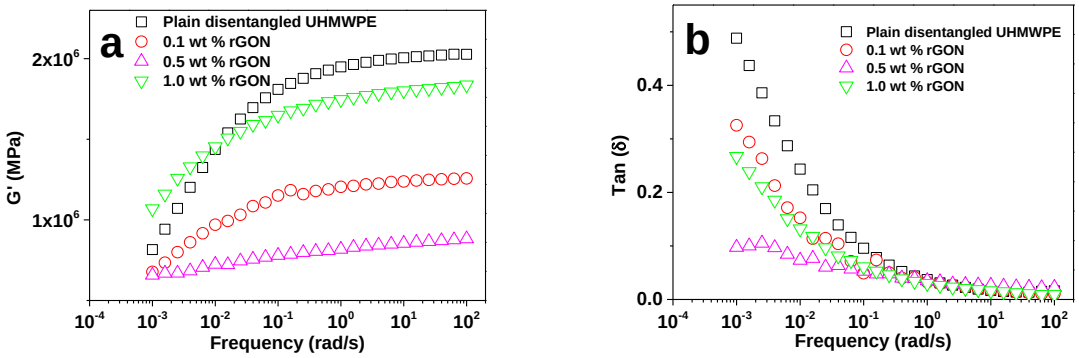

Figure 5-5 a) Storage modulus, *G'*, as a function of frequency, obtained after the samples reached their plateau in **Figure 5-4**a, and **b)** damping factor, tan (δ), as a function of frequency, obtained from **a)**.

The sample having 0.5 wt % rGON shows a plateau of *G'* that stretches over the measured frequency region including the terminal region, confirming that the chain reptation is highly inhibited by the strong chain-filler interaction within the experimental time scale [4]. In the non-equilibrium state of plain disentangled UHMWPE, it has been found that the constraint renewal time increases as the entanglement density increases [28]; however, in the systems of the disentangled UHMWPE composites, where the chains stay less entangled due to the presence of filler, the constraint renewal time tends to increase even compared to that of plain fully-entangled UHMWPE, strongly indicating the arrest of the chain dynamics by the filler. The chain-filler interaction is also evident from the phase angle in Figure 5-5b.

It is important to recall at this point that the differences in molar masses due to the presence of filler may also have influence on the rheological properties. By inspection of the reaction kinetic and catalyst activity in Table 5-3, it is reasonable to conclude that, the samples having rGON may have longer chain component. However, according to earlier research of the molar mass influence on the rheological response of disentangled UHMWPE, it is found that for plain sample having comparable molar mass (3600 s reaction), a continuous increment in *G'* is observed and finally reaches thermodynamic equilibrium state at ~2.0 MPa after a certain time (> 5×10^5 s) [3,9], whereas in the composites, the storage modulus reaches a plateau in a much shorter time (< 2×10^5 s) and at a much lower value (~ 0.8 MPa). This helps to rule out the molar mass influence on the decrease in the plateau value of the composites.

5.3.4 Influence of Entanglement Density in the Crystallisation Kinetic of Dis-UHMWPE in the Presence of rGON Filler

In Chapter 4 the DSC annealing of disentangled UHMWPE showed double endothermic peaks: one peak at 135 °C and the other at 141.5 °C, that we have assigned to crystals that form from entangled domains and disentangled domains in the heterogeneous melt, respectively. The crystals which are responsible for the low temperature endothermic peak are found to form during melt crystallisation during e-f, and the crystals related to high temperature endothermic peak form during isothermal crystallisation, d-e, in Scheme 4-1.

To have insight on the influence of the well dispersed filler on the crystallisation of the heterogeneous melts, both plain and composite samples are subjected to the protocol that is used for Figure 4-2a, and the corresponding DSC plots, collected from ramp g-h of Scheme 4-1, are shown in Figure 5-6a, b and c.

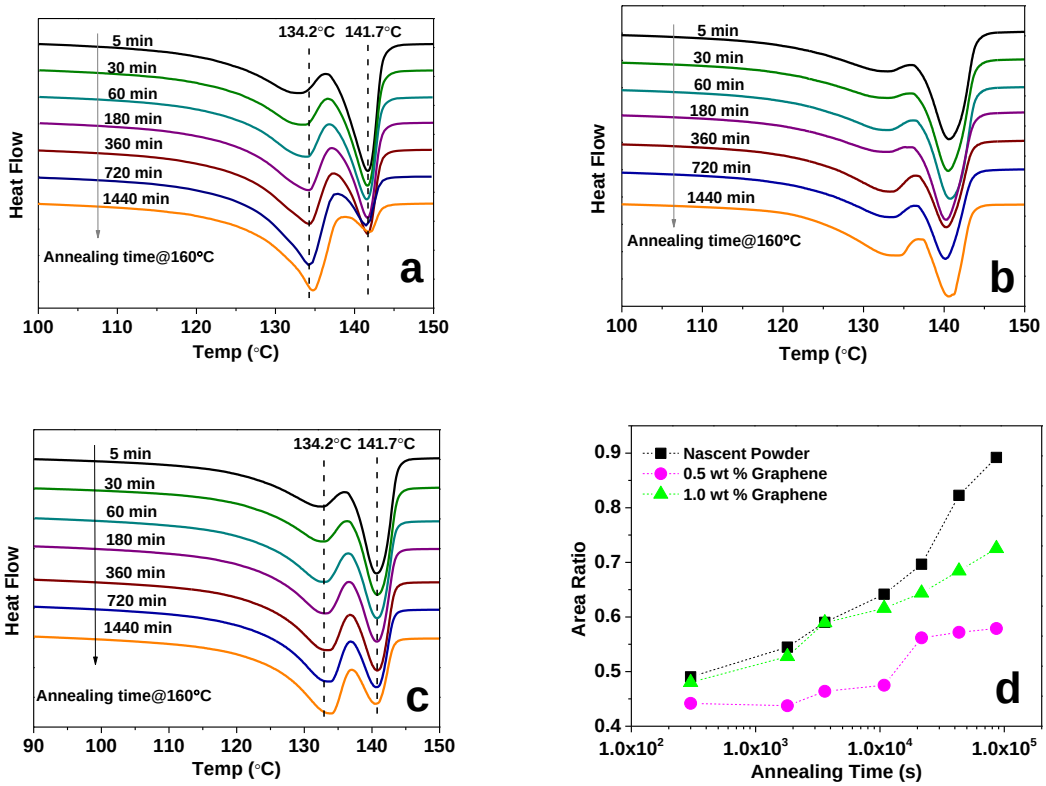

Figure 5-6 DSC plots, obtained from ramp g-h, **Scheme 4-1**, of **a)** plain sample, **b)** 0.5 wt % UHMWPE/rGON sample, and **c)** 1.0 wt % UHMWPE/rGON sample. The samples are annealed for different times at 160 °C followed by isothermal crystallisation at 128 ºC for 180 min; **d)** area ratio of the low temperature endothermic peak to the overall endothermic peak, versus annealing time at 160 °C, of the samples **a)**, **b)** and **c)**.

It is apparent that both the plain and composite samples show the split of the endothermic peak, as observed in Figure 5-6a, b and c, suggesting the presence of heterogeneous melt having disentangled and entangled domains. For the plain sample, the ratio between the low and high temperature endothermic peaks increase with annealing time at 160 ºC, indicating the progressive transformation of the heterogeneous melt from non-equilibrium to equilibrium state. However, at a filler concentration of 0.5 wt %, the increase in the enthalpy of low temperature endothermic peak with annealing time at 160 °C is suppressed, being nearly independent of the annealing time and suggesting that the non-equilibrium melt stays stable for a relatively long time. With further increment in filler concentration to 1.0 wt %, the change in the two endothermic peaks becomes obvious again, suggesting the heterogeneous melt transforms more rapidly into the homogeneous state. This can be attributed to the aggregation of the filler at this concentration that reduces the effective contact between polymer chains and the filler.

Figure 5-6d shows the area ratio of the low temperature endothermic peak normalised by the total area of the double peaks as a function of annealing time at 160 °C based on Figure 5-6a, b and c. A good agreement between the inverse of the endothermic peaks and the corresponding rheological response in Figure 5-4a further strengthens the hypothesis that the chain dynamics are arrested due to the presence of strong chain-filler interaction, especially at the filler concentration of 0.5 wt %.

In Chapter 4, the disentangled UHMWPE composites prepared by physical mixing also show similar trend in the DSC results; however, in agreement with the rheological response, at filler content of 0.8 wt %, the area of high melting peak stays stable and unchanged, whereas the *in-situ* polymerised sample shows the same phenomenon at the concentration of 0.5 wt %, supporting the idea that composites prepared by *in-situ* polymerisation have more uniform filler dispersion thus having more efficient chain-filler interaction.

5.3.5 Influence of rGON on the Mechanical Properties of UHMWPE Composites

All the samples, in nascent state prior to first melting, can be ultra-drawn in the solid state at temperatures below the equilibrium melting point, at least up to a draw ratio of 250, which confirms the low content of entanglements in the polymer matrix [9]. Figure 5-7a depicts the modulus as a function of filler content at different draw ratios. The values of the modulus increase with increasing draw ratio, and the samples reach their maximum values at a draw ratio of 250. The presence of rGON leads to an appreciable enhancement in the modulus. For instance, at a draw ratio of 250, the modulus increases from 167.2 N/Tex for the plain sample to 194.1 N/Tex for the 0.5 wt % composite, an increase of 20%. However, when further increasing the filler content to 1.0 wt %, the modulus tends to drop at all draw ratios comparing to that of 0.5 wt % composite, but it is still higher than that of the plain sample. The phenomenon can be attributed to a balance between chain-filler interaction that increase with increasing chain-filler contacts and aggregation of filler which reduces chain-filler contacts. At concentration of 0.5 wt %, as observed from rheology and DSC, the maximum contact between chain and filler is achieved and as a consequence, the Young's modulus is considerably enhanced. When the filler content increases to 1.0 wt %, aggregation of filler occurs, slightly reducing Young's modulus. This observation is in agreement with previous finding in the literature [29] and our DSC and rheology studies.

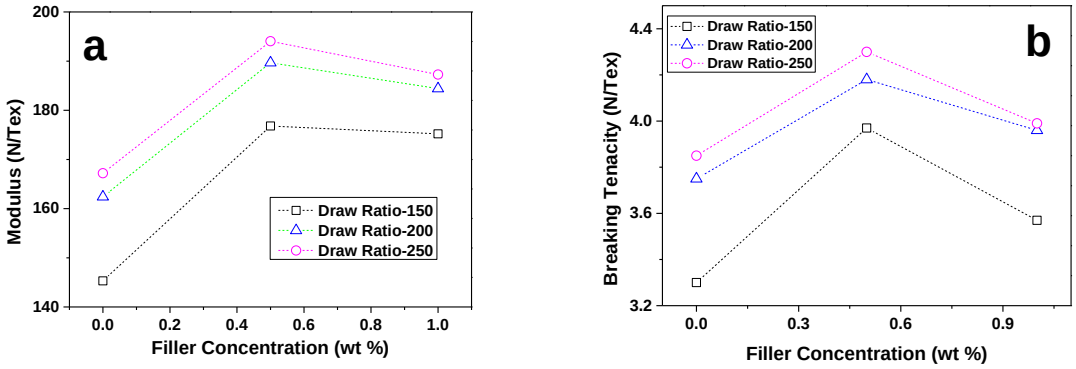

Figure 5-7 Mechanical properties of the samples with different concentration of nanofiller at different draw ratios; a) Young's modulus; b) tensile strength (breaking tenacity).

Figure 5-7b shows the tensile strength as a function of filler content at different draw ratios. The tensile strength shows the same trend as the modulus. It increases with increasing draw ratio for all the samples, and the samples reach high values above 3.8 N/Tex at draw ratio of 250. A 13% increase in tensile modulus and tensile strength is observed on addition of 0.5 w t% of rGON. However, the tensile modulus and tensile strength decreases or stays constant with increase in concentration of rGON above 0.5 wt %. The increase in modulus and tensile strength at the specific concentration region can be attributed to the strong interaction between rGON to polyethylene chain segments that increases resistance to deformation and bridges between chain ends. The former increases the tensile modulus, whereas the latter has implications on tensile strength.

5.4 Conclusions

In this chapter, we have addressed the rheological properties, thermal analysis and mechanical properties of disentangled UHMWPE/rGON samples synthesised via *in-situ* polymerisation, and a comparison with the composites prepared by physical mixing, as reported in Chapters 3 and 4, is made. It is conclusively shown that the *in-situ* composites polymerisation allows a more homogeneous dispersion of the filler across the polymer matrix, maximising the contact area between chains and the filler, and at the same time maintaining the disentangled state of the polymer. The rheological experiment shows a minimum in the plateau value at lower filler concentration (0.5 wt %) compared to the physical mixed sample (0.8 wt %). The minimum value has been related to the most homogeneous filler dispersion

and the most effective contact between chains and fillers that arrest the chain mobility. The strong chain-filler interaction thus inhibits the transition of the melt from non-equilibrium state to the equilibrium state, within the experimental timescale.

Rheological observations regarding the formation of entanglement in melt state were corroborated using differential scanning calorimetry. Similar to the results from physical mixed samples in Chapter 4, we have further found that at the filler concentration of 0.5 wt %, the change in the amount of crystals that is responsible for the high temperature endothermic peak is nearly independent on annealing time at 160 °C, whereas in the same conditions these crystals quickly diminish in the plain polymer. These observations are in line with the results from rheology, and both of them indicate the presence of a strong chain-filler interaction that inhibits the chain entanglement formation. Both the plain and the composite samples show ease in solid-state deformation, indicating an initial low entanglement density.

The strong interaction between chain and filler is also contributing to the enhancement of the mechanical properties. The composite having 0.5 wt % rGON shows the most effective enhancement of the mechanical properties, as the tensile strength and modulus of the uniaxially stretched sample reach considerable higher values of 4.3 N/Tex and 195 N/Tex, respectively.

Acknowledgement:

Here the author would like to take the chance to acknowledge Niek Tops in Teijin Aramid, the Netherlands, for the mechanical property measurements performed on the *in-situ* polymerised disentangled UHMWPE/rGON composites.

References

[1] Tervoort-Engelen, Y. M. T.; Lemstra, P. J. Morphology of nascent ultrahigh-molecular-weight polyethylene reactor powder: chain-extended versus chain-folded crystals. *Polym. Commun.* **1991**, 32, 343-345.

[2] Rastogi, S.; Yao, Y.; Ronca, S.; Bos, J.; Van der Eem, J. Unprecedented high-modulus high-strength tapes and films of ultrahigh molecular weight polyethylene via solvent-free route. *Macromolecules* **2011**, 44, 5558-5568.

[3] Pandey, A.; Champouret, Y.; Rastogi.; S. Heterogeneity in the distribution of entanglement density during polymerization in disentangled ultrahigh molecular weight polyethylene. *Macromolecules* **2011**, 44, 4952-4960.

[4] Liu, K.; Ronca, S.; Andablo-Reyes, E.; Forte, G.; Rastogi, S. Unique rheological response of Ultrahigh Molecular Weight Polyethylenes in the presence of reduced graphene oxide. *Macromolecules* **2015**, 48(1), 131-139.

[5] Feng, W.; Bai, X. D.; Lian, Y. Q.; Liang, J.; Wang, X. G.; Yoshino, K. Well-aligned polyaniline/carbon-nanotube composites films grown by in-situ aniline polymerization. *Carbon* **2003**, 41, 1551-1557.

[6] Ronca, S.; Forte, G.; Tjaden, H.; Yao, Y.; Rastogi, S. Tailoring molecular structure via nanoparticles for solvent-free processing of ultra-high molecular weight polyethylene composites. Polymer **2012**, 53, 2897-2907.

[7] Liu, P.; Gong, K.; Xiao, P.; Xiao, M. J. Preparation and characterization of poly(vinyl acetate)-intercalated graphite oxide nanocomposite. *Mater. Chem.* **2000**, 10, 933-935.

[8] Talebi, S.; Duchateau, R.; Rastogi, S.; Kaschta, J.; Peters, G. W. M.; Lemstra, P. J. Molar mass and molecular weight distribution determination of UHMWPE synthesized using a living homogeneous catalyst. *Macromolecules* **2010**, 43 (6), 2780-2788.

[9] Romano, D.; Tops, N.; Andablo-Reyes, E.; Ronca, S.; Rastogi, S. Influence of polymerization conditions on melting kinetics of low entangled UHMWPE and its implications on mechanical properties. *Macromolecules* **2014**, 47 (14), 4750-4760.

[10] Rastogi, S.; Odell, J. A. Stress stabilization of the orthorhombic and hexagonal phases of UHM PE gel-spun fibres. *Polymer* **1993**, 34, 1523-1527.

[11] Sturzel, M.; Kempe, F.; Thomann, Y.; Mark, S.; Enders, M.; Mulhaüpt, R. Novel graphene UHMWPE nanocomposites prepared by polymerization filling using single-site catalysts supported on functionalized graphene nanosheet dispersions. *Macromolecules* **2012**, 45, 6878-6887.

[12] Gao, X.; Jang, J.; Nagase, S. Hydrazine and thermal reduction of graphene oxide: reduction mechanisms, product structures, and reaction design. *J. Phys. Chem. C* **2010**, 114, 832-842.

[13] Drahushuk, L. W.; Strano, M. S. Mechanics of gas permeation through single layer graphene membranes. *Langmuir* **2012**, 28 (48), 16671-16678.

[14] Krishnamoorti, R.; Chatterjee, T. Rheology and processing of polymer nanocomposites, in applied polymer rheology: polymer fluids with industrial applications (ed M. Kontopoulou). John Wiley&Sons, inc, Hoboken, NJ, USA 2011.

[15] Pandey, A.; Toda, A.; Rastogi, S. Influence of amorphous component on melting of semicrystalline polymers. *Macromolecules* **2011**, 44(20), 8042-8055.

[16] McNally, T.; Potschke, P.; Halley, P.; Murphy, M.; Martin, D.; Bell, S. E. J.; Brennan, G. P.; Bein, D.; Lemoine, P.; Quinn, J. P. Polyethylene multiwalled carbon nanotube composites. *Polymer* **2005**, 46, 8222-8232.

[17] Zhang, Q.; Rastogi, S.; Chen, D.; Lippits, D.; Lemstra, P. J. Low percolation threshold in single-walled carbon nanotube/high density polyethylene composites prepared by melting processing technique. *Carbon* **2006**, 44, 778-785.

[18] Xiao, K.; Zhang, L.; Zarudi, I. Mechanical and rheological properties of carbon nanotube reinforced polyethylene composites. *Compos. Sci. Technol.* **2007**, 67, 177-182.

[19] Kim, H.; Abdala, A. A.; Macosko, C. W. Graphene/polymer nanocomposites. *Macromolecules* **2010**, 43, 6515-6530.

[20] Ferry, J. D. Viscoelastic Properties of Polymers, 3rd ed. Wiley: New York, 1980.

[21] Dealy, J. M.; Larson, R. G. Structure and rheology of molten polymers: from structure to flow behavior and back again. Hanser Publishers, Munch, 2005.

[22] Vega, J. F.; Martinez-Salazar, J.; Trujillo, M.; Arnal, M. L.; Müller, A. J.; Bredeau, S.; Dubois, Ph. Rheology, processing, tensile properties, and crystallization of polyethylene/carbon nanotube nanocomposites. *Macromolecules* **2009**, 42, 4719-4727.

[23] Litvinov, V. M.; Steeman, P. A. M. Vulcanized siloxane chains swollen by polymer chains: NMR investigations into free-chain dynamics. *Macromolecules* **1999**, 32, 8476-8490.

[24] Litvinov, V. M.; Orza, R. A.; Klüppel, M.; Van Duin, M.; Magusin, P. C. M. M. Rubber-filler interaction and network structure in relation to stress-strain behavior of vulcanized, carbon black filled EPDM. *Macromolecules* **2011**, 44, 4887-4900.

[25] Cheng, S.; Chen, X.; Hsuan, G. Y.; Li, C. Y. Reduced graphene oxide-induced polyethylene crystallization in solution and nanocomposites. *Macromolecules* **2011**, 45, 993-1000.

[26] Li, Y. Effect of nano inclusions on the structural and physical properties of polyethylene polymer matrix. *Polymer* **2011**, 52, 2310-2318.

[27] Mead, D. Determination of molecular weight distributions of linear flexible polymers from linear viscoelastic material functions. *J. Rheol.* **1994**, 38, 1797-1827.

[28] Andablo-Reyes, E. A.; de Boer, E. L.; Romano, D.; Rastogi, S. Stress Relaxation in the nonequilibrium state of a polymer melt. *J. Rheol.* **2014**, 58, 1981-1991.

[29] Yang, S.; Lin, W.; Huang, Y.; Tien, H.; Wang, J.; Ma, C.; Li, S.; Wang, Y. Synergetic effects of graphene platelets and carbon nanotubes on the mechanical and thermal properties of epoxy composites. *Carbon* **2011**, 49, 793-803.

6 Conclusions and Future Work

6.1 Conclusions

In this work, influence of rGON filler on the linear chain dynamics has been studied by means of linear rheology, DSC and X-ray scattering. Different PE/rGON composites, such as HDPE/rGON, commercial UHMWPE/rGON and disentangled UHMWPE/rGON composites prepared by physical mixing method or by in-situ polymerisation, are investigated. The filler influence on the physical properties of the composites, such as electrical conductivities and mechanical properties, are also investigated.

The GON filler is synthesised by a modified Hummers method that does not generate any toxic gases. It is found that the graphene oxide nanoplatelets are successfully exfoliated and oxidised, and they can be easily reduced to rGON by a combination of pressures and temperatures.

In the HDPE/rGON composites, it is found in the terminal region of linear rheology that with addition of the filler, the chain relaxation is hindered and with increasing filler concentration, the relaxation becomes more hindered. It is apparent when the concentration reaches 4.0 wt % or above, there is a jump in the absolute values of G', suggesting that at this concentration it reaches rheological percolation where a solid network forms. Interestingly, storage modulus at high frequencies (above cross-over frequency) decreases with increasing filler content and followed by an increase. At filler content of 2.0 wt %, it shows minima at frequency of 100 rad/s. This has been attributed to the disturbance of the polymer network by large aspect ratio filler which attracts the chain segments to the surface of the filler by strong chain-filler interaction. The electrical conductivities of the composites are also investigated, and it is found that the electrical conductivity percolation is at filler concentration of ~4.5 wt %, which is similar to that of rheological percolation. The influence of chain-filler interaction on the anisotropic structure formation is also studies under mild shear using wide and small angle X-ray scattering techniques. It has shown that with addition of filler concentration, the chain orientation is more pronounced after shear. The oriented chains are likely to form precursors and further cause anisotropic structure. The Deborah Number was calculated and $D_{\text{e-stre}} < 1$ is obtained and in line with speculation, no chain stretching (shish) is observed from SAXS. In this chapter, it has conclusively shown the presence of strong chain-filler

interaction that can alter chain dynamics in melt and further cause anisotropic structures when subjected to shear.

In the commercial UHMWPE/rGON composites, the influence of rGON on the chain dynamics is investigated by removing the grain boundaries at high compression temperature, for instance 230 °C. At low compression temperature, such as 160 °C, obvious grain boundaries are observed from plain polymer due to its high viscosity. With addition of filler, it is found that most of the fillers only reside along the boundaries, and with increasing concentration, most of the further added fillers mainly reside and accumulate along the boundaries. This gives rise to the enhancement of absolute value of *G'* within measurable frequencies. At higher compression moulding temperature, most of the boundaries are supposed to be removed and more chain-filler contact is expected. As a result, decrease of *G'* is observed, indicating a disturbance of the polymer melt by chain-filler interaction, as observed in HDPE/rGON samples.

In the disentangled UHMWPE/rGON composites, the influence of the filler on the polymer rheological properties is more obvious. It is found that the entanglement formation of the disentangled chains during dynamic sweep is hindered in the presence of rGON. At concentration of 0.8 wt %, the entanglement formation is almost stopped being independent of annealing time at 160 °C. Low plateau values are reached after long time annealing, indicating higher molar mass between adjacent entanglements. The following dynamic frequency sweep shows that the chain relaxation is hindered at low frequencies and at filler concentration of 0.8 wt %, *G'* is almost independent of frequency. The unique rheological properties are attributed to the porous morphology and low initial viscosity of disentangled UHMWPE, that give rise to homogeneous distribution of filler in the polymer matrix after compression moulding, thus giving effective contacts between disentangled chains and large aspect area filler. The effective contact between chain and filler hence enhances the chain-filler interaction and further hinders the chain dynamics. The electrical conductivity of the disentangled UHMWPE composites compressed at 160 °C, at filler concentration of 2.0 wt % and above, is found at least 2 orders higher than that of commercial UHMWPE compsoites, indicating formation of refined filler-filler network due to homogeneous distribution of the filler in the matrix. When subjected to 230 °C compression moulding, the commercial samples show similar conductivity values of that of disentangled UHMWPE samples. This is attributed to the removal of the polymer powder boundaries and formation of a refined filler-filler network.

A new approach of understanding the transformation of polymer melt from non-equilibrium to equilibrium state has been carried out. After annealing at 160 °C and isothermal crystallisation at 128 °C, it is found that the melting peak of disentangled UHMWPE is split into two peaks: a high melting peak close it PE's equilibrium melting peak (141.5 °C) and a low melting peak that is close to the melting peak of melt-crystallised UHMWPE samples (135 °C). The split of the peak is attributed to the heterogeneity of the polymer melt, which has two different regions/domains, one entangled region and one disentangled region. It can be concluded that the high melting peak is from melting the crystals that form from disentangled domains, and the low melting peak is due to melting the crystals from entangled region. With increasing annealing time, it is found that the low melting peak area/enthalpy increases at expenses of high melting peak area, indicating the entanglement formation with increasing annealing time. The influence of filler on the crystallisation kinetics is also investigated. It has shown that with addition of filler, the increase of the low melting peak area is hindered, and at filler concentration of 0.8 wt %, the peak areas almost stay independent of the annealing time. This is assigned to the hindering of entanglement formation by the presence of filler, and the less entangled region is relatively stable with annealing time. The DSC results are found in line with their corresponding rheological responses.

Disentangled UHMWPE/GON composites prepared by in-situ polymerisation are also investigated in order to understand the filler influence on the chain dynamics and crystallisation behaviours. Similar to the results of disentangled UHMWPE composites prepared by physical mixing method, the chain entanglement formation is hindered when filler is added and the chain relaxation is also hindered at low frequency region due to the strong chain-filler interaction. The hindering in chain entanglement is further supported by DSC annealing experiments, where it shows that the decrease in high melting peak area stays less independent of annealing time, indicating the lasting of less entangled region for longer time. The maximum chain-filler interaction happens at lower concentration comparing to that of physical mixed samples. Mechanical properties are also characterised after the samples are ultra-drawn into 1 D film, and it has shown both Young's modulus and tensile strength are enhanced in the presence of filler.

6.2 Future Work Recommendations

Very important to notice is the reappearance of the high melting peak (141.5 ^{o}C) after disentangled UHMWPE is subjected to melt, even after it reaches equilibrium state. The high melting peak can be either from extended crystals or non-extended crystals but have adjacent re-entrant loops that provide constraint. Due to the heat treatment, extended crystals are less likely to form, and the adjacent re-entrant crystals may be the answer to the high melting peak. However, the formation of adjacent re-entrant crystals requires disentangled state of the chains. This suggests that after the disentangled UHMWPE subjected to melt and even after it reaches its equilibrium state, the chains are still disentangled. How this works? This could be explained by unhooked entanglement which differs from hooked entanglements. However, non-direct evidence has been found during my PhD project, and further work on the entanglement type of disentangled UHMWPE when subjected to melt is highly suggested, and this may reveal new entanglement behaviour for disentangled polymers having high molar mass and result in fabrication of high dimension (3D for instance) products that have ultra-high modulus and strength. Following this point, the influence of filler on the entanglement formation and crystallisation behaviour of the heterogeneous melts can be further explored and explained.

The reduction of the viscosity of disentangled UHMWPE when added rGON filler could lead to ease in processability of the intractable material, attracting industrial interest. However the explanation behind the phenomena is not well answered in this thesis, for an example, the exact chain-filler interaction stays vague. Further investigation on the chain-filler interaction could provide a thorough understanding on the reduction of the viscosity and this may be applied to other composite systems, facilitating processbility of composites especially those having long chain components.

Appendices

Appendix 1

wt % and vol % conversion of filler in the composites

The conversion of added GON from wt % to vol % was done by considering the density of dried GON to be 2.2 g/cm^3 and 0.96 g/cm3 [1] of PE after compression moulding. Considering the high crystallinity of the nascent UHMWPE samples (> 82%) the density of the compressed linear UHMWPE sample is obtained close to 0.96 g/ cm^3. The vol % is used for the calculation of the electrical percolation.

Table A1-1 wt % to vol % conversion of the GON in UHMWPE/GON composites.

wt %	0.1	0.3	0.5	0.8	2.0	4.0
vol %	0.04	0.13	0.22	0.35	0.88	1.79

Reference

[1] Stankovich, S.; Dikin, D. A.; Dommett, G. H. B.; Kohlhaas, K. M.; Zimney, E. J.; Stach, E. A.; Piner, R. D.; Nguyen, S. T.; Ruoff R. S. Graphene-based composite materials. *Nature* **2006**, 442, 282-286.

Appendix 2

Calculation of τ_s at 136 °C:

τ_e@190°C is 7×10^{-9} s, and τ_e@136°C is calculated according to WLF equation:

$$a_T = \frac{\tau_e(@136°C)}{\tau_e(@190°C)} = EXP(\frac{E_a}{R}(\frac{1}{T_1} - \frac{1}{T_2}))$$

T_1=136+273.15=409.15 (K);

T_2=190+273.15=463.15 (K);

E_a= 26.7 kJ/mol; R=8.314 $JK^{-1}mol^{-1}$

Hence τ_e@136 °C = 1.75×10^{-8} s.

$$Z = \frac{Mz}{Me} = \frac{3200000}{828} \approx 3854$$

$$\tau_s = Z^2 \times \tau_e(@136°C) = 3854^2 \times 1.75 \times 10^{-8} \approx 0.26\ (s)$$

Calculation of τ_{rep} at 136 °C:

$$\tau_d = 3 \times Z^3 \times \tau_e = 3 \times 3854^3 \times 1.75 \times 10^{-8} \approx 3000\ s$$

$$\frac{\tau_{rep}}{\tau_d} = 1 - \frac{3.38}{Z^{0.5}} + \frac{4.17}{Z} - \frac{1.55}{Z^{1.5}}$$

Hence,

$$\tau_{rep} = \tau_d \times 0.95 \approx 2840\ (s)$$